

COLD-FORMED STEEL SECTIONS FOR TRANSMISSION TOWERS

by

David Odaisky

A Thesis
Submitted to the Faculty of Graduate Studies
in Partial Fulfilment of the Requirements
for the Degree of

MASTER OF SCIENCE

Department of Civil Engineering
University of Manitoba
Winnipeg, Manitoba
Canada

(c) February, 1994



National Library
of Canada

Acquisitions and
Bibliographic Services Branch

395 Wellington Street
Ottawa, Ontario
K1A 0N4

Bibliothèque nationale
du Canada

Direction des acquisitions et
des services bibliographiques

395, rue Wellington
Ottawa (Ontario)
K1A 0N4

Your file Votre référence

Our file Notre référence

The author has granted an irrevocable non-exclusive licence allowing the National Library of Canada to reproduce, loan, distribute or sell copies of his/her thesis by any means and in any form or format, making this thesis available to interested persons.

L'auteur a accordé une licence irrévocable et non exclusive permettant à la Bibliothèque nationale du Canada de reproduire, prêter, distribuer ou vendre des copies de sa thèse de quelque manière et sous quelque forme que ce soit pour mettre des exemplaires de cette thèse à la disposition des personnes intéressées.

The author retains ownership of the copyright in his/her thesis. Neither the thesis nor substantial extracts from it may be printed or otherwise reproduced without his/her permission.

L'auteur conserve la propriété du droit d'auteur qui protège sa thèse. Ni la thèse ni des extraits substantiels de celle-ci ne doivent être imprimés ou autrement reproduits sans son autorisation.

ISBN 0-315-92194-3

Canada

Name DAVID ODAISKY

Dissertation Abstracts International is arranged by broad, general subject categories. Please select the one subject which most nearly describes the content of your dissertation. Enter the corresponding four-digit code in the spaces provided.

ENGINEERING / CIVIL

SUBJECT TERM

0543

SUBJECT CODE

U·M·I

Subject Categories

THE HUMANITIES AND SOCIAL SCIENCES

COMMUNICATIONS AND THE ARTS

Architecture 0729
Art History 0377
Cinema 0900
Dance 0378
Fine Arts 0357
Information Science 0723
Journalism 0391
Library Science 0399
Mass Communications 0708
Music 0413
Speech Communication 0459
Theater 0465

EDUCATION

General 0515
Administration 0514
Adult and Continuing 0516
Agricultural 0517
Art 0273
Bilingual and Multicultural 0282
Business 0688
Community College 0275
Curriculum and Instruction 0727
Early Childhood 0518
Elementary 0524
Finance 0277
Guidance and Counseling 0519
Health 0680
Higher 0745
History of 0520
Home Economics 0278
Industrial 0521
Language and Literature 0279
Mathematics 0280
Music 0522
Philosophy of 0998
Physical 0523

Psychology 0525
Reading 0535
Religious 0527
Sciences 0714
Secondary 0533
Social Sciences 0534
Sociology of 0340
Special 0529
Teacher Training 0530
Technology 0710
Tests and Measurements 0288
Vocational 0747

LANGUAGE, LITERATURE AND LINGUISTICS

Language
General 0679
Ancient 0289
Linguistics 0290
Modern 0291
Literature
General 0401
Classical 0294
Comparative 0295
Medieval 0297
Modern 0298
African 0316
American 0591
Asian 0305
Canadian (English) 0352
Canadian (French) 0355
English 0593
Germanic 0311
Latin American 0312
Middle Eastern 0315
Romance 0313
Slavic and East European 0314

PHILOSOPHY, RELIGION AND THEOLOGY

Philosophy 0422
Religion
General 0318
Biblical Studies 0321
Clergy 0319
History of 0320
Philosophy of 0322
Theology 0469

SOCIAL SCIENCES

American Studies 0323
Anthropology
Archaeology 0324
Cultural 0326
Physical 0327
Business Administration
General 0310
Accounting 0272
Banking 0770
Management 0454
Marketing 0338
Canadian Studies 0385
Economics
General 0501
Agricultural 0503
Commerce-Business 0505
Finance 0508
History 0509
Labor 0510
Theory 0511
Folklore 0358
Geography 0366
Gerontology 0351
History
General 0578

Ancient 0579
Medieval 0581
Modern 0582
Black 0328
African 0331
Asia, Australia and Oceania 0332
Canadian 0334
European 0335
Latin American 0336
Middle Eastern 0333
United States 0337
History of Science 0585
Law 0398
Political Science
General 0615
International Law and
Relations 0616
Public Administration 0617
Recreation 0814
Social Work 0452
Sociology
General 0626
Criminology and Penology 0627
Demography 0938
Ethnic and Racial Studies 0631
Individual and Family
Studies 0628
Industrial and Labor
Relations 0629
Public and Social Welfare 0630
Social Structure and
Development 0700
Theory and Methods 0344
Transportation 0709
Urban and Regional Planning 0999
Women's Studies 0453

THE SCIENCES AND ENGINEERING

BIOLOGICAL SCIENCES

Agriculture
General 0473
Agronomy 0285
Animal Culture and
Nutrition 0475
Animal Pathology 0476
Food Science and
Technology 0359
Forestry and Wildlife 0478
Plant Culture 0479
Plant Pathology 0480
Plant Physiology 0817
Range Management 0777
Wood Technology 0746
Biology
General 0306
Anatomy 0287
Biostatistics 0308
Botany 0309
Cell 0379
Ecology 0329
Entomology 0353
Genetics 0369
Limnology 0793
Microbiology 0410
Molecular 0307
Neuroscience 0317
Oceanography 0416
Physiology 0433
Radiation 0821
Veterinary Science 0778
Zoology 0472
Biophysics
General 0786
Medical 0760

Geodesy 0370
Geology 0372
Geophysics 0373
Hydrology 0388
Mineralogy 0411
Paleobotany 0345
Paleoecology 0426
Paleontology 0418
Paleozoology 0985
Palynology 0427
Physical Geography 0368
Physical Oceanography 0415

HEALTH AND ENVIRONMENTAL SCIENCES

Environmental Sciences 0768
Health Sciences
General 0566
Audiology 0300
Chemotherapy 0992
Dentistry 0567
Education 0350
Hospital Management 0769
Human Development 0758
Immunology 0982
Medicine and Surgery 0564
Mental Health 0347
Nursing 0569
Nutrition 0570
Obstetrics and Gynecology 0380
Occupational Health and
Therapy 0354
Ophthalmology 0381
Pathology 0571
Pharmacology 0419
Pharmacy 0572
Physical Therapy 0382
Public Health 0573
Radiology 0574
Recreation 0575

Speech Pathology 0460
Toxicology 0383
Home Economics 0386

PHYSICAL SCIENCES

Pure Sciences
Chemistry
General 0485
Agricultural 0749
Analytical 0486
Biochemistry 0487
Inorganic 0488
Nuclear 0738
Organic 0490
Pharmaceutical 0491
Physical 0494
Polymer 0495
Radiation 0754
Mathematics 0405
Physics
General 0605
Acoustics 0986
Astronomy and
Astrophysics 0606
Atmospheric Science 0608
Atomic 0748
Electronics and Electricity 0607
Elementary Particles and
High Energy 0798
Fluid and Plasma 0759
Molecular 0609
Nuclear 0610
Optics 0752
Radiation 0756
Solid State 0611
Statistics 0463
Applied Sciences
Applied Mechanics 0346
Computer Science 0984

Engineering
General 0537
Aerospace 0538
Agricultural 0539
Automotive 0540
Biomedical 0541
Chemical 0542
Civil 0543
Electronics and Electrical 0544
Heat and Thermodynamics 0348
Hydraulic 0545
Industrial 0546
Marine 0547
Materials Science 0794
Mechanical 0548
Metallurgy 0743
Mining 0551
Nuclear 0552
Packaging 0549
Petroleum 0765
Sanitary and Municipal 0554
System Science 0790
Geotechnology 0428
Operations Research 0796
Plastics Technology 0795
Textile Technology 0994

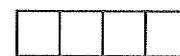
PSYCHOLOGY

General 0621
Behavioral 0384
Clinical 0622
Developmental 0620
Experimental 0623
Industrial 0624
Personality 0625
Physiological 0989
Psychobiology 0349
Psychometrics 0632
Social 0451



Nom _____

Dissertation Abstracts International est organisé en catégories de sujets. Veuillez s.v.p. choisir le sujet qui décrit le mieux votre thèse et inscrivez le code numérique approprié dans l'espace réservé ci-dessous.



U·M·I

SUJET

CODE DE SUJET

Catégories par sujets

HUMANITÉS ET SCIENCES SOCIALES

COMMUNICATIONS ET LES ARTS

Architecture	0729
Beaux-arts	0357
Bibliothéconomie	0399
Cinéma	0900
Communication verbale	0459
Communications	0708
Danse	0378
Histoire de l'art	0377
Journalisme	0391
Musique	0413
Sciences de l'information	0723
Théâtre	0465

ÉDUCATION

Généralités	515
Administration	0514
Art	0273
Collèges communautaires	0275
Commerce	0688
Économie domestique	0278
Éducation permanente	0516
Éducation préscolaire	0518
Éducation sanitaire	0680
Enseignement agricole	0517
Enseignement bilingue et multiculturel	0282
Enseignement industriel	0521
Enseignement primaire	0524
Enseignement professionnel	0747
Enseignement religieux	0527
Enseignement secondaire	0533
Enseignement spécial	0529
Enseignement supérieur	0745
Évaluation	0288
Finances	0277
Formation des enseignants	0530
Histoire de l'éducation	0520
Langues et littérature	0279

Lecture	0535
Mathématiques	0280
Musique	0522
Orientation et consultation	0519
Philosophie de l'éducation	0998
Physique	0523
Programmes d'études et enseignement	0727
Psychologie	0525
Sciences	0714
Sciences sociales	0534
Sociologie de l'éducation	0340
Technologie	0710

LANGUE, LITTÉRATURE ET LINGUISTIQUE

Langues	
Généralités	0679
Anciennes	0289
Linguistique	0290
Modernes	0291
Littérature	
Généralités	0401
Anciennes	0294
Comparée	0295
Médiévale	0297
Moderne	0298
Africaine	0316
Américaine	0591
Anglaise	0593
Asiatique	0305
Canadienne (Anglaise)	0352
Canadienne (Française)	0355
Germanique	0311
Latino-américaine	0312
Moyen-orientale	0315
Romane	0313
Slave et est-européenne	0314

PHILOSOPHIE, RELIGION ET THÉOLOGIE

Philosophie	0422
Religion	
Généralités	0318
Clergé	0319
Études bibliques	0321
Histoire des religions	0320
Philosophie de la religion	0322
Théologie	0469

SCIENCES SOCIALES

Anthropologie	
Archéologie	0324
Culturelle	0326
Physique	0327
Droit	0398
Économie	
Généralités	0501
Commerce-Affaires	0505
Économie agricole	0503
Économie du travail	0510
Finances	0508
Histoire	0509
Théorie	0511
Études américaines	0323
Études canadiennes	0385
Études féministes	0453
Folklore	0358
Géographie	0366
Gérontologie	0351
Gestion des affaires	
Généralités	0310
Administration	0454
Banques	0770
Comptabilité	0272
Marketing	0338
Histoire	
Histoire générale	0578

Ancienne	0579
Médiévale	0581
Moderne	0582
Histoire des noirs	0328
Africaine	0331
Canadienne	0334
États-Unis	0337
Européenne	0335
Moyen-orientale	0333
Latino-américaine	0336
Asie, Australie et Océanie	0332
Histoire des sciences	0585
Loisirs	0814
Planification urbaine et régionale	0999
Science politique	
Généralités	0615
Administration publique	0617
Droit et relations internationales	0616
Sociologie	
Généralités	0626
Aide et bien-être social	0630
Criminologie et établissements pénitentiaires	0627
Démographie	0938
Études de l'individu et de la famille	0628
Études des relations interethniques et des relations raciales	0631
Structure et développement social	0700
Théorie et méthodes	0344
Travail et relations industrielles	0629
Transports	0709
Travail social	0452

SCIENCES ET INGÉNIERIE

SCIENCES BIOLOGIQUES

Agriculture	
Généralités	0473
Agronomie	0285
Alimentation et technologie alimentaire	0359
Culture	0479
Élevage et alimentation	0475
Exploitation des pâturages	0777
Pathologie animale	0476
Pathologie végétale	0480
Physiologie végétale	0817
Sylviculture et taune	0478
Technologie du bois	0746
Biologie	
Généralités	0306
Anatomie	0287
Biologie (Statistiques)	0308
Biologie moléculaire	0307
Botanique	0309
Cellule	0379
Écologie	0329
Entomologie	0353
Génétique	0369
Limnologie	0793
Microbiologie	0410
Neurologie	0317
Océanographie	0416
Physiologie	0433
Radiation	0821
Science vétérinaire	0778
Zoologie	0472
Biophysique	
Généralités	0786
Médicale	0760

SCIENCES DE LA TERRE

Biogéochimie	0425
Géochimie	0996
Géodésie	0370
Géographie physique	0368

Géologie	0372
Géophysique	0373
Hydrologie	0388
Minéralogie	0411
Océanographie physique	0415
Paléobotanique	0345
Paléocéologie	0426
Paléontologie	0418
Paléozoologie	0985
Palynologie	0427

SCIENCES DE LA SANTÉ ET DE L'ENVIRONNEMENT

Économie domestique	0386
Sciences de l'environnement	0768
Sciences de la santé	
Généralités	0566
Administration des hôpitaux	0769
Alimentation et nutrition	0570
Audiologie	0300
Chimiothérapie	0992
Dentisterie	0567
Développement humain	0758
Enseignement	0350
Immunologie	0982
Loisirs	0575
Médecine du travail et thérapie	0354
Médecine et chirurgie	0564
Obstétrique et gynécologie	0380
Ophtalmologie	0381
Orthophonie	0460
Pathologie	0571
Pharmacie	0572
Pharmacologie	0419
Physiothérapie	0382
Radiologie	0574
Santé mentale	0347
Santé publique	0573
Soins infirmiers	0569
Toxicologie	0383

SCIENCES PHYSIQUES

Sciences Pures

Chimie	
Généralités	0485
Biochimie	0487
Chimie agricole	0749
Chimie analytique	0486
Chimie minérale	0488
Chimie nucléaire	0738
Chimie organique	0490
Chimie pharmaceutique	0491
Physique	0494
Polymères	0495
Radiation	0754
Mathématiques	0405
Physique	
Généralités	0605
Acoustique	0986
Astronomie et astrophysique	0606
Électrique et électricité	0607
Fluides et plasma	0759
Météorologie	0608
Optique	0752
Particules (Physique nucléaire)	0798
Physique atomique	0748
Physique de l'état solide	0611
Physique moléculaire	0609
Physique nucléaire	0610
Radiation	0756
Statistiques	0463

Sciences Appliquées Et Technologie

Informatique	0984
Ingénierie	
Généralités	0537
Agricole	0539
Automobile	0540

Biomédicale	0541
Chaleur et thermodynamique	0348
Conditionnement (Emballage)	0549
Génie aérospatial	0538
Génie chimique	0542
Génie civil	0543
Génie électronique et électrique	0544
Génie industriel	0546
Génie mécanique	0548
Génie nucléaire	0552
Ingénierie des systèmes	0790
Mécanique navale	0547
Métallurgie	0743
Science des matériaux	0794
Technique du pétrole	0765
Technique minière	0551
Techniques sanitaires et municipales	0554
Technologie hydraulique	0545
Mécanique appliquée	0346
Géotechnologie	0428
Matériaux plastiques (Technologie)	0795
Recherche opérationnelle	0796
Textiles et tissus (Technologie)	0794

PSYCHOLOGIE

Généralités	0621
Personnalité	0625
Psychobiologie	0349
Psychologie clinique	0622
Psychologie du comportement	0384
Psychologie du développement	0620
Psychologie expérimentale	0623
Psychologie industrielle	0624
Psychologie physiologique	0989
Psychologie sociale	0451
Psychométrie	0632



COLD-FORMED STEEL SECTIONS FOR TRANSMISSION TOWERS

BY

DAVID ODAISKY

**A Thesis submitted to the Faculty of Graduate Studies of the University of Manitoba
in partial fulfillment of the requirements of the degree of**

MASTER OF SCIENCE

© 1994

**Permission has been granted to the LIBRARY OF THE UNIVERSITY OF MANITOBA
to lend or sell copies of this thesis, to the NATIONAL LIBRARY OF CANADA to
microfilm this thesis and to lend or sell copies of the film, and LIBRARY
MICROFILMS to publish an abstract of this thesis.**

**The author reserves other publication rights, and neither the thesis nor extensive
extracts from it may be printed or other-wise reproduced without the author's written
permission.**

ABSTRACT

Cold-formed steel sections are becoming more popular in the construction of transmission towers, both in Europe and North America. In addition to conventional 90° angles, a wide range of shapes can be produced, in sizes to suit individual project requirements.

An investigative project was carried out at the University of Manitoba to examine the axial compressive load capacity of a number of cold-formed shapes suitable for transmission tower construction.

Test parameters included: five different cross-sections, two steel grades, three different slenderness ratios, and three temperature levels. Specimens were tested in setups designed to simulate end conditions representative of actual web members by loading through single legs bolted to gusset plates. Some sections were tested as axially loaded leg members with hinged end conditions. Three special test setups were constructed to accommodate the wide range in length, which varied from 552 mm to 8200 mm. A total of 201 static tests were performed.

Test results were compared to predicted loads using the Canadian Standards CAN/CSA-S136-M89 Cold Formed Steel Structural Members, and CAN/CSA-S37-M86 Antennas, Towers, and Antenna Supporting Structures, ASCE Manual 52

Guide for Design of Steel Transmission Towers, and ECCS Recommendations for Angles in Lattice Transmission Towers. Ultimate, and factored capacity curves were prepared for each specimen shape, and for a wide range of slenderness ratios using the above design methods. In general, test results were adequately predicted by the design methods. Some discrepancies were observed, and simple modifications are proposed to in order to avoid unconservative designs.

Cold temperature was observed to increase the capacity of the sections. The amount of increase varied with the specimen length and failure mode, but in any case was not found to be detrimental.

ACKNOWLEDGEMENTS

This research project was carried out under the direct supervision of Dr. Dimos Polyzois. The author wishes to express his gratitude to Dr. Polyzois for his advice, guidance, encouragement, and support throughout the investigation.

The author also wishes to thank the project members: Mr. T. Jerome, Dr. G. Morris, Mr. W.J. Muzyczka, Dr. S. Rizkalla, and Mr. C.W. Wong for bringing their experience and knowledge to the project meetings during the investigation. Their input and comments were gratefully appreciated.

Financial support provided by Manitoba Hydro, The Canadian Electrical Association, and the University of Manitoba is gratefully acknowledged.

For their advice and assistance during testing, the author thanks Messrs. Ed Lemke, and Rob Graham of the Civil Engineering Department.

The author also wishes to thank his fellow graduate students for their help.

TABLE OF CONTENTS

ABSTRACT	i
ACKNOWLEDGEMENTS	iii
TABLE OF CONTENTS	iv
LIST OF TABLES	viii
LIST OF FIGURES	ix
CHAPTER 1 INTRODUCTION	1
1.1 General	1
1.2 Objectives	3
1.3 Scope	4
CHAPTER 2 LITERATURE REVIEW	6
2.1 General	6
2.2 Canadian Standard CAN/CSA-S136-M89 Cold-Formed Steel Structural Members	16

2.3	CAN/CSA-S37-M86 Antennas, Towers, and Antenna-Supporting Structures	22
2.4	ASCE Manual 52 Guide For Design of Steel Transmission Towers	25
2.5	ECCS Recommendations for Angles in Lattice Transmission Towers	31
CHAPTER 3 EXPERIMENTAL PROGRAM		35
3.1	Introduction	35
3.2	Specimens	35
3.3	Test Setup and Procedure	37
3.3.1	Test Setup No. 1	37
3.3.1.1	Test Procedure	41
3.3.2	Test Setup No. 2	42
3.3.2.1	Test Procedure	43
3.3.3	Test Setup No. 3	44
3.3.3.1	Test Procedure	46
CHAPTER 4 TEST RESULTS		47
4.1	Introduction	47
4.2	Material Tests	47
4.3	Dimensions and Section Properties	48

4.4	Static Load Results	48
CHAPTER 5 ANALYSIS AND DISCUSSION OF TEST RESULTS		49
5.1	Introduction	49
5.2	Material Properties	49
5.3	Effect of Temperature	51
5.4	BA And HBA Specimens	52
5.4	BB And HBB Specimens	59
5.5	BC and HBC Sections	61
5.6	BG Sections	65
5.7	BN and HBN Sections	71
5.9	Concentrically Loaded Angles	78
5.10	Unstiffened Angles Bolted Through One Leg	81
CHAPTER 6 SUMMARY, CONCLUSIONS, AND		
RECOMMENDATIONS		85
6.1	Summary	85
6.2	Conclusions	86
6.3	Recommendations	88
REFERENCES		92

	vii
TABLES	96
FIGURES	114
APPENDIX A	197
APPENDIX B	212

LIST OF TABLES

TABLE NO.	TITLE	PAGE NO.
1.1	Test Parameters	97
4.1	Specified and Measured Yield Strengths	98
4.2	Average Section Properties	99
4.3	Static Test Results Summary	100
5.1	Temperature Affect on Load Capacity	106
5.2	BA and HBA Sections Predicted Load Comparison	107
5.3	BB and HBB Sections Predicted Load Comparison	108
5.4	BC and HBC Sections Predicted Load Comparison	109
5.5	BG Section Predicted Load Comparison	110
5.6	BN and HBN Sections Predicted Load Comparison	111
5.7	Concentrically Loaded Specimen Comparison	112
5.8	Proposed Upper Compressive Limit For Unstiffened Angles Bolted through one Leg	113

LIST OF FIGURES

FIGURE NO.	TITLE	PAGE NO.
1.1	Transmission Tower in Service	115
1.2	Member Failure in a Tower Leg	116
3.1	BA and HBA Section Measurements	117
3.2	BB and HBB Section Measurements	118
3.3	BC and HBC Section Measurements	119
3.4	BG Section Measurements	120
3.5	BN and HBN Section Measurements	121
3.6	Test Setup No. One	122
3.7	Typical Gusset Plates	123
3.8	BN-40 End Fitting	124
3.9	BG-40 End Fitting	124
3.10	Motion Transducers at MidHeight of Specimen	125
3.11	Setup No. 2: Cold Chamber and Load Frame	126
3.12	Setup No. 2: Typical Angle Connection	127
3.13	Setup No. 2: BN-100 End Fitting	127
3.14	Setup No. 2: BG-100 End Fitting	128
3.15	Setup No. 3	129
3.16	Setup No. 3: End Blocks	130
3.17	Setup No. 3: Jack and Load Cell	131
3.18	Setup No. 3: Gusset Plate Hinge	131
3.19	Setup No. 3: Motion Transducer at Midlength	132
3.20	Schematic of Setup No. 1	133
3.21	Schematic of Setup No. 2	134
3.22	Schematic of Setup No. 3	135
3.23	Schematic of Gusset Plate for Angle Connections	136
3.24	Schematic of Gusset Plate for (H)BN Sections: Setup No. 1	137
3.25	Schematic of Gusset Plate for (H)BN Sections: Setup No. 2 & 3	137
3.26	Schematic of Gusset Plate for BG Sections	138
5.1	Load vs. Temperature - BA Section	139
5.2	Load vs. Temperature - HBA Section	140
5.3	Load vs. Temperature - BB Section	141
5.4	Load vs. Temperature - HBB Section	142
5.5	Load vs. Temperature - BC Section	143
5.6	Load vs. Temperature - HBC Section	144
5.7	Load vs. Temperature - BG Section	145
5.8	Load vs. Temperature - BN Section	146
5.9	Load vs. Temperature - HBN Section	147
5.10	Average Failure Load Increase at -50° C vs. Slenderness	148

5.11	Average Failure Load Increase at 0° C vs. Slenderness	149
5.12	BA-40 Specimens at Failure	150
5.13	BA-100 Specimen at Failure	151
5.14	BA-200 Specimen at Failure	151
5.15	BA Section Analysis: CAN/CSA-S136-M89	152
5.16	HBA Section Analysis: CAN/CSA-S136-M89	153
5.17	BA Section Analysis: ASCE Manual 52	154
5.18	HBA Section Analysis: ASCE Manual 52	155
5.19	BA Section Analysis: CAN/CSA-S37-M86	156
5.20	HBA Section Analysis: CAN/CSA-S37-M86	157
5.21	BA Section Analysis: ECCS Recommendations	158
5.22	HBA Section Analysis: ECCS Recommendations	159
5.23	HBB-40 Specimen at Failure	160
5.24	BB-100 Specimen at Failure	160
5.25	BB-100 Midheight Twist and Lateral Deflection	161
5.26	BB-100 Distortion at Connection	161
5.27	BB Section Analysis: CAN/CSA-S136-M89	162
5.28	HBB Section Analysis: CAN/CSA-S136-M89	163
5.29	BB Section Analysis: ASCE Manual 52	164
5.30	HBB Section Analysis: ASCE Manual 52	165
5.31	BC-40 Specimen at Failure	166
5.32	BC-200 Specimen at Failure	166
5.33	BC Section Analysis: CAN/CSA-S136-M89	167
5.34	HBC Section Analysis: CAN/CSA-S136-M89	168
5.35	BC Section Analysis: ASCE Manual 52	169
5.36	HBC Section Analysis: ASCE Manual 52	170
5.37	BC Section Analysis: CAN/CSA-S37-M86	171
5.38	HBC Section Analysis: CAN/CSA-S37-M86	172
5.39	BG-40 Specimen at Failure	173
5.40	BG-40: Distortion of Stiffened Flange at Failure	173
5.41	BG-40 Specimen at Failure	174
5.42	BG-40: Distortion of Web at Failure	174
5.43	BG-100 Specimen after Failure	175
5.44	BG Section Analysis: CAN/CSA-S136-M89	176
5.45	BG Section Analysis: CAN/CSA-S136-M89 $K_t = 0.7$	177
5.46	BG Section Analysis: ASCE Manual 52	178
5.47	BG Section Analysis: ASCE Manual 52 $K_t = 0.7$	179
5.48	BN-40 Specimen at Failure	180
5.49	BN-40 Specimen Lip Distortion	180
5.50	BN-100 Specimen at Failure	181
5.51	BN-200 Specimen at Failure	181

5.52	BN Section Analysis: CAN/CSA-S136-M89	182
5.53	BN Section Analysis: CAN/CSA-S136-M89 Neglecting Torsional Buckling	183
5.54	HBN Section Analysis: CAN/CSA-S136-M89	184
5.55	HBN Section Analysis: CAN/CSA-S136-M89 Neglecting Torsional Buckling	185
5.56	BN Section Analysis: CAN/CSA-S16.1-M89	186
5.57	BN Section Analysis: CAN/CSA-S16.1-M89 Neglecting Torsional Buckling	187
5.58	HBN Section Analysis: CAN/CSA-S16.1-M89	188
5.59	HBN Section Analysis: CAN/CSA-S16.1-M89 Neglecting Torsional Buckling	189
5.60	BN Section Analysis: ASCE Manual 52	190
5.61	BN Section Analysis: ASCE Manual 52 Neglecting Torsional Buckling	191
5.62	HBN Section Analysis: ASCE Manual 52	192
5.63	HBN Section Analysis: ASCE Manual 52 Neglecting Torsional Buckling	193
5.64	BA-40 Specimen with Both Legs Connected	194
5.65	Proposed Upper Compressive Limit for Unstiffened Angles Loaded Through One Leg	195
5.66	Comparison of Experimental Results with Modified Manual 52	196
A.1	Typical Load-Displacement curves for Specimens BA-40 and HBA- 40	198
A.2	Typical Load-Displacement curves for Specimens BA-100 and HBA- 100	199
A.3	Typical Load-Displacement curves for Specimens BA-200 and HBA- 200	200
A.4	Typical Load-Displacement curves for Specimens BB-40 and HBB- 40	201
A.5	Typical Load-Displacement curves for Specimens BB-100 and HBB- 100	202
A.6	Typical Load-Displacement curves for Specimens BB-200 and HBB- 200	203
A.7	Typical Load-Displacement curves for Specimens BC-40 and HBC- 40	204
A.8	Typical Load-Displacement curves for Specimens BC-100 and HBC- 100	205
A.9	Typical Load-Displacement curves for Specimens BC-200 and HBC- 200	206
A.10	Typical Load-Displacement curves for Specimens BG-40 and BG- 100	208
A.11	Typical Load-Displacement curves for Specimens BG-200	209

A.12	Typical Load-Displacement curves for Specimens BN-40 and HBN 40	209
A.13	Typical Load-Displacement curves for Specimens BN-100 and HBN- 100	210
A.14	Typical Load-Displacement curves for Specimens BN-200	211

CHAPTER 1

INTRODUCTION

1.1 General

Hydro-electric transmission structures are traditionally built primarily of hot-rolled angle sections of various sizes. Angles are advantageous for both main legs and web members due to the simplicity of bolting members directly together without the use of gusset plates. Simplified fabrication and erection procedures help to reduce overall structure cost.

Cold-formed angles are becoming more popular as replacements for hot-rolled angles, especially in the smaller angle sizes. In addition to conventional 90° angles, a wide range of shapes can be produced, in sizes to suit individual project requirements. In particular, cold-forming can be used to provide stiffening lips to prevent local buckling of thin, wide elements, to optimize shapes so that longer unbraced lengths can be used, and to create shapes such as 60° angles for triangular towers.

By using stiffened edges, the designer is able to increase the width of thin sections without reductions for local buckling. Wider elements can lead to an increase in the sections' moment of inertia and to a decrease in a members' slenderness. This allows the use of longer unbraced lengths and reduces the number of bracing members and connections. As a result, cost savings can be realized through

reductions in the required weight of steel. Savings may also arise due to decreased fabrication requirements, and reduced labour costs in tower erection, since a reduction in the number of members, and bolted connections simplifies the tower construction. In addition, the lips are beneficial in improving resistance to damage in shipping and handling.

Lips have the disadvantage of preventing the nesting of sections, thus requiring more volume in shipping. The lips also make connections to the inside of the leg difficult compared to a plain angle which can be easily connected on either side of the leg.

Creating shapes such as the 60° angle to suit special applications, can simplify fabrication details. In the case of triangular towers, the bracing members intersect at 60° and cannot be bolted directly to a plain angle without using additional gusset plates; however they can bolt directly to a 60° angle leg member. The 60° angle offers another benefit in that it increases the minimum radius of gyration relative to a 90° angle, thereby increasing the flexural buckling strength. The 60° angle has the disadvantage of a reduced torsional-flexural buckling strength.

Web members in a tower are most commonly connected to legs members by simply bolting through one leg. This is advantageous in simplifying construction and fabrication, however it results in eccentricity of load in the web member. The eccentricity reduces the axial load capacity, and must therefore be accounted for in

design. At the same time, the bolted connection provides some rotational restraint to the web member, thus increasing the capacity. This benefit can be accounted for to avoid excessively conservative designs.

A number of cold-formed shapes suitable for transmission tower construction are examined in this project. Experimental work was performed to determine the axial load capacity of these shapes.

1.2 Objectives

The main objective of the research work was to determine the axial load capacity of five different cold-formed steel sections suitable for transmission tower construction.

The test results were compared to design capacities calculated using: Canadian Standards CAN/CSA-S136-M89 Cold-Formed Steel Structural Members (CSA 1989), henceforth referred to as CSA-S136, CAN/CSA-S37-M86 Antennas, Towers, and Antenna Supporting Structures (CSA 1986) henceforth referred to as CSA-S37, ASCE Manual 52 Guide for Design of Steel Transmission Towers (ASCE 1988) henceforth referred to as Manual 52, and ECCS Recommendations for Angles in Transmission Towers (European Convention for Constructional Steelwork 1985) henceforth referred to as the ECCS Recommendations.

1.3 Scope

The scope of the project included the testing of 189 cold-formed members. There were four main parameters:

- (1) Shape
- (2) Steel Grade
- (3) Slenderness ratio
- (4) Temperature

Table 1.1 summarizes the test program and indicates the number of tests performed for each parameter. Each of these parameters is discussed below.

Five different shapes were investigated:

- 1) BA: Plain 90° angle.
- 2) BB: Lipped 90° angle.
- 3) BC: 60° angle.
- 4) BG: T-Shape.
- 5) BN: Back-to-Back Lipped Channels.

Each shape was produced from two different types of steel. The first type, supplied by SAE Towers of Milano, Italy, was A715 Grade 60 with a specified yield strength of 415 MPa. The second type was G40.21-300W and was selected in order to represent a grade which is readily available in Canada.

Each shape was fabricated in three lengths in order to represent a wide range of slenderness ratios. The lengths were selected to correspond to slenderness ratios of approximately 40, 100, and 200. The exact slenderness ratios varied, so the values shown in Table 1.1 are referred to as the "nominal slenderness ratios".

Specimens produced from the first steel type (A715) were tested at three temperature levels; -50°C , 0°C , and room temperature (approximately 20 to 23°C). The second set of specimens (G40.21 steel) were tested at -50°C , and room temperature only. These are the specimens designated as HBA, HBB, HBC, HBN. The longest specimens, designated as BG-200, and BN-200 were only tested at room temperature.

Three separate test setups were required to accommodate the variety of shapes and lengths. In addition, a large refrigeration unit was designed and built for the tests.

Material tests were also performed in a separate project (Polyzois et al 1994). project, dealing specifically with material tests. The results of these material tests are referred to in this work. All measured yield strength values are based on these material tests.

CHAPTER 2

LITERATURE REVIEW

2.1 General

The design and construction of steel transmission towers has evolved over the past century from the simple use of windmill towers modified to carry wires, to, as an extreme example, towers over 700 ft. high, spanning 12000 ft. across the Messina Straits between Sicily and the Italian mainland (Bergstrom et al.).

Transmission tower design differs from normal individual building design in that a typical transmission line of considerable length makes use of the same tower many times over. As a result of this repetition, there is room for significant cost savings by attempting to achieve the utmost economy consistent with adequate safety. Since transmission towers differ from typical structures, special standards have been developed to provide specific guidance to tower designers. Considerable research has been conducted in the area of transmission tower design and construction. The majority of the research relates to plain, hot-rolled angles since these are the most commonly used. The use of cold-formed steel is also generating new areas of research. In this chapter some of the literature related to transmission towers will be reviewed, and some specific design guidelines which are available to the engineer involved in transmission tower design will be examined.

Kravitz (1982) prepared a review of the state of the art and practice of transmission line tower design. Topics covered included loading combinations, analysis procedures, and member design using the ASCE Manual 52. In this reference comments on the design criteria in the manual are given and recommendations regarding future research and testing are made.

The work by Kravitz was extended by Cannon (1989), who conducted a worldwide survey of tower analysis and design methods. In this survey, Cannon obtained information from various tower designers regarding the predicted member forces and member strengths of two full scale experimental tower tests. He found considerable variation in the predictions from country to country, company to company, and designer to designer. ASCE Manual 52 was the choice of 60% of the participants in this survey and was the most commonly referenced design guide. There was also variation in the information supplied between participants who utilized the recommendations of Manual 52. Cannon concludes that a major factor in the design of transmission towers is the professional experience and judgement of designers.

A brief summary of the relevant literature which was found to be useful in the study is given below.

Marsh (1969) conducted tests on small aluminum angles. The test setup consisted of angles loaded eccentrically by bolting through one leg with one or two bolts. The test specimens were bolted to larger angles which resembled chord members in a truss assembly. The use of two bolts was found to increase the member capacity when compared to the capacity of sections connected with only one bolt. An expression was developed which combined the effects of flexure about the weak axis and twisting. This expression was later incorporated in Canadian Standard S136-M89.

Adhuri and Madugula (1991) discussed the concept of schifflerization of 90° angles to form 60° angles. The similarities and differences between 60° and 90° angles were presented. The current design practices in Canada were discussed, and the limitations of the commonly used design standard CAN/CSA-S37-M86 were also examined. The process of bending the angle legs from 90° to 60° was found to increase the minimum moment of inertia by approximately 20% to 50%. At the same time, there is a decrease in the maximum moment of inertia by a similar amount. The shear centre was also found to move slightly away from the intersection of the legs, resulting in an increase in the warping constant C_w . Overall, the 60° angles were found to be stronger in flexural buckling, and weaker in torsional-flexural buckling when compared to a 90° angle. Due to the decreased torsional-flexural buckling strength, 60° angles could be subject to torsional flexural buckling at longer lengths than similar sized 90° angles. In the design of 60° angles

according to the CSA-S37-M86 standard, the effect of torsional-flexural buckling is not included. The authors intended to bring this to the attention of engineers involved in tower design. In order to account for torsional flexural-buckling properly, the authors proposed a modification to the existing design method used in CSA-S37. Load capacity tables were presented for typical angle sizes and lengths, where factored capacities according to the existing method and the proposed method were compared. The authors also provided a number of expressions for calculating the geometric properties of 60° angles.

Adluri, Madugula, and Monforton (1992) reported on the results of tests performed on 18 concentrically loaded, schifflerized angles. Test results were compared to predicted loads using the ASCE Manual 52 and AISC-LRFD specifications (1986). In the paper the authors pointed out that there is a lack of published information on the strength and behaviour of schifflerized angles. Emphasis was placed on determining the appropriate width to be used in calculating the w/t ratio. The AISC-LRFD (1986) specification, which accounts for torsional-flexural buckling, was found to provide results which were in good agreement with the test results. The ASCE Manual 52, which is more commonly used in the design of lattice towers, does not specifically account for torsional-flexural buckling. The results provided by Manual 52 overestimated test results which were governed by torsional-flexural buckling. The authors proposed two modifications to the methods used by Manual 52 for predicting more accurately the capacity of schifflerized angles. The first

method proposed involved the use of the entire leg width in w/t calculations. The second method, which was considered more rational by the authors, was to use the width of the bent portion of the leg in the calculation of w/t . In addition, in the second method the values of both the flexural and the equivalent torsional-flexural radii of gyration for the member are calculated and the minimum of the two radii is used to compute the slenderness ratio.

Bathon et al (1993) tested 75 equal and unequal leg hot rolled angles under eccentric loads. The specimens were bolted to gusset plates through one leg. The gusset plates were attached to ball and socket supports lubricated with high pressure grease in order to ensure that no rotational restraint was provided by the support. The experimental results were compared to predicted loads using ASCE Manual 52. It was found that the predicted failure loads were generally higher than the experimental loads. However, the authors also referred to full-scale tower test results which showed that the capacity was 2% to 10% higher than that predicted by the ASCE Manual 52. The authors concluded that the design of towers may be safely performed using the ASCE Manual 52, but that close attention should be paid to the provisions limiting the eccentricity of applied load.

A small number of papers dealing specifically with cold-formed steel sections have also been published. These are presented below:

Madugula, Prabhu, and Temple (1983) tested 16 concentrically loaded cold-formed angles with slenderness ratios ranging from 90 to 250. The magnitude and distribution of residual stresses were also investigated. A finite element program was also developed to predict the failure loads, taking into account initial out-of-straightness. Failure loads were compared to results obtained from ASCE Manual 52 (1971), AISI specification (1980), CSA-S136 (1974), and the ECCS Recommendations (1976). The ECCS Recommendations were found to be conservative for most cases, whereas the results obtained from ASCE Manual 52, the AISI specifications, and CSA-S136-1974 were found to be slightly unconservative. The maximum residual stress was found to be approximately 30% of the yield stress. The magnitude and distribution of the residual stresses was found to be similar to that observed in hot-rolled angles.

Madugula and Ray (1984) tested 24 equal and unequal leg cold-formed angles under eccentric loads. In contrast to the tests performed by Bathon, these specimens were tested in a setup designed to simulate one panel of one face of a latticed tower. This setup therefore provided some degree of fixity to the ends of the specimens. Three slenderness ratios were examined, 80, 120, and 170. Specimens were bolted at the ends through one leg, with either one, two, or three bolts. The objectives of the investigation were to study the following: the effect of the number of bolts in the end connections, the difference in strength of unequal leg angles with long leg connected and with long leg out, the effect of the assumed location of the shear centre, and the effect of the magnitude of warping constant used. Test results were

compared to loads computed from the general theory of torsional-flexural buckling, the ASCE Manual 52, and the ECCS Recommendations. It was found that failure loads computed according to the ECCS Recommendations were generally conservative. For specimens with slenderness ratios less than 120 that were connected with only one bolt, the ASCE Manual 52 predicted failure loads higher than the experimental failure loads. For specimens with slenderness ratios less than 120 which were connected by two or three bolts and for specimens with slenderness ratios exceeding 120, the experimental failure loads were in good agreement with the loads computed according to the ASCE Manual 52. The strength of the members was found to increase when the number of bolts in the end connection was increased. Unequal leg angles were found to carry higher loads when the long leg was unconnected. The authors also concluded that the exact location of the shear centre, and magnitude of the warping constant have an insignificant effect on the predicted failure loads.

Faggiano (1985) discussed the design philosophy of cold-formed steel towers, as related to the potential member shapes, and tower configurations. Areas of potential cost savings were highlighted and some limitations were addressed in the reference. Some difficulties associated with cold-formed steel member detailing were also examined.

Gaylord and Wilhoite (1985) provided recommendations for the design of plain and lipped cold-formed angles used in transmission towers. The reference was of considerable interest to other researchers in the field as evidenced by the discussion given by Bryant M.E, Marsh C., Ray S.K., and Madugula K.S. The methods provided allow the designer to use the same criteria used for the design of hot-rolled angles in transmission towers, as outlined in ASCE Manual 52. The authors verified their recommendations through comparison with test results from four different sources. The sources of test data included: Chajes, Fang, Pen, and Winter (1966), Madugula, Prabhu, and Temple (1983), Technologic Papers of the Bureau of Standards No. 218 Department of Commerce (1922), as well as unpublished data.

The effect of temperature and galvanization on the compressive strength of cold-formed angles was studied by Polyzois et al (1990). The study involved the testing of 10 galvanized and 10 ungalvanized cold-formed steel angles with a slenderness ratio of 70. Tests were performed at temperatures ranging from -45 to 25° C. Angles were attached to gusset plates by bolting through one leg. In addition, 48 standard tension coupon tests were conducted at various temperatures. Several observations were made by the authors, as summarized below. The capacity of angles tested at -45° C was approximately 8% higher than the capacity at room temperature. Similar results were found for tension coupon tests. Corner coupons were found to have yield strength ranging from 13% to 27% higher than the yield strength of flat coupons. Galvanized angles were found to have ultimate

compressive resistances 9% higher than ungalvanized angles. Ultimate predicted loads were calculated using Canadian standard S136, and the American specification (AISI 1986). When the angles were treated as beam columns, it was found that the predicted loads were very conservative. The ultimate test results were approximately 2.6 times higher than the predicted loads.

While the above papers dealt primarily with angle shaped members, cold-formed shapes other than angles have also been investigated as alternatives for transmission tower construction. Zavelani and Faggiano (1985) provided recommendations for the design of cold-formed latticed transmission towers using shapes other than angles. Their recommendations were based on the AISI Specification for the design of cold-formed members, and on test experience. Recommendations regarding items such as galvanizing, tolerances, and connections were also provided. In addition, several experimental testing programs which demonstrated the validity of the recommendations were reviewed in the reference. These included the work by: Carpena who carried out a series of tests on open 60° lipped and unlipped channel at the SAE Test Station (Italy) in 1964. The test setup consisted of a triangular tower configuration, with the channels acting as the leg members. Horizontal loading was applied at the top of the tower in order to induce compression in the channels. The work of Fang who investigated torsional-flexural buckling of cold-formed thin-walled columns in 1966 at Cornell University is also cited. In Fang's work specimens were loaded concentrically with fixed end supports, and columns

were tested both in the elastic and inelastic range. An interaction equation which combined twisting and bending was established. W-shaped post angles for use in triangular towers were investigated by Cauzillo (1976). Specimens were tested with flanged ends, and spherical supports. An experimental line was built using triangular towers with W-shaped posts based on the results of the test program. Casarico, Catenacci, and Faggiano investigated the use of back-to-back lipped channels, and lipped T-shapes (1981). Two experimental 500kV towers were built at the SAE research centre. Tests confirmed the validity of the design criteria based on the AISI specifications. Tests on T-shaped specimens were performed by Wilhoite, Zandonini, and Zavelani (1984) at the Technical University of Milan. The specimens were subjected to both concentric and eccentric loads, and were loaded by bolting to gusset plates with ball bearing headings at each end.

Four experimental cold-formed steel towers were constructed by the American Electric Power Research Institute (AEPRI) at their testing station near Fort Worth Texas. The towers utilized various shapes, including 90° angles, 60° angles, T-shapes, back-to-back lipped channels, and W-shapes. Catenacci, Finzi, and Rossi (1989) reported on the design of these towers, and compared the towers to similar configurations designed using hot-rolled angles. The authors also refer to some similar work performed in Italy (SAE and ENEL). The four experimental towers were found to have significant reductions in the total tower weight, and in the number of members, plates, and bolts. These reductions were said to result in

reductions in fabrication, packaging, transportation, and erection costs. The authors conclude that these towers demonstrate that the use of cold-formed members in electrical transmission towers is feasible, reliable, and economical.

An extensive literature review relating to hot-rolled and cold-formed angles was prepared by Kennedy and Madugula (1982). The review included theoretical analyses for flexural, torsional-flexural, and plate buckling of angles, experimental investigations, and design practices in North America and Europe. The authors also made a number of recommendations for further research.

In the following section the various codes of practice which were utilized in order to analyze the test specimens are reviewed.

2.2 Canadian Standard CAN/CSA-S136-M89 Cold-Formed Steel Structural Members

The basic column curve adopted by CSA-S136 consists of the Euler buckling curve at stresses below $0.5 F_y$, and an approximation to a tangent modulus curve at stresses above $0.5 F_y$. The curve is specified in Clause 6.6.1.3 as follows:

When $F_p > F_y/2$

$$F_a = F_y - \frac{(F_y)^2}{4F_p}$$

When $F_p \leq F_y/2$

$$F_a = F_p$$

Where

F_y = Yield stress in Mpa, and

F_p = least value of elastic buckling stress for Euler-flexural, torsional, torsional-flexural buckling (given in MPa), as specified by Clauses 6.6.2, 6.6.3, 6.6.7, and 6.7.4, all of which are defined below.

The compressive resistance of the section is determined as:

$$C_r = \phi_a A_e F_a$$

Where

F_a is defined above

A_e = effective cross sectional area determined from Clause 5.6.2 using the stress level = F_a (which may be less than the gross area).

ϕ_a = 0.9 for doubly symmetric sections

= 0.75 for singly symmetric sections

The above provisions are limited to sections 4.5 mm or less in thickness. For sections greater than 4.5 mm the axial stress is computed according to CSA Standard S16.1.

Flexural Buckling

The critical flexural buckling stress is given by Clause 6.6.2

$$F_p = 0.833 F_e$$

where

$$F_e = \pi^2 E / (KL/r)^2$$

$$KL/r = \text{Maximum effective slenderness ratio}$$

$$K = \text{Effective length factor}$$

$$r = \text{radius of gyration of fully effective area about the principal axes}$$

The above expression is modified by Clause 6.6.7 for built up sections connected at discrete points. The sections have a reduced shear rigidity compared to sections which are continuously joined. The critical stress is modified by combining the member slenderness with the slenderness of an individual component between points of connection. A modified slenderness ratio is thus created by combining the two ratios.

$$F_p = 0.833 F_e$$

where

$$F_e = \frac{\pi^2 E}{(KL/r)^2 + (a/r_1)^2}$$

KL/r = overall slenderness of the built-up section

a = spacing of fasteners between components

r_1 = radius of gyration of individual section

Torsional and Torsional-flexural Buckling Clause 6.6.3.1

The critical buckling stress is given as the lesser of the reduced flexural buckling stress F_p defined above, or the reduced torsional flexural buckling stress given by

$$F_p = 0.833 F_{st}$$

where

$$F_{st} = \frac{1}{2} \beta [F_s + F_t - \sqrt{(F_s + F_t)^2 - 4\beta F_s F_t}]$$

$$F_s = \pi^2 E / (KL/r)^2$$

$$F_t = \frac{1}{A(r_o)^2} [GJ + \frac{\pi^2 EC_w}{(K_t L_t)^2}]$$

$$\beta = 1 - (x_o/r_o)^2$$

$$r_o = \sqrt{(r_x)^2 + (r_y)^2 + (x_o)^2}$$

A = fully effective area of member

r_x, r_y = radii of gyration of fully effective area about centroidal principal axes

K_t = effective length factor for torsional buckling

L_t = unsupported length for twisting

- x_o = distance between shear centre and centroid
 KL/r = effective slenderness ratio for bending about the axis of symmetry
 J = St. Venant's torsion constant

Local Buckling

The stress on sections with unstiffened flanges is further limited by the local buckling limit imposed by Clause 6.6.3.2

$$C_r = \frac{\phi_a k \pi^2 EA}{12(1-\mu^2)W^2}$$

where

- ϕ_a = 0.9
 k = 0.43
 A = fully effective section area
 W = flat width ratio of unstiffened flange

Single Angles Loaded Through One Leg Clause 6.7.4

Angles loaded eccentrically through one leg fail by combined bending about the weak axis and twisting. An equivalent slenderness ratio which combines the modes of buckling. The reduced elastic buckling stress is given as

$$F_p = \frac{0.833\pi^2 E}{[(KL/r_y)^2 + (5b/t)^2]}$$

where

- L** = unbraced length of the member
- r_v** = least radius of gyration of the fully effective area
- b** = flat width of the leg
- t** = leg thickness
- K** = effective length factor depending on the connection
- = 0.7 for translation fixed connections with two or more bolts or welds
- = 0.8 for translation fixed connections with a single bolt

The compressive resistance is given by Clause 6.6.1.3 using $\phi = 0.75$, but is limited to $0.5AF_y$ for single bolted members, and $0.67AF_y$ for members connected by welds or two or more bolts.

Effective Areas

Clause 5.6.2 of the Standard specifies flat width limits beyond which a section's full area is not effective. The basic flat width thickness limit is given as

$$W_{\text{lim}} = 0.644\sqrt{kE/f}$$

When the limit is exceeded the reduced effective width is given by

$$B = 0.95\sqrt{kE/f} \left[1 - \frac{0.208}{W}\sqrt{kE/f} \right]$$

where k and W depend on the section shape and loading conditions and are specified in detail in the standard, but will not be presented here. The value of f is the calculated stress in the effective element.

2.3 CAN/CSA-S37-M86 Antennas, Towers, and Antenna-Supporting Structures

Both the CSA-S37 and CSA-S136 standards are based on limit states design principles which requires that the effect of factored loads must not exceed the factored load resistance. The CSA-S37 standard allows cold formed steel angles to be used as substitutes for hot rolled angles, but limits such angles to leg dimensions of 55 mm or less. Although the sections used in the experimental investigation exceeded this limit, the standard will still be examined.

According to the CSA-S37 standard, member resistances are based on the Canadian standard CSA/CAN-S16.1-M84 Steel Structures for Buildings. This standard is primarily intended for hot-rolled steel products. The basic axial stress is defined in terms of the dimensionless parameter λ defined as

$$\lambda = \frac{KL}{r} \sqrt{\frac{F_y}{\pi^2 E}}$$

The axial resistance is given by S16.1 Clause 13.3 as

$$C_r = \phi A F_y \quad \text{for } 0 < \lambda \leq 0.15$$

$$C_r = \phi A F_y (1.035 - 0.202\lambda - 0.222\lambda^2) \quad \text{for } .15 < \lambda \leq 1.0$$

$$C_r = \phi A F_y (-0.111 + 0.636/\lambda + .087/\lambda^2) \quad \text{for } 1.0 < \lambda \leq 2.0$$

$$C_r = \phi A F_y (0.009 + 0.877/\lambda) \quad \text{for } 2.0 < \lambda \leq 3.6$$

$$C_r = \phi A F_y / \lambda^2 \quad \text{for } 2.0 < \lambda \leq 3.6$$

The values of K , and ϕ depend on the member type, slenderness, and connection type. For concentrically loaded leg members with maximum effective slenderness less than 120, Clause 6.2 specifies $K=1.0$, and $\phi=0.9$.

Clause 6.2.4 provides recommendations for web members loaded through one leg only. For members connected with two or more bolts (or equivalent in welding) the standard neglects the eccentricity, and specifies $K=0.9$. The resistance factor depends on the slenderness, i.e., for $KL/r > 120$ $\phi=0.9$, and for $KL/r < 120$ $\phi=0.72$. The factored resistance below $KL/r = 120$ need not be less than the resistance at $KL/r = 120$ with $\phi=0.9$.

When members are connected with only one bolt the member is still treated as an axially loaded member except that no restraint is considered, and $K = 1.0$. The resistance factor is set at 0.72 for all slenderness ratios. (Clause 6.2.4.3)

From the above discussion it can be seen that the CSA-S37 standard recognizes the end restraint provided by multiple bolt connections by specifying K . The effect of eccentricity is accounted for by simply reducing the resistance factor.

As mentioned, Standard S37 bases the axial resistance on the provisions of Standard S16.1, which limits the width to thickness ratio of angle legs to $200/\sqrt{F_y}$. For sections exceeding this limit S16.1 refers to the cold formed steel standard CSA-S136. In order to make the CSA-S37 standard more comprehensive, this limit was modified to account for sections which may be subject to local buckling. Amendment No. 12 (September 1992) was issued in order to account for local buckling. A reduced effective yield stress is used when width-to-thickness ratios exceed $200/\sqrt{F_y}$. The effective stress is calculated as follows:

$$200/\sqrt{F_y} < w/t \leq 380/\sqrt{F_y}$$

$$F_y = F_y \left[1.677 - .677 \frac{w/t}{200/\sqrt{F_y}} \right]$$

$$\text{for } 380/\sqrt{F_y} < w/t \leq 25$$

$$F_y = 56415 / (w/t)^2$$

For cold formed 90° angles w is taken as the lesser of the flat width or the total leg width less $3t$. For schifflerized 60° angles the standard specifies w as the flat width to the bend line; but does not specifically refer to cold-formed 60° angles.

The calculated value of reduced effective yield stress is substituted for the yield stress F_y in the calculation of the compressive resistance.

This simple method of accounting for local buckling by reducing the effective yield stress contrasts with the more involved method of the CSA-S136 standard which reduces the effective area of the section to account for local buckling.

2.4 ASCE Manual 52 Guide For Design of Steel Transmission Towers

Developed by the American Society of Civil Engineers, this manual serves as a major source of information for transmission tower design. Whereas the previous two standards are based on limit states design, the ASCE Manual 52 utilizes the ultimate strength design. In the ultimate strength design, the specified loads are multiplied by overload capacity factors depending on the loading type, and members are designed to approach failure at these loads. In contrast to limit states design, no performance factors are applied to the member resistance. ASCE committees are currently studying the feasibility of revising the recommendations to incorporate load and resistance factor design principles.

Allowable Compression (Section 4.6)

Section 4.6 of the manual specifies the following allowable compression stress (in imperial units)

$$F_a = \left[1 - \frac{1}{2} \left(\frac{KL/r}{C_c}\right)^2\right] F_y \quad \text{For } \frac{KL}{r} \leq C_c$$

$$F_a = \frac{286000}{\left(\frac{KL}{r}\right)^2}$$

$$\text{For } \frac{KL}{r} \geq C_c$$

$$C_c = \pi \sqrt{\frac{2E}{F_y}}$$

Where F_y = yield stress (ksi), E = modulus of elasticity = 29000 ksi, KL = effective length (in.), and r = radius of gyration (in.).

Angles

The Manual is limited for use to angles with b/t ratios less than 25. A reduced effective yield stress is calculated when the flat width ratio exceeds $(w/t)_{\text{lim}} = 80/\sqrt{F_y}$.

$$F_{\text{crit}} = \left[1.677 - 0.677 \frac{w/t}{(w/t)_{\text{lim}}}\right] F_y \quad \left(\frac{w}{t}\right)_{\text{lim}} \leq \frac{w}{t} \leq \frac{144}{\sqrt{F_y}}$$

$$F_{\text{cr}} = \frac{9500}{(w/t)^2} \quad \frac{144}{\sqrt{F_y}} \leq \frac{w}{t}$$

The effect of the reduced local buckling strength on flexural buckling strength is accounted for by substituting the reduced effective yield stress for F_y in the equations from section 4.6 listed above.

Section 4.7 of the Manual provides modified effective length formulas to account for eccentricity and end restraint on angles members.

For members with a concentric load at each end:

$$\frac{KL}{r} = \frac{L}{r} \quad 0 \leq \frac{L}{r} \leq 120$$

For members with a concentric load at one end and normal framing eccentricity at the other end of the unsupported panel:

$$\frac{KL}{r} = 30 + 0.75 \frac{L}{r} \quad 0 \leq \frac{L}{r} \leq 120$$

For members with normal framing eccentricities at each end:

$$\frac{KL}{r} = 60 + 0.5 \frac{L}{r} \quad 0 \leq \frac{L}{r} \leq 120$$

For members unrestrained against rotation at both ends:

$$\frac{KL}{r} = \frac{L}{r} \quad 120 \leq \frac{L}{r} \leq 200$$

For members partially restrained against rotation at one end:

$$\frac{KL}{r} = 28.6 + 0.762 \frac{L}{r} \quad 120 \leq \frac{L}{r} \leq 225$$

For members partially restrained against rotation at each end:

$$\frac{KL}{r} = 46.2 + 0.615 \frac{L}{r} \quad 120 \leq \frac{L}{r} \leq 250$$

For members unrestrained against rotation at both ends:

$$\frac{KL}{r} - \frac{L}{r} \quad 120 \leq \frac{L}{r} \leq 200$$

The manual limits maximum modified effective lengths to $KL/r \leq 150$ for leg members, $KL/r \leq 200$ for other compression members, and $KL/r \leq 250$ for redundant members. Members connected with only one bolt are not considered to be restrained against rotation, whereas members connected with two or more bolts are considered partially restrained if the connection is to a member capable of resisting rotation of the joint.

Lipped Angles

The w/t limits and reduced effective yield stress defined for plain angles do not apply to lipped angles since the local buckling strength is increased by the lips. The ratio w/t for the leg shall not exceed 60. The Manual neglects lateral torsional buckling for the plain angle, and only considers flexural and local buckling. Lateral torsional buckling must be considered for the lipped angle since it is no longer very close in value to the local buckling strength. An equivalent radius of gyration for torsional and flexural buckling is given in Section 4.8 as

$$\frac{2}{r_{tf}^2} - \frac{1}{r_t^2} + \frac{1}{r_u^2} + \sqrt{\left(\frac{1}{r_t^2} - \frac{1}{r_u^2}\right)^2 + 4\left(\frac{u_o}{r_{tf} r_u r_{ps}}\right)^2}$$

$$r_t = \sqrt{\frac{C_w + 0.04J(K_t L)^2}{I_{ps}}}$$

where

r_{tf} = equivalent torsional flexural radius of gyration

C_w = warping constant

J = St. Venant torsion constant

$K_t L$ = effective length for warping

I_{ps} = polar moment of inertia = $I_u + I_z + Au_o^2$

u_o = distance between shear centre and centroid

I_u = moment of inertia about axis symmetry

I_z = moment of inertia about non-symmetrical axis

The axial stress is provided by section 4.6 using the larger of KL/r_z or KL/r_{tf} . The effective length formulas of Section 4.7 may be applied to lipped angles, but K_t listed above must be then be set equal to 1.0. If the width-to-thickness ratio w/t of the leg exceeds $220/\sqrt{F_y}$ then the axial stress acts over a reduced effective area, calculated according to section 4.5 of the manual.

For lips at 90° to the leg the minimum required depth is specified in section 4.8.4 as:

$$d = 2.8t \left[\left(\frac{w}{t} \right)^2 - \frac{4000}{F_y} \right]^{\frac{1}{6}} \geq 4.8t$$

For sections other than plain angles, the manual provides formulas for calculating effective widths when flat widths exceed the limits for stiffened or unstiffened elements.

Doubly-Symmetric Sections (section 4.9.4)

The manual requires that doubly symmetric sections be designed for flexural buckling using section 4.6, and for torsional buckling using the radius of gyration r_t defined above.

Singly Symmetric Sections (section 4.9.5)

In addition to flexural buckling about the axis of symmetry, torsional flexural buckling should be checked using the equivalent radius of gyration r_{tf} as provided for lipped angles above.

2.5 ECCS Recommendations for Angles in Lattice Transmission Towers

The effect of local and torsional buckling on the overall buckling strength of members is accounted for by calculating a reduced effective yield stress when flat width ratios exceed the specified limits. The approach taken is similar to ASCE Manual 52, and CSA-S37, but differs in that the reductions differentiate between cold formed and hot rolled angles. Two reasons are given treating the angles differently:

- Cold formed angles have a smaller torsional stiffness than hot rolled angles due to the lack of a heel and fillet.
- Cold formed angles have an increased yield strength at the corners due to the strain hardening caused by bending.

The effect of these factors is to reduce the buckling strength of cold formed angles with low b/t ratios and low slenderness compared to hot rolled angles. At higher b/t and L/r ratios the increased yield at the corners offsets the lack of a heel, and the two types of angles are treated the same. The limits and reduction formulas for the cold formed angle are given by

$$\left(\frac{b}{t}\right)_{\text{lim}} = 0.503 \sqrt{\frac{E}{\sigma_r}}$$

$$\bar{\sigma} = \sigma_r \left[\frac{5}{3} - \frac{2}{3} \frac{b/t}{(b/t)_{\lim}} \right] \quad \text{for } \left(\frac{b}{t} \right)_{\lim} < \frac{b}{t} < \frac{3}{2} \left(\frac{b}{t} \right)_{\lim}$$

$$\bar{\sigma} = \frac{\pi^2 E}{(5.1 \frac{b}{t})^2} \quad \text{for } \left(\frac{b}{t} \right) > \frac{3}{2} \left(\frac{b}{t} \right)_{\lim}$$

where

$\bar{\sigma}$ = reduced effective yield stress

σ_r = yield stress (MPa)

E = modulus of elasticity, taken as 210000 MPa

Note that b is taken as the full leg width for these formulas, and not the flat width.

A basic non-dimensional column curve "a₀" is adopted from the European Convention for Constructional Steelwork. The curve is summarized in table format in the ECCS Recommendations for Angles. This curve is used as the basis for design of concentrically loaded leg members. Eccentrically loaded web members are designed using the same basic column curve by modifying the members slenderness to take into account end fixity, and eccentricity. This basic approach is very similar to that taken by ASCE Manual 52. The ECCS approach is slightly different in that it differentiates between which axis the buckling occurs about. Different slenderness modifications are specified for buckling about the minor principle axis, and buckling about geometric axes. The mode of buckling is determined by the bracing

configuration. The correction formulas listed below apply to the specimens tested in this research program, based on the following conditions:

- eccentricity at both ends
- buckling about the v-v axis (minor principal axis)
- discontinuous members with 2 bolts at each end
- discontinuous members with single bolts at each end.

For $\Lambda \leq \sqrt{2}$

$$\bar{\Lambda} = 0.5 + 0.6464\Lambda \quad \text{for 2 bolts at end}$$

For $\Lambda > \sqrt{2}$

$$\bar{\Lambda} = 0.5 + 0.6464\Lambda \quad \text{for 2 bolts at end}$$

$$\bar{\Lambda} = \Lambda \quad \text{for single bolts at ends}$$

Where Λ = non dimensional slenderness ratio

$$\Lambda = \frac{\lambda}{(\pi \sqrt{E/\sigma})}$$

and λ = slenderness ratio - L/r_v

In these expressions it is implied that for non-dimensional slenderness ratios below $\Lambda = \sqrt{2}$ the eccentricity reduces the allowable load. For $\Lambda > \sqrt{2}$ the restraint provided by a 2 bolt connection offsets the eccentricity and the allowable axial load may be increased relative to an axially loaded pin ended member. Once the modified non-dimensional slenderness ratio is evaluated, the value of allowable stress is determined using the tables provided in the appendix of the ECCS Recommendations.

The tables provide the ratio of the buckling stress to the reduced effective yield stress as follows:

$$N = \frac{\sigma_{ult}}{\sigma}$$

CHAPTER 3

EXPERIMENTAL PROGRAM

3.1 Introduction

The objective of the program was to determine the axial load capacity of various cold-formed steel shapes used in the construction of lattice transmission towers. The experimental investigation included the scheduled testing of 189 galvanized, cold-formed steel sections under a variety of parameters. There were 5 extra specimens tested under the same parameters. Finally, a total of 7 additional specimens were tested in order to investigate a revised end connection condition. In this chapter, the test specimens, test setups, and test procedures are discussed.

3.2 Specimens

SAE Towers of Milano, Italy supplied 129 of the specimens used in the investigation. These specimens were identified as BA, BB, BC, BG, AND BN. Additional tests were performed on specimens fabricated locally, using a steel which is more commonly used in Canada as an alternative to the A715 steel. The additional specimens are identified as HBA, HBB, HBC, and HBN. The second series of specimen was identical to the first one with the exception of the T-shaped BG specimen could not be produced to acceptable tolerances.

All the specimens used in this test program were hot-dip galvanized by the fabricators (or their subcontractors) prior to delivery to us.

The following specimen designation system was used in this investigation:

(H)BA-40-1

The first letter, H is used to identify the second set of specimens which were made of a G40.21 steel, and is only indicated on these shapes. The second two letters refer to the specimen shape as follows: BA for plain angles, BB for lipped angles, BC for 60° angles, BG for T-shaped sections, and BN for back-to-back channels. Figures 3.1 to 3.5 illustrate the shapes. The first number, 40 in this example, refers to the nominal slenderness ratio of the specimen, and is either 40, 100, or 200. The last number refers to the individual specimen identification within each shape and slenderness group. Under this system, each specimen has a unique identifying number.

To simulate actual tower conditions, bolted connections were used for load application. Ideally these bolt holes would be punched by the fabricator prior to forming and galvanizing. However, under the specimen procurement and project scheduling conditions, this option was not possible. Therefore all bolt holes were drilled in the lab. The bolt diameter of 5/8" required 11/16" holes. This size of hole required that small pilot holes be drilled first, before drilling to the final size. Approximately 1500 holes were required. The BN and HBN specimens were to be

bolted back-to-back with 1/2" spacer plates. The specimens were connected at approximately the 1/4, 1/2, and 3/4 length points with two 3/8" diameter bolts. The connection design for each specimen was based on preliminary load capacity calculations. The number of bolts used to connect each specimen decreased as the predicted capacity decreased for each different shape and slenderness ratio. Only as many bolts as required by design were used in the connections.

3.3 Test Setup and Procedure

Due to the very large number of samples, and variation in length (from 552 mm to 8245 mm) three separate test setups were required to perform the tests. Each setup and procedure will be discussed separately.

3.3.1 Test Setup No. 1

The first setup made consisted of an existing custom-built cold chamber used in previous investigations. This setup was able to accommodate specimens ranging in length from 552 mm to 1950 mm.

The cold chamber measures 810 by 950 by 2440 mm tall, and has two 200 mm diameter holes through the cooler floor and ceiling to allow for loading. The chamber is equipped with a full height, hinged door for access. The door has a window, and the chamber has an interior light to allow for visual observations during testing. Temperatures of -50°C and 0°C could be achieved. Room temperature tests

were simply performed with the door left open. A steel platform was built in order to support the chamber within the loading machine, to provide a working space for installing the specimens, and to allow for periodic removal of the entire test setup from the loading machine.

A 5000 kN capacity model 810 Closed Loop Testing System Machine was used to apply loads. Loads were applied to the specimen by two 168 mm diameter steel pipes connected to the MTS machine and extended through the holes in the top and bottom of the cooler. The bottom pipe extension is fixed, and the top pipe moves down vertically in order to apply load. Two different top pipes were required in order to accommodate the range in specimen length. Gusset plates were bolted to the ends of the pipes, and the specimens were bolted to the gusset plates. Figure 3.6 illustrates the test setup features described above, and figure 3.20 presents a schematic of the setup.

Due to the large number of tests being performed, it was decided to bolt channel shape extensions to the gusset plates to help prevent damaging the plates. If the channels became damaged during testing they could be easily replaced. The main gusset plate was stiffened at the base to help prevent excessive bending of the vertical plate. Figures 3.7 and 3.23 illustrate the gusset plate setup used. Due to height restrictions within the chamber, the channels had to be removed for testing the (H)BB-100, and (H)BC-100 specimens. All angle specimens were tested by

bolting to the gussets. Seven additional tests were performed by connecting bolting both legs of the angles to the support. This was achieved by simply bolting a clip angle to the main gusset plate, and then bolting the outstanding leg of the specimen to the clip angle. The opposite leg was bolted to the gusset plate.

The BN, HBN, and BG specimens tested in the same setup were also bolted to gusset plates at each end, but in this case the gusset plates were not bolted to the pipe extensions. Instead, these gusset plates had curved bottoms to act as hinges. The specimens were thus free to rotate about the hinges at top and bottom. The hinges were oriented about the weak principal axis of each section.

Figure 3.8 shows the (H)BN gusset plate and hinge. The vertical gusset extends into the 12.7 mm gap between the backs of the channels, an additional plate is then placed on each side of the webs, and the whole connection is secured by six 5/8" diameter bolts. This connection is considered to provide a concentric load condition. A schematic of the connection is given in figure 3.24.

Figures 3.9 and 3.26 show the gusset plate used to connect the BG sections. The vertical gusset plate extends into the gap between the two parallel webs, and three bolts are installed. A clip angle is connected to the section flanges on each side of the vertical gusset, and then the clip angles are bolted to the vertical gusset. Due to its' shape, this section is difficult to connect. Drilling holes at the location of the

centroidal axis was impossible due to interference by the ends of the flanges. By connecting through the web on one side of the centroid, and through the flanges at the opposite side of the centroid it was assumed that centroidal loading was achieved. In practice, of course, a truly concentric load is unlikely to be achieved with a section such as this.

Temperatures in the chamber were controlled by thermostat, and monitored by a thermocouple connected directly to the specimen. In addition, a thermometer was placed near the window to confirm the thermocouple readings. The chamber required approximately 3-4 hours to achieve -50°C , and approximately 1 hour to reach 0°C .

Initially four Linear Variable Transducers (LVDT's) were placed at midheight of the specimens to monitor the twist and lateral deflections. However, at cold temperatures the LVDT's tended to freeze, and using plastic bags to prevent moisture from freezing also seemed to interfere with the free movement of the LVDT's. This problem was solved by using wire extension displacement transducers. These were placed outside of the chamber to prevent freezing, and the wires run in to the cooler using a system of fixed pulleys. Figure 3.10 illustrates how this system was used to monitor the deflection of the extreme points of the specimens.

During loading, the stroke of the MTS piston was monitored and recorded, and the load was measured by a load cell attached to the pipe extension. A Hewlett Packard Data Acquisition System was used to monitor and record the data during testing.

3.3.1.1 Test Procedure

Prior to testing, the specimen dimensions and midlength out of straightness were recorded. The average dimensions for each cross section are given in figures 3.1 to 3.5.

The gusset plates were aligned using a carpenter level, and after the specimens were bolted in place, they were again checked for alignment using the level. The BG and (H)BN specimens were installed by bolting the gusset plates onto the member on the ground, hoisting the specimens in place, aligning with the carpenter level, and then applying a small load (approximately 5 to 10 kN) to hold the specimen in place.

Once, the specimens were in place, the motion transducers were connected to the specimen. The thermocouple lead was connected to the specimen for cold temperature tests, and the chamber door closed and allowed to cool.

Load was applied to the specimen using stroke control on the MTS machine. Stroke was applied gradually at approximately 0.02 mm/second. A typical test required approximately 10 minutes to reach maximum load. Stroke was increased until the measured load peaked and began decreasing.

3.3.2 Test Setup No. 2

The first setup was too small to accommodate the longer specimens, and a second setup had to be designed and built. In designing the second setup it was determined that it was not feasible to accommodate the longest specimens of approximately 8000 mm length. It was therefore decided that the very long specimens would be tested in a third, separate setup at room temperature only. Setup number two had to accommodate specimens ranging in length from about 2000 mm to 4500 mm.

A new custom built chamber was built, measuring 1050 mm wide by 1420 mm deep by 5300 mm high . It has similar features to the first chamber, including 200 mm diameter access holes at the top and bottom for loading, interior lighting, and a window in the door to allow observation. The chamber is different in that economic considerations prevented using a simple hinged access door. Access is provided by a full height removable front panel on the cooler. The door was bolted in place at 4 locations, and clasped at the very top. In order to allow installation by one person, a special support system was designed allowing the door to be lifted with a chain hoist and slid out of the way to provide access inside the chamber.

The entire chamber was built within two 8230 mm tall steel columns which were fixed to a structural floor and acted as the load frame. The top pipe extension into the chamber was connected to cross beams bolted to the tops of the columns. The bottom pipe extension into the chamber rested on top of a load cell and hydraulic

jack which reacted directly against the structural floor. Angle frames were installed at the top and bottom to provide lateral stability to the pipes. The bottom stabilizer frame used teflon pads to allow the pipe to slide up and down freely. An LVDT was placed between the jack and the bottom of the cooler support frame to measure the vertical stroke of the jack during loading. Figure 3.11 illustrates the loading frame and cooler, and figure 3.22 shows a schematic representation of the setup.

Two different top pipe extensions were required to accommodate the different lengths. In addition, the top cross beams were designed to be raised or lowered to accommodate different specimen lengths.

The gusset plates were bolted to the pipe extensions, and the angles specimens were bolted to the gussets. The gusset plates used in first setup were used in this setup as well. The BN and HBN specimens were tested using roller hinges at the top and bottom of the gusset plates as described in Setup no. 1. BG specimens were tested in this setup first, and were tested without any hinge system, that is the gusset plates were bolted directly to the pipe extensions. Figures 3.12 to 3.14 and figures 3.24 to 3.26 indicate the end fittings described above.

3.3.2.1 Test Procedure

Installation and removal of the specimens was performed with a chain hoist. An 8 m. high steel scaffold frame was required to access the top of the specimen.

Temperature control and monitoring was performed as described for Setup no. 1. Midheight specimen lateral movements were also monitored as in Setup no. 1. Load was measured with a load cell placed between the jack and bottom pipe, and an LVDT measured the stroke. Data was recorded using the Hewlett Packard Data Acquisition System shown in figure 3.11.

The test procedures were similar to those described in Setup no. 1, except that the load was applied using an 1800 kN capacity hydraulic jack. The load was increased in small increments of about 2 to 5% of predicted specimen capacity. The stroke of the jack was increased beyond the point of maximum load measurements until the load dropped approximately 10 %.

3.3.3 Test Setup No. 3

Six specimens were tested in a third setup; three BG-200, and three BN-200 specimens. These specimens were approximately 8000 mm long. Tests were performed at room temperature only, since the elastic buckling of these members was unlikely to be affected by temperature, and they could not be accommodated in the cold chambers.

A test setup which was previously used for testing long wooden poles was modified to suit the specimens. These tests were performed with the members in a horizontal position, as illustrated in figures 3.15 and 3.22. The setup consists of two

end supports to provide the end reactions. Figure 3.16 illustrates the two end blocks. Each end block has an overhead support and chain hoist to facilitate installation and removal of the specimens. The blocks were tied together by 4 long dywidag bars; one at each corner of the blocks. The dywidag bars were supported vertically at three points along their length to prevent sag. Load was applied at one end using two 445 kN capacity hydraulic jacks. The jacks and a load cell were placed between the end block and a large steel plate which was supported on a system of rollers to allow the plate to slide in the direction of loading. Applying hydraulic pressure to the jacks forces the plate to slide toward the opposite end block, inducing compression in the specimen. The dywidag bars act in tension to provide the reaction at each end block. Figure 3.17 shows the hydraulic jacks and load cell.

The specimens were tested with vertical hinges at each end to allow the specimens to buckle laterally without restraint. Figure 3.18 illustrates the hinge system. Figures 3.25 and 3.26 illustrate the connections for the (H)BN and BG specimens. The specimens were installed with the weak axis vertical to allow buckling about the hinge. The specimens rested on vertical supports with teflon pads that allowed the specimen to slide sideways at midlength without restraint, as illustrated in figure 3.19

3.3.3.1 Test Procedure

Before installing the test specimen, the end blocks were aligned by measuring the perpendicular, and diagonal distances between the corners of each end block.

The specimens were bolted to the gusset plates, lifted into position, and aligned with the centre points on each end block. A small load of about 5 to 10 kN was then applied to hold the specimen in position. Position transducers were connected to the specimens at midlength as illustrated in figure 3.19. The axial displacement was measured with a motion transducer installed between the fixed end block, and the sliding end plate as illustrated in figure 3.17. The load was applied in small increments of 2 to 5% of the ultimate load.

CHAPTER 4

TEST RESULTS

4.1 Introduction

In this chapter, the results of the experimental testing program are presented. These results include: material tests, measured dimensions, tabulated failure loads, load-deflection curves, and results of additional static tests which were performed.

4.2 Material Tests

As discussed in Chapter 1, the material tests were performed as part of the Galvanizing Embrittlement studies, and the tests were not performed by the author. Standard Tension Coupon Tests were performed on coupons taken from flat and corner sections of the specimens. Tests were performed according to ASTM-E370 to obtain the yield strengths. The tests were performed at various temperature levels, and both galvanized and ungalvanized specimens were examined. Full details of these investigations can be seen in the Galvanizing Embrittlement report submitted as part of the CEA project 340 T 844 (Polyzois et al 1994). The room temperature results from flat section coupons are used in Chapter 5 of this report and will therefore be summarized in this section.

Table 4.1 summarizes the yield strengths obtained from the room temperature, flat coupon tension tests.

4.3 Dimensions and Section Properties

Figures 3.1 to 3.5 illustrate the average measured dimensions for each shape. The figures identify the net dimension after deducting galvanizing thicknesses. Dimensions in parenthesis are the specified dimensions. Calculated section properties listed in table 4.2 are based on the average measured dimensions with the galvanizing deducted. Galvanizing thickness was approximately 0.1 mm on average. The average section properties were used to calculate load capacities in Chapter 5. Note that all of the specimens made from G40.21 steel have specified thicknesses of 4.5 mm, while the specimens made from ASTM A715 grade 60 steel have specified thicknesses of 4.0 mm, with the exception of the BN shapes which had a thickness of 5.0 mm.

4.4 Static Load Results

Table 4.3 lists the results of all the static tests performed. This table represents a total of 196 tests, and includes results from 7 extra tests performed beyond the planned 189 tests. The left column breaks the tests down into groups representing each individual shape and length. The results are divided according to the temperature at which each test was performed. The average load of each temperature, length, and shape group is listed in the far right column.

Typical plots of load vs. displacement for each shape and length are provided in appendix A.

CHAPTER 5

ANALYSIS AND DISCUSSION OF TEST RESULTS

5.1 Introduction

In this chapter, the results of the axial load tests and material tests are discussed. The effect of cold temperature on the results is also examined.

The results of the material tests, and section properties based on the average of all the section measurements will be used to analyze the sections. Sections will be analyzed according to both the "specified" yield strengths, and the measured yield strengths.

Each shape will be examined separately, and the results compared to predicted capacities to determine the accuracy of different design approaches. The methods of analysis were presented in Chapter 2. In order to avoid redundancy, the applicable formulas used for the analysis of the results in this chapter will not be listed again.

5.2 Material Properties

The yield strength used in this chapter was obtained from coupons taken from flat portions of cold-formed members similar to those tested in the experimental program. The material testing program was extensive and the results are presented elsewhere (Polyzois 1994). A short summary of these results is given below.

In the material testing program, it was found that the yield strength of the test coupons increased with decrease in temperature. The average increase of all tension tests at -50°C compared to tests at room temperature was approximately 10%.

It was also found that galvanizing affected the yield strengths of the tension coupons. In general, the yield strength of the galvanized coupons was greater than the ungalvanized coupons. The increase ranged from a low of 7.5% for the A715 steel to a high of 36.5% for the G40.21 steel. The results of tests on ungalvanized A715, and G40.21 steel specimens seem to confirm the specified yield strength of 415 MPa and 300 MPa respectively.

The results of tests on the G40.21 steel specimens also demonstrated a much larger increase in yield strength when galvanized compared to the A715 steel coupons. From table 4.1, the average increase in yield strength for the A715 coupons due to galvanizing was 8.5%; whereas the average increase in yield strength for the G40.21 coupons due to galvanizing was 36.3%. This increase in yield strength is quite large. Previous testing at the University of Manitoba by Polyzois, Charnvarnichborikarn, and Rizkalla (1989) demonstrated an average increase due to galvanizing in the range of 10% which agrees with the A715 steel results above. It was felt that the large increase in yield strength for the G40.21 steel may be attributed to the galvanizing process.

For each specimen shape, the coupon test result used in the analysis will be based on the galvanized strengths listed in table 4.1, since the specimens themselves were all galvanized. The analysis will also consider the specified yield strength. The specified yield strength of the A715 steel is 415 MPa, while for the G40.21 steel the specified yield strength was 300 MPa. Both values are based on the ungalvanized coupon strengths.

5.3 Effect of Temperature

The effect of temperature on the behaviour of the actual test specimens was noticeable, but not as significant as observed for the material tests. Figures 5.1 to 5.9 demonstrate the relation between temperature and failure load for each specimen shape and slenderness. A linear regression analysis was used to provide a straight line relation for the measured data within the temperature ranges used. The general trend of increased ultimate loads can be observed from these figures.

Table 5.1 summarizes the effect of temperature on the specimen ultimate load. The table lists the average ultimate load for all specimens in each shape and length category in column number two. The second (and third) column is the ratio of the average ultimate load for tests performed at 0° C (and -50° C) divided by the average results obtained at room temperature. For example, for the BA-40 specimens, the test results at 0° C do not show any increase, and the test results at -50° C show an average increase of 2%. The average increase for all the tests is

listed at the bottom of the table and is 1.3% at 0° C, and 3.8% at -50° C. When reviewing the table it becomes apparent that the largest increases in strength at both cold temperatures tend to occur for the smallest slenderness level for each shape. For example, BB-40 specimens show an increase of 10% at -50° C and an increase of only 2% for the longer BB-200 members. Figures 5.10 and 5.11 illustrate this difference. These graphs compare the relative increase in strength at each temperature level depending on the nominal slenderness ratio. In figure 5.10 it can be seen that the shortest members show an average increase of 7.4% at -50° C, and the longest members ($L/r=200$) show an average increase of only 2%.

This behaviour can be explained by the fact that as the members slenderness increases into the elastic range, the members strength is not affected by an increase in yield strength; whereas as the member becomes shorter, the capacity becomes more affected by the material strength. It can also be observed that the largest increases in strength at cold temperature occurred in the BG, BN, and HBN-40 specimens. Failure in these specimens was characterized by material failure in the form of local buckles at the stiffened edges.

5.4 BA And HBA Specimens

Behaviour

The angles were loaded through one leg, bolted to a gusset plate. The specimens began to bend and twist upon application of load, and increased until failure. The

angles with $L/r = 40$ were only 552 mm long, and measured 452 mm between centroids of connections. Consequently, they did not deflect and twist as much as longer specimens before failure. At maximum loading, buckles developed in the bolted leg, resulting in a rapid drop in capacity. Figure 5.12 shows BA-40 test specimens after failure, illustrating the local buckle in the bolted leg. Specimens with $L/r = 100$ demonstrated larger lateral deflections and twist at failure. The specimens deflected primarily perpendicular to the bolted leg. Some of the specimens still developed buckles in the bolted leg near the gusset plate. This location coincides with a point of reverse curvature in the leg, caused by the rotational restraint of the bolted connection. The drop in load capacity after ultimate was less rapid than for the shorter angles. Figure 5.13 illustrate a typical specimen with $L/r = 100$. At $L/r = 200$ the specimens twisted and deflected (primarily perpendicular to the loaded leg), and did not develop any buckles in the loaded leg. Figure A4.11 shows a typical load-deflection curve for these specimens, indicating a gradual drop in load after ultimate. Figures 5.14 shows a specimen at ultimate.

CAN/CSA-S136-M89 Analysis

The angles were analyzed according to Clause 6.7.4 Single Angles Loaded Through One Leg. This clause is discussed in Chapter 2. In using this clause, "b" is taken as the average leg flat width. The effective length factor K was taken as 0.7 for slenderness ratios less than 150 to account for the fixity provided by the two bolt connections. Beyond $L/r = 150$, only one bolt was used in testing, and K is taken as

0.8. The compressive stress limit F_a is computed by Clause 6.6.1.3, to account for buckling in the inelastic range.

Once the compressive stress limit F_a is known, the section must be checked to see if the flat width ratios do not exceed the limits specified in Clause 5.6.2 . If the limits are exceeded, then the reduced effective area is calculated, and is used to calculate the compressive strength of the section, as per Clause 6.6.1.3. It was found that both BA and HBA specimens had reduced effective areas for slenderness ratios less than about 100.

The capacity was not found to be limited by the local buckling strength limit imposed by clause 6.6.3.2, or by the limits imposed by clause 6.7.4.

Figures 5.15 and 5.16 show the results of the analysis for BA and HBA specimens respectively. Table 5.2 compares the average experimental ultimate loads with the predicted loads at the slenderness ratios of the specimens, and provides some detailed results not shown on the graphs (for example: factored capacity based on coupon yield). In all cases, the factored predicted loads based on coupon yield strengths, and specified strengths fall safely below the experimental loads. The predicted ultimate loads for BA specimens agreed fairly closely to the experimental loads. However for the HBA specimens, test results at $L/r=40$ were only 82 % of the ultimate predicted capacity based on the coupon yield, and 94 % based on the

specified yield. For the HBA-200 specimens, the average test result was only 91 % of the ultimate predicted load based on either yield value.

ASCE Manual 52

The specimens were analyzed in accordance with section 4.7 Compression Members: Angles. Flat width-to-thickness ratios of the angles exceeded the specified limit values, above which, local buckling may occur. Therefore the effective yield stresses were reduced as per section 4.7.3 to account for the effect of reduced local buckling strength on the flexural buckling strength. BA section critical stress was reduced to 289 MPa and 281.3 MPa for yields of 469 and 415 respectively. HBA stress was reduced to 319.5 MPa and 272.9 MPa for yields of 409 MPa and 300 MPa respectively. The effective length used in calculating the capacity was determined in accordance with section 4.7.4.2 to account for eccentricity of load, and end fixity. Allowable axial stresses on the gross section were computed as per section 4.6, substituting the reduced critical stresses for F_y .

Figures 5.17 and 5.18 show the predicted capacities and experimental results for BA and HBA shapes respectively. Note that although the effective slenderness used in analysis may be larger or smaller than the actual value of L/r , the test results are still plotted at the actual value L/r . The test results can be seen to fall near the predicted loads for most of the results. The notable exception was the HBA-40 results which fell below the predicted values. Table 5.2 lists the predicted values at

the exact slenderness of the test specimens. The average experimental result for HBA-40 tests was only 84 % and 94 % of the predicted value based on the coupon yield strength and specified yield strength respectively. This discrepancy was not evident for the BA-40 specimens where the average experimental load of 120 kN was exactly equal to the predicted load.

CAN/CSA-S37-M86 Analysis

Specimen capacity was calculated using the standard's clause 6.2.4 Web Members. Accordingly, a K value of 0.9 was assumed for members with two or more bolts, and a K value of 1.0 for members with only one bolt (assumed at $L/r=150$ in the curves). The width-thickness ratios of the specimens exceeded the limits imposed by clause 6.2.5, thereby requiring the calculation of a reduced effective yield stress " F_y ". This value was equal to 271 MPa and 266.8 MPa for yields of 469 and 415 MPa respectively for BA specimens; and equal to 300.6 MPa and 261 MPa for HBB yields of 409 and 300 MPa. The reduced effective yields and effective lengths were then used in the axial compressive strength equations given in Clause 13.3.1 of CSA Standard CAN3-S16.1.

Figures 5.19 and 5.20 show the ultimate loads calculated on the basis of this standard. The factored curves are also shown. The value of the resistance factor varies depending on the value of L/r , and the number of bolts: $\phi=0.72$ for $L/r < 120$, $\phi=0.9$ for $L/r > 120$ when 2 bolts are used, $\phi=0.72$ when one bolt is used (at

$L/r > 150$ on the curves). The horizontal section on the factored capacity curve relates to the point at which the resistance factor changes from 0.9 to 0.72. The lower limit of the factored resistance is that obtained using $\phi=0.9$ at $L/r=120$. The results for both BA-40 and HBA-40 specimens fall below the predicted curve. This can be explained by the fact that the analysis does not implicitly take into account the eccentricity of load. At short lengths, the end fixity is not as significant as the eccentricity, thus the capacity is overestimated. It must be noted, however, that in all cases, the factored resistance falls conservatively below the average experimental loads. The results at $L/r = 100$ and 200 fall above the ultimate capacity curve. It can be seen that the resistance factors have been reduced from the typical value of 0.9 to account for the eccentricity. For slenderness ratios greater than 120, it is implied that the beneficial effect of a two bolt connection offsets the eccentricity, and the member is assumed to be axially loaded, with $\phi=0.9$. If only one bolt is used than the standard neglects any end fixity, and specifies $\phi=0.72$.

Table 5.2 lists the predicted failure loads from the graphs discussed above. Again, it can be seen that the factored capacities are all below the experimental results.

ECCS Recommendations

This method is very similar to the approach taken by Manual 52. The width to thickness ratio in this case is specified as the full leg width divided by thickness. Both angles' b/t ratios exceeded the specified limit. Therefore a reduced effective

yield stress was calculated. For the BA specimens the width-thickness ratio exceeded $3/2(w/t)_{lim}$, and the effective yield stress was reduced to 253.2 MPa. This value depended only on the width-thickness ratio, and was independent of the actual yield strength. The HBA specimens had reduced effective yield stresses of 296.5 MPa and 258 MPa for yields of 409 MPa and 300 MPa respectively. It should be noted that to be consistent with previous calculations, the modulus of elasticity was taken as 200,000 MPa, and not 210,000 as specified by the ECCS.

The calculated curve is based on the following conditions identified in the ECCS method: eccentric load at both ends of specimen, bending about the weak, non-symmetric axis of the section, end fixity due to two or more bolts at each end (for slenderness less than 120), members with slenderness greater than 120 are assumed to be discontinuous, and connected with only one bolt.

Figures 5.21 and 5.22 show the predicted capacities using the ECCS Recommendations for Angles in Lattice Transmission Towers. In general, the experimental results fell above the predicted loads, with the exception of some BA-40 test results. The HBA-40 results once again did not reach as high as predicted. Table 5.2 indicates that the HBA-40 average result of 123 kN was only 79 % of the predicted value of 156 kN (based on the measured yield strength), and only 90 % of the predicted load based on the specified yield.

5.4 BB And HBB Specimens

Behaviour

The lipped angles behaved similar to the plain angles, and began to bend and twist upon application of loading. The specimens tended to deflect primarily perpendicular to the plane of the gusset plate as did the plain angles. The most significant difference in the member's behaviour was that at short lengths the specimens did not develop any local buckles in the loaded legs near the gusset plates as did occur for all the short plain angles. During testing, the gusset plates could be seen to be bending slightly in the direction of the member's lateral deflection. Figures 5.23 through 5.26 illustrate the member behaviour during testing.

CAN/CSA-S136-M89

The sections were analyzed using the same method used for the plain angles as given by clause 6.7.4, to determine whether it could be safely used to predict the load capacity of lipped angles loaded through one leg. It is recognized, however, that the method was developed for plain angles without the benefit of lips. The flat width of the stiffened leg was used as "b". Both HBB and BB specimens were found to be adequately stiffened to allow fully effective areas.

Figures 5.27 and 5.28 show the results of the analysis, compared to the experimental results. A significant difference in performance can be seen between the HBB and BB specimens. All BB test results fell above the ultimate capacity based on the

measured yield strengths; whereas almost all of the HBB test results fell below the ultimate predicted loads based on the measured yield. For the HBB specimens, the test results at $L/r = 100$ also fell below the ultimate capacity based on the specified yield strength. The results do fall safely above the factored curves in all cases. Table 5.3 lists the predicted loads and average ultimate experimental loads. This also illustrates the discrepancy between the ultimate HBB-100 and HBB-40 experimental loads and the predicted loads.

ASCE Manual 52 Analysis

The sections were analyzed according to the same methods used for the plain angles, using section 4.8 of the Guide. The dimensions of the lip were checked according to section 4.8.4. Section BB's lip were found to be adequate. Section HBB's lips were not adequate. They measured 25 mm overall, but were required to be 27.9 mm. However, since the lip was very close to the required size, it was assumed to be adequate. The sections satisfied the flat width-thickness ratios specified by equation 4.9.3 of the Manual for stiffened elements. This assumption seemed more reasonable than completely neglecting the lip. The analysis of lipped angles is different than plain angles in that in addition to checking the flexural buckling of the specimen about the weak axis, torsional flexural buckling is also checked. An equivalent radius of gyration is calculated as per section 4.8.3. In using the expressions for r_{tf} , K was taken as 1.0 as specified. The allowable compression is

then calculated using the minimum radius of gyration, and the effective lengths provided by section 4.7.4.2.

For nominal slenderness ratios of 40 and 100, it was found that r_{if} was smaller than r_y . Therefore the buckling stress was calculated using r_{if} . Figures 5.29 and 5.30 illustrate the design capacity curve. The predicted loads agree very closely with the experimental results. The BB results all fall slightly above the predicted loads, and the HBB results are centred on the curve. Table 5.3 summarizes the analysis.

5.5 BC and HBC Sections

Behaviour

Specimen behaviour was very similar to the plain angles, characterized by continuous bending and twisting at loading. The short specimens developed buckles in the loaded leg near the top or bottom gusset as indicated in figure 5.31. Intermediate length specimens deflected laterally at mid-height and twisted approximately 30°. The lateral deflection was primarily perpendicular to the gusset plate. At ultimate load, some specimens developed buckles in the loaded legs at the gusset plates in the area of reverse curvature in the specimen. The longest specimens behaved similarly, but did not develop any buckles in the bolted legs. Figure 5.32 illustrates a BC-200 specimen under load, demonstrating a large degree of twist.

Although 60° angles benefit from an increased flexural strength (due to an increased minimum radius of gyration), they are subject to a decreased torsional-flexural buckling strength relative to 90° angles. As the moment of inertia about the non-symmetrical weak axis increases, the moment of inertia about the strong-symmetrical axis decreases. The torsional-flexural buckling capacity decreases as the strong axis inertia decreases. This effect was evidenced by the large amount of twist that occurred during tests.

CAN\CSA-S136-M89 Analysis

As for the BB specimens, the sections were analyzed using Clause 6.7.4 for Single Angles Loaded Through One leg to see how well it could predict the capacity. The procedure is essentially the same as discussed for the plain angles. The flat width value of "b" was taken as the flat leg width to the point of curvature as indicated on figure 3.3. The effective area of the sections was found to be reduced for slenderness values up to approximately 100.

Figures 5.33 and 5.34 show the results of the analysis. BC specimen test results fell above the predicted capacities. HBC test results fell below the predicted capacity at $L/r = 40$ and 100. At $L/r=200$, the average result fell on the curve. All of the test results were higher than the factored capacity based in the measured yield strength. Table 5.4 summarizes the predicted capacities. The bottom row lists the ratio of mean test result for all BC and HBC tests divided by the mean ultimate

predicted capacity. This value is 0.99 when the measured yield strength is used. The ratio of mean test result divided by factored resistance based on measured yield strength is 1.32. The comparable values calculated for BA and HBA specimens in table 5.1 is 0.99 and 1.32 respectively. Based on the test results, it appears that clause 6.7.4 works as well for 60° angles as it does for 90° angles.

ASCE Manual 52

Manual 52 limits the use of the effective length provisions of section 7.4 which account for eccentricity and fixity to 90° angles. The reason for excluding 60° angles is not indicated in the commentary. One reason may be the reduced torsional flexural capacity of 60° angles compared to 90° angles. For simply supported 90° angles free to warp at each end, the critical stress for local buckling and pure torsional buckling are the same. The stress for torsional-flexural buckling is close to the torsional stress. For this reason 90° angles are normally checked for flexural and local buckling only, neglecting torsional-flexural buckling.

In using section 4.7 for the 60° angles, it is therefore unconservatively assumed that the torsional-flexural buckling strength is equivalent to a plain angle.

In checking the specified width-thickness ratios, the flat width of the leg was taken as indicated in figure 3.3. The reduced critical stress for the BC specimen was 250.2 MPa and 249.7 MPa for yields of 477 MPa and 415 MPa respectively. Since they

are so close in value, the difference was neglected, and a value of 250 MPa is assumed. For the HBC specimens, the reduced critical stress was 269.5 MPa and 241.0 MPa for yields of 415 and 300 MPa respectively.

Figures 5.35 and 5.36 show the results of the analysis. The BC test results fall close to the predicted capacity. HBC test results at slenderness levels of 40 and 100 fall below the predicted loads. The discrepancy is greatest at the nominal slenderness ratio of 40. From table 5.4 it can be seen that the mean experimental load at $L/r=40$ was only 78 % of the predicted capacity based on the measured yield strength. In addition, the ratio of mean test result to mean predicted capacity for all BC and HBC tests listed in the bottom row of table 5.4 is only 0.92. That is, on average, the predicted capacity overestimates the failure loads by 8.5 %. If the HBC-40 results are excluded, then the average predicted capacity overestimates the mean failure load by only 2.8 %

CAN\CSA-S37-M86 Analysis

The method of analysis was identical to that for the plain angles. The Standard specifies a flat width value to use for schifflerized 60° angles, but does not specify a similar value for cold-formed angles. Following previous assumptions, and the general approach followed for schifflerized angles, the width was simply taken as the flat width up to the start of the bend. Based on the flat-width ratios, the effective yield stress was reduced to 222.3 MPa and 226.4 MPa for BA yields of 477 and 415

MPa respectively. The reduced critical stress was actually less when based on the higher measured yield stress than when based on the specified yield stress. The reduced stress for the HBC specimens was 247.9 MPa and 227.7 MPa for yields of 415 and 300 MPa respectively.

Figures 5.37 and 5.38 show the results of the analysis. The data is plotted at L/r , where r is radius of gyration about the weak axis. Torsional-flexural buckling is not considered in the analysis. Once again, it was found that the BC test results generally fell above the predicted curve, and the HBC-40 and 100 results fell below the ultimate predicted curve. The HBC-40 results showed the largest discrepancy, with the average result being only 78 % of the predicted ultimate capacity. All but one test result fell above the factored predicted capacity.

5.6 BG Sections

Behaviour

The hat-shaped BG sections are singly symmetric, and as such may be susceptible to torsional-flexural buckling. During testing specimens were observed to twist and deflect laterally.

Specimens with slenderness ratios of 40 remained fairly straight during testing with only slight lateral deflection and twist. The specimens failed suddenly as local buckles developed in the stiffened 45° flange on one side of the section. The load

dropped quickly after the flange buckled. Figure 5.39 shows a specimen after buckling at mid height; and figure 5.40 shows the distorted flange and stiffening lip after failure. A different type of failure is shown in figure 5.41, where the member failed by buckling of the web section near the bottom of the member. A closer view of the buckled web is shown in figure 5.42. Table 5.1 shows that there was a 16% increase in load resistance for these specimens when tested at -50°C as compared to room temperature tests. The specimen material failure is directly affected by the increased material strength at cold temperature.

The intermediate length specimens ($L/r = 100$) twisted and deflected laterally about the symmetric axis. Failure was sudden as the 45° flange buckled on the concave side of the deflected member. The lateral deflection increased suddenly, and the load dropped off substantially. This can be observed in a typical load-deflection curve such as figure A4.106. Figure 5.43 illustrates a specimen after failure. These specimens were tested using the same gusset plate as at the other two slenderness ratios, except the base of the gusset was bolted down, and not allowed to hinge. The BG-100 specimens were tested first. After performing these tests it was decided to install a hinge on the gusset to allow rotation about the axis of symmetry for the BG-40 and BG-200 specimens.

The longest specimens were very long and noticeably flexible, especially about the axis of symmetry. The out of straightness about this axis ranged from 4 to 15 mm.

Specimens began to deflect laterally gradually as the load increased. Most of the twist occurred as the load approached the maximum. The load did not peak and drop off quickly, but rather was maintained at a near constant level while the lateral deflection continued to increase. When the load was released, the specimen returned very near to the original shape.

CAN\CSA-S136-M89 Analysis

The specimen was analyzed as a concentrically loaded, singly-symmetric section according to section 6.6.3. Accordingly, the critical stress is the lower of the torsional-flexural stress provided in clause 6.6.3.1, or the flexural buckling stress of Clause 6.6.2. Torsional flexural buckling was found to be the governing mode at all test lengths considered.

In calculating the torsional buckling stress, the effective length factor for torsional buckling " K_t " was initially taken as 1.0. The analysis was then repeated using an assumed " K_t " = 0.7 to reflect the warping restraint provided by the connection. Both flanges of the section are bolted, and both thicknesses of web are connected. It was felt that this connection definitely provided some restraint, and that neglecting the restraint may be overly conservative.

Once the critical stress was evaluated, the effective area of the section is evaluated using Clause 5.6.2 of the Standard. The flat flange, and 45° flange were both found

to be effective at the maximum stresses. In evaluating the web, it was assumed that it could be treated as being stiffened on each edge by a web or flange, and that the curved radius connecting the two webs together combined with one web to stiffen the opposite web. Using this assumption allowed the calculation of effective area according to Clause 5.6.2.2. Alternatively, the web could be simply assumed as stiffened on one edge by a flange, and by a stiffener on the other edge. However then the "simple lip stiffener" would be made up of a completely curved section. The standard only considers the flat width of a stiffener. Therefore the entire stiffener would be neglected, and the web would not be considered as stiffened. This would be an overly conservative assumption since the radius does provide some stiffening effect to the web. Using the first assumption, it was found that at the maximum measured yield stress of 438 MPa, the web was almost fully effective. The total web area was theoretically reduced by 2.4 mm^2 . This small reduction was ignored since it represented an amount of only 0.1 % of the gross area.

Figure 5.44 and 5.45 shows the results of the analysis using $K_t = 1.0$ and 0.7 respectively. The capacities are summarized in table 5.5. The experimental results fall above the ultimate predicted capacities for both curves. When $K_t = 0.7$ was used, the predicted results were higher (less conservative), particularly for lower slenderness ratios. The results at $L/r = 100$ fall significantly higher than the predicted ultimate loads for both values of K_t . These specimens did not have an actual hinge installed at the base of the gusset plate. It appears that neglecting the

restraint provided by the gussets is overly conservative. From table 5.5 it can be seen that ratio of the mean test result to mean ultimate predicted load is 1.63 when $K_t = 1.0$, and 1.37 when a less conservative value of $K_t = 0.7$ was assumed. Table 5.5 also shows a capacity in parenthesis below the results for $K_t = 0.7$. The results in brackets are the predicted capacity for the $L/r = 100$ specimens if it is assumed that $K_t = K_x = 0.7$ to reflect both the torsional restraint, and the gusset plate fixity. The ultimate predicted capacity based on this assumption is 318 kN.

ASCE Manual 52

Section 4.9.5 of the Manual requires that the section be checked for flexural buckling in the plane of symmetry and for torsional flexural buckling. An equivalent radius of gyration is calculated as per Section 4.8.3. The value of K_t was used as 1.0 and then as 0.7, consistent with the previous analysis. It should be noted that when using equation 4.8-1 from the manual to calculate r_{tf} , the terms $1/r_t$ and $1/r_u$ are replaced with K_t/r_t and K_u/r_u to account for mixed end fixity conditions. Used in this form the equation gives K_t/r_{tf} . Torsional flexural buckling governed for all specimen lengths, and therefore the buckling stress is based on KL/r_{tf} . The data, however, is plotted at x-axis coordinates corresponding to L/r_y , in order to maintain a uniform scale.

The effective area is calculated at the computed allowable compressive stress (Section 4.6). The average dimension of the lip measured 14.3 mm, and according

to section 4.8.4 the minimum lip depth should be 19.5 mm. If the lip is neglected and the flange treated as unstiffened, the maximum allowable flat-width ratio at maximum stresses is 36.1. The actual ratio is only slightly larger at 38.4. Based on this, and the fact that the lip does provide some benefit, the flange was considered stiffened, and the full area was effective. The web was treated as stiffened at both ends, and was found to have a reduced effective area at high stresses. The reduced area was taken into account in the capacity calculations.

Figures 5.46 and 5.47 show the results of the analysis. The results fall mostly above the predicted curve. When $K_t = 0.7$ was used, the predicted loads increased, yet were still conservative. Table 5.5 lists the predicted loads for each case. The table also lists the predicted ultimate load using $K_t = K_x = 0.7$. This load is listed in parenthesis below the predicted load at $L/r = 100$.

The predicted loads at $L/r = 100$ are very conservative. While the mean experimental failure load was 470 kN, the ultimate predicted load varied from a minimum of 256 kN to 384 kN depending on the effective length assumptions. In the most conservative case, the predicted load is only 54 % of the ultimate.

A non-typical section such as this might best be utilized by performing prototype tests to study the effect of various assumptions necessary for design. For example, if based on these tests, a section was designed using less conservative effective length

assumptions, the design capacity increases by 50 % from 256 to 384 kN. The potential savings in steel may be substantial.

5.7 BN and HBN Sections

Behaviour

The back to back channel sections are doubly symmetric sections with relatively large cross-sections. They would be suitable for very heavily loaded leg members. The end fixity for these sections is likely to be less of a factor in design than it is for angles. Discontinuous ends of channel sections would likely be joined with web connected gusset plates. The gusset plates would not provide as much rotational restraint to the channels as they did for angles (since the channels are much stiffer). The test specimens were loaded concentrically by bolting to a 12.7 mm thick gusset plate positioned in the gap between the backs of the channels. The first two BN-100 tests were performed with the gusset plates fixed at their base, by bolting down to the pipe extensions. During testing, as the members buckled laterally, they bent the gusset plates with them, leaving some permanent bend in the plates. It was then decided to perform all remaining BN and HBN tests with pinned ends, free to rotate about the weak axis.

Specimens with $L/r = 40$ remained fairly straight during testing, with only slight lateral deflection. At ultimate, local buckles developed in the lips, at about midheight on the concave side of the member, and the lateral deflection quickly

increased, while the load dropped off quickly. Figures 5.48 and 5.49 illustrate the behaviour of the member, and show the buckles in the lips. Table 5.1 shows that these sections developed almost 10 % higher loads at cold temperatures than at room temperature.

At $L/r = 100$ the specimens displayed two distinct behaviour modes. The specimens which developed the highest loads remained fairly straight right up until failure, whereupon the specimens suddenly buckled laterally. The lips on the concave side buckled slightly at about midheight. Unfortunately, the orientation of the specimen in the cold chamber sometimes prevented observing whether the local buckles developed at ultimate load, or if they developed as the members lateral deflection increased upon continued application of load after failure had occurred. The second type of behaviour was characterized by gradually increasing lateral deflection, and lower ultimate loads. The lips did not always distort. The specimens gradual increase in lateral deflection indicates imperfect member performance. This may be attributed to member out of straightness, small alignment errors, and lack of perfect symmetry in the sections due to manufacturing tolerances. Although the method of loading through the webs is reasonably concentric, in practice a purely concentric load is highly unlikely, thus creating moments in the section, and reducing the axial capacity. The first type of failure may be unlikely to be achieved for members of actual structures, at the lengths similar used in testing. Figures 5.5 illustrates a typical test specimen behaviour. In some cases a small amount of twist

was observed during testing, but the ultimate failure was always in the form of lateral buckling about the weak axis.

The test specimens with $L/r = 200$ were 8200 mm long, and had significant out of straightness (between 7 mm and 13 mm) about the weak axis. These specimens began to deflect laterally upon application of load, and continued increasing to the maximum load, at which point the deflection increased quickly. Figure 5.51 illustrates the behaviour of a BN-200 specimen.

CAN/CSA-S136-M89 analysis

The BN specimens had a thickness of 5.0 mm, and the HBN specimens were 4.5 mm thick. This standard specifies that sections greater than 4.5 mm in thickness must be designed for axial stresses provided by CSA Standard S16.1. Therefore CSA-S136 is actually only applicable to the HBN specimens. For comparison purposes, both sections were analyzed using S16.1 and S136.

Clause 6.6.7 provides a modification to the basic Euler buckling expression to account for the reduced shear rigidity of built-up sections joined together at discrete points. In using Clause 6.6.7, K is taken as 1.0 (since the ends are hinged), L is the distance between the hinges, r is the weak axis radius of gyration. Using the critical elastic buckling stress calculated by Clause 6.6.7, the compressive stress limit F_a is calculated as per clause 6.6.1.3 for the elastic and inelastic ranges.

The above analysis assumes that the section is not critical in torsional buckling. For shorter length specimens, torsional buckling may govern. Therefore the sections were also checked for torsional buckling according to clause 6.6.3.1. In calculating the torsional buckling stress F_t , the effective length factor K_t was assumed equal to 1.0.

Using the compressive stress limits from above, calculated at each specific slenderness ratio, the effective area can be calculated. Both BN and HBN sections were found to be adequately stiffened to allow the full effective area to act.

Figures 5.52 and 5.54 illustrate the results of the analysis, and table 5.6 lists the predicted capacities. BN-40, HBN-40, and HBN-100 section capacities were found to be governed by torsional buckling critical stresses. Since the actual failure modes did not appear to be governed by torsional buckling, the section capacities based on flexural buckling are also indicated in parenthesis in table 5.6, and are shown on figures 5.53 and 5.55. In general, the predicted capacities based on flexural buckling seemed to better predict the average failure load, but because of the scatter of test results, some of the failure loads were overestimated. The ultimate predicted loads based on torsional buckling were all conservative. In the event that torsional buckling is neglected, as is normally the practice for doubly symmetric sections, the predicted loads are generally still conservative.

CAN/CSA-16.1-M89

This standard applies when the section thickness is greater than 4.5 mm, as were the BN sections. Axial stress levels are computed according to CSA-S16.1 column curves, and effective areas are calculated according to CSA-S136, at the level of axial stress provided by CSA-S16.1. The sections were all found to be fully effective. A modified effective length was calculated to account for the reduced shear rigidity due to the spacing of the back to back channel connections:

$$\text{Modified } \frac{KL}{r} = \sqrt{\left(\frac{KL}{r}\right)^2 + \left(\frac{a}{r_1}\right)^2}$$

Where

KL/r = overall slenderness ratio of the entire section about the built-up member (weak) axis. ($K=1.0$)

a = fastener spacing

r_1 = radius of gyration of individual section

This modified effective length was used to calculate the dimensionless slenderness parameter λ .

The sections were also checked for torsional buckling by substituting the equivalent radius of gyration r_t for r in calculating the dimensionless parameter λ . When checking torsional buckling, the modified slenderness as discussed above was not

considered. The data was plotted at an X-axis coordinate of L/r_y , regardless of whether flexural or torsional buckling governed, but the curve itself does account for the torsional buckling strength as indicated.

The results are presented in figures 5.56 to 5.59, and in table 5.6. In general, this method predicted lower loads at low and intermediate slenderness (40 and 100), and higher loads at high slenderness ratios ($L/r=200$) than the Cold-Formed Steel Standard S136. For the BN sections which applied in this case, the flexural buckling predicted loads were unconservative for all the long members, and for two of the intermediate length members. The torsional buckling predicted loads were generally conservative. As indicated in table 5.6, the ratio of mean failure load to mean predicted load was 1.28 when torsional buckling was considered, and 1.09 when only flexural buckling was considered.

ASCE Manual 52

Section 4.9.4 Doubly Symmetric Open Cross Sections requires that torsional buckling be checked if the unsupported length for torsional buckling exceeds the flexural buckling length. For the test conditions it is assumed that the lengths are the same, suggesting that only flexural buckling needs to be considered according to the guide. Both modes were considered. For BN-40 and HBN-40 sections the equivalent radius of gyration r_t was smaller than the weak axis radius of gyration, and torsional buckling governed.

HBN sections were found to have fully effective areas. The lips on BN sections measured 15.5 mm, and were required to be 26.6 mm according to the minimum lip depth requirements of section 4.8.4. The stiffening effect of the lips was neglected in the analysis and a slightly reduced effective area was calculated at higher stresses.

The manual does not recognize the detrimental effect of the spacing of back to back connections. Therefore, in contrast to the CSA-S136 and S16.1 methods already discussed, the effective length was taken simply as KL/r (with $K = 1.0$), and no modification was applied. For comparison purposes, the capacities were then also calculated assuming that the modification did apply.

The results of the analysis are shown in figures 5.60 to 5.63, and in table 5.6. Results listed under column two of the table were calculated using a modified effective length as discussed above. Experimental failure loads generally fell below the predicted curves for BN-100 and 200, and HBN-40 and 100 specimens when torsional buckling was neglected. Considering torsional buckling resulted in safer load predictions for members at $L/r=40$. When the modified slenderness was considered, the predicted loads reduced to provide better predictions, yet were still unconservative in some cases, particularly for HBN-100 and BN-200 sections. For these sections, the predicted loads were the same for specified yield strength, and measured yield strength.

The ratio of mean test result to mean predicted load, based on measured yields, and considering torsional buckling was only 0.98. By comparison, the comparable ratios based on CSA-S16.1 and CSA-S136 were conservative at 1.27 and 1.17 respectively. The design method used in CSA-S136 provided better ultimate load predictions than ASCE Manual 52. However, the primary difference between the two methods relates to the use of the modified slenderness ratio in calculating the elastic Euler buckling stress, and in multiplying the buckling stress by a factor of 0.833.

5.9 Concentrically Loaded Angles

Seven additional tests were performed on the angle shaped specimens in order to examine the effect of bolting to both legs of the section. Clip angles were bolted to the gusset plates so that the outstanding legs of the angles could be connected as well. Figure 5.64 illustrates a BA-40 specimen connected in this manner.

Specimens behaviour was not completely as expected. In some cases the specimen behaviour was no different than when only one leg was connected. Specimens HBA-100-7, and HBC-100-7 were examples of this. The member ultimate loads were very similar to the results with one leg bolted. Specimens were observed to twist and deflect primarily perpendicular to the gusset plate, similar to the single leg connected specimens. In contrast, some sections were observed to deflect primarily about the weak principal axis, with little twist. For these specimens the ultimate load was found to be higher than when connected by one leg.

The reason for the difference between specimens is not clear, but the behaviour does suggest that the connection did not consistently achieve concentric loading. If the bolts connecting the leg directly to the main gusset plate went into bearing before the bolts to the outstanding leg, then the initial loading on the specimen is as if loaded through one leg. Small differences in bolt end distances could cause this. As the load is initially applied through the one leg, the specimen begins to bend and deflect perpendicular to the gusset plate. In turn, the gusset plate tends to bend slightly due to the end restraint. As the gusset plate rotates, the clip angle also rotates, and the bolt holes in the clip angle move slightly down, away from the load, thus forcing more load to the opposite leg. Under these circumstances the member behaves as if loaded through one leg, and the connection to the clip angle does not provide any benefit.

Specimens HBB-100-7 and 8, and HBA-100-9 were tested by modifying the gusset plate. The clip angle was bolted to the gusset plate, but it was located so that the bottom of the clip angle was in bearing against the horizontal section of the gusset plate. Any rotation induced in the main gusset plate was then prevented by the clip angle. And similarly, the clip angle could not rotate in the direction parallel to the gusset plate as the length of the gusset plate provided substantial stiffness in that direction. As expected, the sections tested in this manner reached much higher loads than when connected by one leg. The results of these tests are listed in table 4.3, and are identified as being bolted through both legs.

CAN/CSA-S136-M89: The sections were assumed to be concentrically loaded, and Clause 6.7.4 was not followed. Section capacity was checked according to Clause 6.6.3 Singly Symmetric Sections. Accordingly, the section capacity is given by the lower of the flexural buckling capacity about the weak axis, or the torsional flexural buckling capacity. The latter was found to be the limiting factor. The calculated capacity is compared to the test results in table 5.7. Two of the test results were significantly overestimated; falling below even the factored capacity based on specified yield strength. Section HBA-100-9 which was tested with the more rigid gusset plate (as described above), reached a higher ultimate load than predicted.

ASCE Manual 52: For sections bolted in both legs, effective length provisions of section 4.7.4.2 assume a concentric load, and neglect any end fixity. Using the specified effective length, the capacity is calculated exactly as for the members loaded through a single leg. Predicted loads were lower than those of CSA-S136.

CAN/CSA-S37-M86: The sections were treated as leg members, and analyzed according to Clause 6.2.3. The effective length factor K is taken as 1.0, and the sections are analyzed as axially loaded sections. The section capacity is calculated as for the eccentrically loaded sections, with two exceptions: the effective length factor K is taken as 1.0, and the value of the resistance factor is specified as 0.9. In contrast, the single bolted leg analysis used K varying from 0.9 to 1.0, and the resistance factor ranging from 0.72 to 0.9.

ECCS: The analysis is similar to the ASCE Manual 52. The sections are treated as concentrically loaded, and no modification is made to the basic slenderness ratio of L/r ($K=1$). With the above modifications, section capacity is calculated as for the eccentrically loaded angles.

Table 5.7 compares the experimental test results with the calculated capacities from above. In general, the specimens that behaved as expected by buckling about the weak principal axis with little twist, achieved loads higher than predicted by the various methods. The sections that behaved similarly to their single bolted leg counterparts reached loads significantly below the predicted loads. These failure loads were very close to the loads achieved with only one bolted leg.

The method of testing does not closely simulate the condition of leg members butt spliced at the ends or lap spliced together. Unconservative designs may result in a situation where the designer may attempt to increase a web members capacity by adding clip angles in order to bolt to both legs. The web member connected in this may not achieve the predicted strength in some cases.

5.10 Unstiffened Angles Bolted Through One Leg

The experimental testing program indicated a tendency for unstiffened angles with low slenderness ratios to develop distortions in the bolted leg very close to the

gusset plate. Once the leg began to distort, the axial load resistance dropped. The load in the angle immediately adjacent to the connection is primarily distributed in the bolted leg only, with very little load distributed to the outstanding leg. The design methods which have been reviewed in the previous discussions consider member buckling at the critical midheight location, at which point a more uniform stress distribution can be assumed. The actual stress in the angle at the connection, involves both axial stresses and bending stresses, due to the rotational restraint provided at the bolted connection. There is a general lack of test experience for specimens in the lower slenderness ranges, and surprisingly, not one of the design methods reviewed takes into account the potential failure of an angle as described above. In many cases, the specimens failed at loads significantly lower than predicted by the design methods. It is therefore apparent that an additional limit should be imposed on unstiffened angles loaded through one leg.

Based on correlation to the experimental test results, the following simple modification is recommended to avoid premature failure of such angles. An upper limit to the compressive strength should be calculated as the product of the yield strength multiplied by the area of the flat portion of the bolted leg for 90° angles, or 90% of the area of the flat portion of the bolted leg for 60° angles. If the local stress distribution in the bolted leg near the connection exceeds the yield stress, the leg begins to buckle, leading to failure. The proposed compressive limit is defined below.

For 90° angles

$$C_{r_{max}} = F_y w t$$

For 60° angles

$$C_{r_{max}} = F_y (0.9w) t$$

where

w = flat width of leg

t = leg thickness

F_y = yield strength

Although the method is simplistic, and does not necessarily account precisely for the actual stress distribution in the vicinity of the connection, it does result in more reasonable ultimate load predictions for very short angles than provided by any of the design methods. It is therefore recommended that the upper limits defined above be considered in addition to buckling loads defined in the design methods. Table 5.8 compares the results of BA-40, HBA-40, BC-40, and HBC-40 tests, with the proposed upper compressive limits as defined above. The yield strengths for each section were obtained from tension tests performed on flat portions of sections, at the three temperature levels used in the static compression tests. The calculated

compressive limit for each specimen is based on the yield strength measured at the same temperature as the static test. The mean ratio of the experimental failure loads to the upper limit loads calculated for the BA-40, HBA-40, BC-40, and HBC-40 angles is equal to 1.0, and the standard deviation is 0.058. Figure 5.65 provides illustration to the results listed in table 5.8. Figure 5.66 compares the experimental results with the loads predicted using ASCE Manual 52's recommendations, with two modifications. The first modification includes the proposed limit for short unstiffened angles. The second modification is that the back-to-back channel capacity is modified utilizing the recommendations of CSA-S136. By comparing the data with the 1:1 correspondence line it can be seen that the experimental results are predicted very well by the methods of ASCE Manual 52 (when modified as described above). Data which falls below the 1:1 line indicates unconservative predicted loads, and as evidenced on the figure, such instances are limited in number of occurrences.

CHAPTER 6

SUMMARY, CONCLUSIONS, AND RECOMMENDATIONS

6.1 Summary

A research program was performed at the University of Manitoba to examine the axial load carrying capacity of a number of cold-formed shapes suitable for transmission tower construction. The project was jointly sponsored by The Canadian Electrical Association, Manitoba Hydro, and The University of Manitoba.

The extensive testing program included a total of 201 axial load tests. The testing was carried out over a fifteen month period. Three different test setups were used in this investigation.

Test parameters included: two types of steel, five different shapes, three slenderness ratios, and three temperatures. Specimens were tested in setups designed to simulate end conditions representative of tower members by loading through single legs bolted to gusset plates. Some sections were tested as axially loaded leg members with hinged end conditions.

Test results were compared to predicted loads using the Canadian Standards CAN/CSA-S136-M89 Standard for Cold Formed Steel Structural Members, and CAN/CSA-S37-M86 Standard Antennas, Towers, and Antenna Supporting Structures. The ASCE Manual 52 Guide for Design of Steel Transmission Towers,

and the ECCS Recommendations for Angles in Lattice Transmission Towers were also used.

6.2 Conclusions

- The average of all experimental failure loads when tested at 0° C was 1.3 % higher than at room temperature.
- The average of all experimental failure loads when tested at -50° C was 3.8 % higher than at room temperature.
- The amount of load increase at -50° C was the largest for members with $L/r = 40$. These specimens averaged loads 7.4 % higher than at room temperature. Specimens with $L/r = 100$ and 200 only showed a 1 to 2 % increase.
- For BA and HBA specimens, the ratio of mean experimental failure load divided by mean predicted ultimate load based on measured yield strength was as follows:

CAN/CSA-S136-M89 -----	0.99
CAN/CSA-S37-M86 -----	0.99
ASCE MANUAL 52 -----	1.01
ECCS -----	1.03

- For BB and HBB specimens, the ratio of mean experimental failure load divided by mean predicted ultimate load based on measured yield strength was as follows:

CAN/CSA-S136-M89 ----- 0.99

ASCE MANUAL 52 ----- 1.10

- For BC and HBC specimens, the ratio of mean experimental failure load divided by mean predicted ultimate load based on measured yield strength was as follows:

CAN/CSA-S136-M89 ----- 0.96

CAN/CSA-S37-M86 ----- 0.91

ASCE MANUAL 52 ----- 0.92

- For BN and HBN specimens, the ratio of mean experimental failure load divided by mean predicted ultimate load based on measured yield strength was as follows:

CAN/CSA-S136-M89 ----- 1.18

CAN/CSA-S16.1-M89 ----- 1.28

ASCE MANUAL 52 ----- 0.98

- For BG specimens, the ratio of mean experimental failure load divided by mean predicted ultimate load based on measured yield strength was as follows:

CAN/CSA-S136-M89 ----- 1.63

ASCE MANUAL 52 ----- 1.45

- Seven additional tests were performed with specimens bolted through one leg to the gusset plate, and through the other leg to a clip angle in order to simulate concentric load conditions. They did not behave consistently. Failure loads varied substantially, from no increase in capacity, to capacities in excess of concentric loading predictions.

6.3 Recommendations

Based on the results of the research and analysis, the following recommendations are made:

- The increase in axial load capacity at cold temperatures was variable, depending on specimen length and failure mode. Within the test parameters, temperature was not found to be detrimental, and may be conservatively neglected in design.

- Caution should be exercised in designing eccentrically loaded unstiffened angles with slenderness ratios of approximately 40. Code prediction reliability was much lower for these sections than for longer sections. Members of this length are likely to be uncommon in transmission towers, especially as eccentrically loaded web members. The test specimens of concern ranged in length from 552 mm to 736 mm.
- The proposed upper compressive limit to prevent premature failure near the connection of short angles bolted through one leg was found to provide better ultimate load predictions than the available design methods, and it is recommended that it be included in design.
- It should be recognized that Canadian Standards CSA-S136 and CSA-S37 are intended to provide safe and economical design capacities. Therefore the goal is to predict loads that members can support, but not necessarily the loads at which the members will actually fail.
- The resistance factors (ϕ) provided by the Standards mentioned above, are an integral part of the design resistance, reflecting the performance and reliability of the member type, and not just simply the material strength. For singly symmetric sections, and for eccentrically loaded members the standards recognize the potential lack of conservatism in the guidelines. Consequently,

the resistance factors ranged from 0.72 to 0.9 depending on the section shape, length, and connection type. When using the Canadian Standards, the calculated factored resistances were found to be safe for 181 out of 189 tests (based on the measured yield strength) When using the specified strengths, the factored resistances were safe for 186 out of 189 tests.

- CSA Standard CAN/CSA-S37-M86 presently limits the use of cold-formed steel sections as a substitute for hot-rolled steel angles to angles with leg dimensions of 52 mm or smaller. All of the sections used in this study were larger than this. Consideration should be made to increasing this limit.
- The method used in CSA Standard CAN/CSA-S136-M89 to account for eccentricity in angles loaded through one leg by bolts or welds, should be generalized to account for 60° and lipped angles.
- Although test results are limited, modifying a simple gusset plate with clip angles in order to attach to both legs of a web member did not provide reliable increases in load capacity. Caution is advised against relying on such a detail to provide increases in member capacity.
- The design of back-to-back channels should include the affect of the spacing of the back-to-back connections. Further, the elastic stress levels provided

by the Euler expression modified as such should be reduced by a factor of 0.833 as in the CSA-S136-M89.

- In general, with the exceptions mentioned, the design methods reviewed in this study provided acceptable results and appear to be adequate for the design of cold-formed steel sections for transmission towers. However, ASCE Manual 52 was found by the author to be the preferred guide. The Manual is widely accepted by tower designers, and its recommendations are supported by numerous laboratory and full-scale tests. In particular, the effective length formulas used to design angles were found to accurately account for both connection eccentricity and end fixity.

REFERENCES

- Adluri S.M.R., Madugula M.K.S., "Factored axial compressive resistance of schifflerized angles," *Canadian Journal of Civil Engineering*, Vol.18, 1991, pp.926-932.
- Adluri S.M.R., Madugula M.K.S., Monforton G.R., "Schifflerized angle struts," *Journal of Structural Engineering*, ASCE, Vol 118, No.71, July, 1992, pp.1920-1936.
- American Iron and Steel Institute, "Specification for The Design of Cold-formed Steel Structural Members," Cold-formed Steel Design Manual-Part I, 1986, Washington DC.
- Arena J.R., Zar M., "Section 24 Towers and Transmission Pole Structures," *Structural Engineering Handbook*, Gaylord E.H., ed, Gaylord C.H., ed, McGraw-Hill, New York, Second Edition, 1979, pp.24-1.
- ASCE, "Electrical Transmission Line and Tower Design Guide," Report of the Task Committee on Tower Design of the Committee on Analysis and Design of Structures, *Journal of the Structural Division*, ASCE, Vol.93, No. ST 4, August, 1967, pp.245-282, see also closure Vol.95, No. ST6, June, 1969, pp.1361-1372.
- ASCE-American Society of Civil Engineers, 1988. "Guide for Design of Steel Transmission Towers," ASCE Manuals and Reports on Engineering Practice No. 52, Second Edition, New York, N.Y.
- Bathon L., Mueller W.H., Kempner L., "Ultimate Load Capacity of Single Steel Angles," *Journal of Structural Engineering*, ASCE, Vol 119, No.1, January, 1993, pp.279-300.
- Bergstrom R.N., Arena J.R., Kramer J.M., "Design of Self Supported Steel Transmission Towers," *Journal of the Power Division*, ASCE, Vol. 86, No. PO 3, June 1960, pp. 55-88.
- Bryant M.E., "Transmission Towers: Design of Cold-Formed Angles," *Journal of Structural Engineering, Discussion*, ASCE, Vol 113, No.3, March, 1987, pp.649-650.
- Cannon D., "Variation in Design Practice for Lattice Towers," Steel Structures Proceedings, ASCE Structures Congress, 1989.
- Catenacci A., Finzi M., Zavelani A., "New Outlines for 500 kV Transmission Towers using Cold-Formed Shapes: The Experimental Line of the American Electric Power Research Institute," Steel Structures Proceedings, ASCE Structures Congress, 1989.

Chajes A., Winter G., "Torsional-Flexural Buckling of Thin-Walled Members," *Journal of the Structural Division*, ASCE, Vol. 91, No. ST 4, August, 1965, pp.103-123.

CSA-Canadian Standards Association, 1986. "CAN/CSA-S37-M86, *Antennas towers and antenna supporting structures*," National Standard of Canada, Rexdale, Ont., Canada.

CSA-Canadian Standards Association, 1987. "CAN/CSA-C22.3 No. 1-M87, *Overhead Systems*," National Standard of Canada, Rexdale, Ont., Canada.

CSA-Canadian Standards Association, 1991. "Special Publication S136.1-M1991 *Commentary on CAN/CSA-S136-M89, Cold formed steel structural members*," National Standard of Canada, Rexdale, Ont., Canada.

CSA-Canadian Standards Association, 1989. "CAN/CSA-S16.1-M89, *Limit states design of steel structures*," National Standard of Canada, Rexdale, Ont., Canada.

CSA-Canadian Standards Association, 1989. "CAN/CSA-S136-M89, *Cold formed steel structural members*," National Standard of Canada, Rexdale, Ont., Canada.

Davalath G.S.R., "Transmission Towers: Design of Cold-Formed Angles," *Journal of Structural Engineering, Discussion*, ASCE, Vol 113, No.3, March, 1987, pp.658-659.

Faggiano P., "Lattice Tower Design using Cold-Formed Shapes," *Innovations in the Design of Electrical Transmission Structures*, Proceedings of a ASCE Conference, Kansas City, Missouri, August 14-16, 1985, pp37-46.

European Convention For Constructional Steelwork, 1985. "Recommendations for Angles in Lattice Transmission Towers," ECCS - Technical Committee 8 - Structural Stability Technical Working Group 8.1 - Components, First Edition 1985 No. 39, Brussels, Belgium.

Gaylord E.H., Wilhoitte G.M., "Transmission Towers: Design of Cold-Formed Angles," *Journal of Structural Engineering*, ASCE, Vol 111, No.8, August, 1985, pp.1810-1825. See also Discussion, Vol 113, No. 3, March, 1987, pp.654-657.

Kalyanaraman V., Pekoz T., Winter G., "Unstiffened Compression Elements," *Journal of the Structural Division*, ASCE, Vol. 103, No. ST 9, September, 1977, pp.1833-1848.

Kennedy J.B., Madugula M.K.S., "Buckling of Angles: State of the Art." *Journal of the Structural Division*, ASCE, Vol.108, No. ST9, September, 1982, pp.1967-1980.

Kennedy J., Madugula K.K.S., "Buckling of Steel Angle and Tee Struts," *Journal of the Structural Division*, ASCE, Vol. 98, No.ST 11, November, 1972, pp.2507-2520.

Karren K.W., Winter G., "Effects of Cold-forming on Light Gage Steel Members," *Journal of the Structural Division*, ASCE, Vol. 93, No.ST 1, February, 1967, pp.433-469.

Karren K.W., "Corner Properties of Cold-formed Steel Shapes," *Journal of the Structural Division*, ASCE, Vol. 93, No.ST 1, February, 1967, pp.401-431.

Knight G.M.S., Santhakumar A.R., "Joint Effects on Behaviour of Transmission Towers," *Journal of Structural Engineering*, ASCE, Vol 119, No.3, March, 1993, pp.698-712.

Kravitz R. A., "Transmission Line Tower Analysis and Design in Review," *IEEE Transactions on Power Apparatus and Systems*, Vol. PAS-101, No. 11, November 1982, pp. 4350-4357.

Lui E.M., "Behaviour of Single Angles under Compression and Biaxial Bending," *Steel Structures Proceedings*, ASCE Structures Congress, 1989.

Madugula M.K.S., Ray K.S., "Ultimate strength of eccentrically loaded cold-formed angles," *Canadian Journal of Civil Engineering*, Vol.11, 1984, pp.225-233.

Madugula M.K.S., Prabhu T.S., Temple M., "Ultimate strength of concentrically loaded cold-formed angles," *Canadian Journal of Civil Engineering*, Vol.10, 1983, pp.60-68.

Madugula M.K.S., Ray K.S., "Cross-sectional properties of cold-formed angles," *Canadian Journal of Civil Engineering*, Vol.11, 1984, pp.649-655.

Madugula M.K.S., Ray K.S., "Biaxial bending of cold-formed angle members," *Canadian Journal of Civil Engineering*, Vol.11, 1984, pp.933-942.

Marsh C., "Transmission Towers: Design of Cold-Formed Angles," *Journal of Structural Engineering, Discussion*, ASCE, Vol 113, No.3, March, 1987, pp.650-652.

Marsh C., "Factored axial compressive resistance of schifflerized angles: Discussion," and "Reply", *Canadian Journal of Civil Engineering*, Vol.20, 1993, pp.330-332.

Marsh C., "Single Angle Members in Tension and Compression," *Proceedings, Journal of the Structural Division*, ASCE, Vol.95, No. ST5, February, 1969, pp.1043-1049.

Mulligan G.P., Pekoz T., "Locally Buckled Thin-Walled Columns", *Journal of Structural Engineering*, ASCE, Vol. 110, No. 11, November 1984, pp.2635-2654.

Pekoz T.B., Winter G., "Torsional-Flexural Buckling of Thin-Walled Sections under Eccentric Load," *Journal of the Structural Division*, ASCE, Vol. 95, No.ST 5, May, 1969, pp.941-962.

Polyzois D., Et Al., "Effect of temperature and galvanization on the compressive strength of cold-formed angles," *Canadian Journal of Civil Engineering*, Vol.17, 1990, pp.440-451.

Polyzois D., Et Al., "Use of Cold Formed Sections for Transmission Towers in Canada," *Technical Report No. 340 T 844*, Canadian Electrical Association, Jan, 1994.

Ray S.K., Madugula M.K.S., "Transmission Towers: Design of Cold-Formed Angles," *Journal of Structural Engineering, Discussion*, ASCE, Vol 113, No.3, March, 1987, pp.652-653.

Weng C.C., Lin C.P., "Study of Maximum Strength of Cold-Formed steel Columns," *Journal of Structural Engineering*, ASCE, Vol 118, No.1, January, 1992, pp.128-146.

Wei-Wen Yu, "Cold-formed Steel Design," John-Wiley and Sons, Inc, New York, 1982.

Zavelani A., "Design and Test of Cold Formed Steel Members," *Innovations in the Design of Electrical Transmission Structures*, Proceedings of a ASCE Conference, Kansas City, Missouri, August 14-16, 1985, pp.69-78.

Zavelani, A., Faggiano P., "Design of Cold-Formed Latticed Transmission Towers," *Journal of Structural Engineering*, ASCE, Vol 111, No.11, November, 1985, pp.2427-2445.

TABLES

TABLE 2.1 Static Test Parameters










SECTION	TYPE OF STEEL	NOMINAL SLENDERNESS (L/r)	OVERALL LENGTH (mm)	NUMBER OF TESTS AT EACH TEMPERATURE			TOTAL NO. OF TESTS FOR EACH SHAPE	TOTAL NO. FOR EACH STEEL TYPE
				-50°C	0°C	ROOM TEMP.		
BA 	ASTM A715 GRADE 60	40	552	3	3	3	27	123
		100	1380	3	3	3		
		200	2760	3	3	3		
BB 		40	855	3	3	3	27	
		100	1950	3	3	3		
		200	4240	3	3	3		
BC 		40	736	3	3	3	27	
		100	1840	3	3	3		
		200	3680	3	3	3		
BG 		40	1640	3	3	3	21	
		100	4120	3	3	3		
		200	8245	0	0	3		
BN 		40	1640	3	3	3	21	
		100	4105	3	3	3		
		200	8210	0	0	3		
HBA 	CSA G40.21 GRADE 300 W	40	552	3	0	3	18	66
		100	1380	3	0	3		
		200	2760	3	0	3		
HBB 		40	780	3	0	3	18	
		100	1950	3	0	3		
		200	3900	3	0	3		
HBC 		40	736	3	0	3	18	
		100	1840	3	0	3		
		200	3680	3	0	3		
HBN 		40	1580	3	0	3	12	
		100	3950	3	0	3		
TOTAL				72	39	78	189	

TABLE 4.1 Tensile Material Properties of Flat Coupons at Room Temperature

SECTION	SPECIFIED STRENGTH (MPa)	COUPON YIELD STRENGTH (MPa)	
		GALVANIZED	UNGALVANIZED
BA	415	469	424
BB	415	445	418
BC	415	477	434
BG	415	438	419
BN	300	481	434
HBA	300	409	289
HBB	300	418	311
HBC	300	415	315
HBN	300	401	290

Source: Polyzois et al (1994)

TABLE 4.2 Average Section Properties

SECTION	A	I_x	I_y	J	C_w	r_x	r_y
	(mm ²)	(10 ³ mm ⁴)	(10 ³ mm ⁴)	(mm ⁴)	(mm ⁶)	(mm)	(mm)
BA	530	434.34	98.076	2759	0	28.6	13.6
HBA	603	481.08	111.77	4073	0	28.2	13.6
BB	787	1132.30	327.4	5174	331	37.9	20.4
HBB	822	941.66	327.41	5353	190	33.8	19.96
BC	595	345.53	201.38	3173	0	24.1	18.4
HBC	700	423.02	260.14	4725	0	24.6	19.3
BG	1925	3376.65	3318.92	10266	3604	41.9	41.5
BN	2564	5115.00	4394.53	21368	4354	44.7	41.5
HBN	2300	3966.00	3850.02	15531	5538	41.5	40.9

TABLE 4.3 Static Test Results Summary

100

SPECIMEN	ULTIMATE LOAD (kN)			
	TEST TEMP. LEVEL			AVERAGE
	-50°C	0°C	ROOM TEMP.	
BA-40-1 BA-40-2 BA-40-3 BA-40-18 BA-40-19			113 126 120 118 120	119
BA-40-4 BA-40-5 BA-40-6		116 125 116		119
BA-40-7 BA-40-8 BA-40-9 BA-40-19-1	122 110 123 127			121
BA-40-19-2 *			140	
BA-100-1 BA-100-2 BA-100-3			93 103 100	99
BA-100-4 BA-100-5 BA-100-6		102 98 100		100
BA-100-7 BA-100-8 BA-100-9	105 104 100			103
BA-200-1 BA-200-2 BA-200-3			29 32 28	30
BA-200-4 BA-200-5 BA-200-6		28 34 28		30
BA-200-7 BA-200-8 BA-200-9	28 28 28			28
HBA-40-1 HBA-40-2 HBA-40-3			115 118 120	118
HBA-40-4 HBA-40-5 HBA-40-6	131 129 124			128
* Both legs of specimen bolted				

TABLE 4.3 Static Test Results Summary

SPECIMEN	ULTIMATE LOAD (kN)			
	TEST TEMP. LEVEL			AVERAGE
	-50°C	0°C	ROOM TEMP.	
HBA-100-1 HBA-100-2 HBA-100-3			119 112 111	114
HBA-100-4 HBA-100-5 HBA-100-6	120 117 117			118
HBA-100-7 * HBA-100-9 *			122 155	
HBA-200-1 HBA-200-2 HBA-200-3			29 30 29	29
HBA-200-4 HBA-200-5 HBA-200-6	30 32 31			31
BB-40-1 BB-40-2 BB-40-3			209 203 204	205
BB-40-4 BB-40-5 BB-40-6		214 213 213		213
BB-40-7 BB-40-8 BB-40-9	223 228 227			226
BB-100-1 BB-100-2 BB-100-3			133 132 132	132
BB-100-4 BB-100-5 BB-100-6		133 132 134		133
BB-100-7 BB-100-8 BB-100-9	136 139 140			138
* Both legs of specimen bolted				

TABLE 4.3 Static Test Results Summary

SPECIMEN	ULTIMATE LOAD (kN)			
	TEST TEMP. LEVEL			AVERAGE
	-50°C	0°C	ROOM TEMP.	
BB-200-1 BB-200-2 BB-200-3			45 46 47	46
BB-200-4 BB-200-5 BB-200-6		46 46 46		46
BB-200-7 BB-200-8 BB-200-9	47 47 47			47
HBB-40-1 HBB-40-2 HBB-40-3			196 187 188	190
HBB-40-4 HBB-40-5 HBB-40-6	205 202 206			204
HBB-100-1 HBB-100-2 HBB-100-3			133 121 120	125
HBB-100-4 HBB-100-5 HBB-100-6	128 128 130			129
HBB-100-7 * HBB-100-8 *			180 169	175
HBB-200-1 HBB-200-2 HBB-200-3			44 45 45	45
HBB-200-4 HBB-200-5 HBB-200-6	47 48 47			47
BC-40-1 BC-40-2 BC-40-3			116 121 116	118
BC-40-4 BC-40-5 BC-40-6		119 124 120		121
BC-40-7 BC-40-8 BC-40-9	125 119 113			119
* Both legs of specimen bolted				

TABLE 4.3 Static Test Results Summary

SPECIMEN	ULTIMATE LOAD (kN)			
	TEST TEMP. LEVEL			AVERAGE
	-50°C	0°C	ROOM TEMP.	
BC-100-1 BC-100-2 BC-100-3			92 95 92	93
BC-100-4 BC-100-5 BC-100-6		92 98 99		96
BC-100-7 BC-100-8 BC-100-9	92 100 96			96
BC-200-1 BC-200-2 BC-200-3			32 35 35	34
BC-200-4 BC-200-5 BC-200-6		36 31 31		33
BC-200-7 BC-200-8 BC-200-9	31 31 33			32
HBC-40-1 HBC-40-2 HBC-40-3			110 117 119	115
HBC-40-4 HBC-40-5 HBC-40-6	119 120 126			122
HBC-100-1 HBC-100-2 HBC-100-3			103 103 101	102
HBC-100-4 HBC-100-5 HBC-100-6	110 109 106			108
HBC-100-7 * HBC-100-8 *			107 119	113
HBC-200-1 HBC-200-2 HBC-200-3			37 38 37	37
HBC-200-4 HBC-200-5 HBC-200-6	39 42 41			41
* Both legs of specimen bolted				

TABLE 4.3 Static Test Results Summary

SPECIMEN	ULTIMATE LOAD (kN)			
	TEST TEMP. LEVEL			AVERAGE
	-50°C	0°C	ROOM TEMP.	
BN-40-1 BN-40-2 BN-40-3			990 1030 1030	1017
BN-40-4 BN-40-5 BN-40-6		1050 1115 1110		1092
BN-40-7 BN-40-8 BN-40-9	1165 1015 1160			1113
BN-100-1 BN-100-2 BN-100-3			499 427 357	428
BN-100-4 BN-100-5 BN-100-6		329 451 430		403
BN-100-7 BN-100-8 BN-100-9	432 351 419			401
BN-200-1 BN-200-2 BN-200-3			75 85 79	80
HBN-40-1 HBN-40-2 HBN-40-3			734 783 765	761
HBN-40-4 HBN-40-5 HBN-40-6	823 819 834			825
HBN-100-1 HBN-100-2 HBN-100-3			361 360 352	358
HBN-100-4 HBN-100-5 HBN-100-6	325 306 319			317

TABLE 4.3 Static Test Results Summary

SPECIMEN	ULTIMATE LOAD (kN)			
	TEST TEMP. LEVEL			AVERAGE
	-50°C	0°C	ROOM TEMP.	
BG-40-1 BG-40-2 BG-40-3			675 723 795	731
BG-40-4 BG-40-5 BG-40-6		767 796 784		782
BG-40-7 BG-40-8 BG-40-9	862 803 872			846
BG-100-1 BG-100-2 BG-100-3 BG-100-10 BG-100-11			486 441 440 463 505	467
BG-100-4 BG-100-5 BG-100-6		459 445 481		462
BG-100-7 BG-100-8 BG-100-9	499 515 440			485
BG-200-1 BG-200-2 BG-200-3			94 94 94	94

TABLE 5.1 Temperature affect on Load Capacity

Specimen Group	Average Load (kN)	<u>P test ave. (0 °C)</u>	<u>P test ave. (-50°C)</u>
		P test ave. (room temp.)	P test ave. (room temp.)
BA-40	120.0	1.00	1.02
HBA-40	123.0		1.08
BA-100	100.7	1.01	1.04
HBA-100	116.0		1.04
BA-200	29.2	1.01	0.94
HBA-200	30.0		1.07
BB-40	214.7	1.04	1.10
HBB-40	197.0		1.07
BB-100	134.3	1.01	1.05
HBB-100	127.0		1.03
BB-200	46.3	1.00	1.02
HBB-200	46.0		1.04
BC-40	119.3	1.03	1.01
HBC-40	118.5		1.06
BC-100	95.0	1.03	1.03
HBC-100	105.0		1.06
BC-200	33.0	0.97	0.94
HBC-200	39.0		1.11
BG-40	786.3	1.07	1.16
BG-100	471.3	0.99	1.04
BG-200	94.0		
BN-40	1074.0	1.07	1.09
HBN-40	793.0		1.08
BN-100	410.7	0.94	0.94
HBN-100	337.2		0.89
BN-200	80.0		
Average Increase For all tests		1.013 (1.3%)	1.038 (3.8%)

TABLE 5.2 BA and HBA Predicted Load Comparison

SPECIMEN GROUP	EXPERIMENTAL (kN)		CODE PREDICTED LOADS (kN)											
			CAN/CSA-S136-M89 Clause 6.7.4				ASCE MANUAL 52 Section 6.4		ECCS Angle Recommendations		CAN/CSA-S37-M86 Clause 6.2.4			
	Mean	Standard Deviation	Fy Coupon *		Fy Specified *		Fy Coupon *	Fy Specified *	Fy Coupon *	Fy Specified *	Fy Coupon *		Fy Specified *	
			$\phi=1.0$	$\phi=0.75$	$\phi=1.0$	$\phi=0.75$					$\phi=1.0$	$\phi=0.72$	$\phi=1.0$	$\phi=0.72$
BA-40	120	5.05	119	89	116	87	120	118	118	118	135	97	133	95
BA-100	101	3.4	85	64	85	64	89	88	78	78	88	64	88	63
BA-200	29	2.1	28	21	28	21	26	26	25	25	24	18	24	18
HBA-40	123	5.8	150	112	131	98	147	131	156	137	169	121	148	106
HBA-100	116	3.4	109	82	106	80	103	99	98	90	105	75	99	71
HBA-200	30	1.1	33	25	33	25	30	30	28	28	28	20	28	20
Mean Test Result	86.5	Mean Predicted Load	87.33	65.50	83.17	62.50	85.83	82.00	83.83	79.33	91.50	65.83	86.67	62.17
Ratio of Mean Test Result to Mean Code Predictions			0.99	1.32	1.04	1.38	1.01	1.05	1.03	1.09	0.95	1.31	1.00	1.39

* Refer to Table 4.1

TABLE 5.3 BB and HBB Predicted Load Comparisons

SPECIMEN GROUP	EXPERIMENTAL (kN)		CODE PREDICTED LOADS (kN)					
			CAN/CSA-S136-M89 Clause 6.7.4				ASCE MANUAL 52 Section 6.4	
	Mean	Standard Deviation	Fy Coupon *		Fy Specified *		Fy Coupon *	Fy Coupon *
			$\phi=1.0$	$\phi=0.75$	$\phi=1.0$	$\phi=0.75$		
BB-40	214.9	8.74	198	148	194	145	187	184
BB-100	134.6	2.91	120	90	120	90	114	114
BB-200	46.3	0.67	39	29	39	29	37	37
HBB-40	197.3	7.65	225	169	186	139	191	168
HBB-100	126.7	4.68	148	111	144	108	126	126
HBB-200	46.0	1.41	47	35	47	35	44	44
Mean Test Result	127.6	Mean Predicted Load	129.5	97.0	121.7	91.0	116.5	112.2
Ratio of Mean Test Result to Mean Code Predictions			0.99	1.32	1.05	1.40	1.10	1.14

* See Table 4.1

TABLE 5.4 BC and HBC Predicted Load Comparison

SPECIMEN GROUP	EXPERIMENTAL (kN)		CODE PREDICTED LOADS (kN)									
			CAN/CSA-S136-M89 Clause 6.7.4				ASCE MANUAL 52 Section 6.4		CAN/CSA-S37-M86 Clause 6.2.4			
	Mean	Standard Deviation	Fy Measured *		Fy Specified *		Fy Measured *	Fy Specified *	Fy Measured *		Fy Specified *	
			$\phi=1.0$	$\phi=0.75$	$\phi=1.0$	$\phi=0.75$			$\phi=1.0$	$\phi=0.72$	$\phi=1.0$	$\phi=0.72$
BC-40	119	3.65	117	88	116	87	121	120	125	90	127	91
BC-100	95.1	3.11	86	64	86	64	94	94	89	64	90	65
BC-200	32.8	1.93	31	23	31	23	30	30	28	20	28	20
HBC-40	118.5	4.70	147	110	133	100	151	139	164	118	151	109
HBC-100	105.3	3.30	111	83	110	83	118	112	116	83	110	79
HBC-200	39	1.92	40	30	40	30	39	39	36	26	36	26
Mean Test Result	84.98	Mean Predicted Load	88.7	66.3	86.0	64.5	92.2	89.0	93.0	66.8	90.3	65.0
Ratio of Mean Test Result to Mean Code Predictions			0.96	1.28	1.10	1.32	0.92	0.95	0.91	1.27	0.94	1.31

* See Table 4.1

TABLE 5.5 BG Section Predicted Load Comparison

SPECIMEN GROUP	EXPERIMENTAL LOADS (kN)		CODE PREDICTED LOADS (kN)											
			CAN/CSA-S136-M89				CAN/CSA-S136-M89				ASCE MANUAL 52			
			Clause 6.6.3		see footnote 1		Clause 6.6.3		see footnote 2		Section 4.9.5			
	Mean	Standard Deviation	Fy Measured **		Fy Specified **		Fy Measured **		Fy Specified **		Fy Measured **		Fy Specified **	
			$\phi=1.0$	$\phi=0.75$	$\phi=1.0$	$\phi=0.75$	$\phi=1.0$	$\phi=0.75$	$\phi=1.0$	$\phi=0.75$	see footnote 1	see footnote 2	see footnote 1	see footnote 2
BG-40	786.3	58.01	542	406	528	396	655	492	630	473	590	687	571	658
BG-100	470.4	26.80	214	160	214	160	257 (318)*	193 (239)*	257 (318)*	193 (239)*	256	309 (384)*	256	309 (384)*
BG-200	94.0	0.00	71	54	71	54	72	54	72	54	86	87	86	87
Mean Test Result	450.2	Mean Predicted Load	275.7	206.7	271.0	203.3	328.0 (348.3)*	246.3 (261.7)*	319.7 (340.0)*	240.0 (255.3)*	310.7	361.0 (388.0)*	304.3	351.3 (376.3)*
Ratio of Mean Test Result to Mean Code Predictions			1.63	2.18	1.66	2.21	1.37 (1.29)*	1.83 (1.72)*	1.41 (1.32)*	1.88 (1.76)*	1.45	1.25 (1.17)*	1.48	1.28 (1.20)*
* Calculated assuming $K_x=K_t=0.7$			1 Calculated assuming $K_t=K_x=1.0$											
** See Table 4.1			2 Calculated assuming $K_t=0.7$, $K_x=1.0$											

TABLE 5.6 BN and HBN Sections Predicted Load Comparison

SPECIMEN GROUP	EXPERIMENTAL FAILURE LOADS (kN)		CODE PREDICTED LOADS (kN)											
			CAN/CSA-S16.1-M89 Clause 13.3				CAN/CSA-S136-M89 Clause 6.6.7				ASCE MANUAL 52 Section 4.9.4			
	Mean	Standard Deviation	Fy Measured **		Fy Specified **		Fy Measured **		Fy Specified **		Fy Coupon **		Fy Specified **	
			$\phi=1.0$	$\phi=0.9$	$\phi=1.0$	$\phi=0.9$	$\phi=1.0$	$\phi=0.9$	$\phi=1.0$	$\phi=0.9$	See Footnote 1	See Footnote 2	See Footnote 1	See Footnote 2
BN-40	1073.9	61.14	729 (952)*	656 (857)*	681 (849)*	613 (764)*	843 (1039)*	759 (935)*	773 (919)*	696 (827)*	907 (1079)*	907 (1060)*	822 (954)*	822 (940)*
BN-100	410.56	51.32	355	320	342	307	347	313	347	313	481	417	481	417
BN-200	79.7	4.11	105	95	104	93	89	80	89	80	124	107	124	107
HBN-40	793	35.64	637 (747)*	573 (673)*	522 (587)*	470 (529)*	712 (805)*	641 (725)*	572 (624)*	515 (562)*	773 (838)*	773 (825)*	606 (643)*	606 (635)*
HBN-100	337.2	21.44	286 (313)*	258 (281)*	263 (287)*	237 (258)*	287 (325)*	258 (292)*	287 (325)*	258 (292)*	454	389	428	385
Mean Test Result	538.9	Mean Predicted Load	422.4 (494.4)*	380.4 (445.2)*	382.4 (433.8)*	344.0 (390.2)*	455.6 (521.0)*	410.2 (472.6)*	413.6 (460.8)*	372.4 (414.8)*	547.8 (595.2)*	518.6 (559.6)*	492.2 (526.0)	467.4 (496.8)*
Ratio of Mean Test Result to Mean Code Predictions			1.28 (1.09)*	1.42 (1.21)*	1.41 (1.24)*	1.57 (1.38)*	1.18 (1.03)*	1.31 (1.14)*	1.30 (1.17)*	1.45 (1.30)*	0.98 (0.91)*	1.04 (0.96)*	1.09 (1.02)*	1.15 (1.08)*

* Calculated neglecting torsional buckling

** See Table 4.1

1. Calculated as per Manual 52

2. Calculated using a modified slenderness as provided in CSA-S136 Cl.6.6.7

To account for back to back connection spacing

TABLE 5.7 Concentrically Loaded Specimen Comparison

SPECIMEN	EXPERIMENTAL FAILURE LOADS (kN)	CODE PREDICTED LOADS (kN)											
		CAN/CSA-S136-M89 Clause. 6.6.3 **				ASCE MANUAL 52 SECTION 6.4		ECCS		CAN/CSA-S37-M86 Clause. 6.2.4			
		Fy Coupon *		Fy Specified *		Fy Coupon *	Fy Specified *	Fy Coupon *	Fy Specified *	Fy Coupon *		Fy Specified *	
		$\phi=1.0$	$\phi=0.75$	$\phi=1.0$	$\phi=0.75$					$\phi=1.0$	$\phi=0.72$	$\phi=1.0$	$\phi=0.72$
HBA-100-7	122												
HBA-100-8	113	143	107	127	95	124	114	110	105	91	82	87	78
HBA-100-9	155												
HBB-100-7	180	127	95	127	110	141	139	(a)	(a)	(a)	(a)	(a)	(a)
HBB-100-8	169												
HBC-100-7	107	109	82	109	82	114	113	(a)	(a)	105	94	101	91
HBC-100-8	119												
Mean Test Result	141	126.3	94.7	121.0	95.7	126.3	122.0	110.0	105.0	98.0	88.0	94.0	84.5
Ratio of Mean Test Result to Mean Code Predictions		1.12	1.49	1.17	1.47	1.12	1.16	1.18	1.24	1.26	1.40	1.31	1.46
* See Table 4.1		** Calculated assuming $K_y=0.7$, $K_t=1.0$						(a) : not applicable					

TABLE 5.8 Proposed upper limit capacity for short unstiffened angles loaded through one leg

Section	Test Temp. (°C)	Coupon Yield (MPa)*	Test Load (kN)	Cr limit (kN)	Test load Cr limit
BA-40-1	23	469	113	112.7	1.00
BA-40-2	23	469	126	112.7	1.12
BA-40-3	23	469	120	112.7	1.06
BA-40-18	23	469	118	112.7	1.05
BA-40-19	23	469	120	112.7	1.06
BA-40-4	0	486	116	116.8	0.99
BA-40-5	0	486	125	116.8	1.07
BA-40-6	0	486	116	116.8	0.99
BA-40-7	-50	519	122	124.8	0.98
BA-40-8	-50	519	110	124.8	0.88
BA-40-9	-50	519	123	124.8	0.99
BA-40-19-1	-50	519	127	124.8	1.02
HBA-40-1	23	409	115	113.9	1.01
HBA-40-2	23	409	118	113.9	1.04
HBA-40-3	23	409	120	113.9	1.05
HBA-40-4	-50	511	131	142.3	0.92
HBA-40-5	-50	511	129	142.3	0.91
HBA-40-6	-50	511	124	142.3	0.87
BC-40-1	23	477	116	112.5	1.03
BC-40-2	23	477	121	112.5	1.08
BC-40-3	23	477	116	112.5	1.03
BC-40-4	0	488	119	115.1	1.03
BC-40-5	0	488	124	115.1	1.08
BC-40-6	0	488	120	115.1	1.04
BC-40-7	-50	510	125	120.3	1.04
BC-40-8	-50	510	119	120.3	0.99
BC-40-9	-50	510	113	120.3	0.94
HBC-40-1	23	415	110	118.4	0.93
HBC-40-2	23	415	117	118.4	0.99
HBC-40-3	23	415	119	118.4	1.00
HBC-40-4	-50	440	119	125.5	0.95
HBC-40-5	-50	440	120	125.5	0.96
HBC-40-6	-50	440	126	125.5	1.00
Mean:					1.00
Standard deviation:					0.058
* Obtained from tension coupons tested at room temp., 0°C, and -50°C					

FIGURES



FIGURE 1.1
Transmission Tower in Service

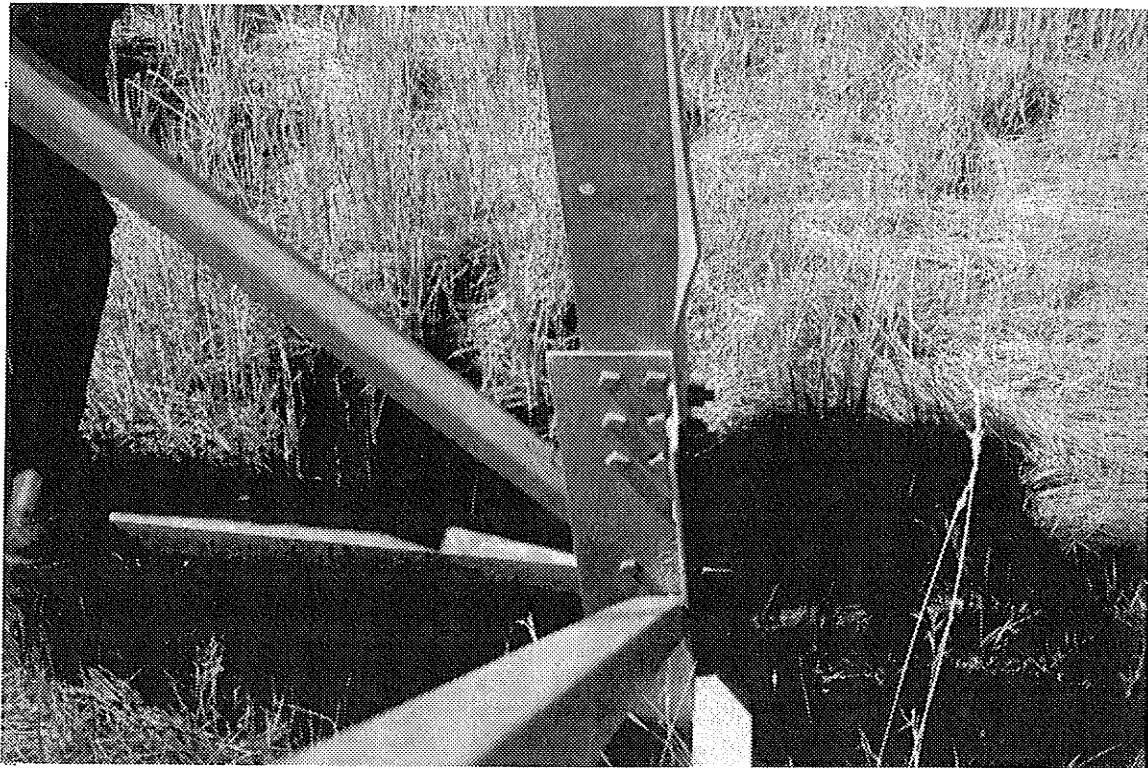
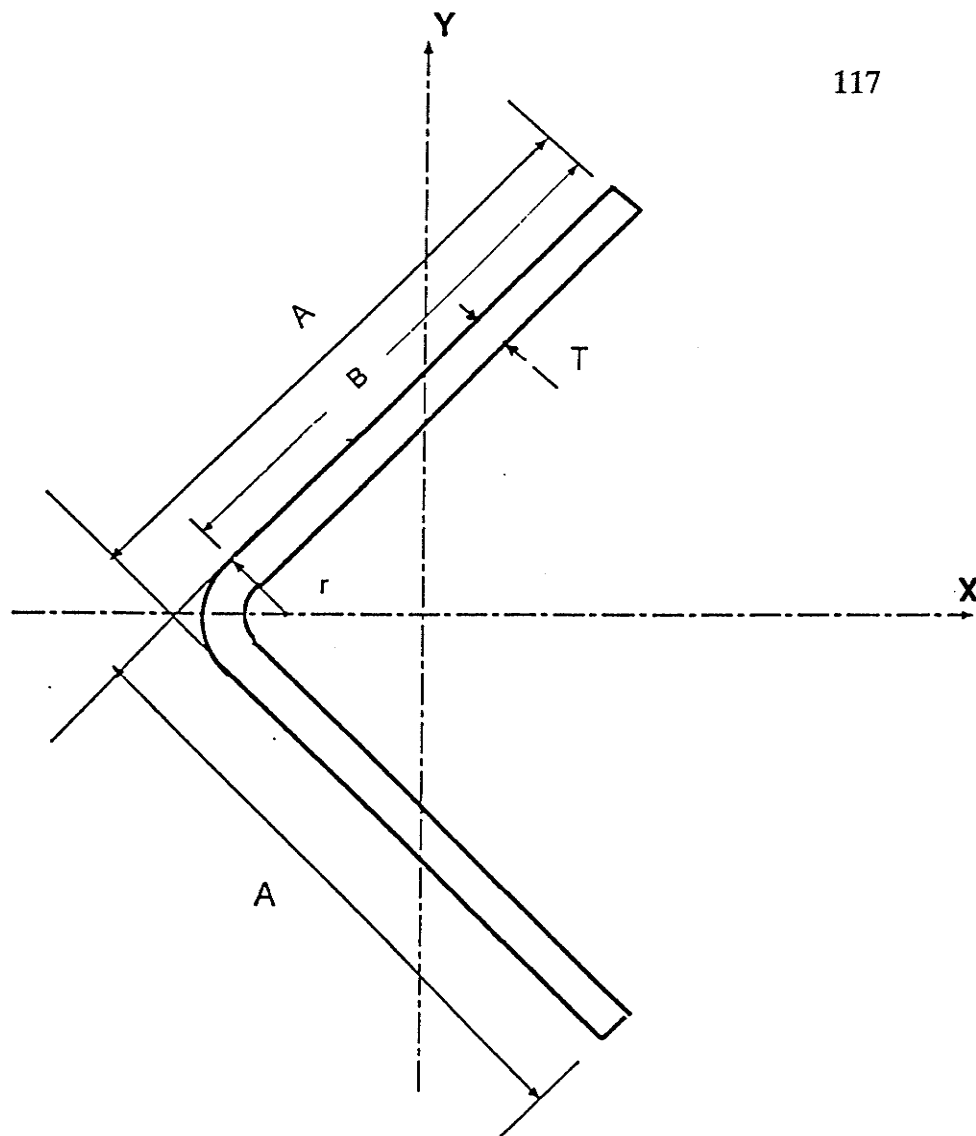


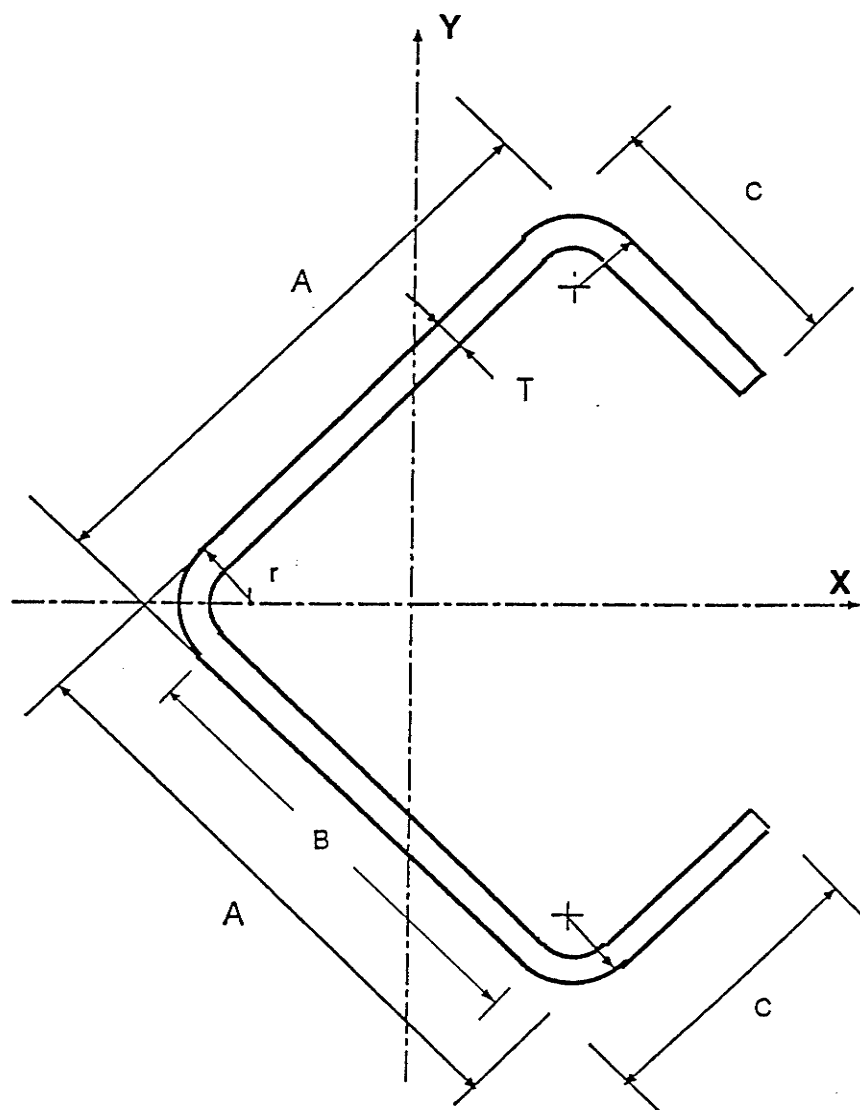
FIGURE 1.2
Member Failure in a Tower Leg



SPECIMEN	DIMENSIONS (mm) *			
	A	B	r	T
BA	71.1	60.1	11	3.95
HBA	70.7	61.9	8.8	4.5

* Galvanizing thickness deducted

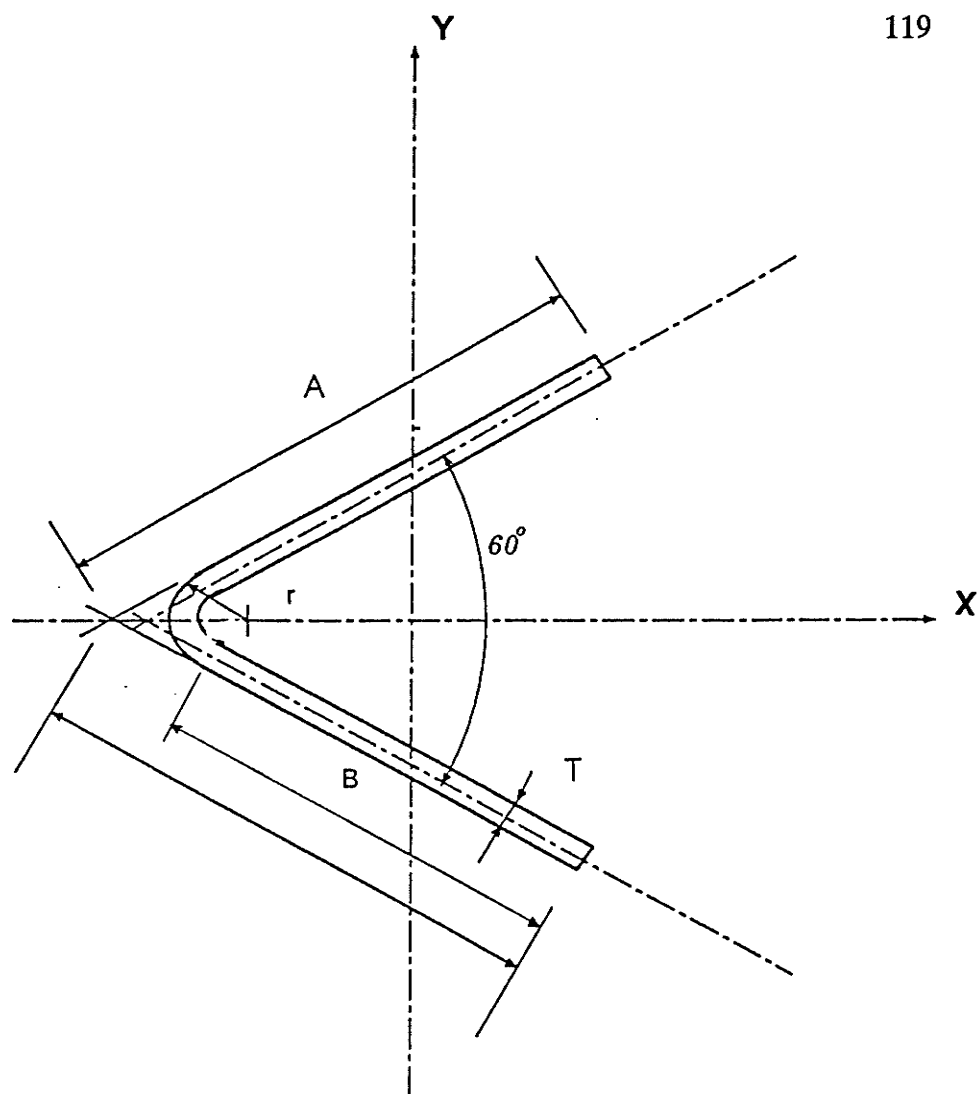
FIGURE 3.1
BA and HBA Section Measurements



SPECIMEN	DIMENSIONS (mm) *				
	A	B	C	r	T
BB	83.6	64.7	30.8	9.45	4.22
HBB	78.9	62.1	24.7	8.4	4.42

* Galvanizing thickness deducted

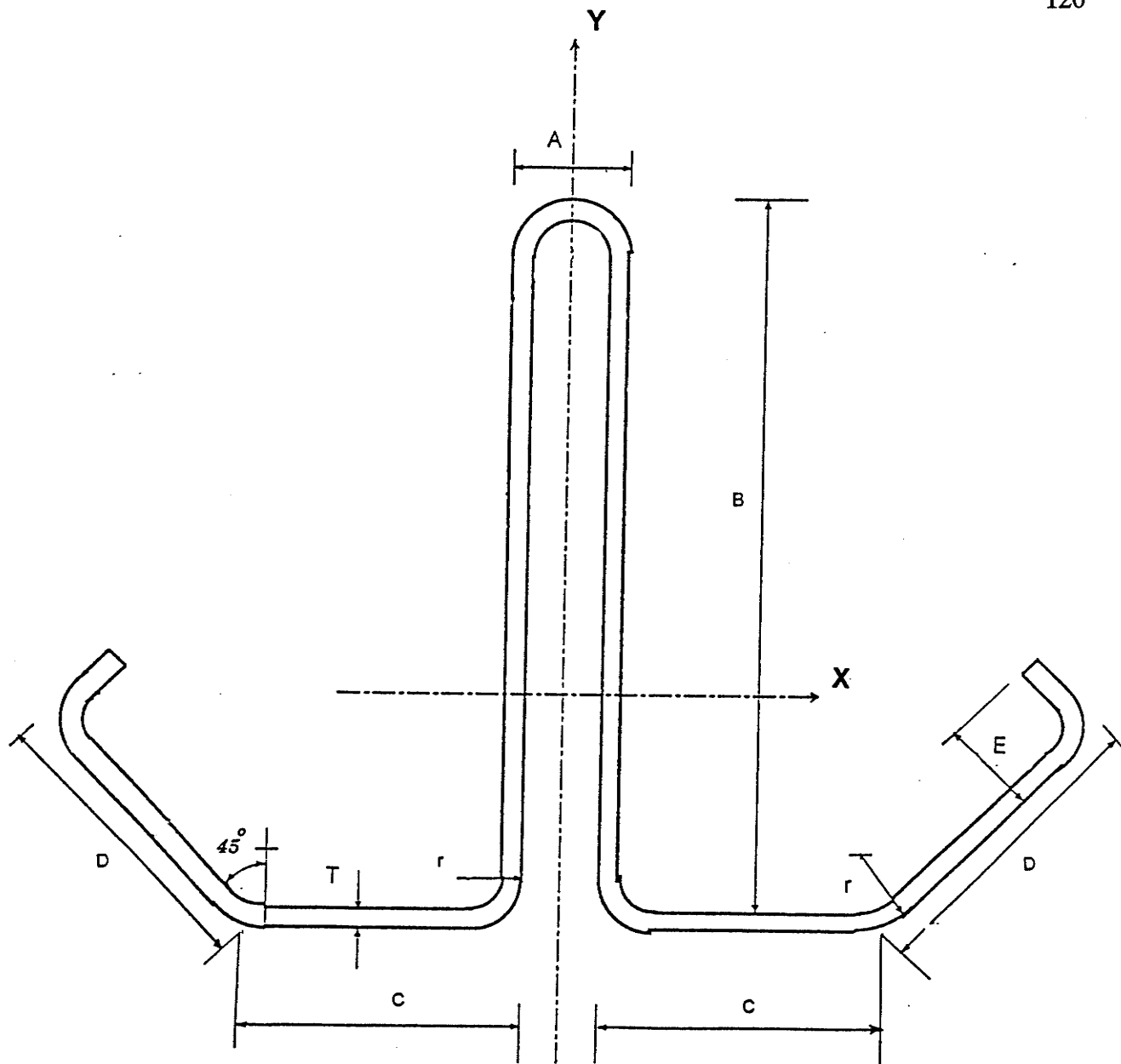
FIGURE 3.2
BB and HBB Section Measurements



SPECIMEN	DIMENSIONS (mm) *			
	A	B	r	T
BC	83.4	65.5	10.5	4.0
HBC	86.4	70.4	9.25	4.5

* Galvanizing thickness deducted

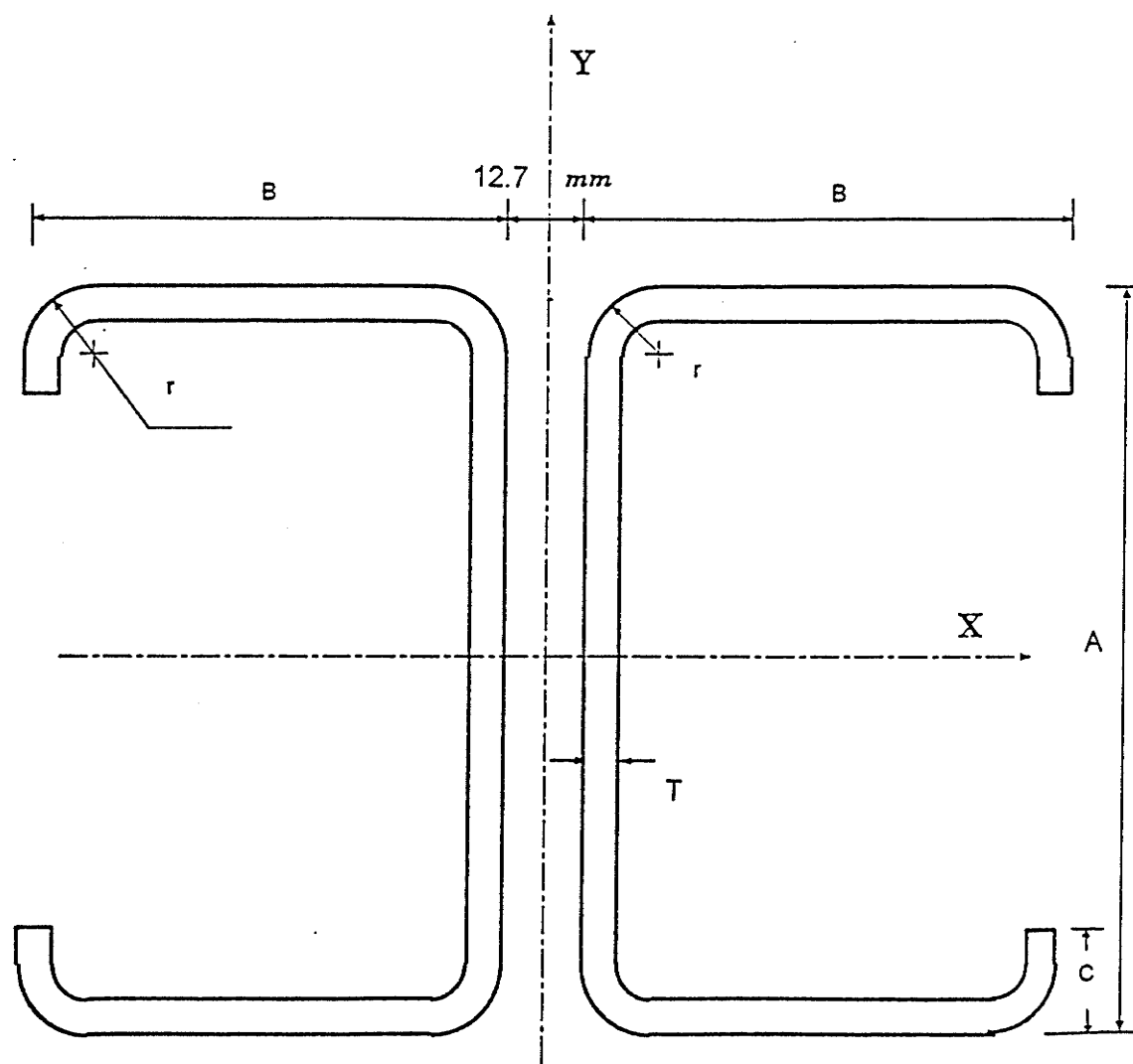
FIGURE 3.3
BC and HBC Section Measurements



SPECIMEN	DIMENSIONS (mm) *						
	A	B	C	D	E	r	T
BG	23.7	131.7	52.6	52.3	14.5	9.9	4

* Galvanizing thickness deducted

FIGURE 3.4
BG Section Measurements



SPECIMEN	DIMENSIONS (mm) *				
	A	B	C	r	T
BN	112.1	74.7	15.5	11.85	5.0
HBN	106.1	66.0	24.4	10.0	4.5

* Galvanizing thickness deducted

FIGURE 3.5
BN and HBN Section Measurements

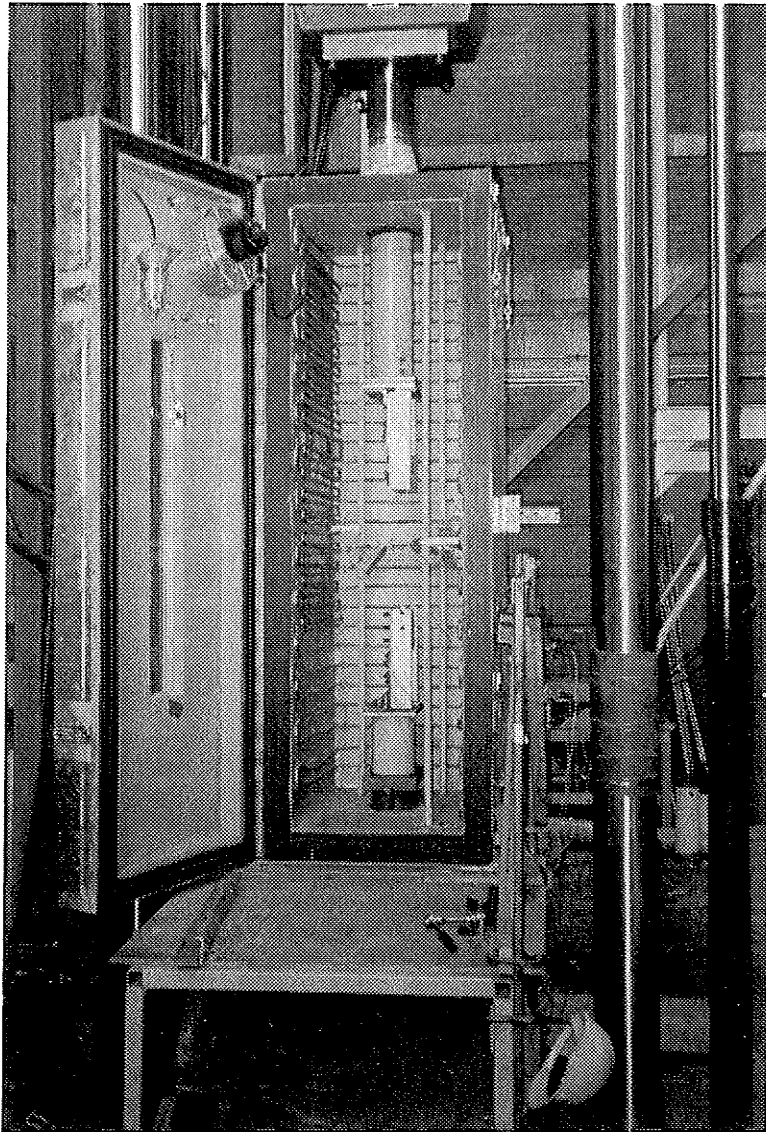


FIGURE 3.6
Test Setup No. One

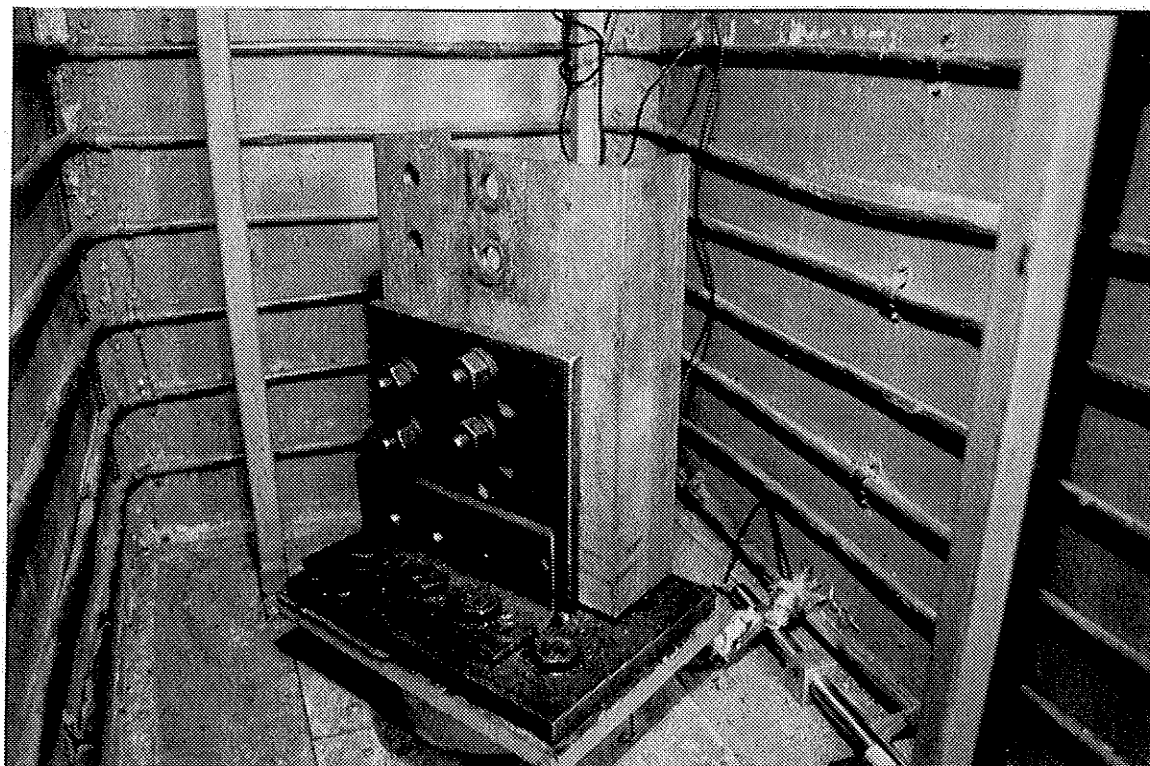
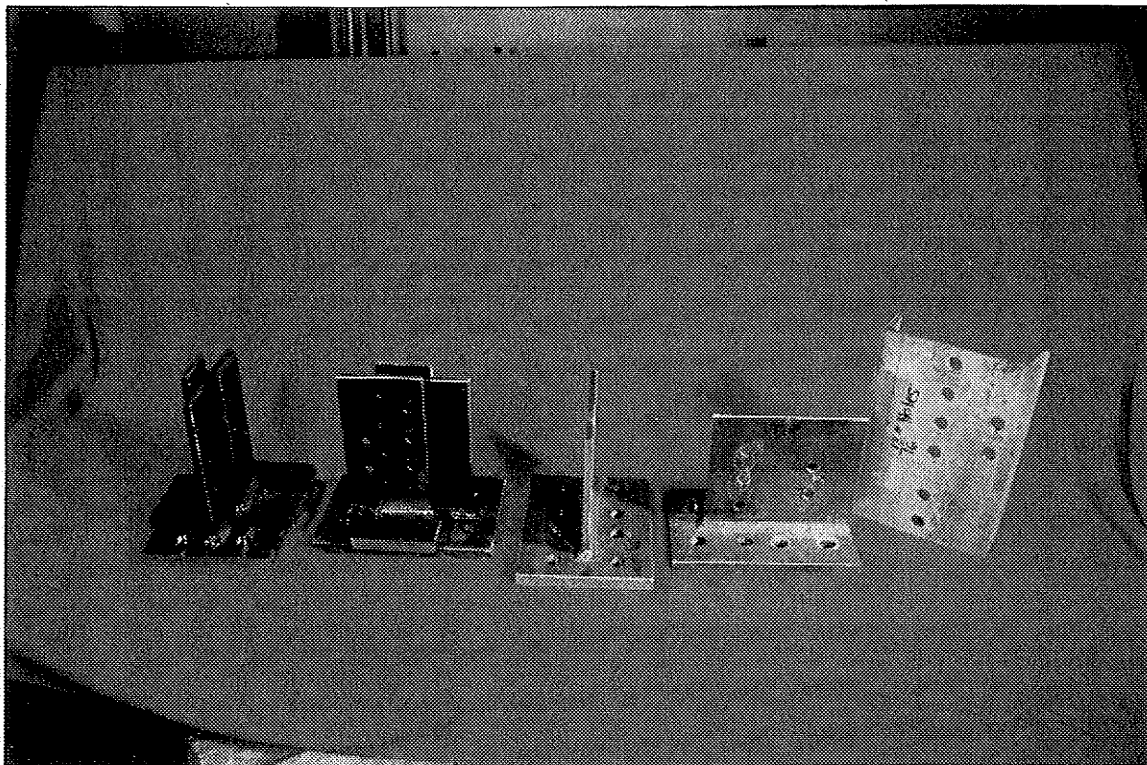


FIGURE 3.7
Typical Gusset Plates

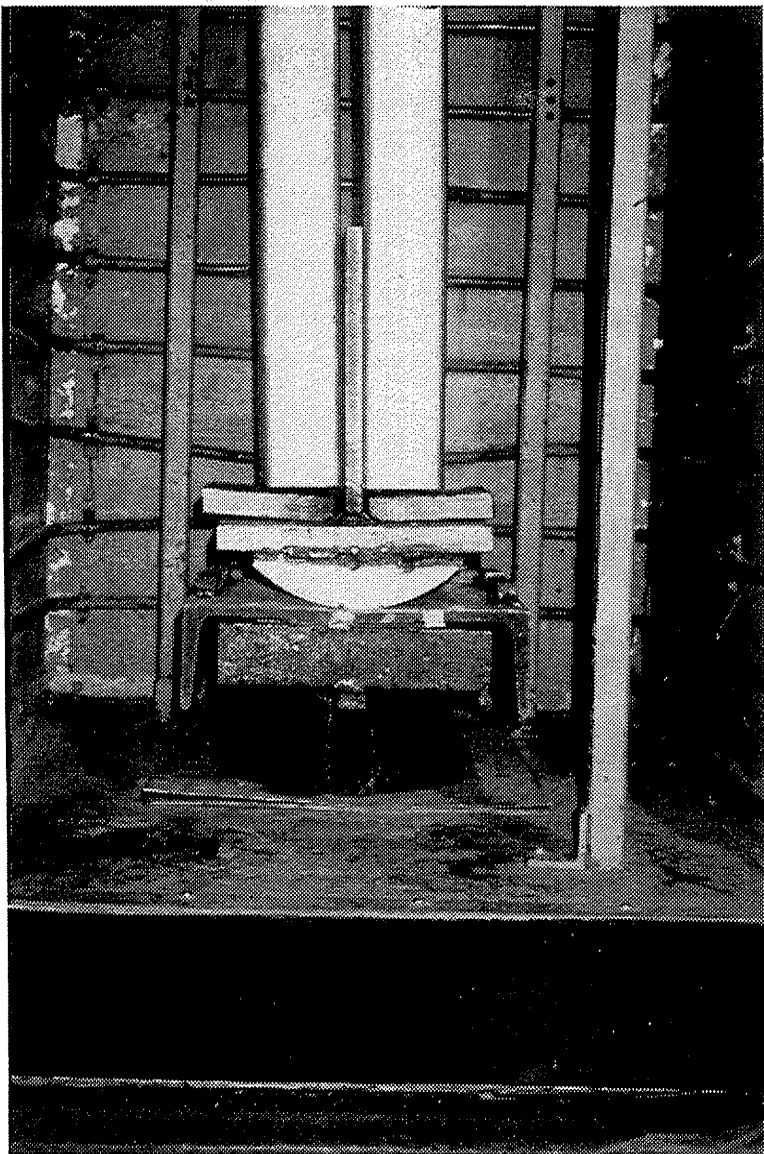


FIGURE 3.8
BN-40 End Fitting

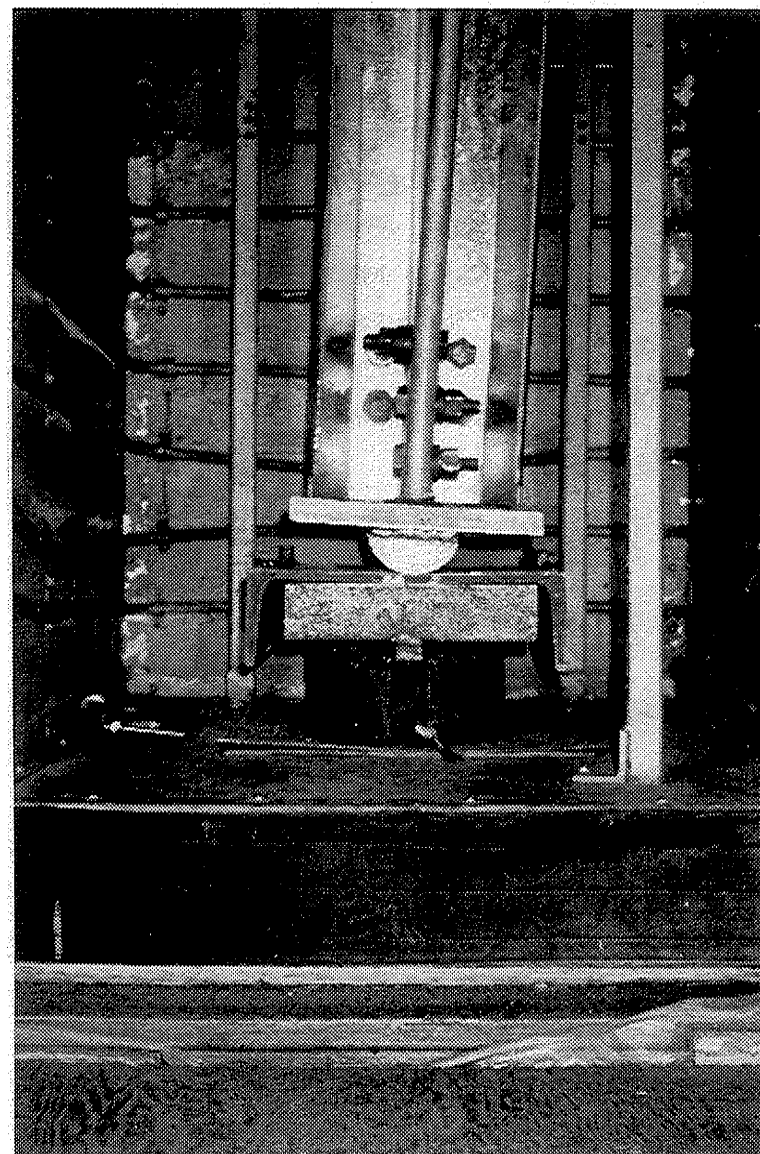


FIGURE 3.9
BG-40 End Fitting



FIGURE 3.10

Motion Transducers at MidHeight of Specimen

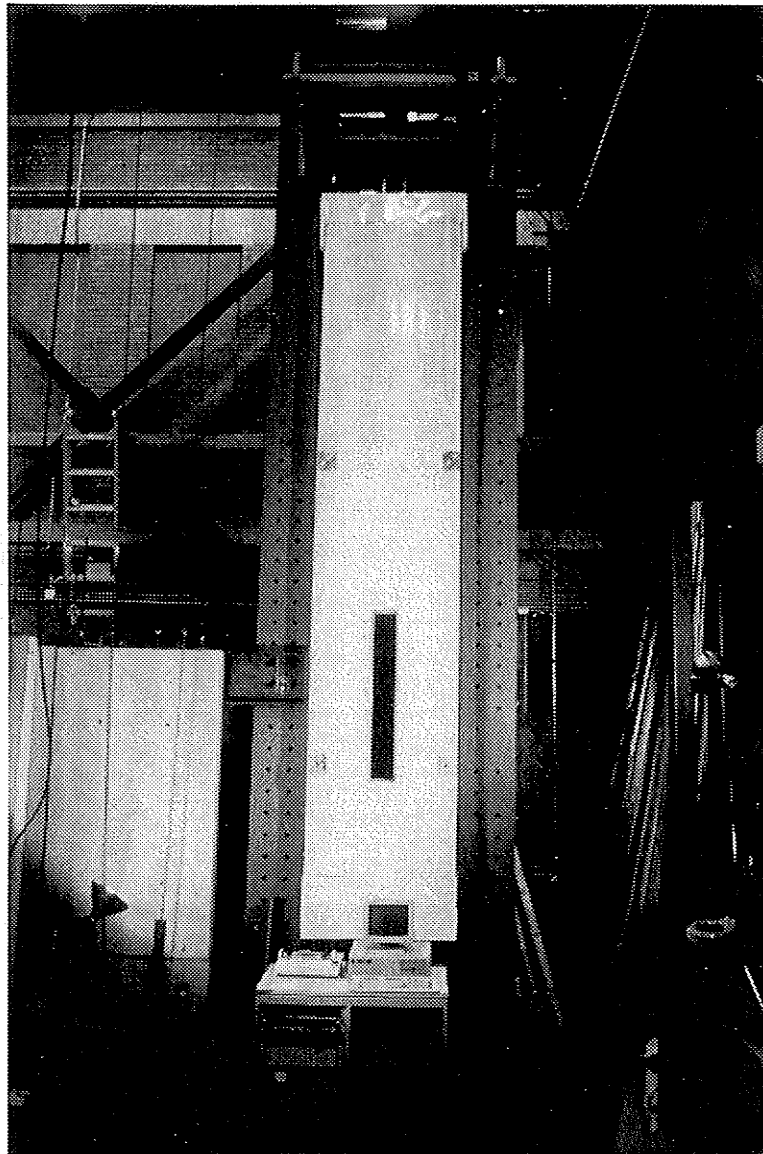


FIGURE 3.11
Setup No. 2: Cold Chamber and Load Frame

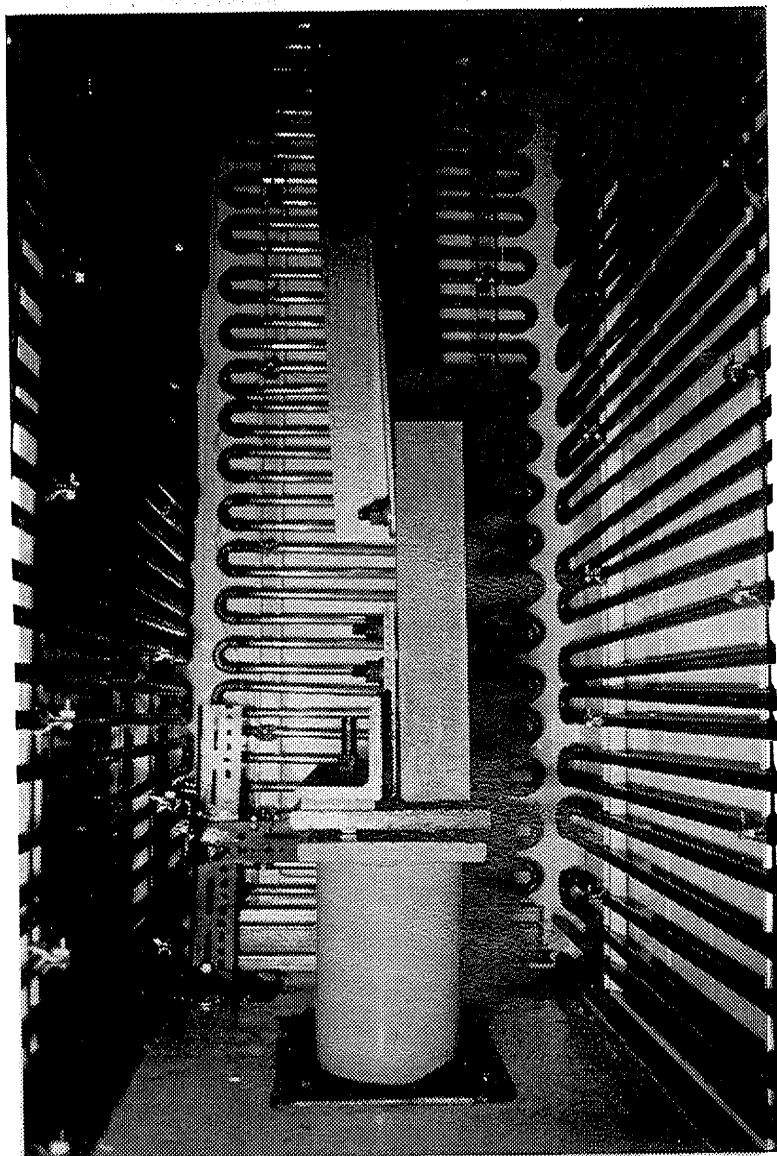


FIGURE 3.12
Setup No. 2: Typical Angle Connection

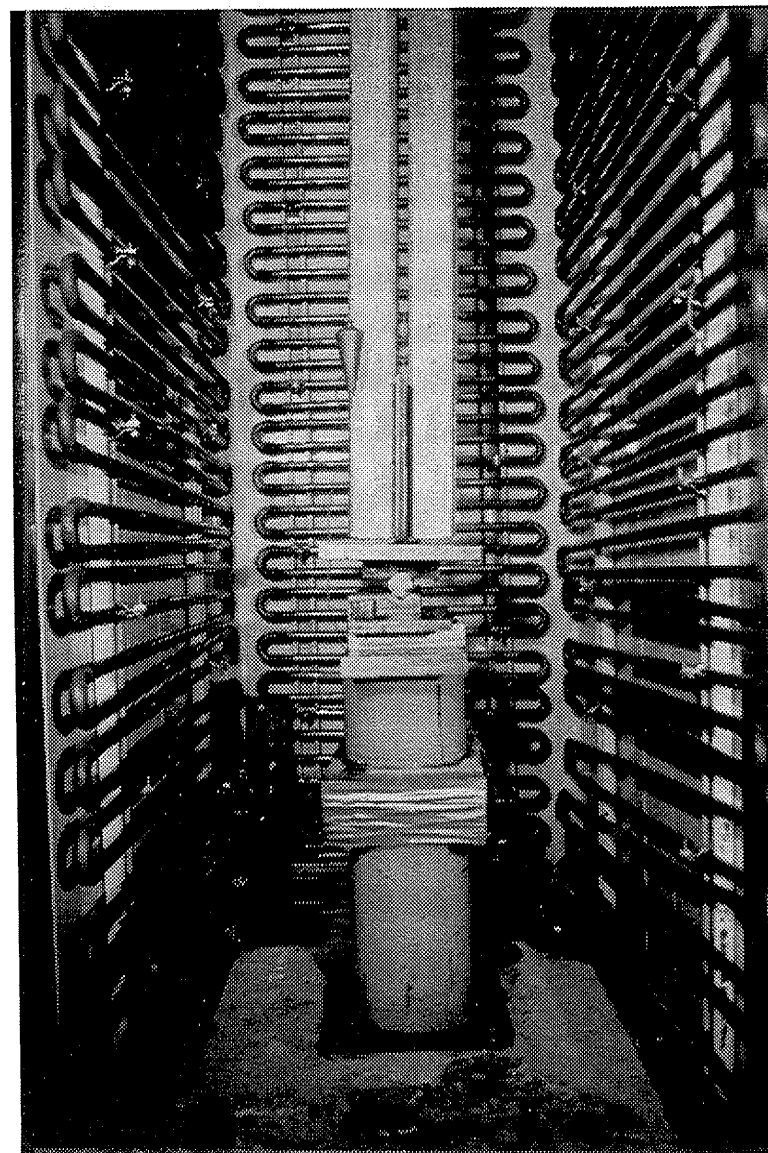


FIGURE 3.13
Setup No. 2: BN-100 End Fitting

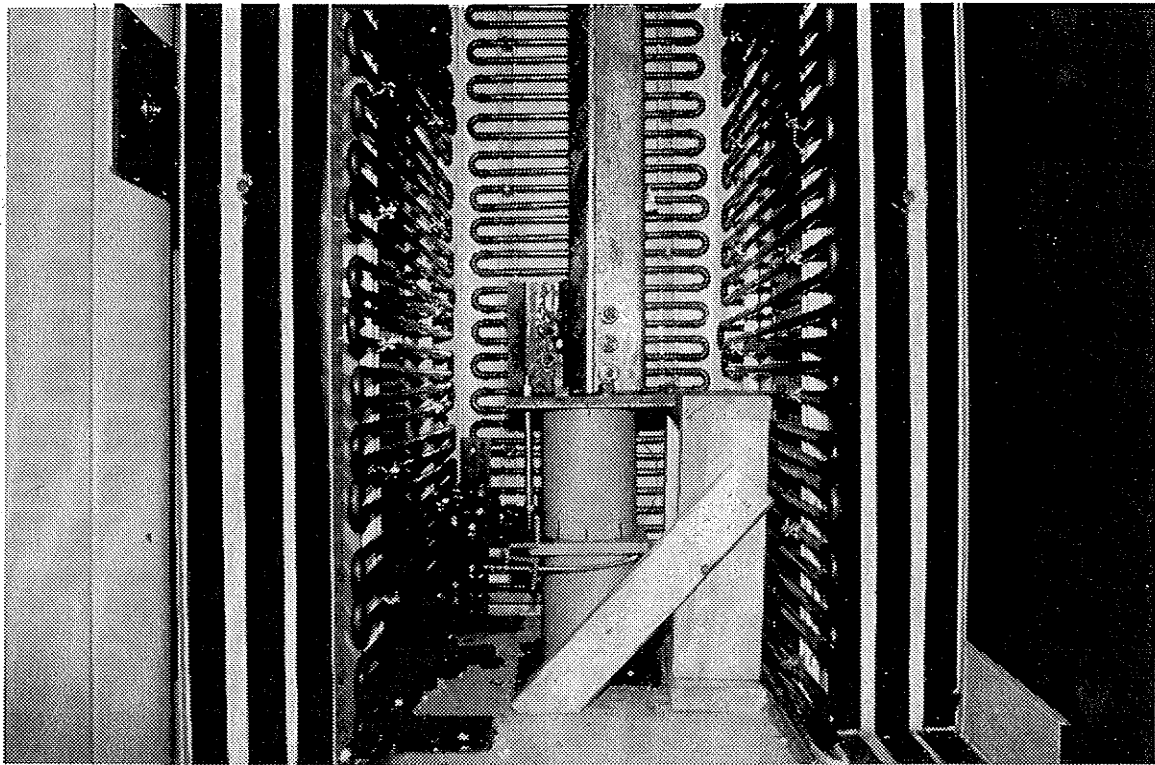


FIGURE 3.14
Setup No. 2: BG-100 End Fitting

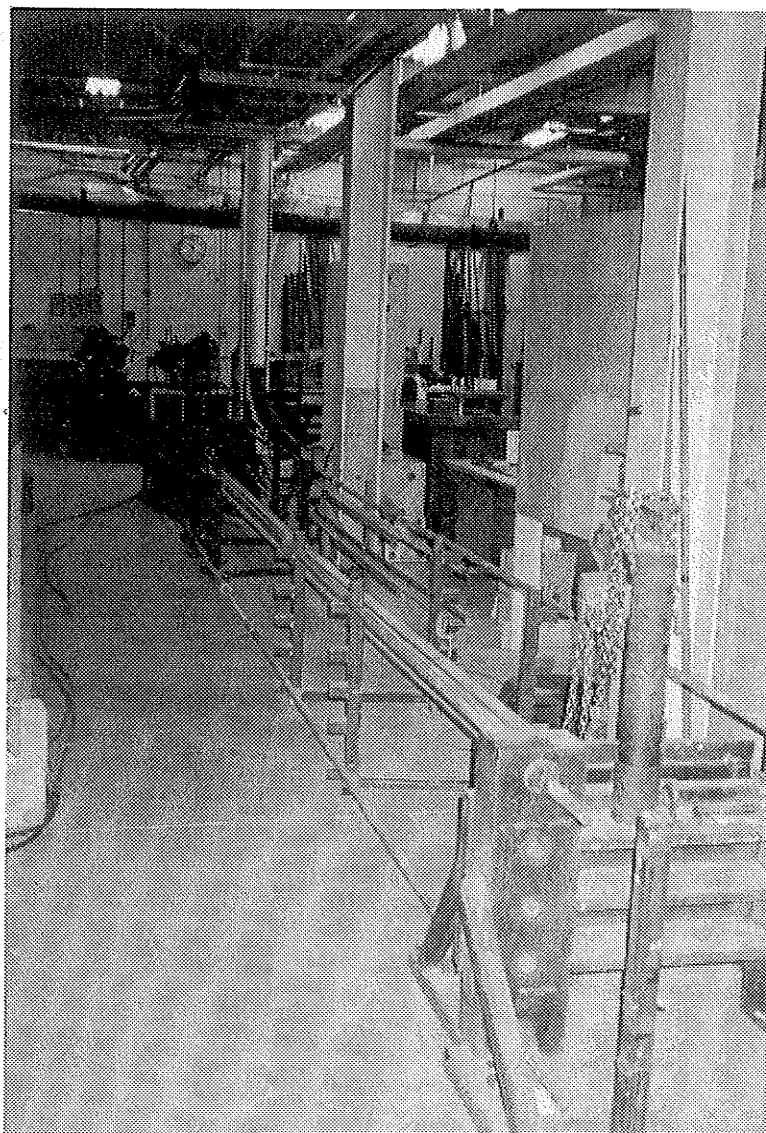


FIGURE 3.15
Setup No. 3

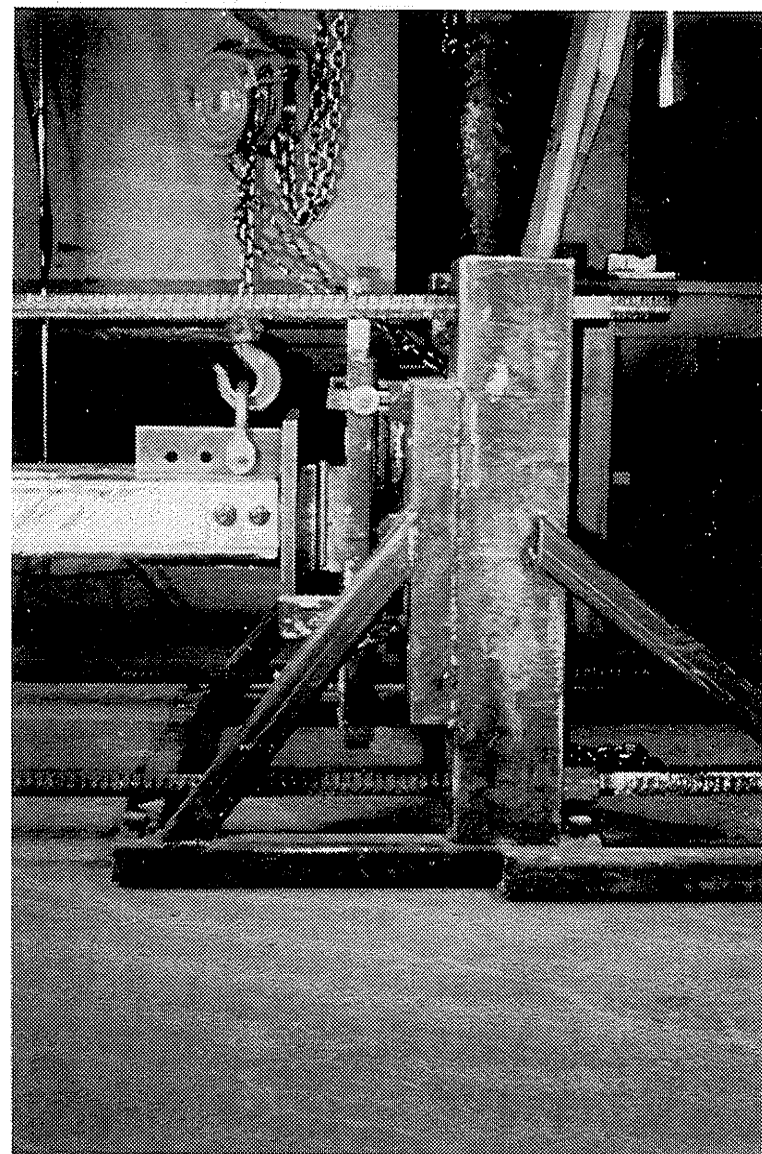
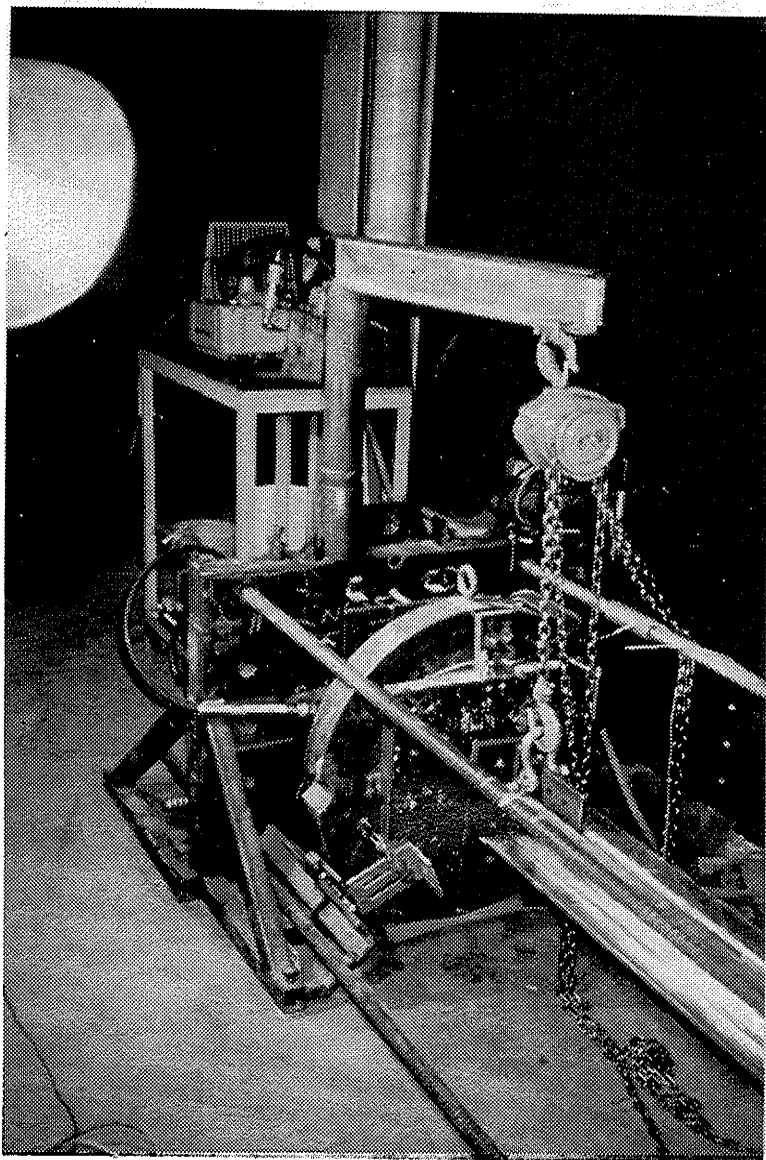


FIGURE 3.16
Setup No. 3: End Blocks

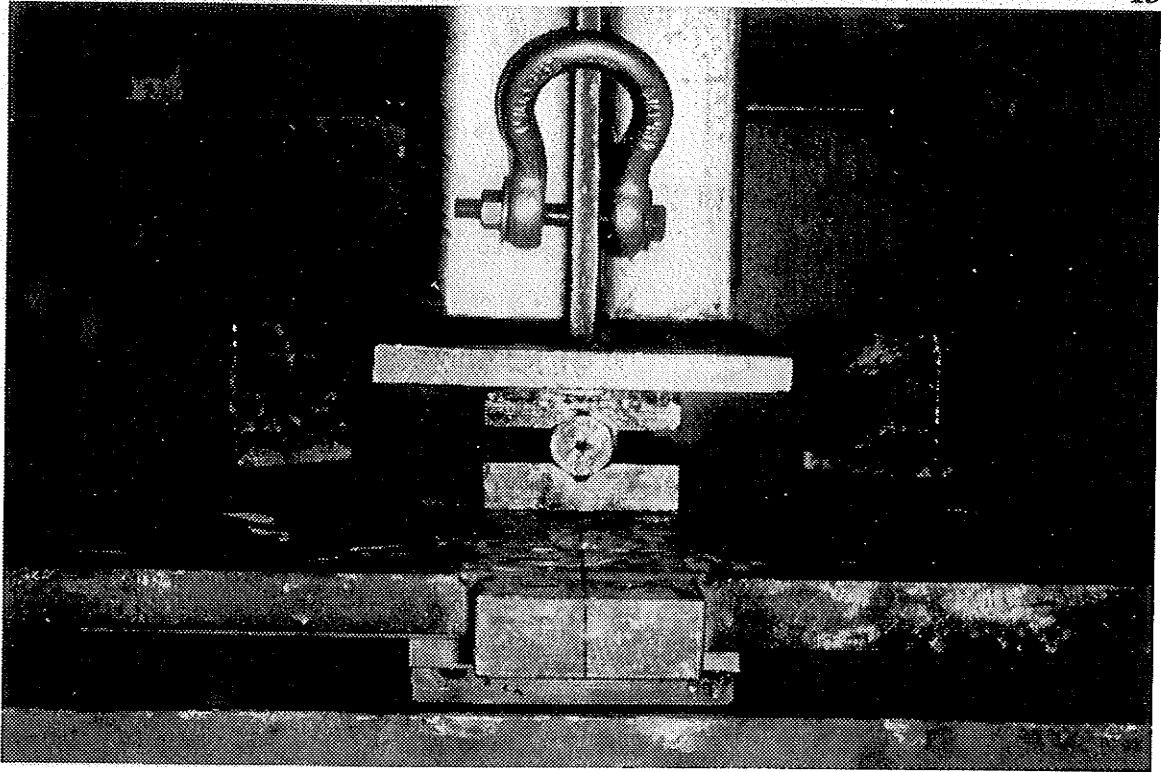


FIGURE 3.18
Setup No. 3: Gusset Plate Hinge

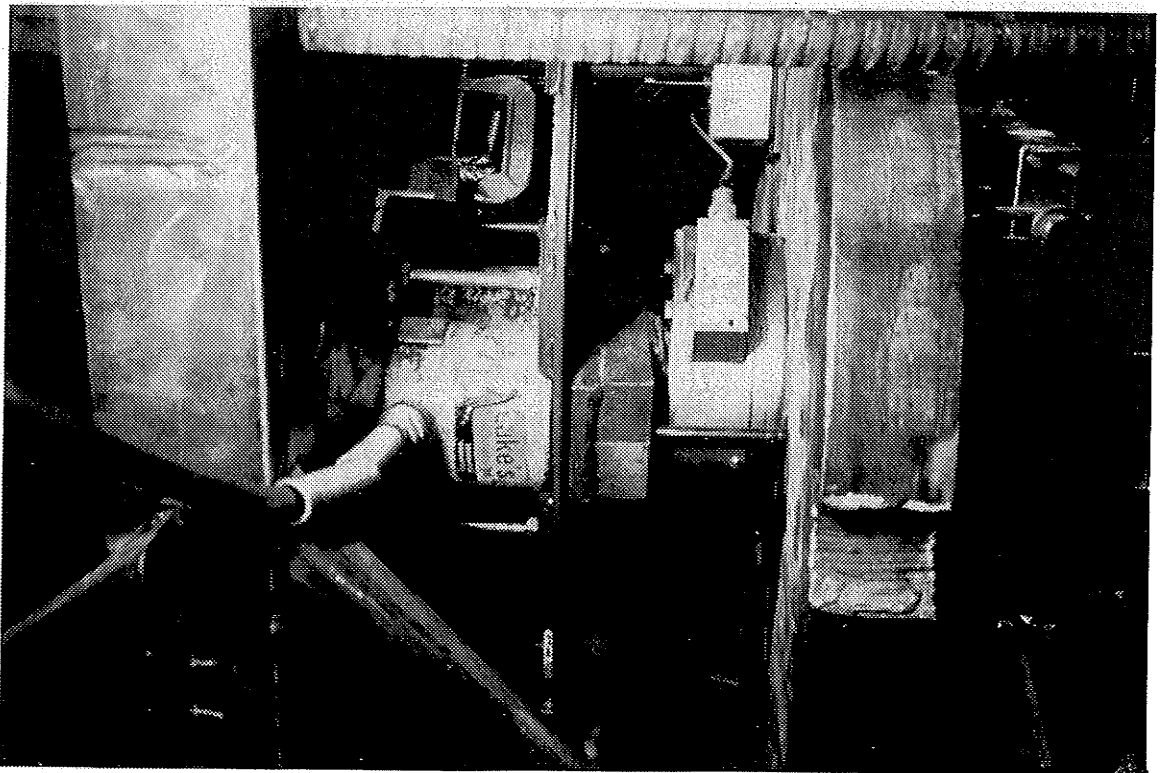


FIGURE 3.17
Setup No. 3: Jack and Load Cell

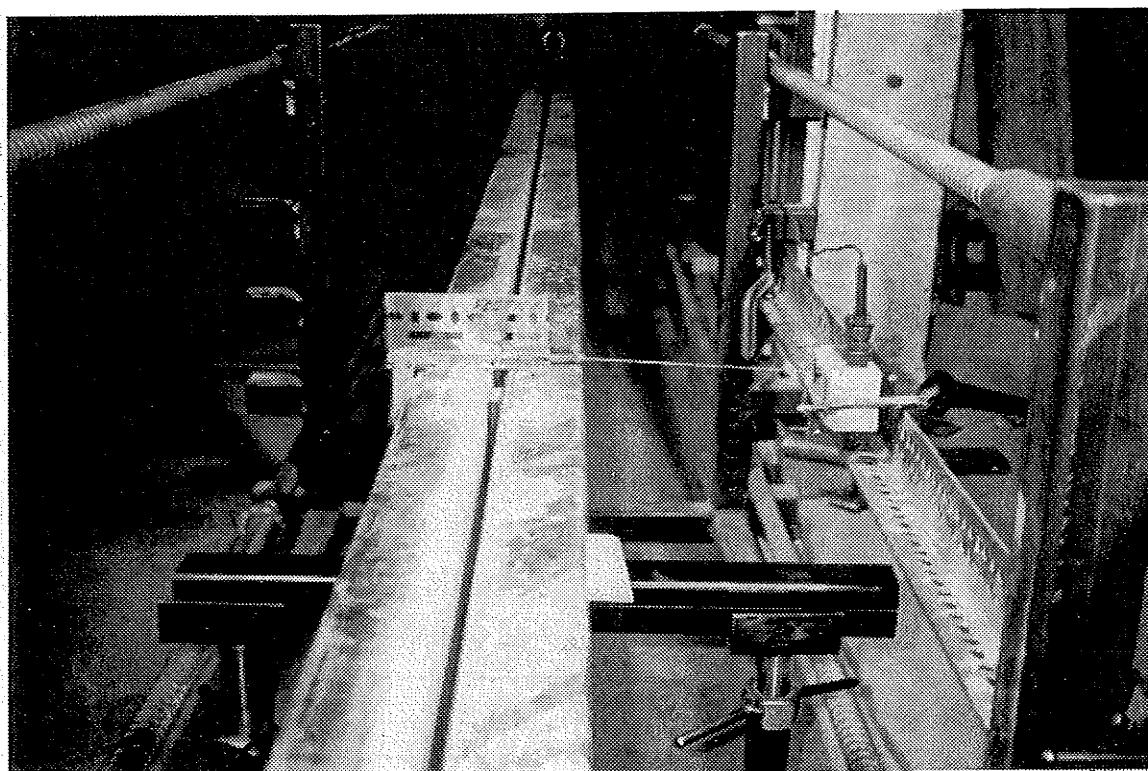


FIGURE 3.19
Setup No. 3: Motion Transducer at Midlength

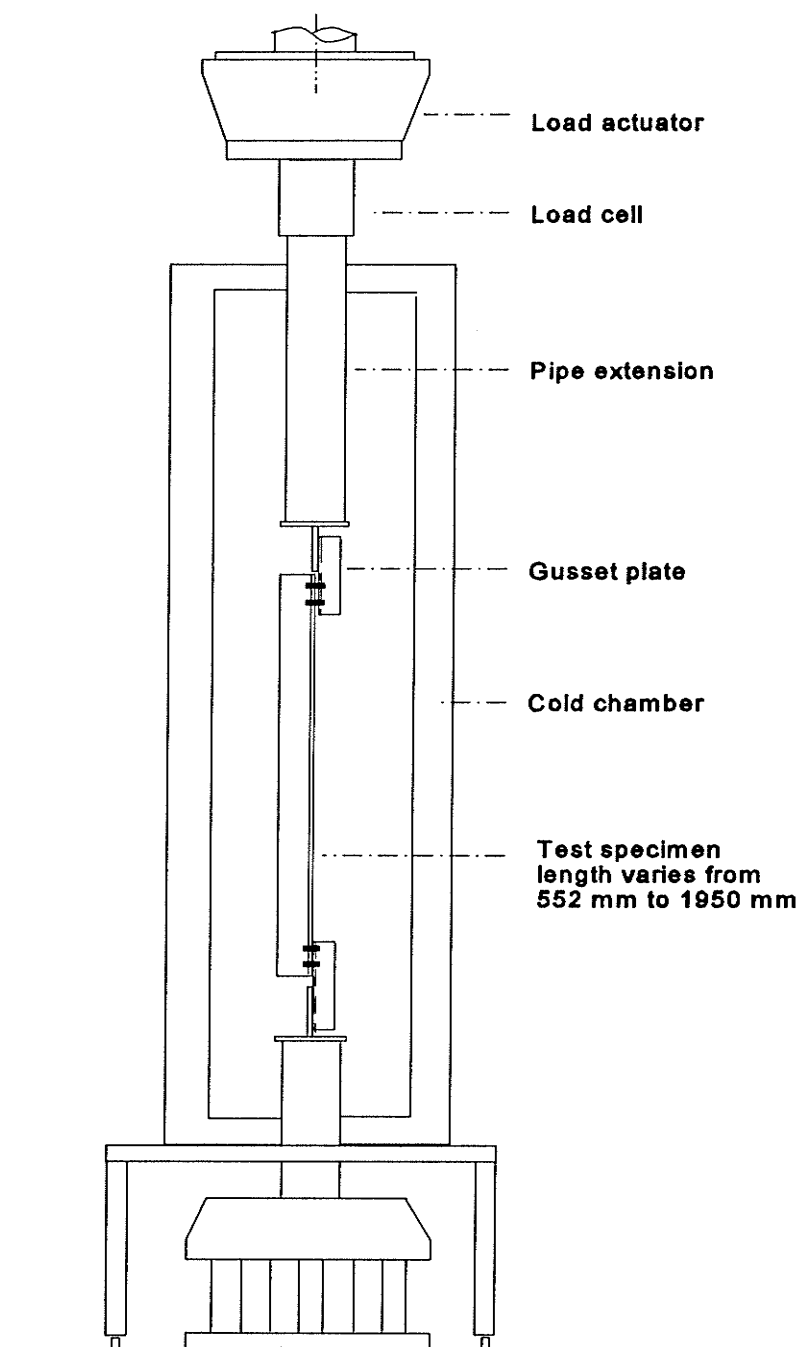


Figure 3.20 Schematic of Setup No. 1

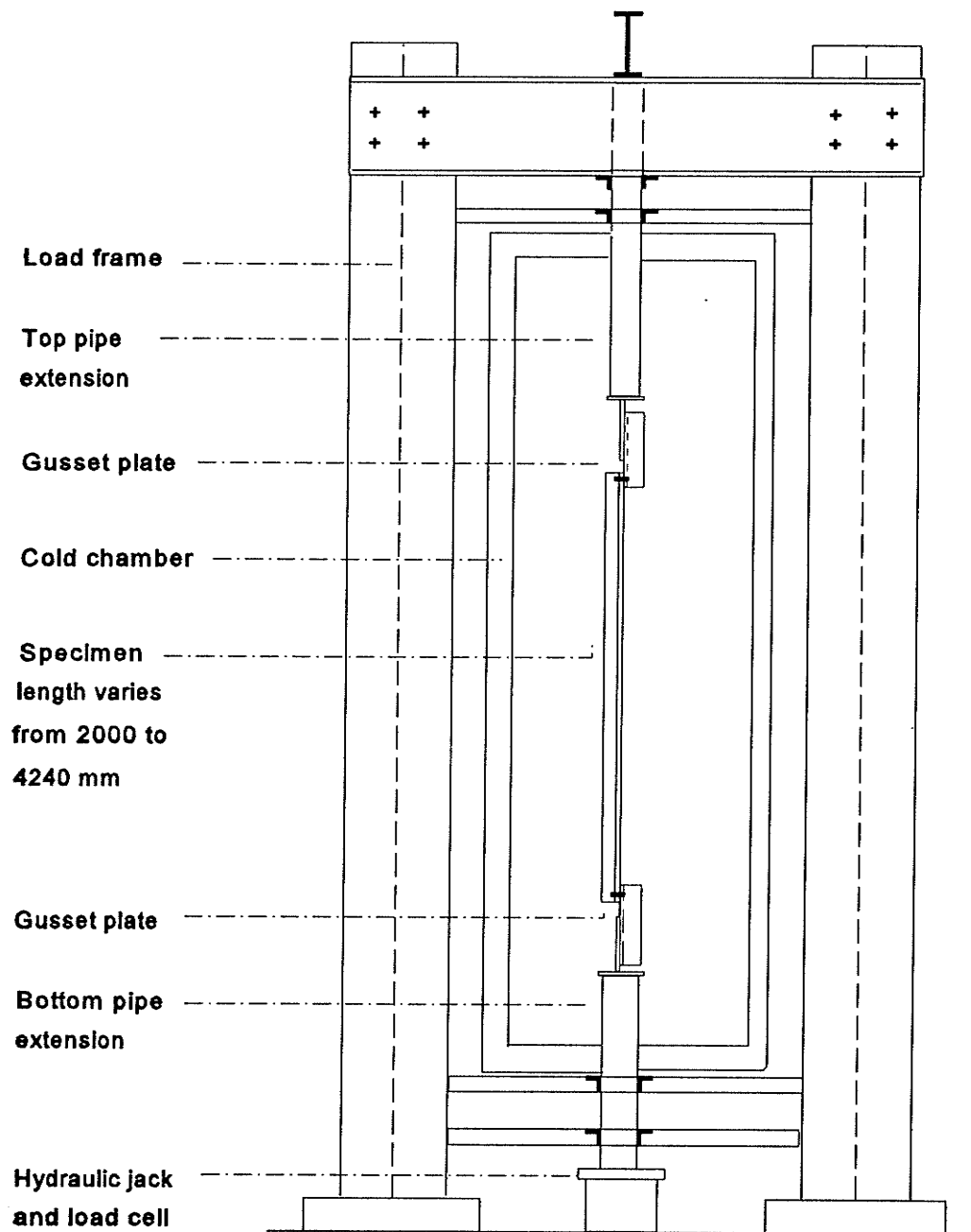


Figure 3.21 Schematic of Test Setup No. 2

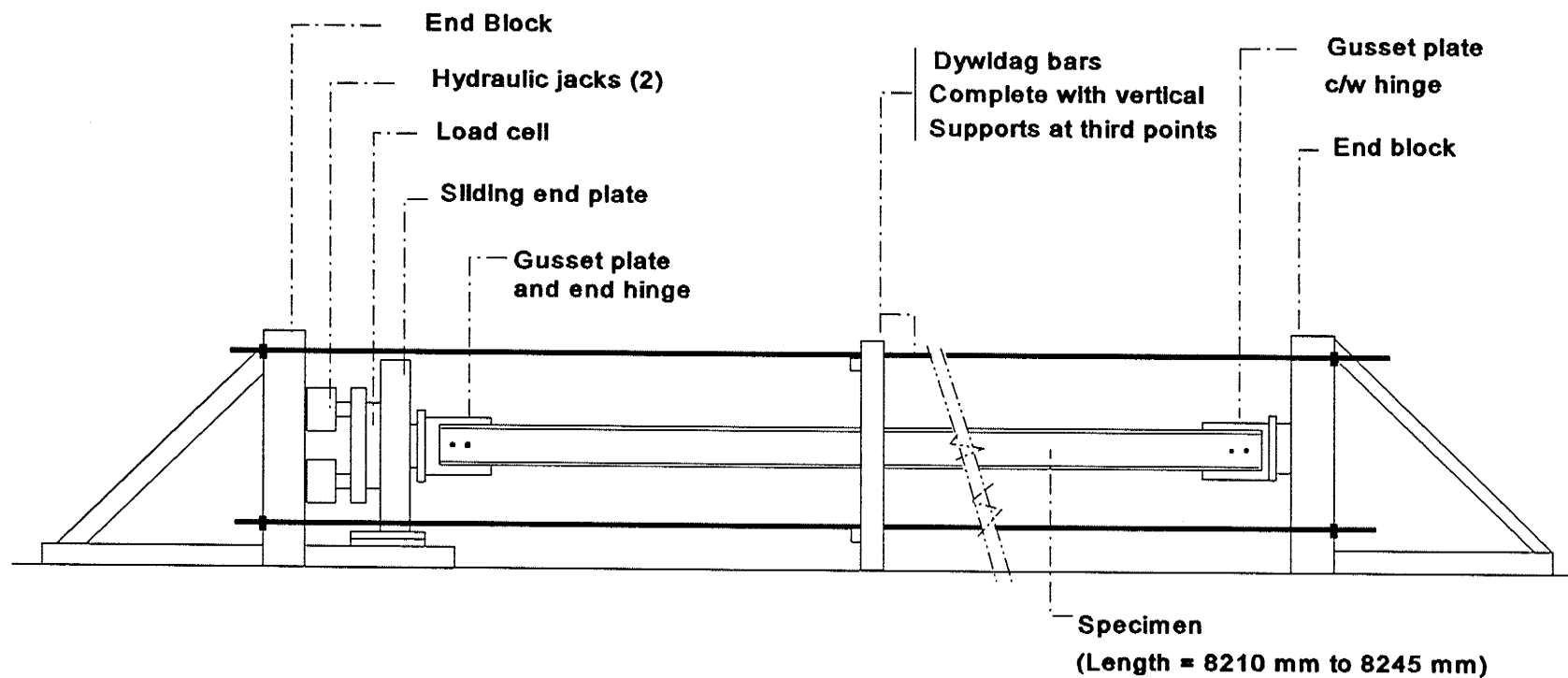


Figure 3.22 Schematic of Setup No. 3

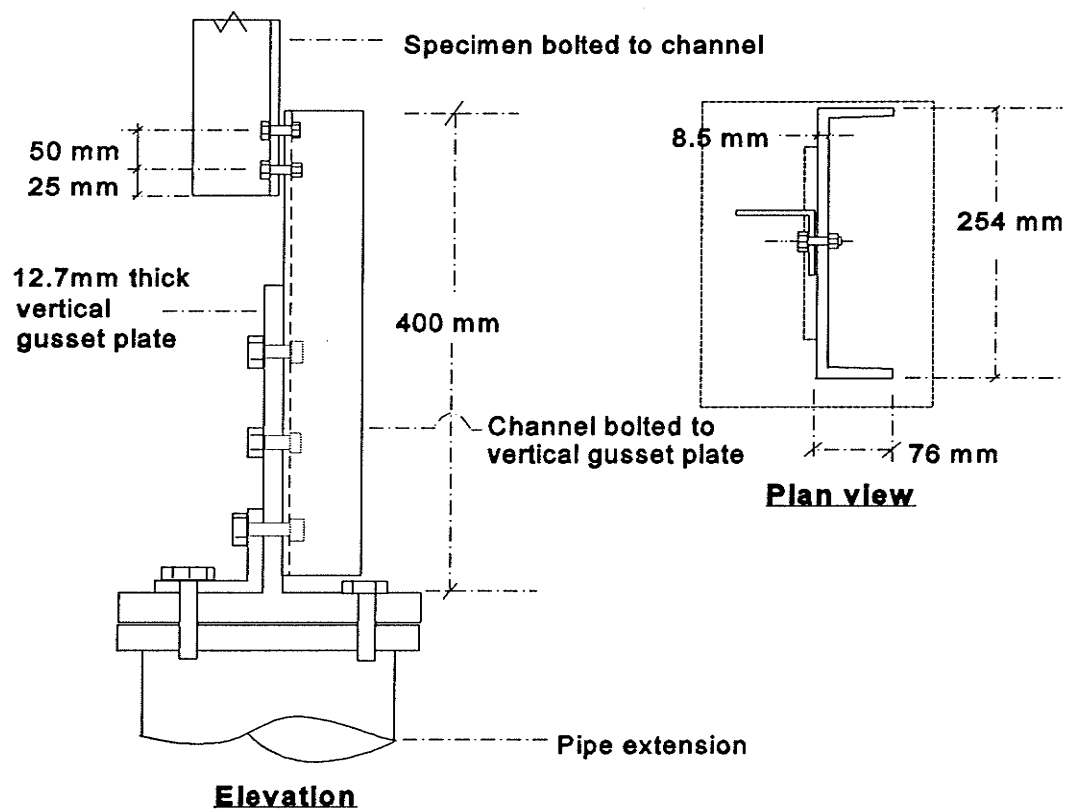


Figure 3.23 Schematic of Gusset Plate for Angle Connections

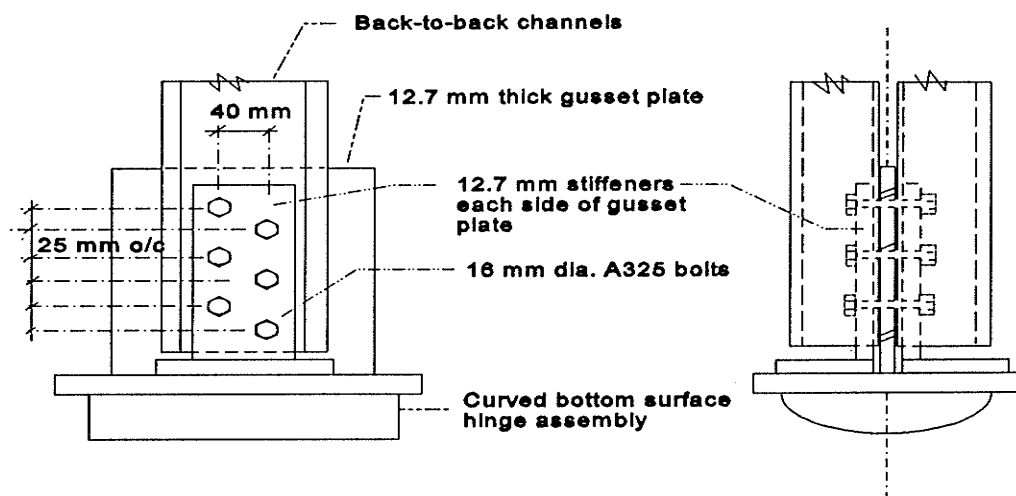


Figure 3.24 Schematic of (H)BN Gusset Plate: Setup No. 1

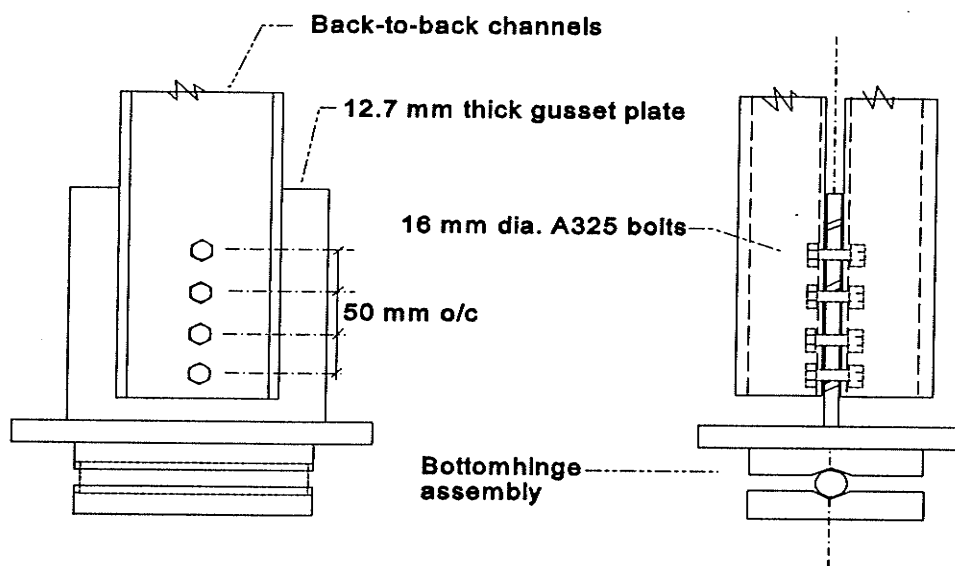


Figure 3.25 Schematic of (H)BN Gusset Plate: Setup No. 2 & No. 3

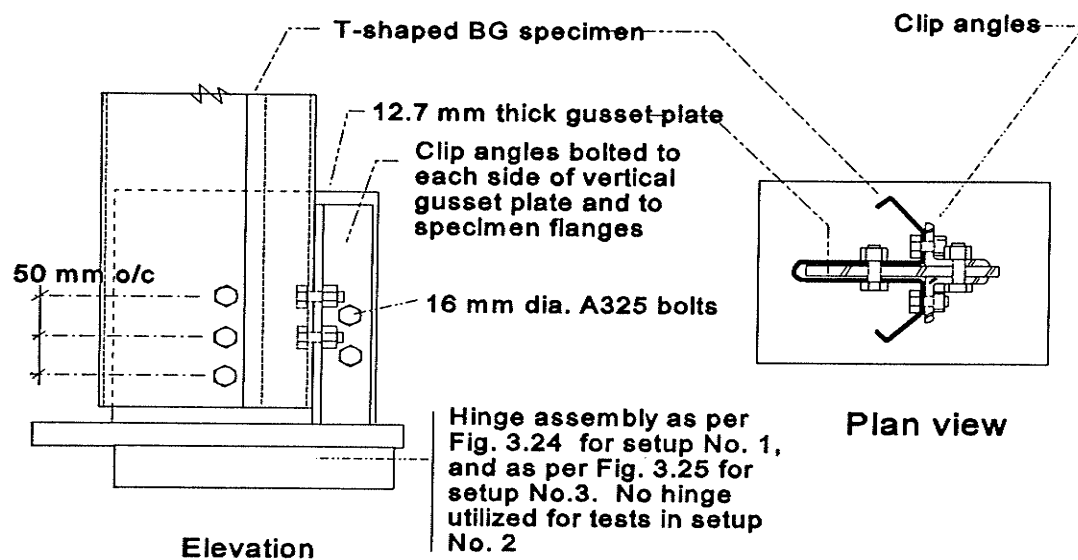


Figure 3.26 Schematic of Gusset Plate for BG Connections

BA SECTION TEST RESULTS .VS. TEMPERATURE

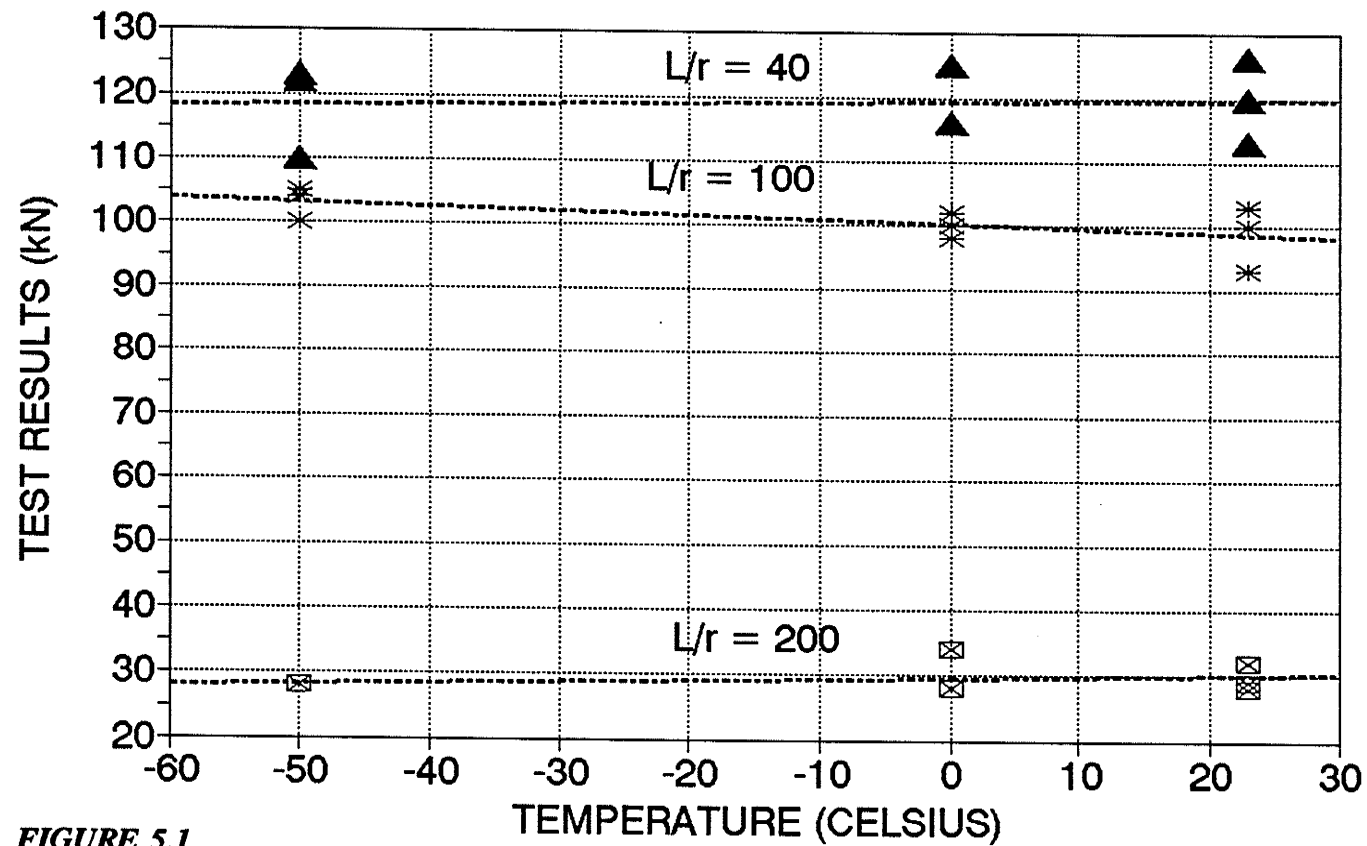


FIGURE 5.1
Load vs. Temperature - BA Section

HBA SECTION TEST RESULTS .VS. TEMPERATURE

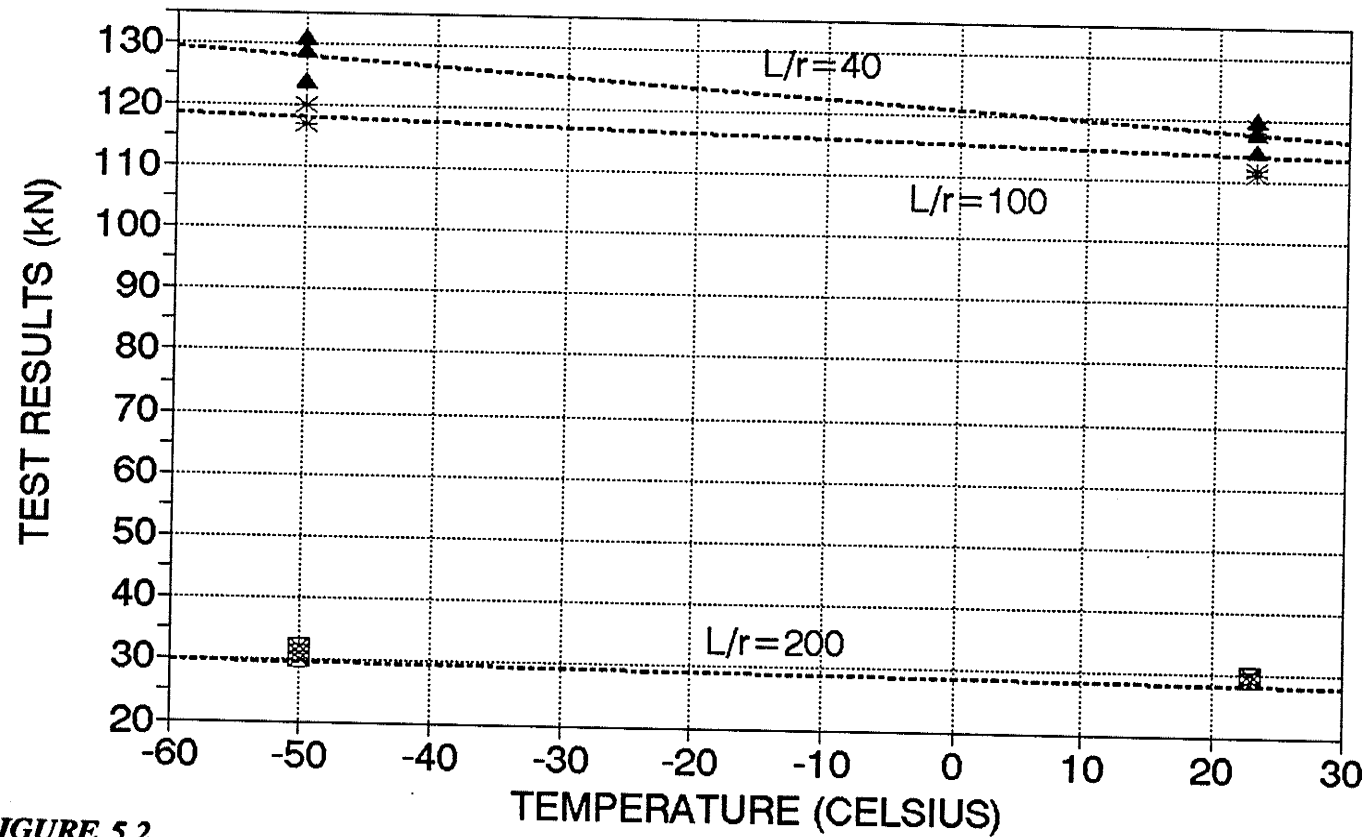


FIGURE 5.2
Load vs. Temperature - HBA Section

BB SECTION TEST RESULTS .VS. TEMPERATURE

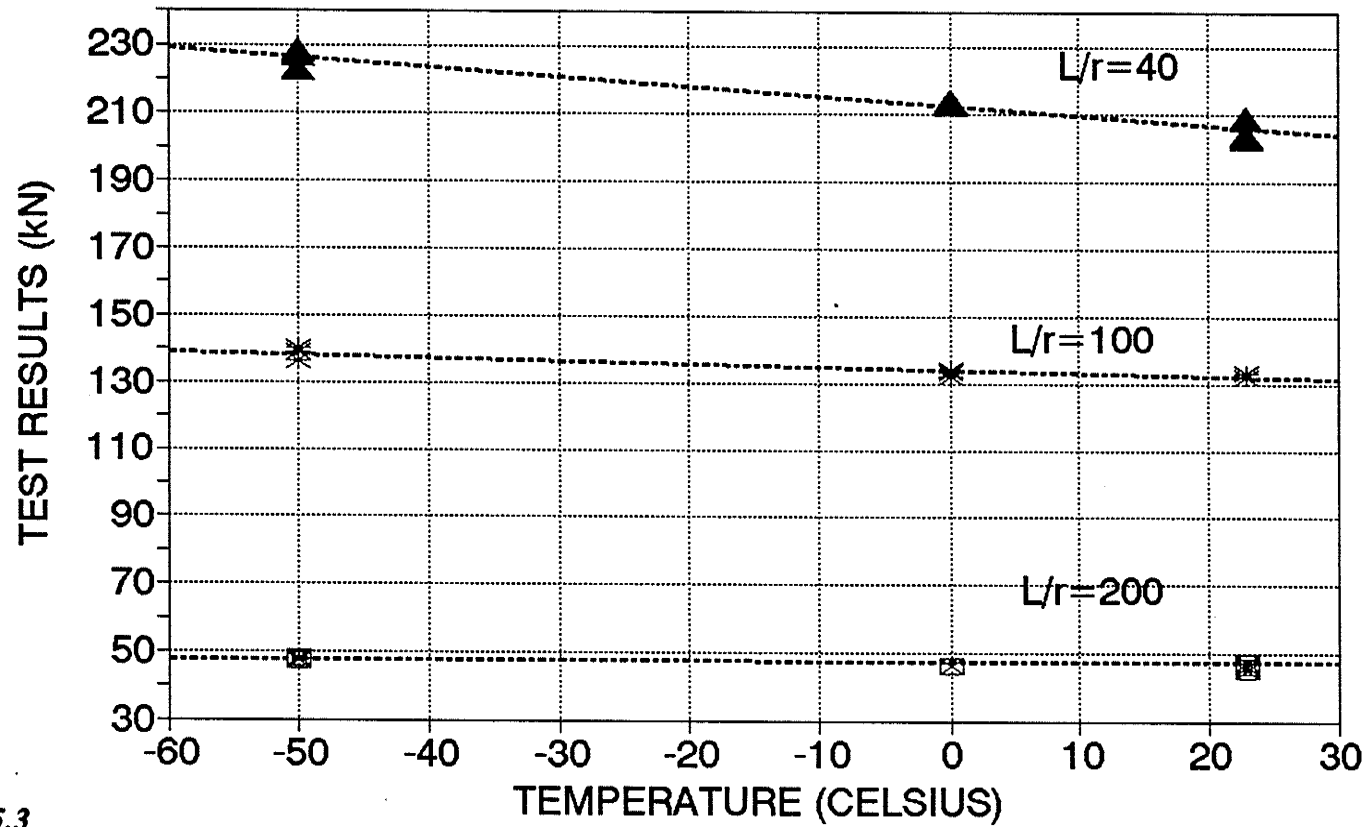


FIGURE 5.3
Load vs. Temperature - BB Section

HBB SECTION TEST RESULTS .VS. TEMPERATURE

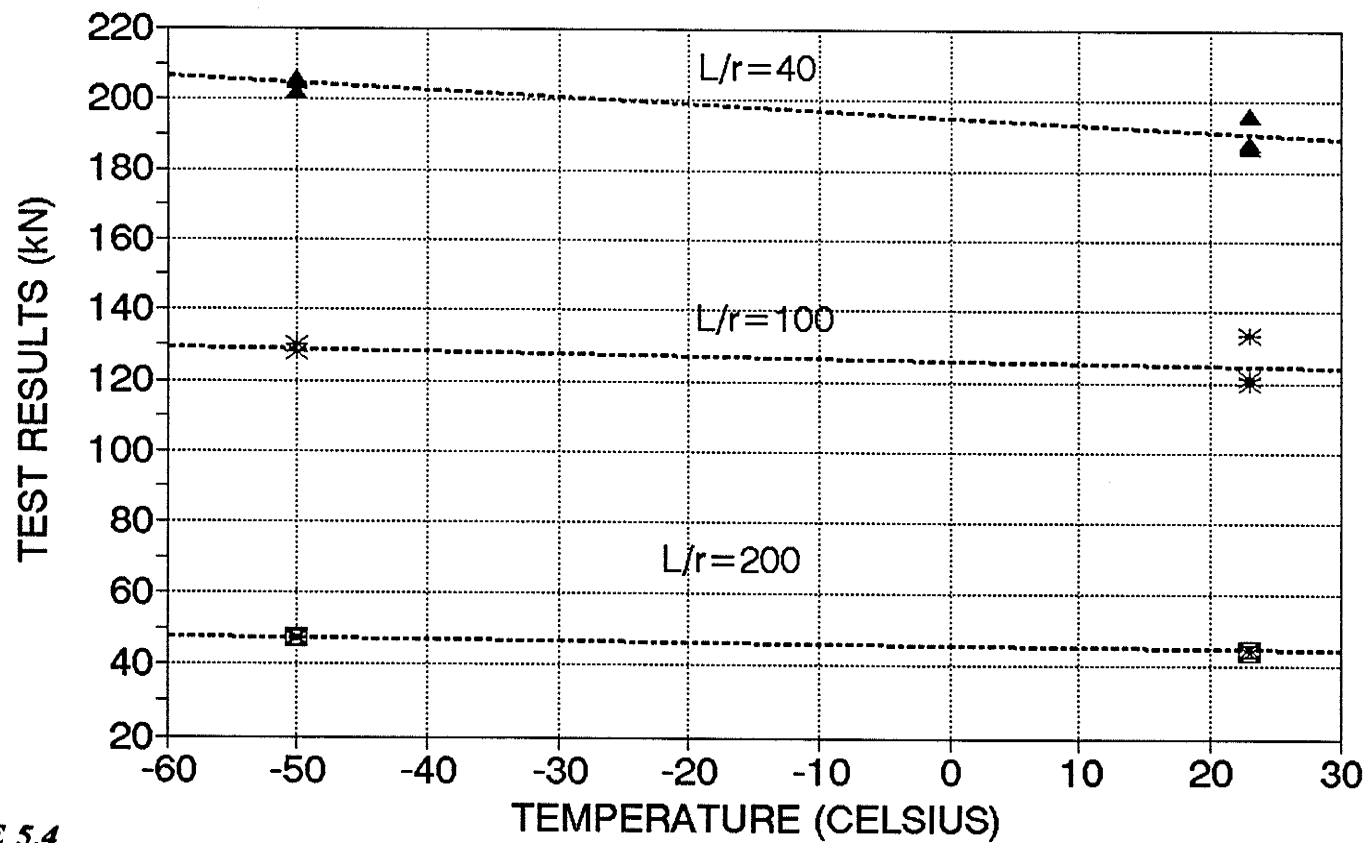


FIGURE 5.4
Load vs. Temperature - HBB Section

BC SECTION TEST RESULTS .VS. TEMPERATURE

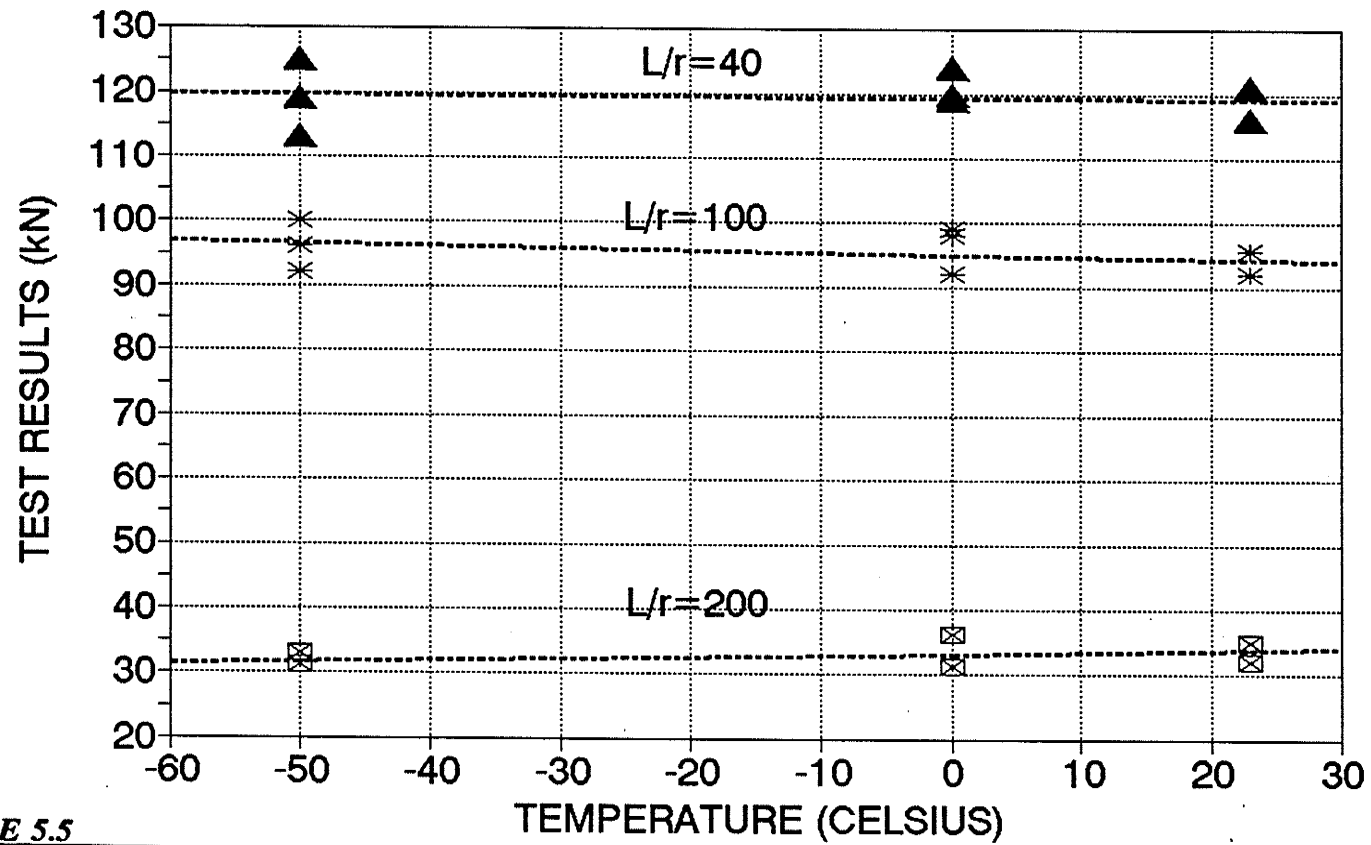


FIGURE 5.5
Load vs. Temperature - BC Section

HBC SECTION TEST RESULTS .VS. TEMPERATURE

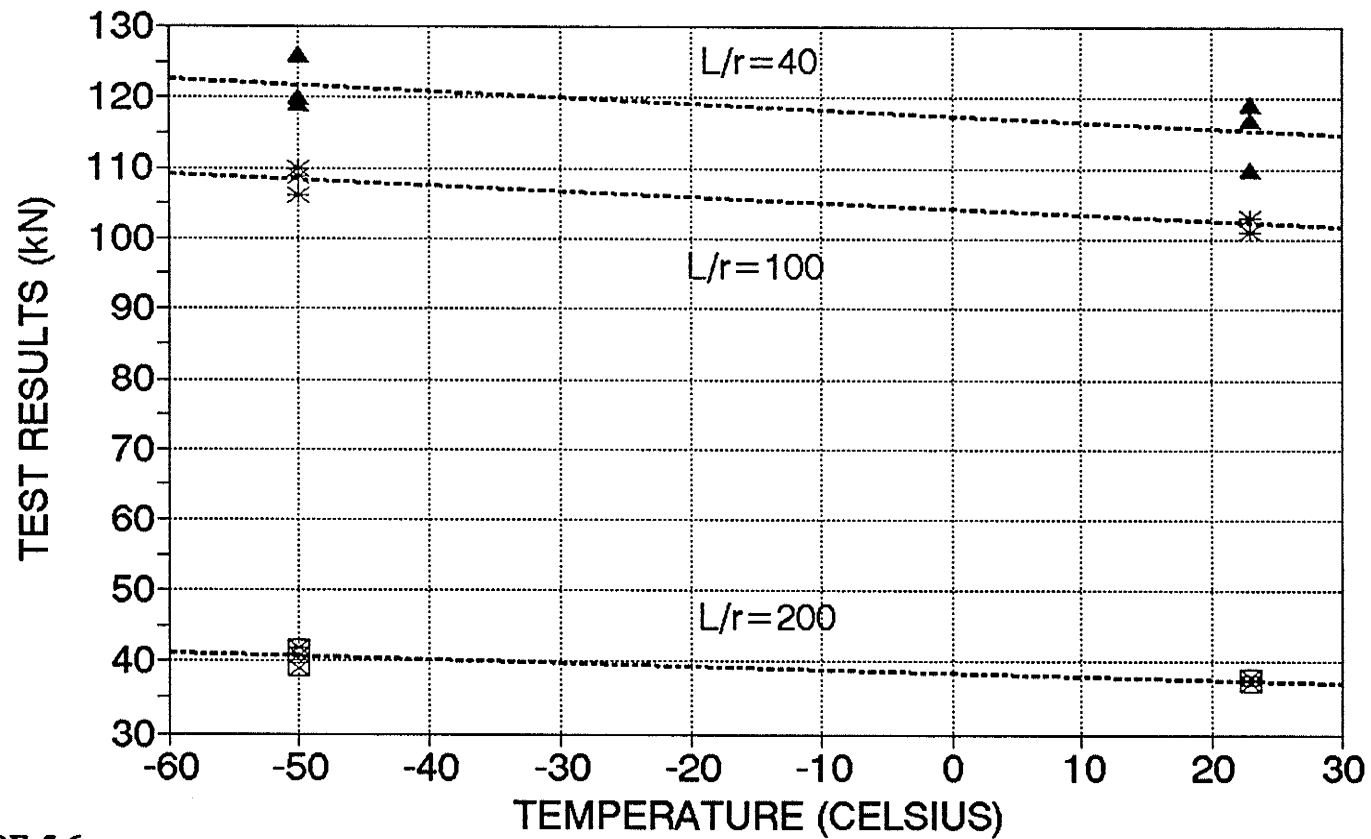


FIGURE 5.6
Load vs. Temperature - HBC Section

BG SECTION TEST RESULTS .VS. TEMPERATURE

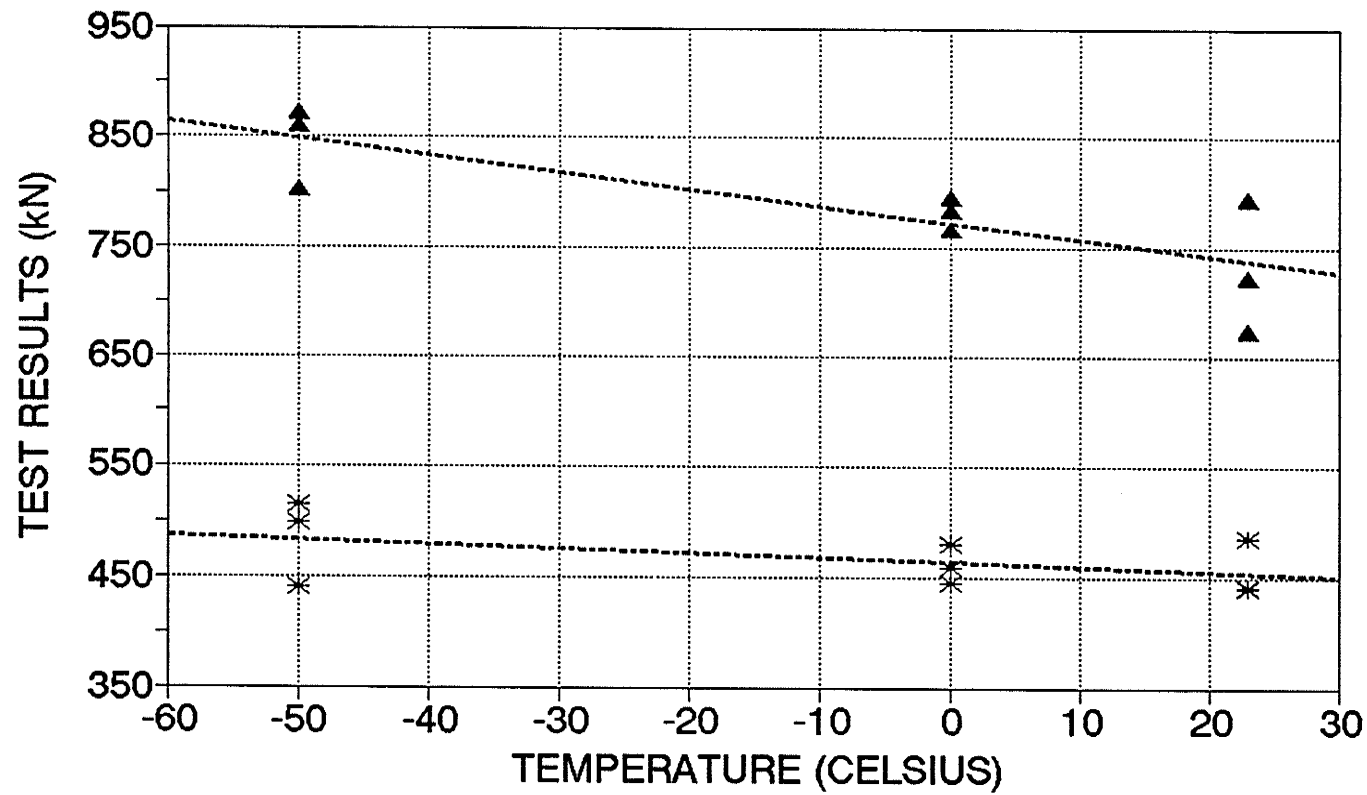


FIGURE 5.7
Load vs. Temperature - BG Section

▲ $L/r = 40$ * $L/r = 100$

BN SECTION TEST RESULTS .VS. TEMPERATURE

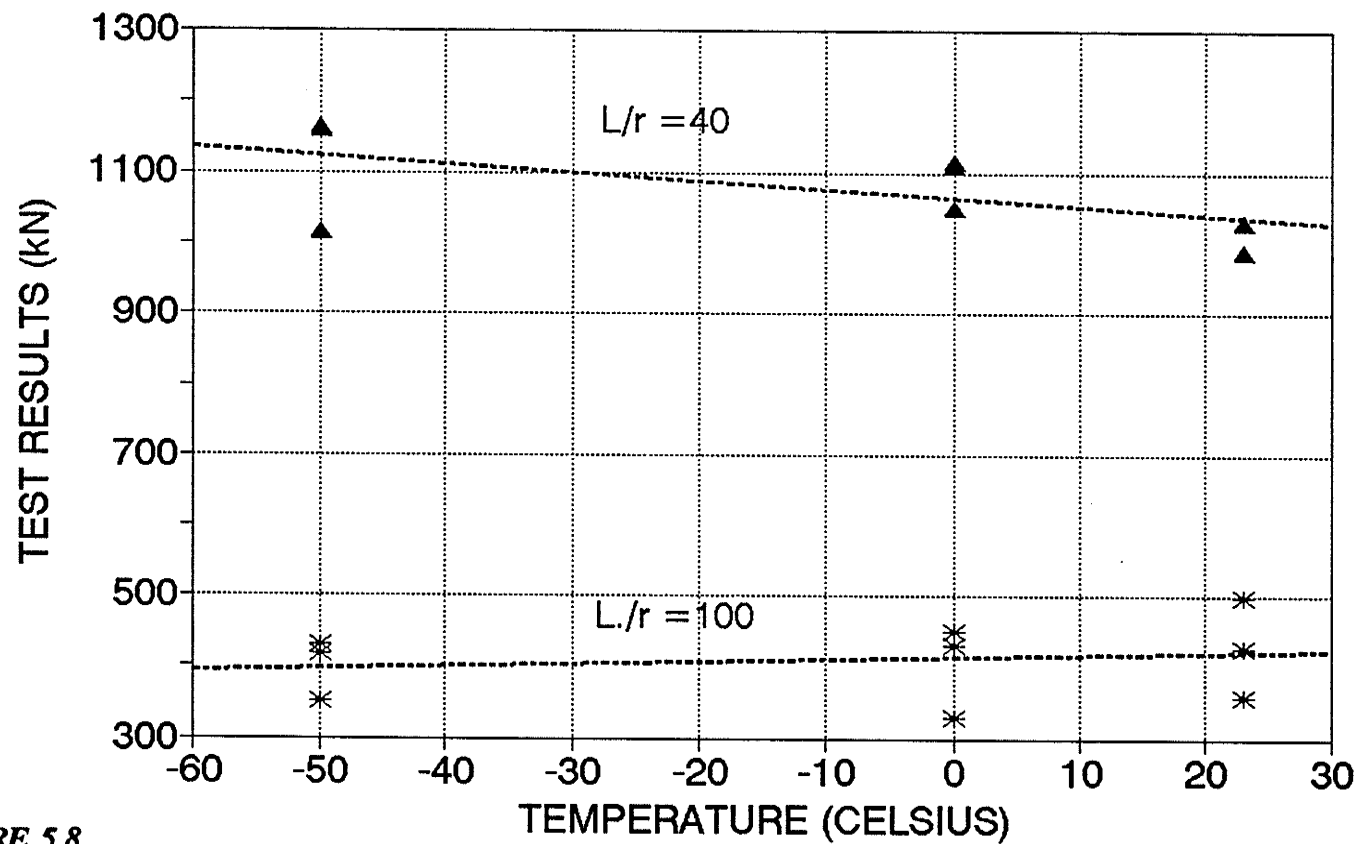


FIGURE 5.8
Load vs. Temperature - BN Section

HBN SECTION TEST RESULTS

.VS. TEMPERATURE

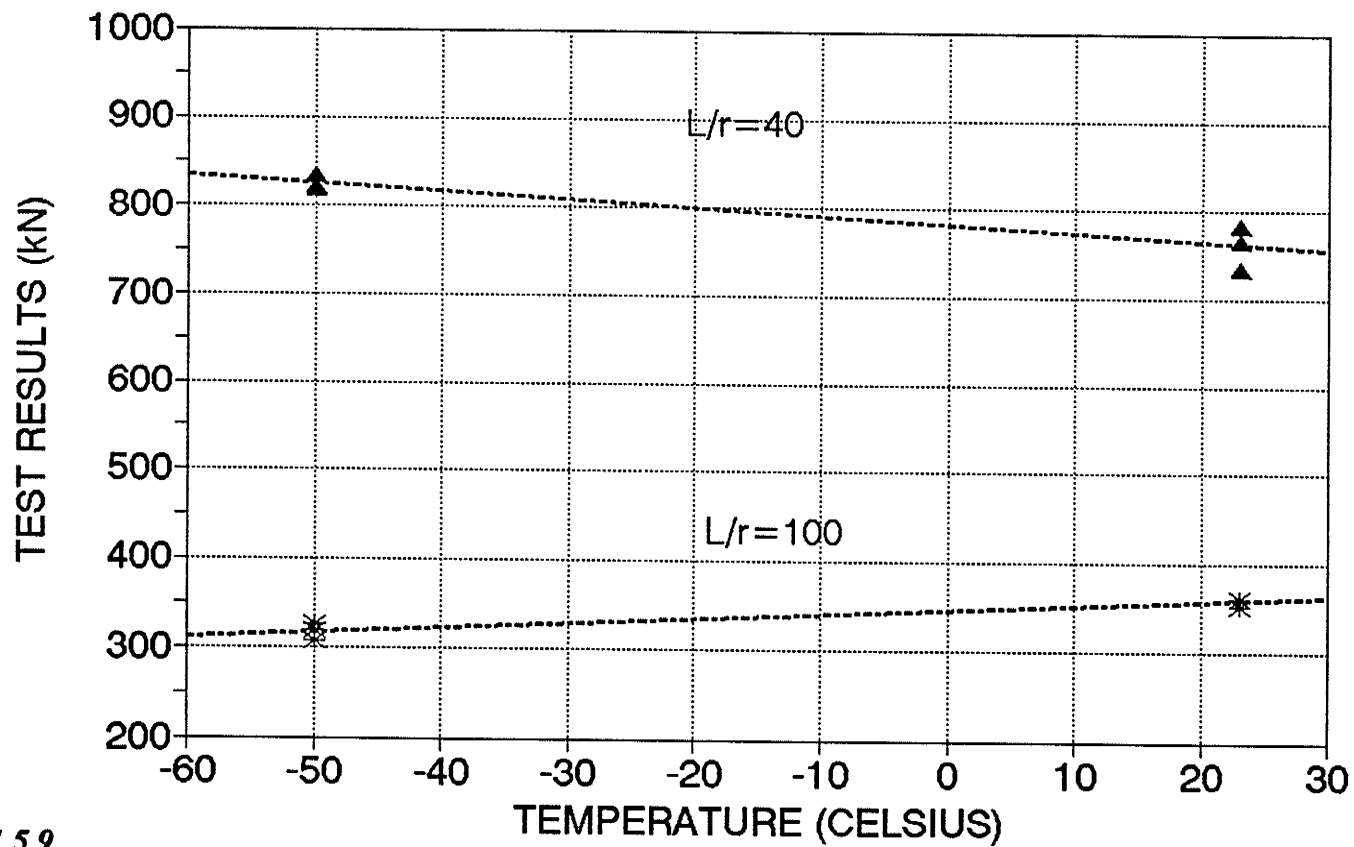


FIGURE 5.9
Load vs. Temperature - HBN Section

**AVERAGE INCREASE IN FAILURE LOAD OF ALL TESTS AT -50 °C
COMPARED TO ROOM TEMPERATURE TESTS**

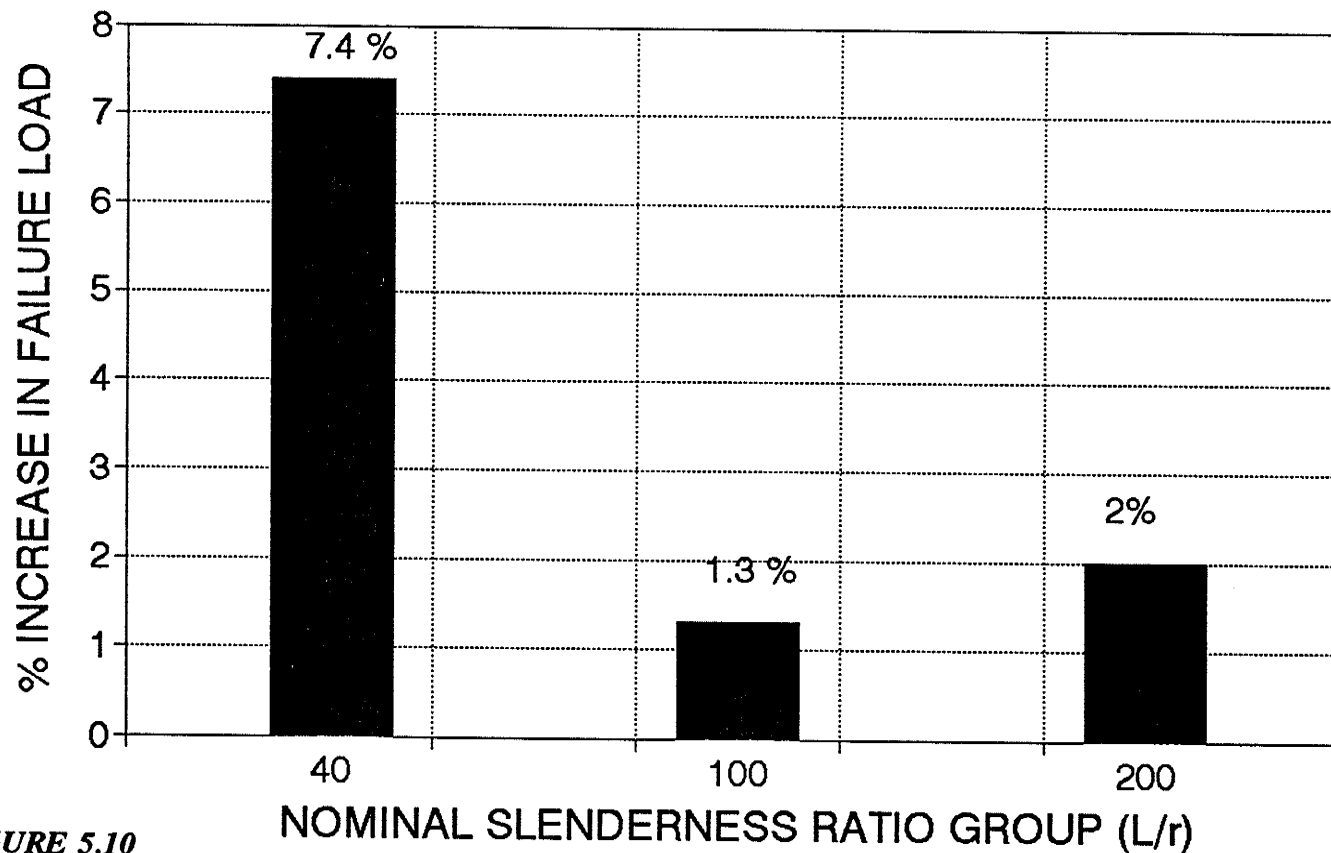


FIGURE 5.10
Average Failure Load Increase at -50° C vs. Slenderness

AVERAGE INCREASE IN FAILURE LOAD OF ALL TESTS @ 0°C

COMPARED TO ROOM TEMPERATURE TESTS

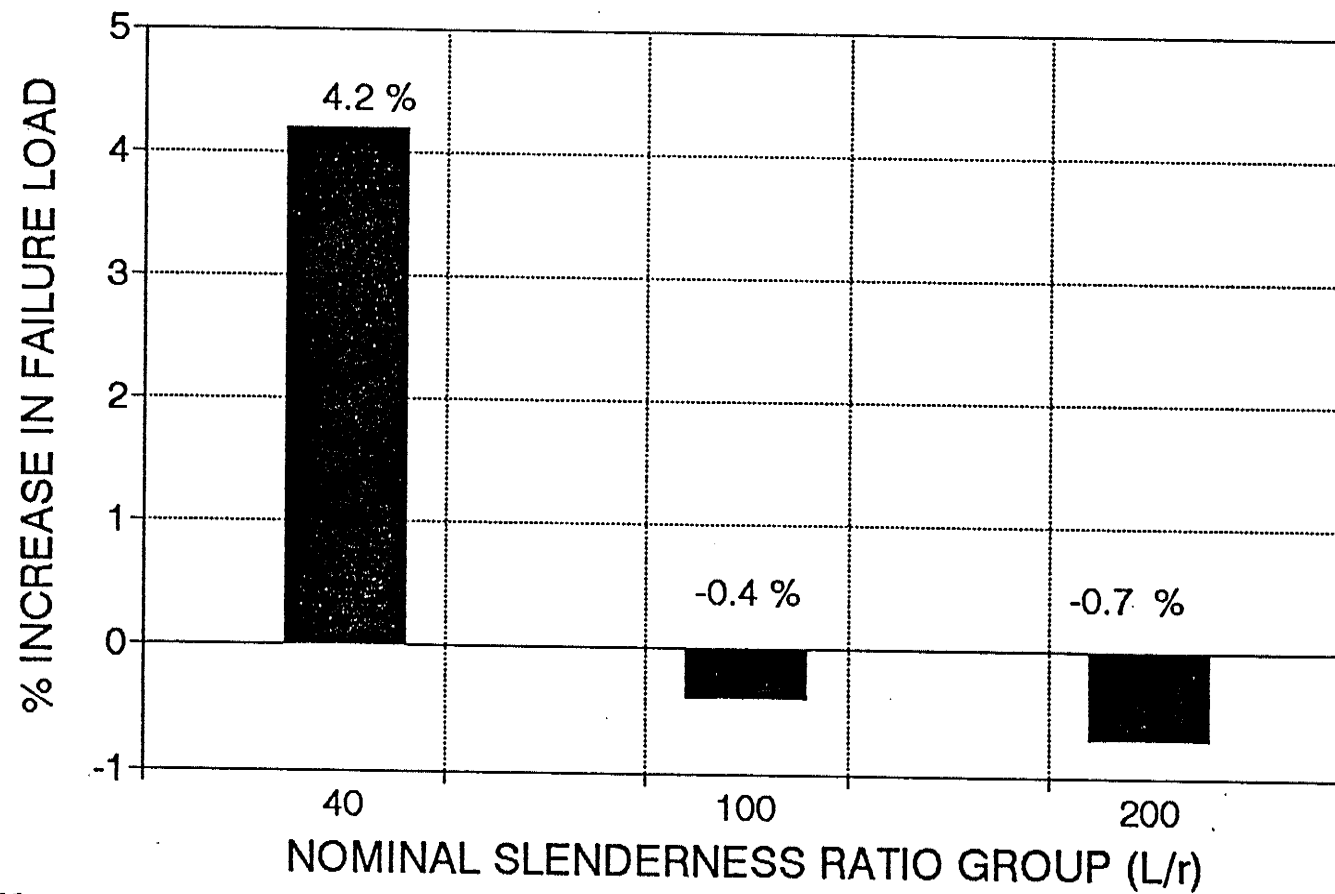


FIGURE 5.11

Average Failure Load Increase at 0°C vs. Slenderness

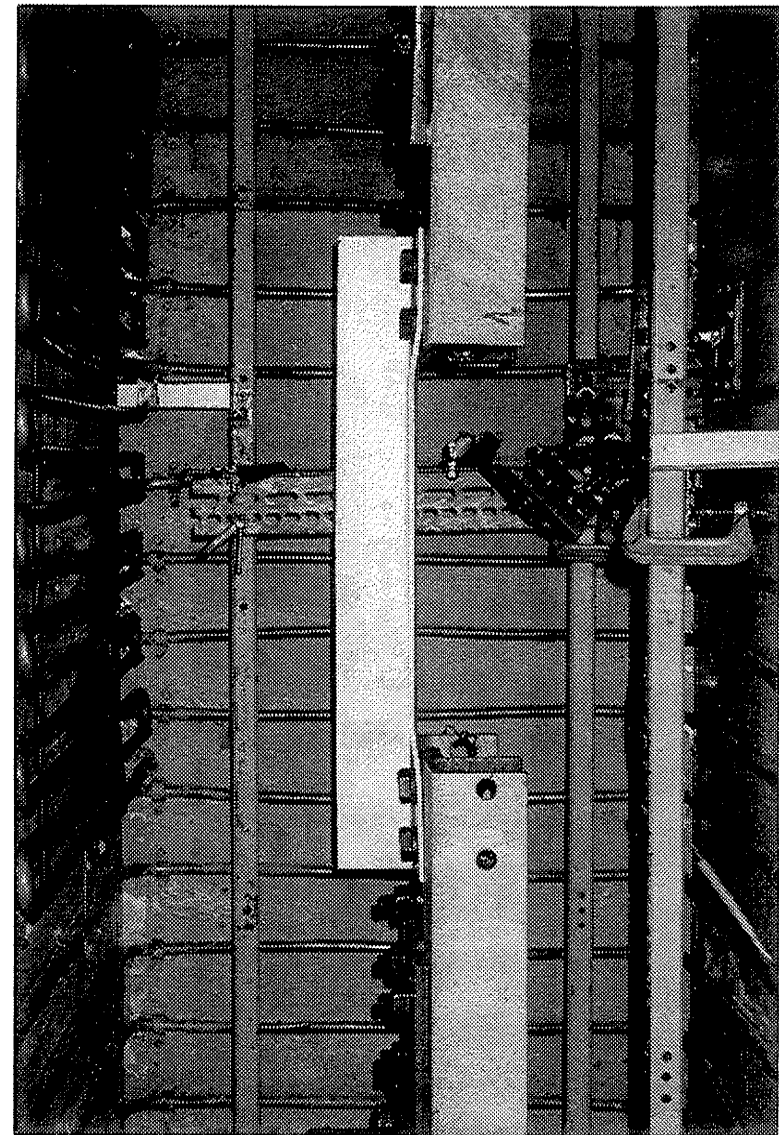
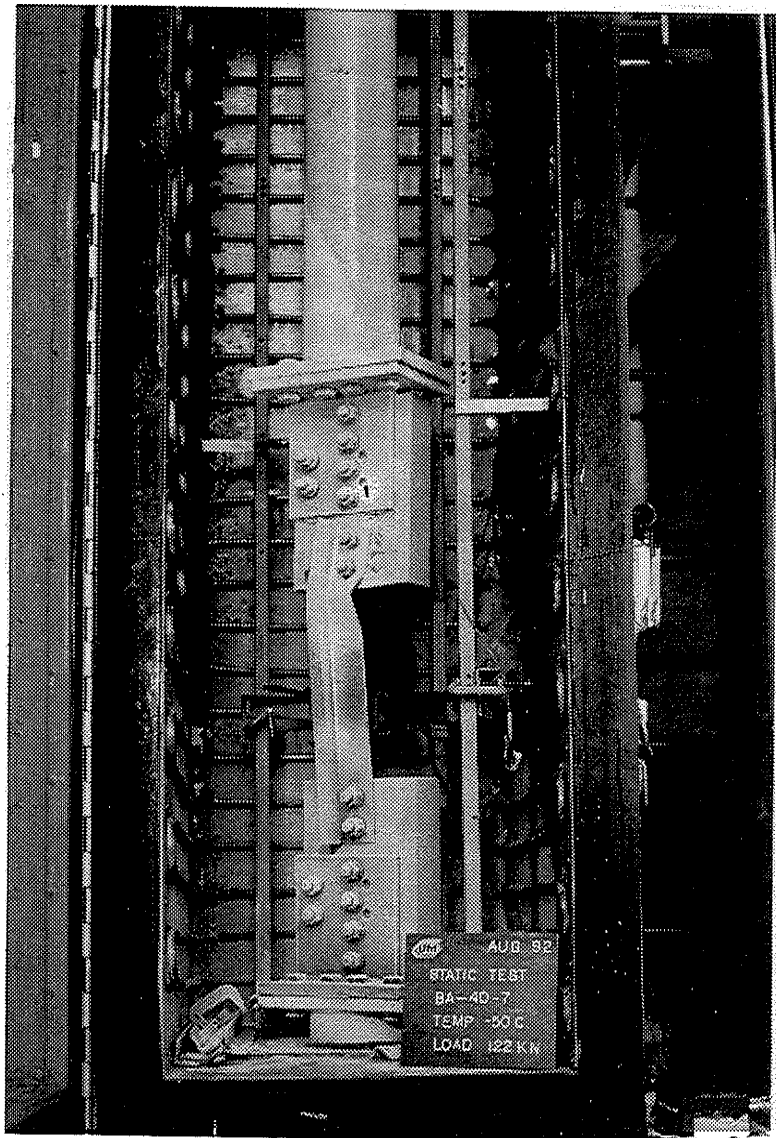


FIGURE 5.12
BA-40 Specimens at Failure

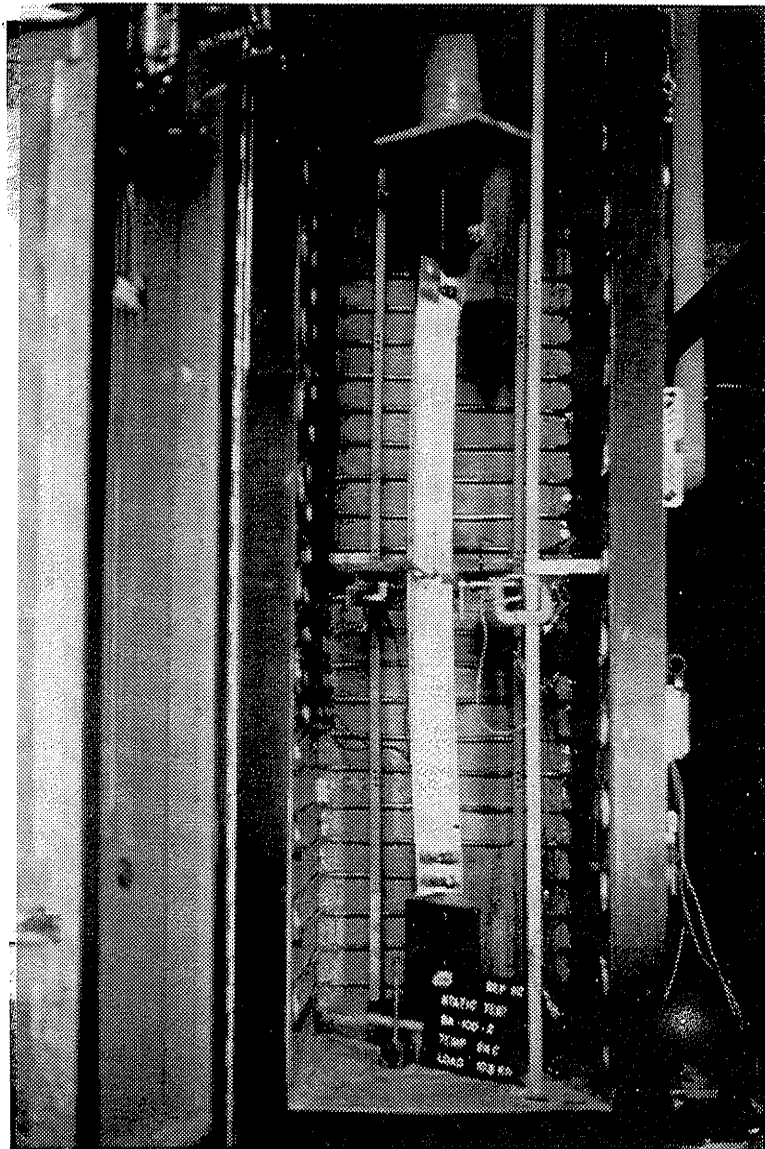


FIGURE 5.13
BA-100 Specimen at Failure

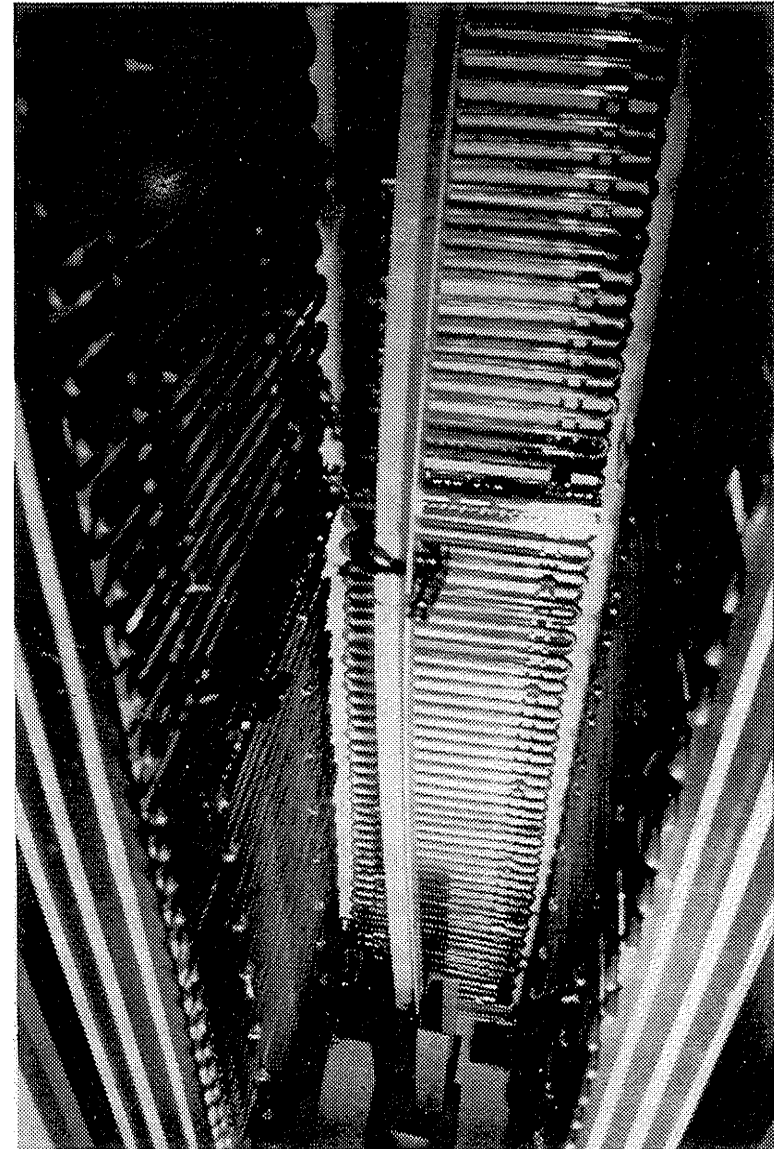


FIGURE 5.14
BA-200 Specimen at Failure

BA SECTION TESTS

CAN/CSA-S136-M89 ANALYSIS

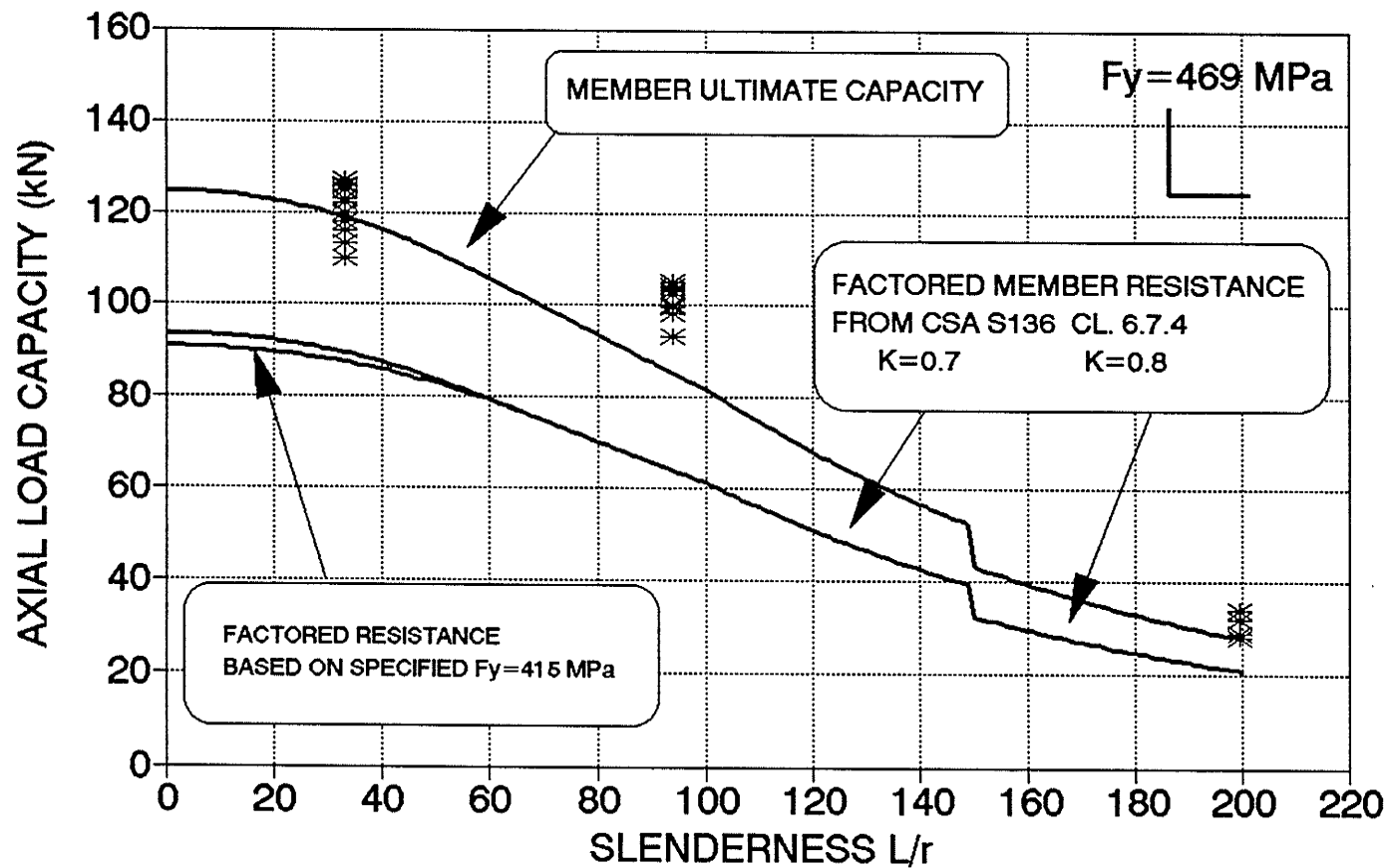


FIGURE 5.15

BA Section Analysis: CAN/CSA-S136-M89

(L =CENTER TO CENTER OF CONNECTIONS)

HBA SECTION TESTS

CAN/CSA-S136-M89

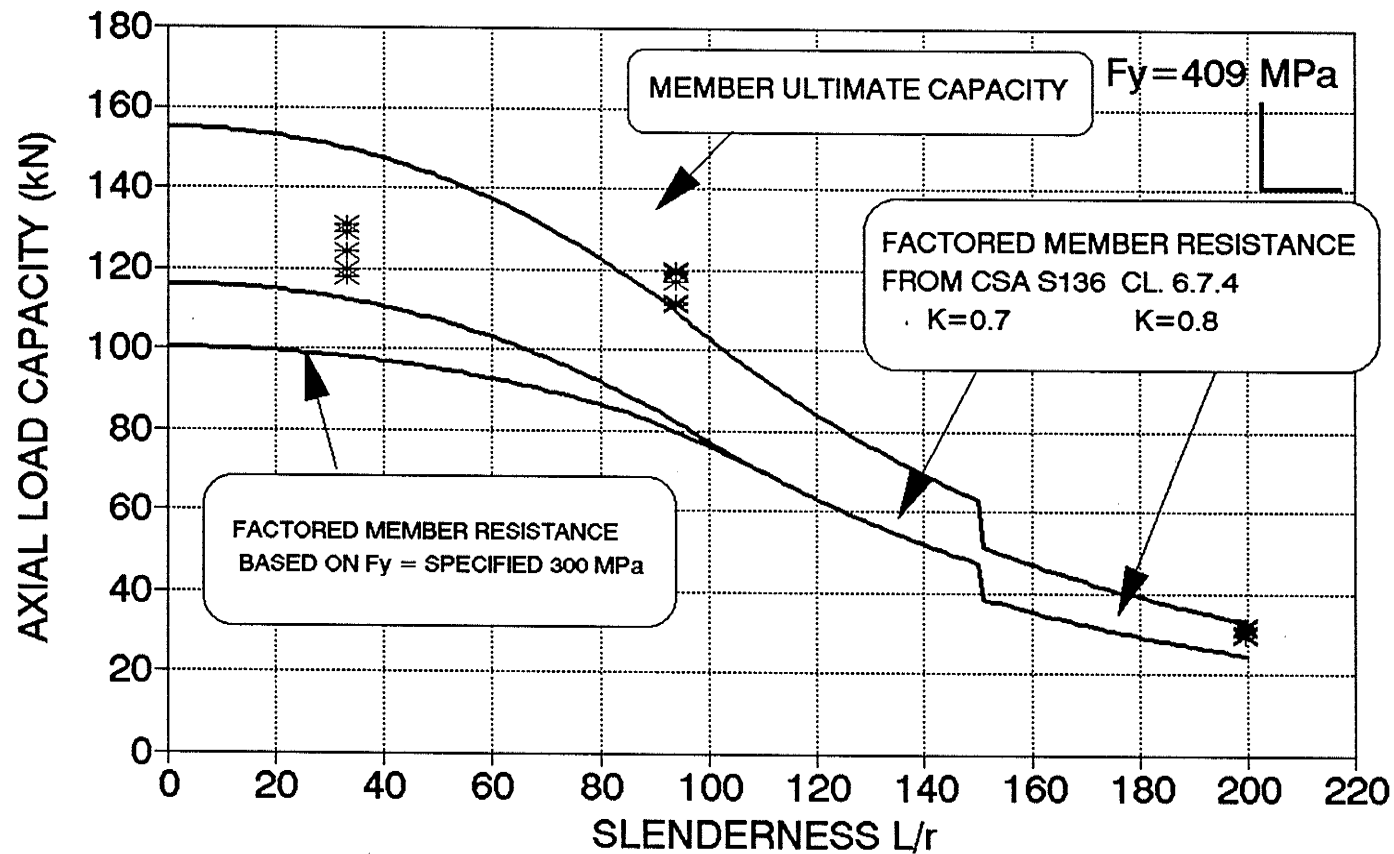


FIGURE 5.16

HBA Section Analysis: CAN/CSA-S136-M89

(L =CENTER TO CENTER OF CONNECTIONS)

BA SECTION TESTS

ASCE MANUAL 52

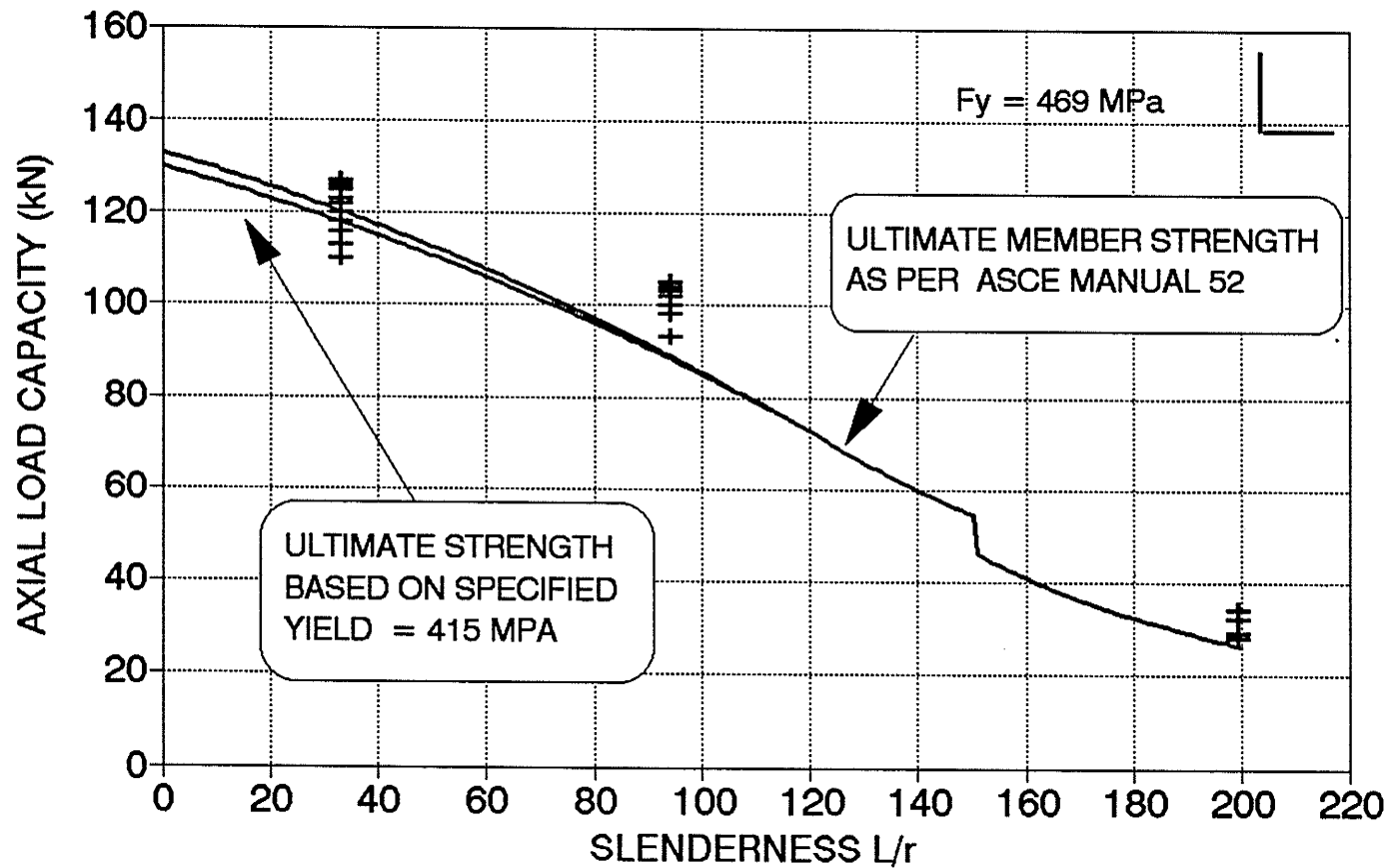


FIGURE 5.17

BA Section Analysis: ASCE Manual 52

(L = CENTER TO CENTER OF CONNECTIONS)

HBA SECTION TESTS

ASCE MANUAL 52

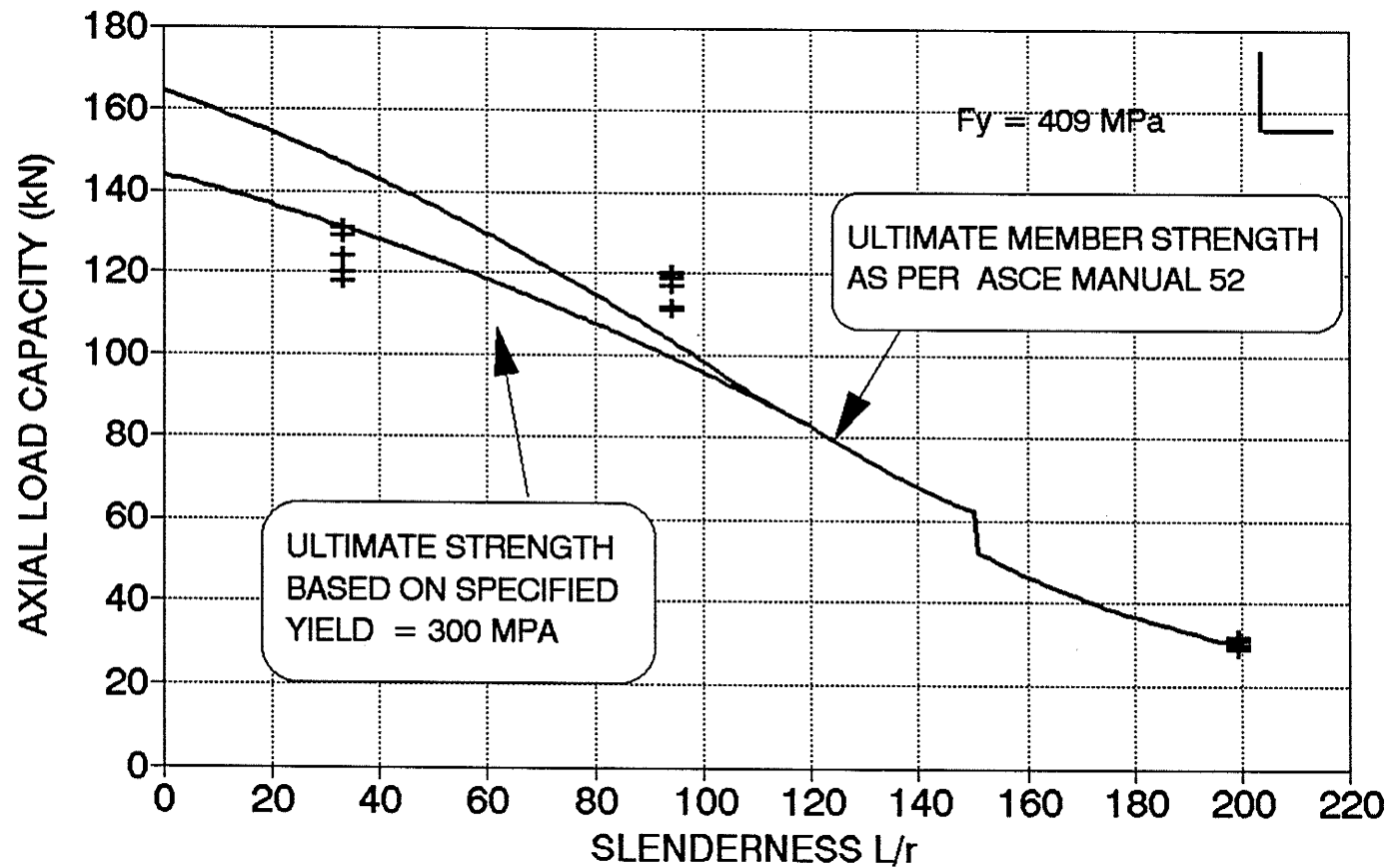


FIGURE 5.18

HBA Section Analysis: ASCE Manual 52 (L = CENTER TO CENTER OF CONNECTIONS)

BA SECTION TESTS

CAN/CSA S37-M86

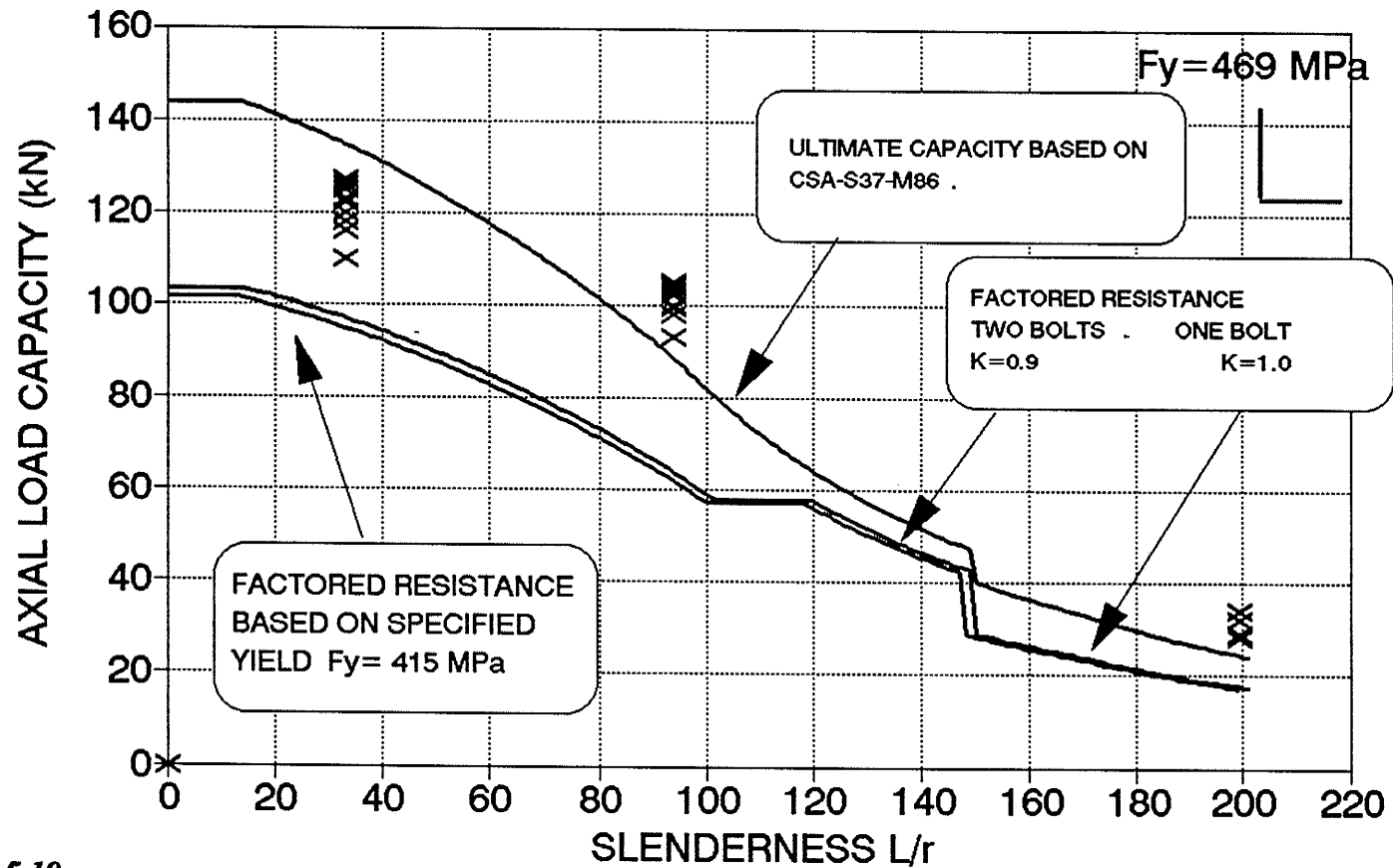


FIGURE 5.19

BA Section Analysis: CAN/CSA-S37-M86

HBA SECTION TESTS

CAN/CSA S37-M86

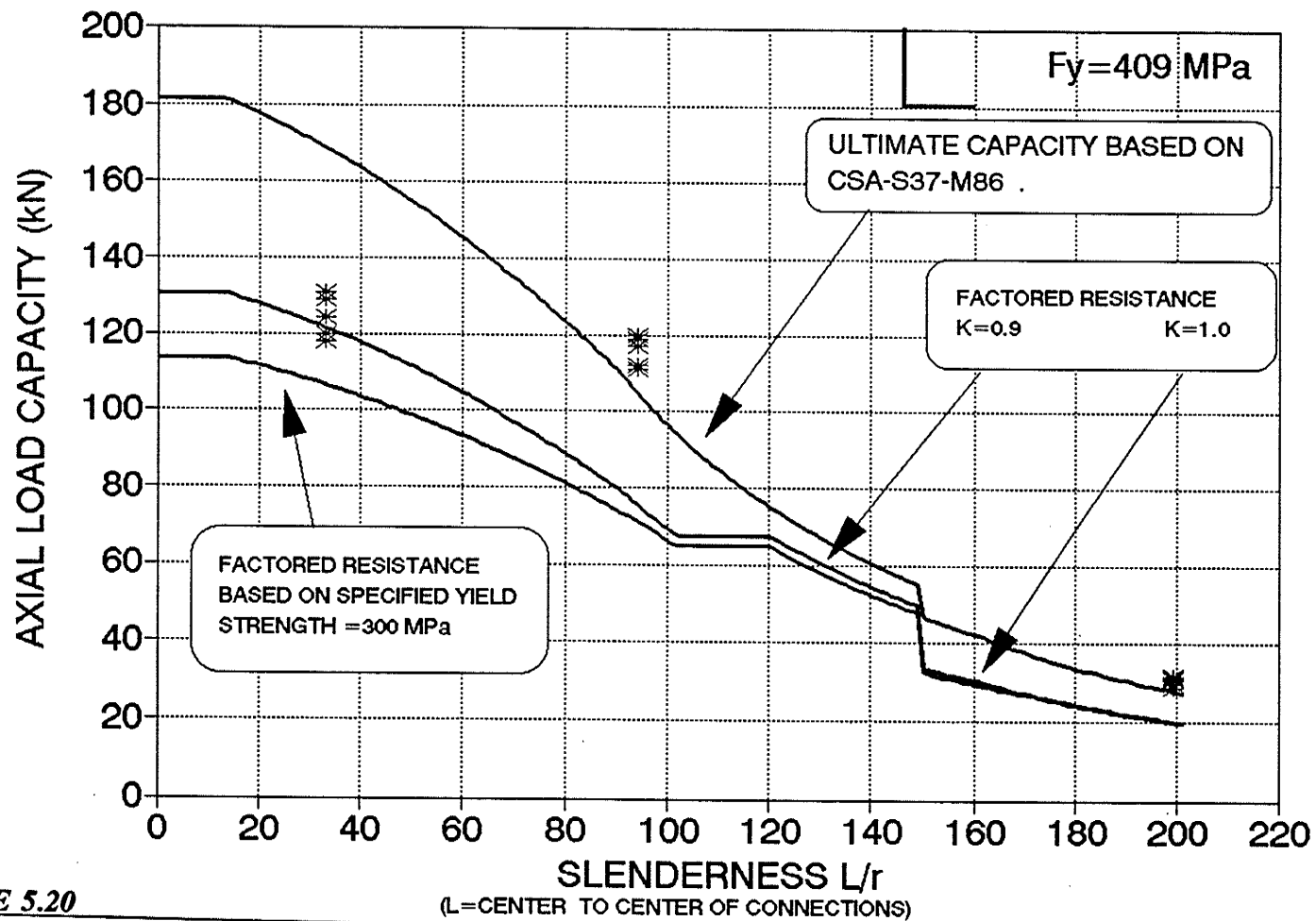


FIGURE 5.20

HBA Section Analysis: CAN/CSA-S37-M86

BA SECTION ANALYSIS

ECCS RECOMMENDATIONS

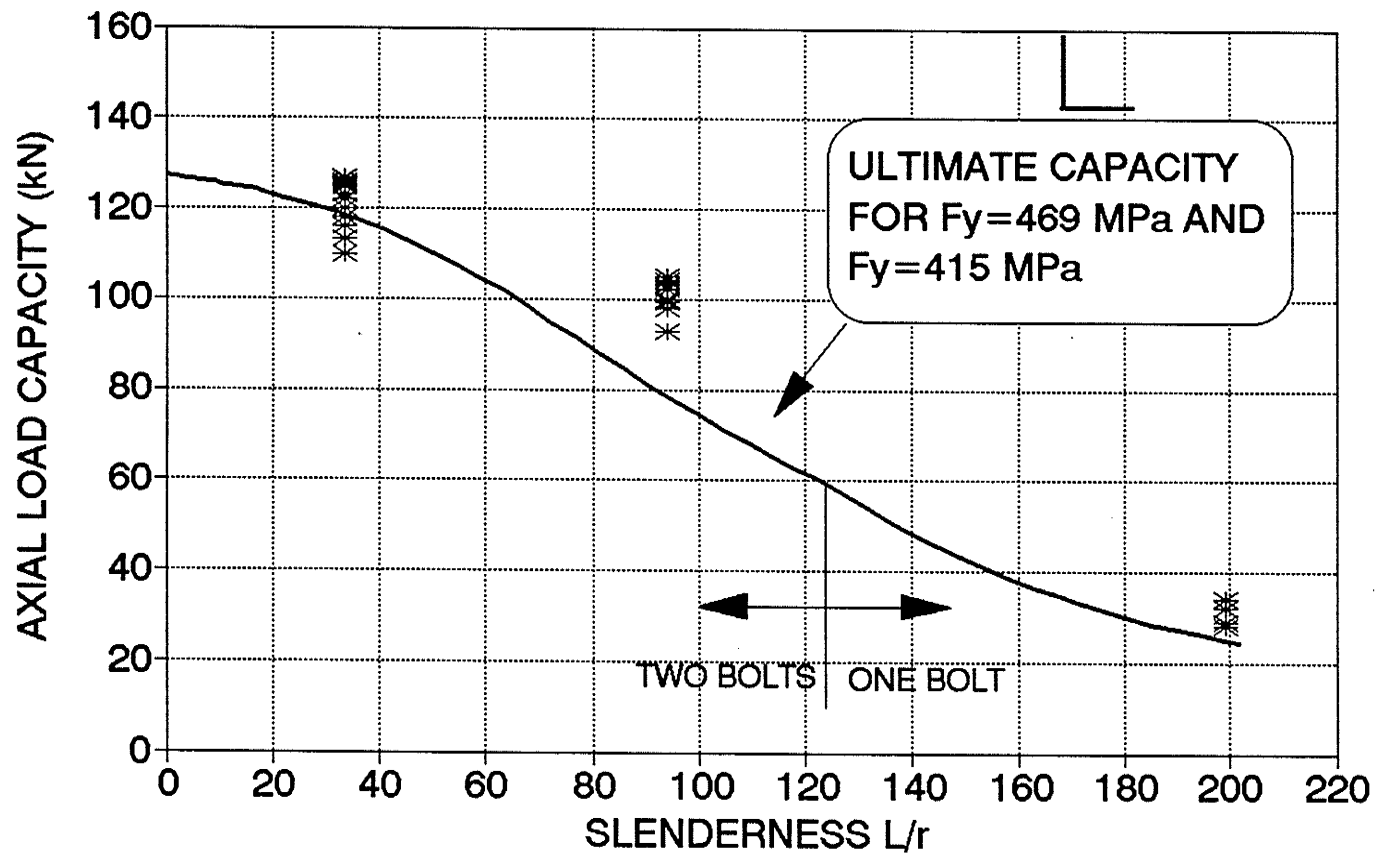


FIGURE 5.21

BA Section Analysis: ECCS Recommendations

L = CENTRE TO CENTRE OF CONNECTIONS

HBA SECTION ANALYSIS

ECCS RECOMMENDATIONS

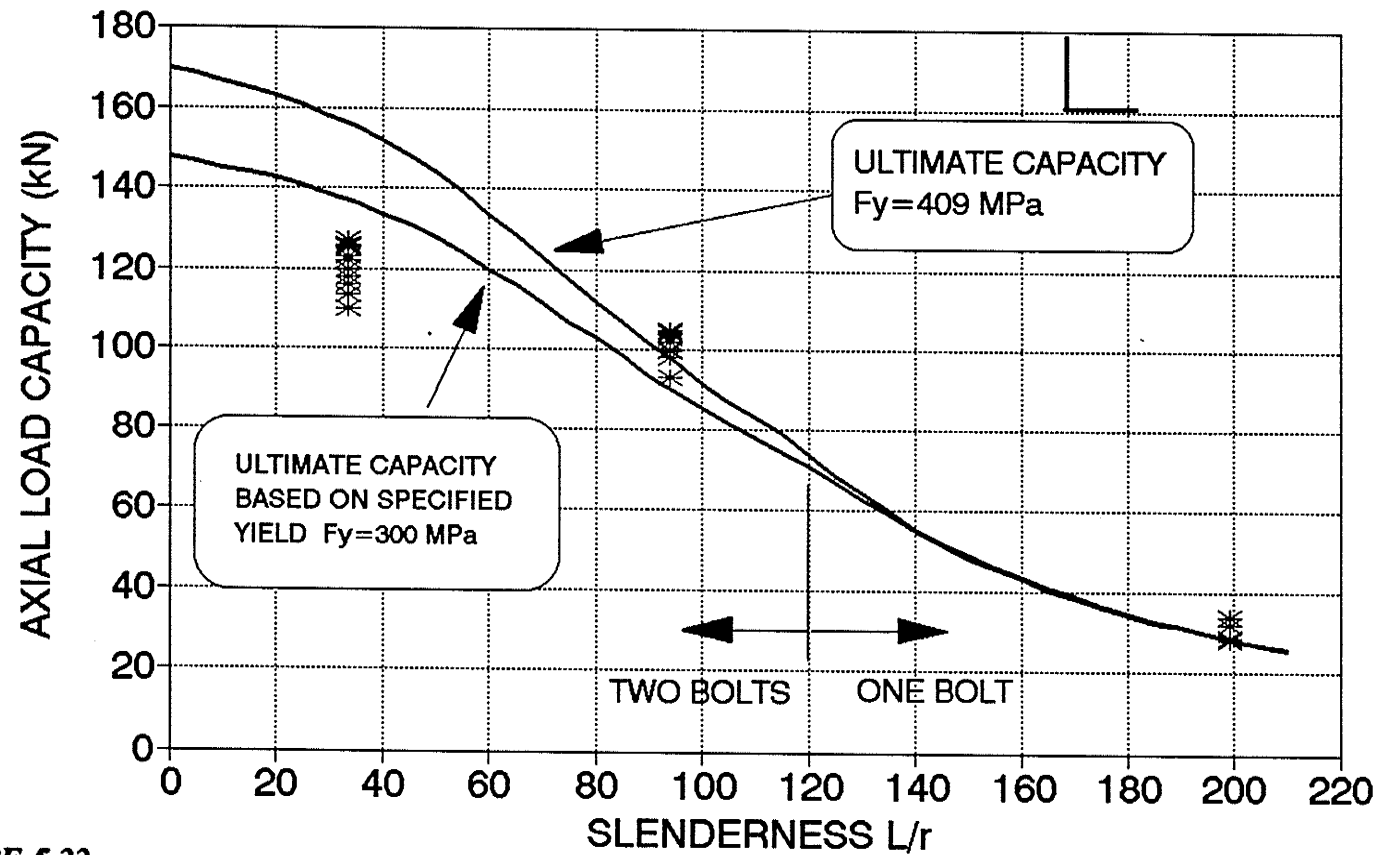


FIGURE 5.22
HBA Section Analysis: ECCS Recommendations

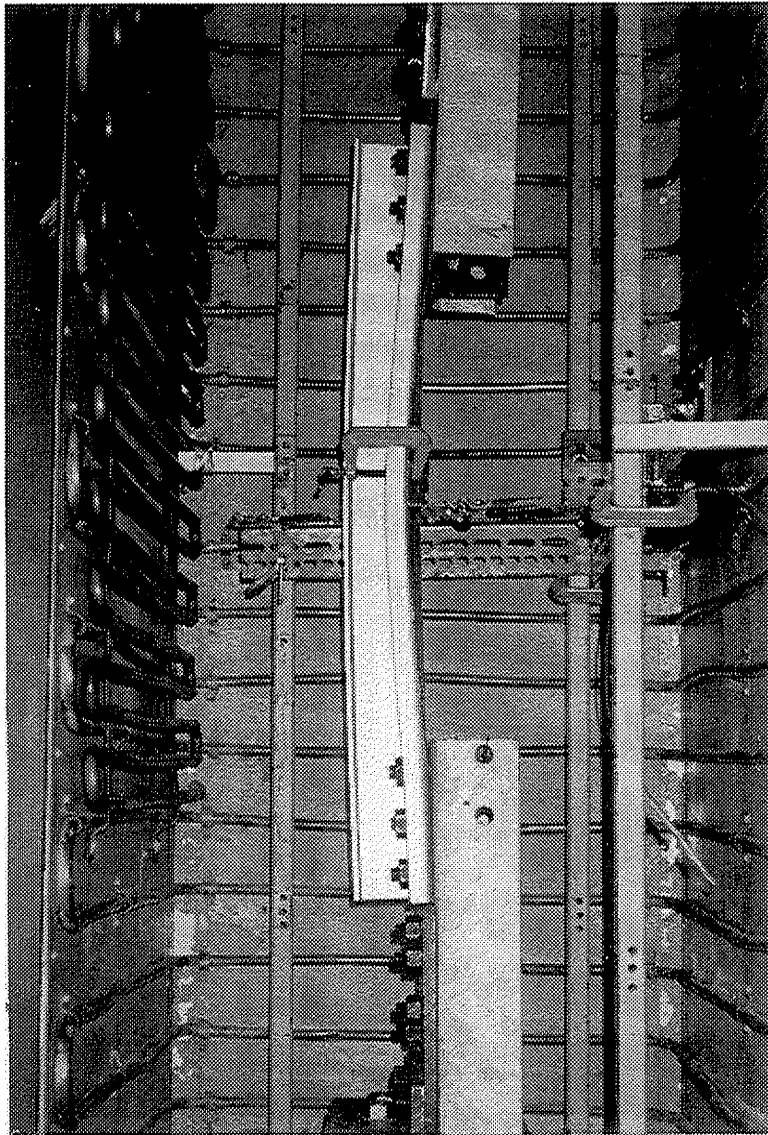


FIGURE 5.23
HBB-40 Specimen at Failure

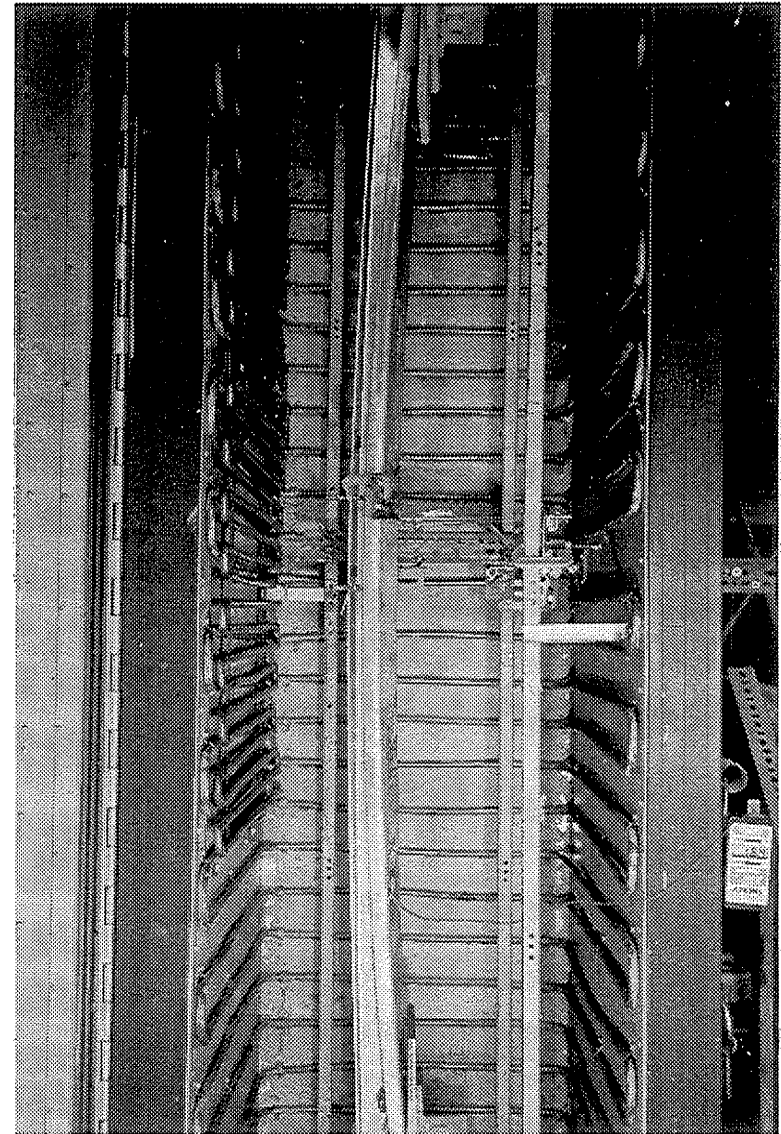


FIGURE 5.24
BB-100 Specimen at Failure

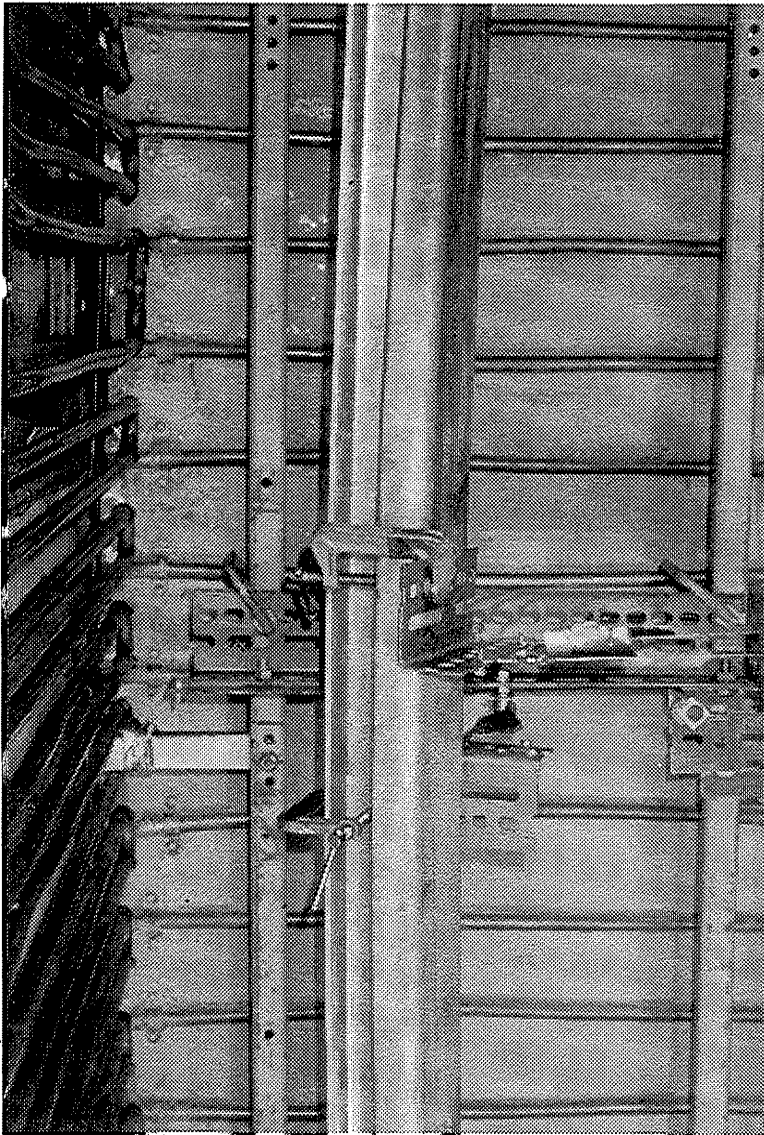


FIGURE 5.25
BB-100 Midheight Twist and Lateral Deflection

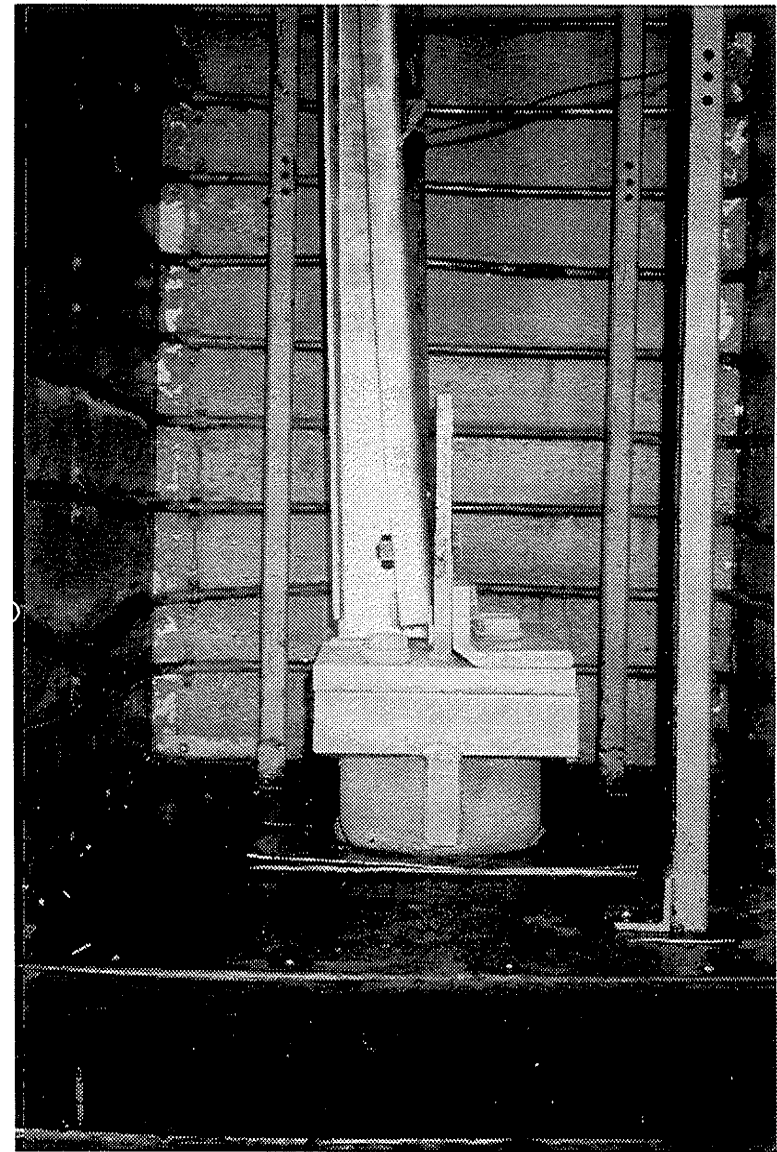


FIGURE 5.26
BB-100 Distortion at Connection

BB SECTION TESTS

CSA S136 CLAUSE 6.7.4

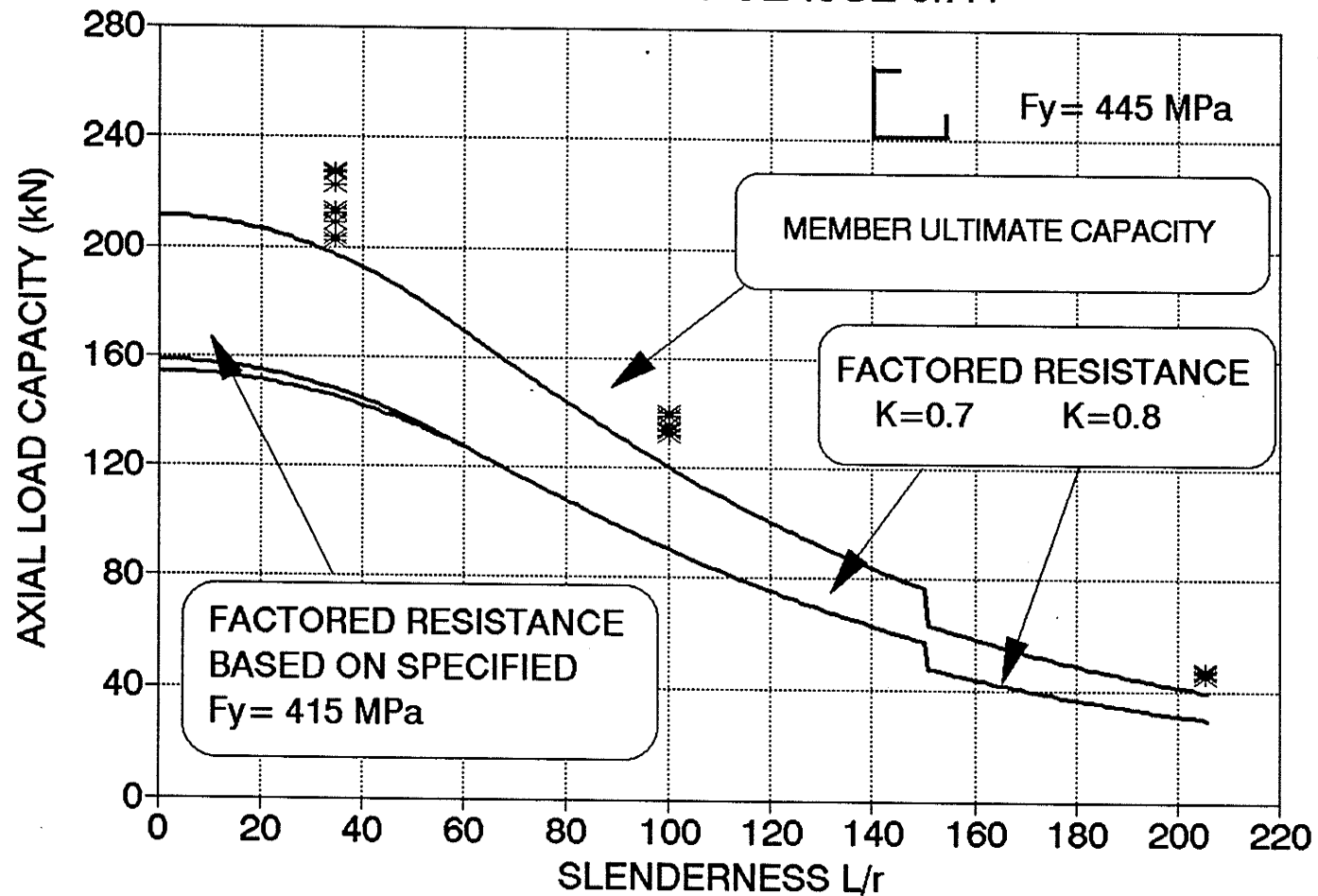


FIGURE 5.27

BB Section Analysis: CAN/CSA-S136-M89

(L = CENTER TO CENTER OF CONNECTIONS)

HBB SECTION TESTS

CSA S136 CLAUSE 6.7.4

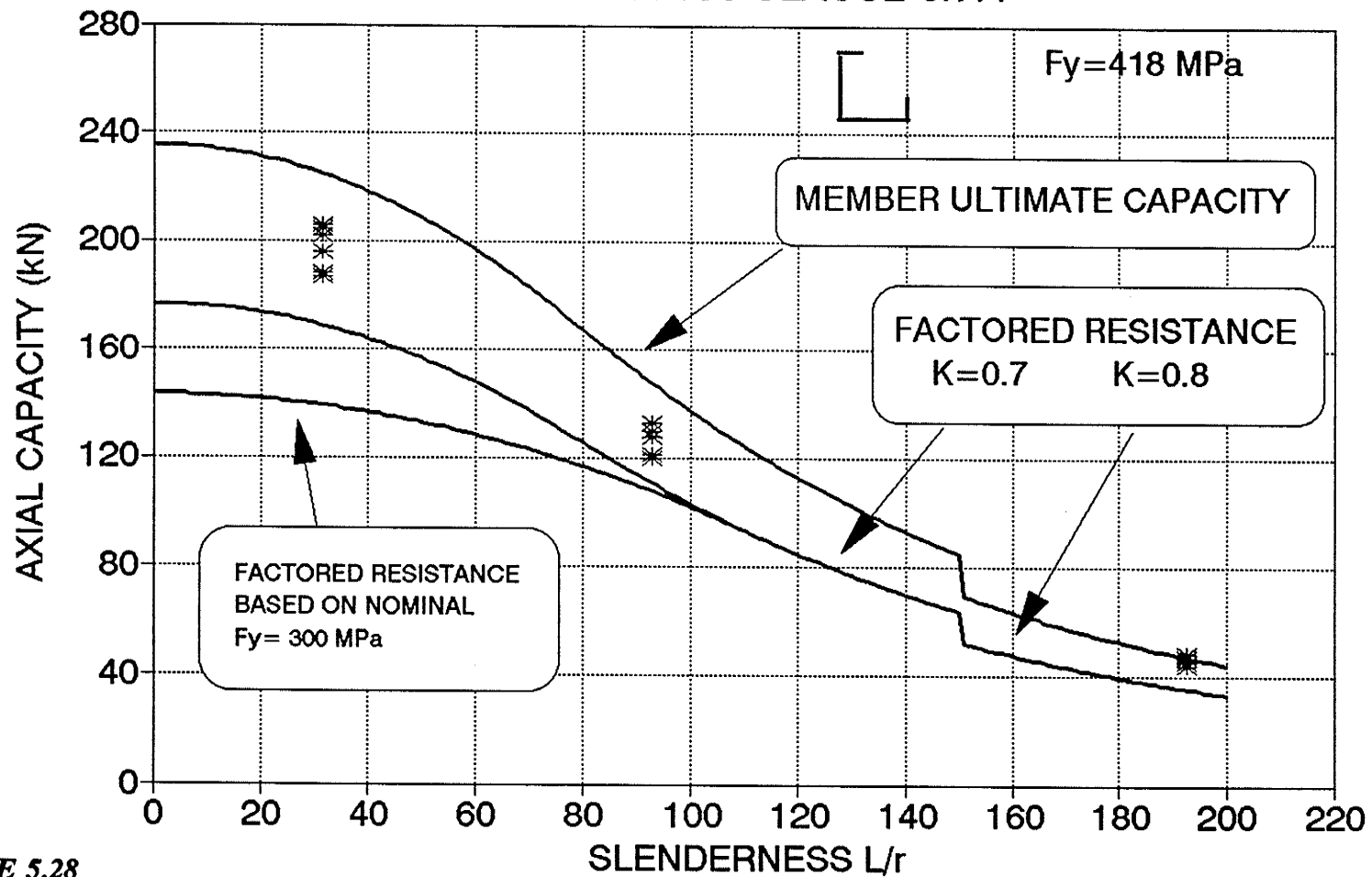


FIGURE 5.28

HBB Section Analysis: CAN/CSA-S136-M89

(L = CENTER TO CENTER OF CONNECTIONS)

BB SECTION TESTS

ASCE MANUAL 52

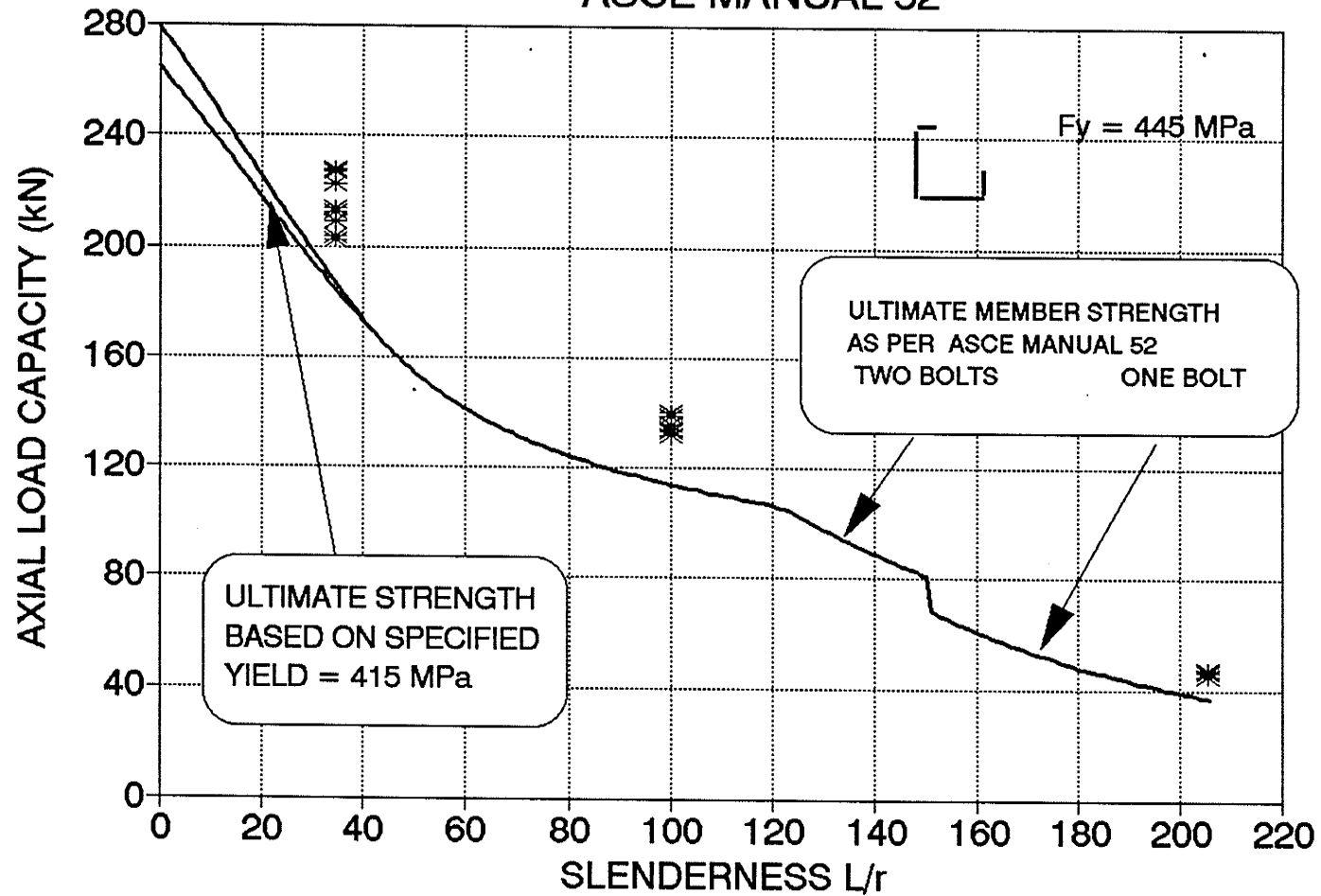


FIGURE 5.29

BB Section Analysis: ASCE Manual 52

(L = CENTER TO CENTER OF CONNECTIONS)

HBB SECTION TESTS

ASCE MANUAL 52

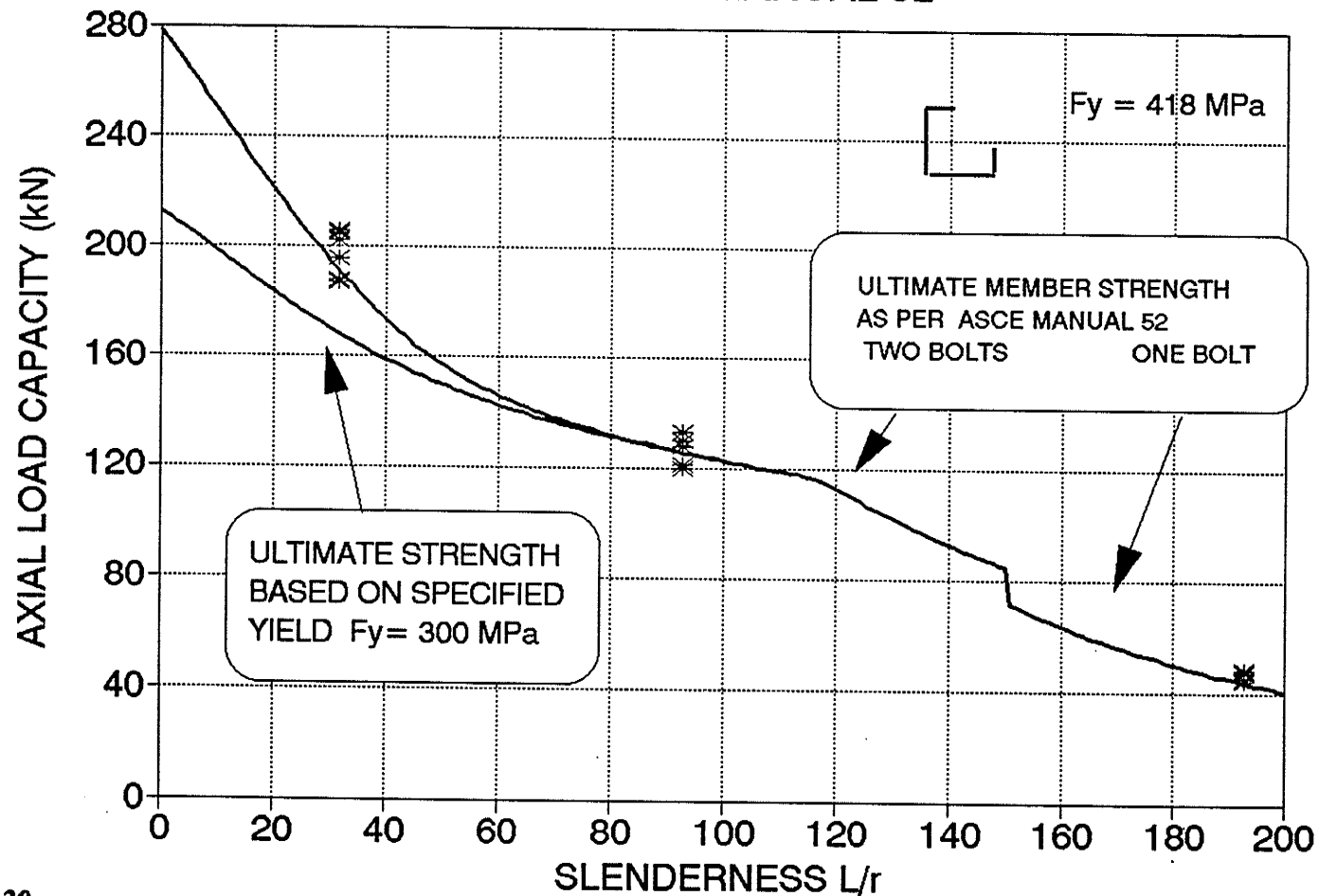


FIGURE 5.30

HBB Section Analysis: ASCE Manual 52

(L = CENTER TO CENTER OF CONNECTIONS)

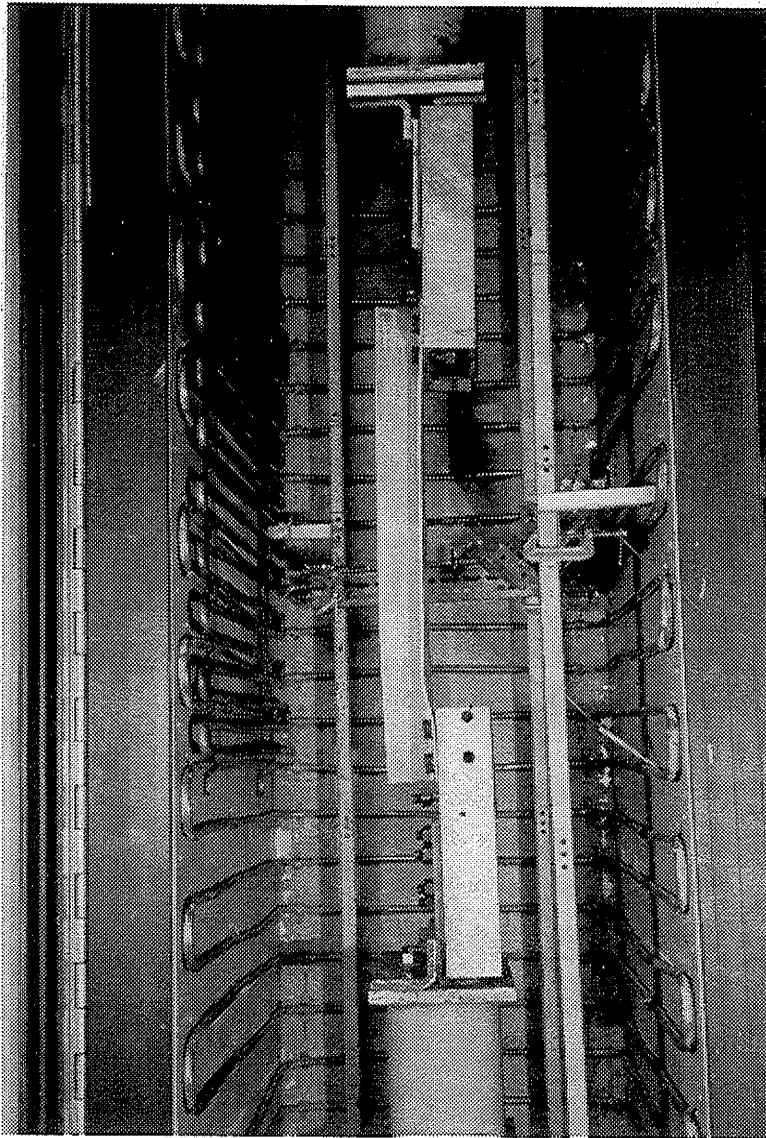


FIGURE 5.31
BC-40 Specimen at Failure

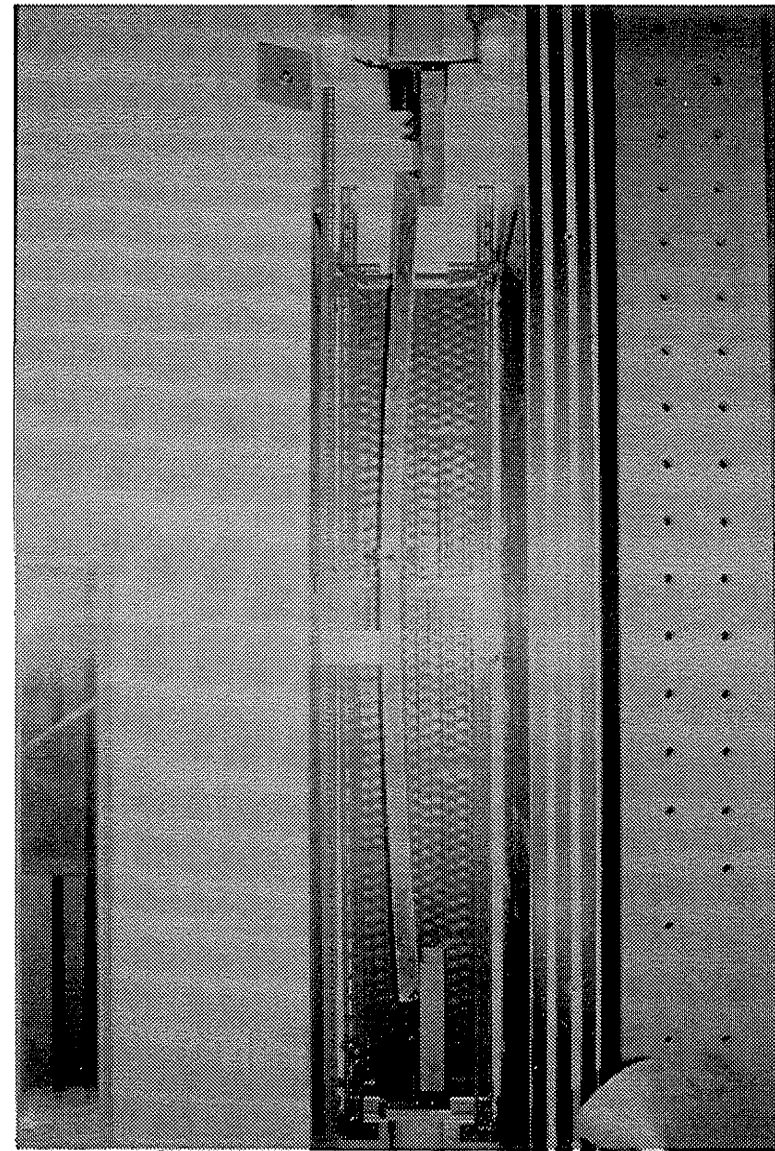


FIGURE 5.32
BC-200 Specimen at Failure

BC SECTION TESTS

CAN/CSA-S136-M89

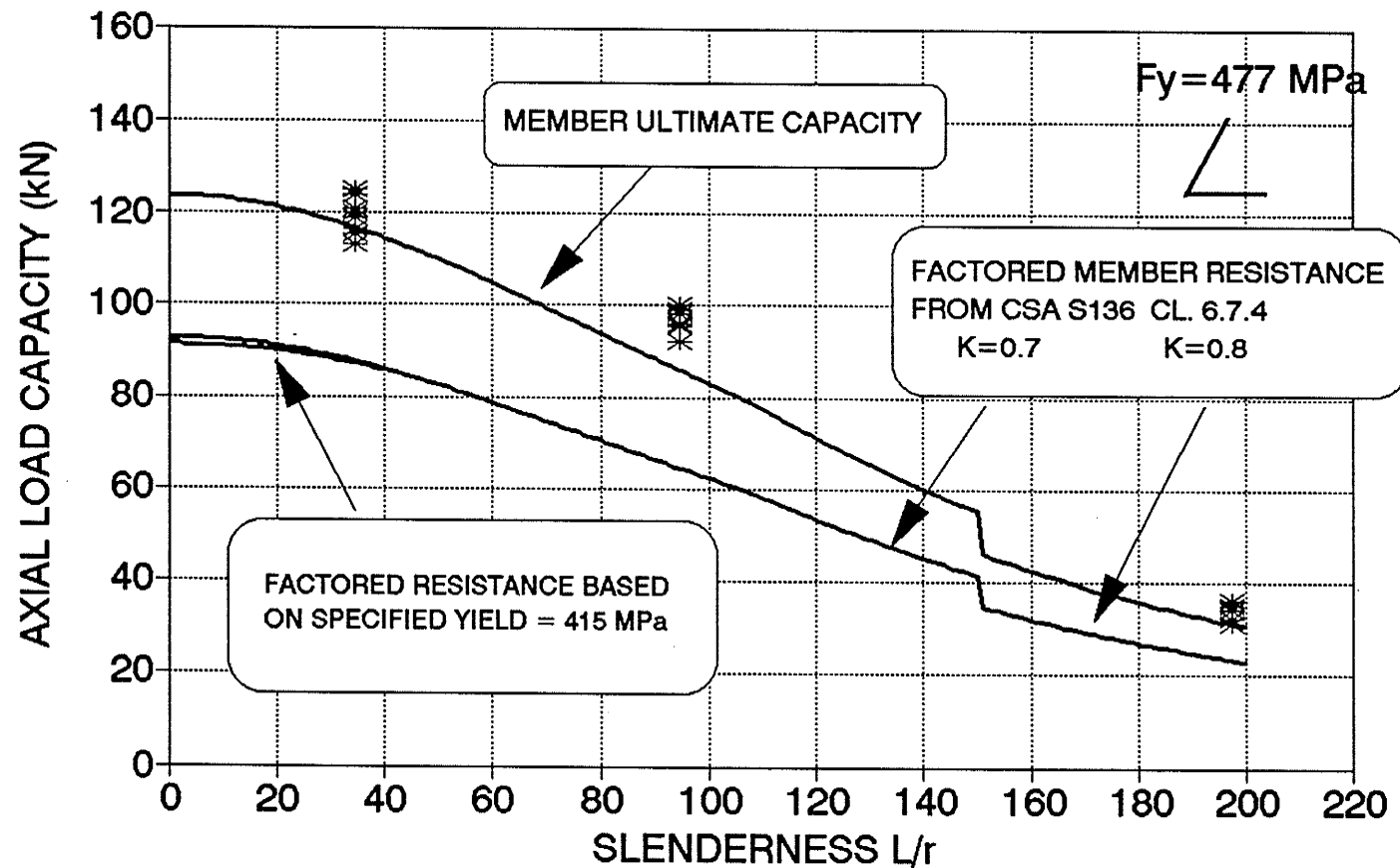


FIGURE 5.33

BC Section Analysis: CAN/CSA-S136-M89

(L =CENTER TO CENTER OF CONNECTIONS)

HBC SECTION TESTS

CAN/CSA-S136-M89

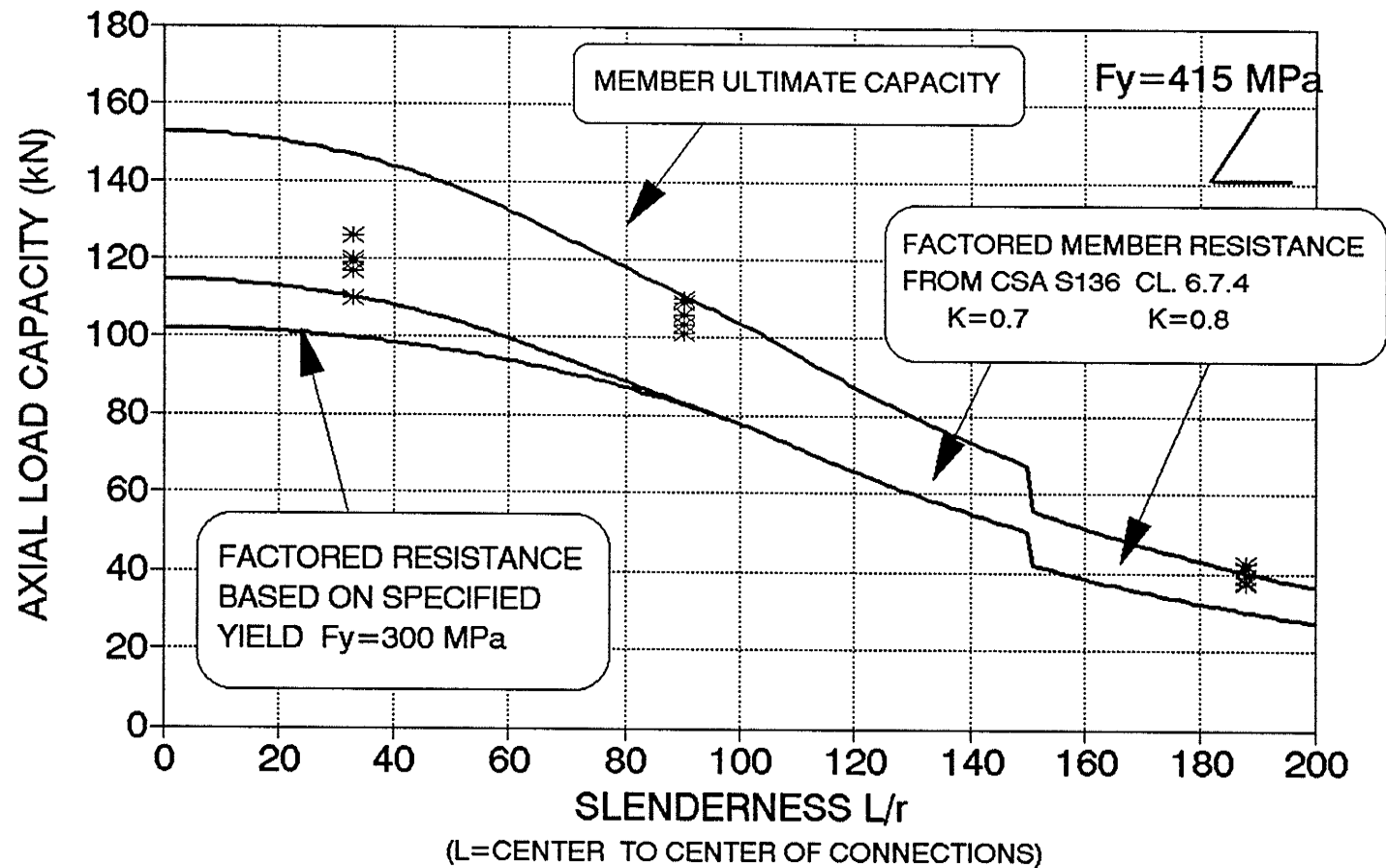


FIGURE 5.34
HBC Section Analysis: CAN/CSA-S136-M89

BC SECTION TESTS

ASCE MANUAL 52

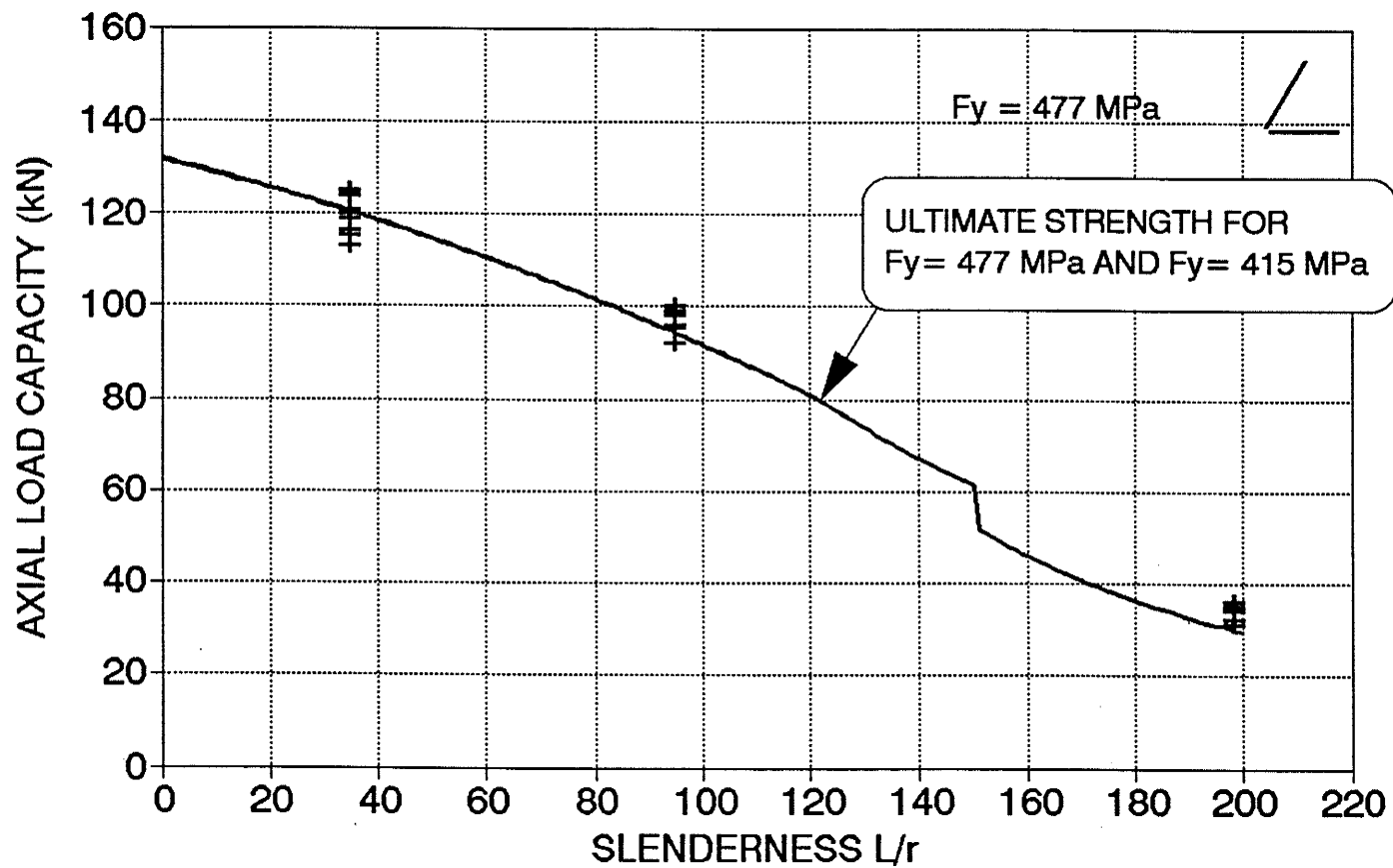


FIGURE 5.35

BC Section Analysis: ASCE Manual 52

(L = CENTER TO CENTER OF CONNECTIONS)

HBC SECTION TESTS

ASCE MANUAL 52

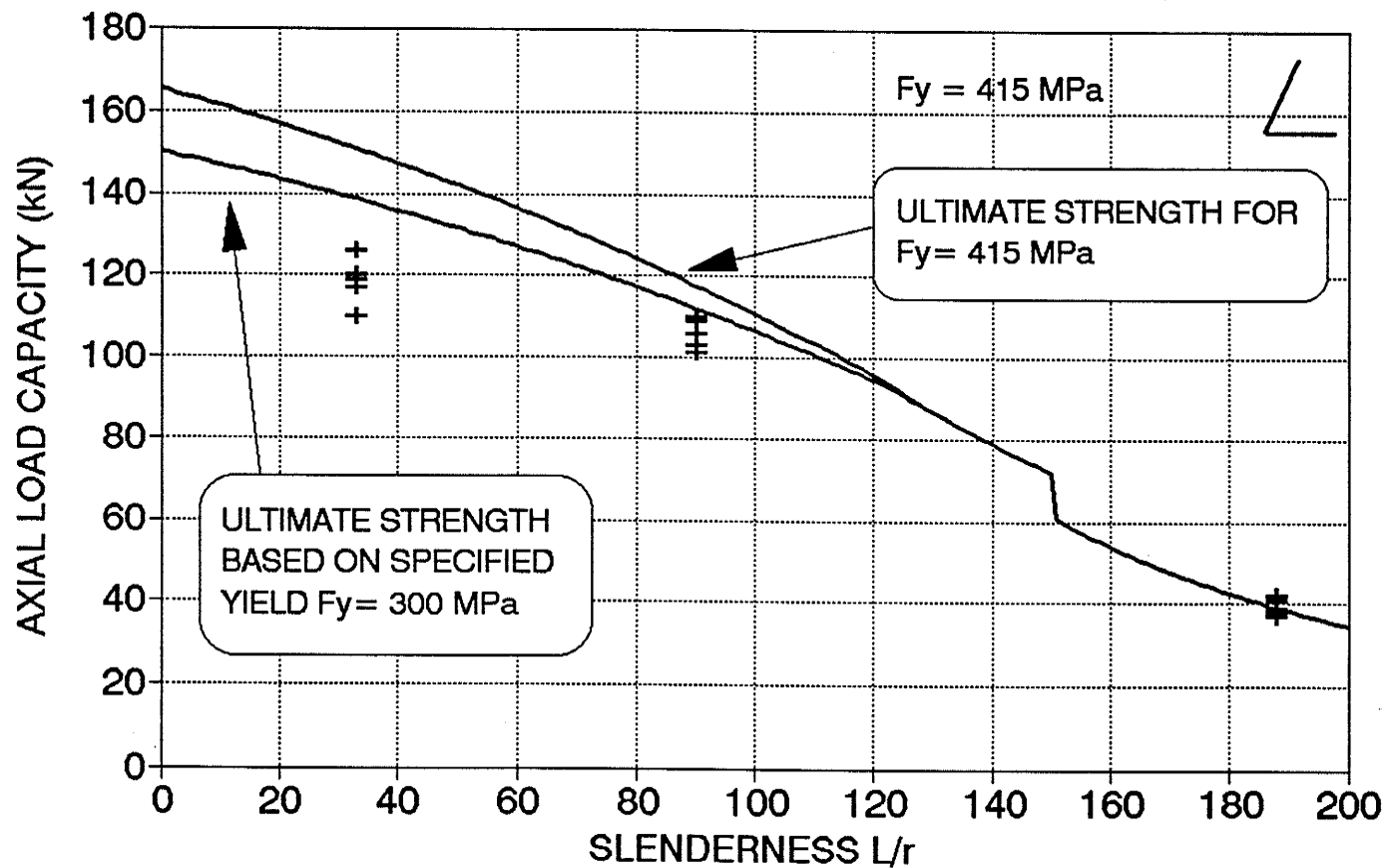


FIGURE 5.36
HBC Section Analysis: ASCE Manual 52

(L = CENTER TO CENTER OF CONNECTIONS)

BC SECTION TESTS

CAN/CSA S37-M86

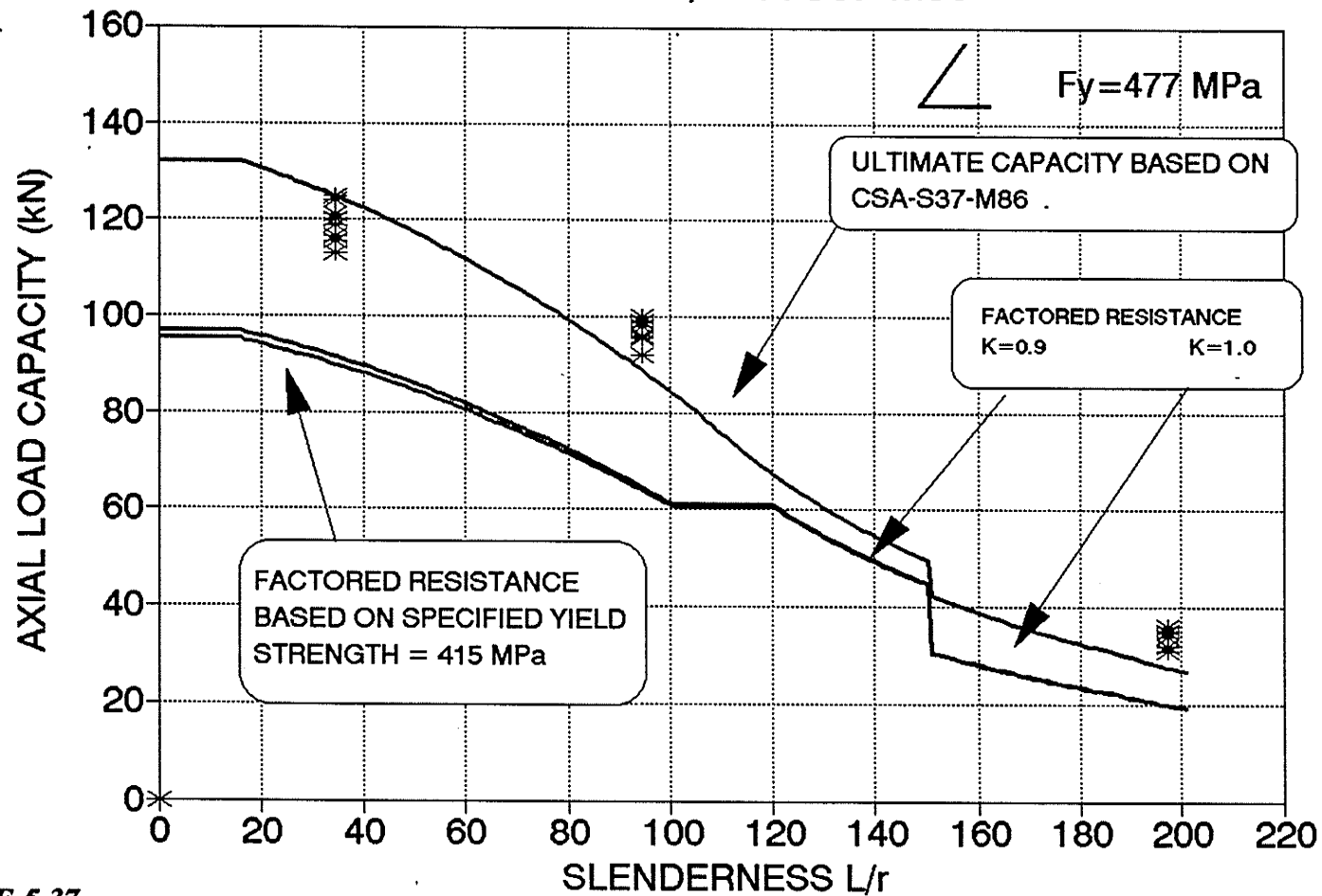


FIGURE 5.37

BC Section Analysis: CAN/CSA-S37-M86 (L =CENTER TO CENTER OF CONNECTIONS)

HBC SECTION TESTS

CAN/CSA S37-M86

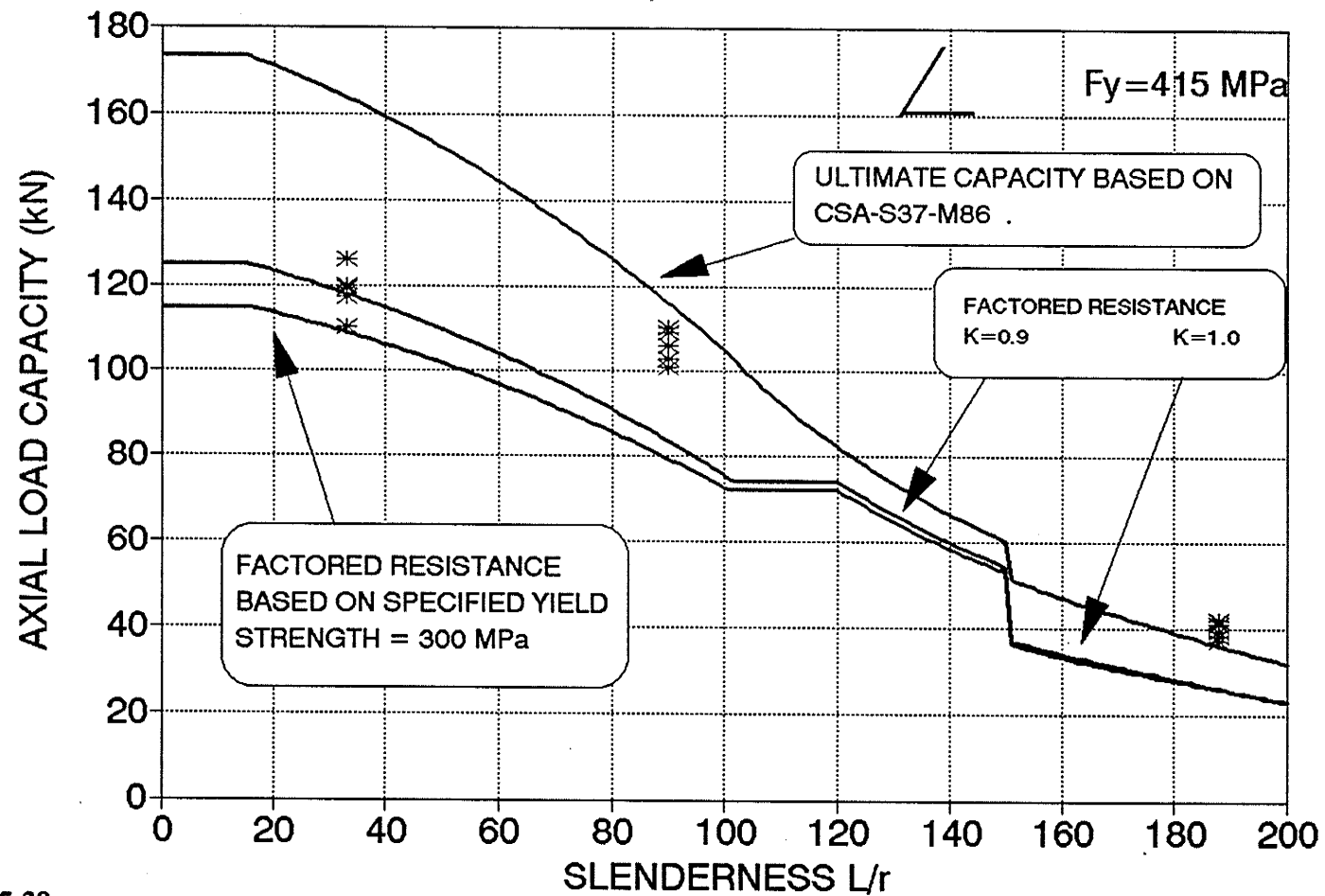


FIGURE 5.38

HBC Section Analysis: CAN/CSA-S37-M86

(L =CENTER TO CENTER OF CONNECTIONS)

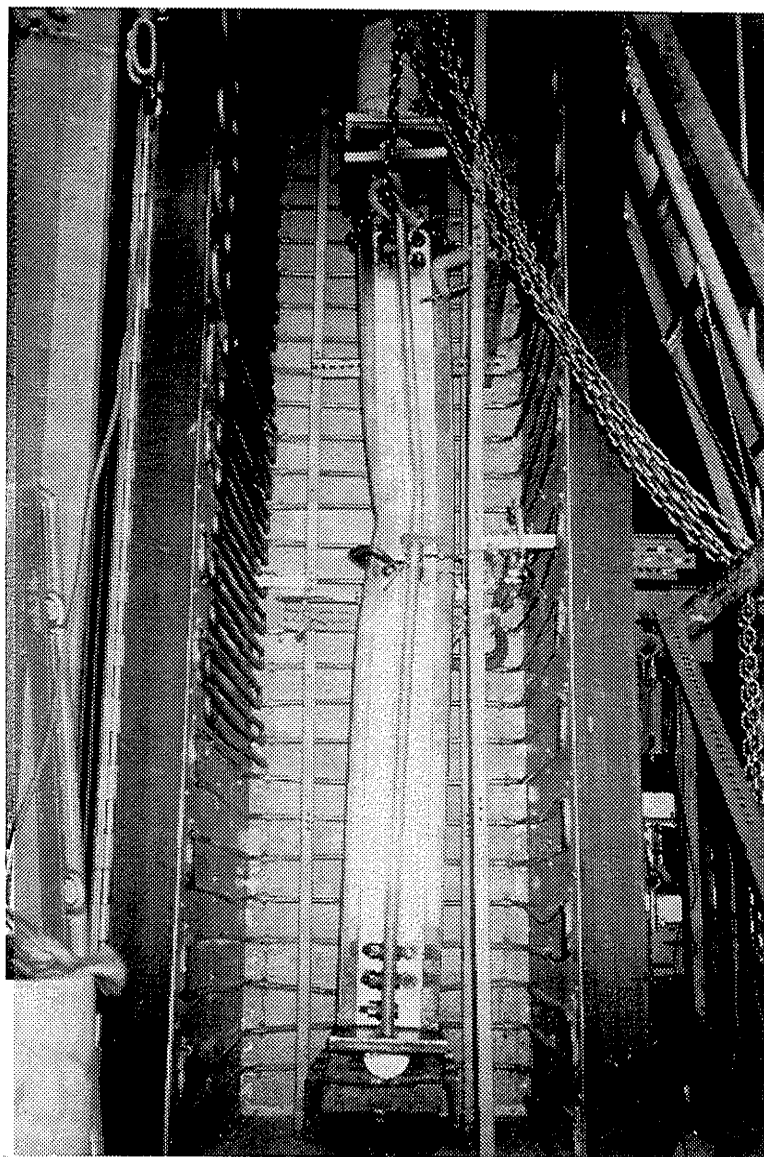


FIGURE 5.39
BG-40 Specimen at Failure

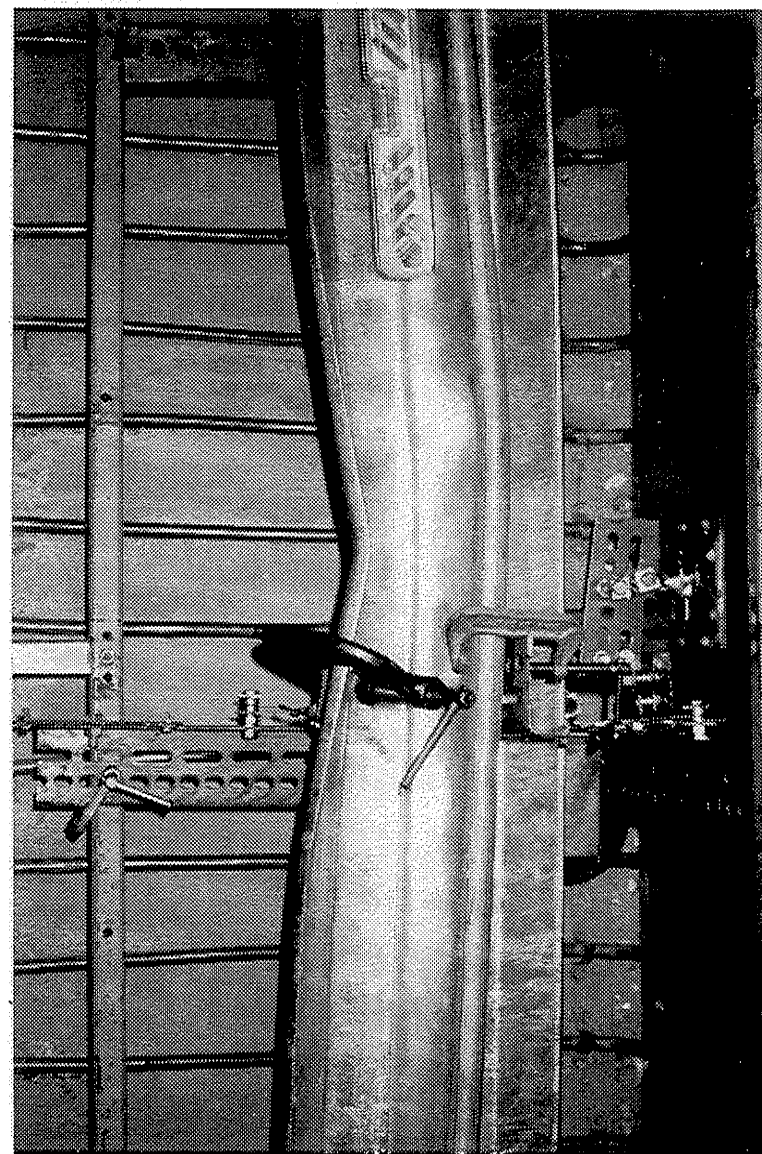


FIGURE 5.40
BG-40: Distortion of Stiffened Flange at Failure

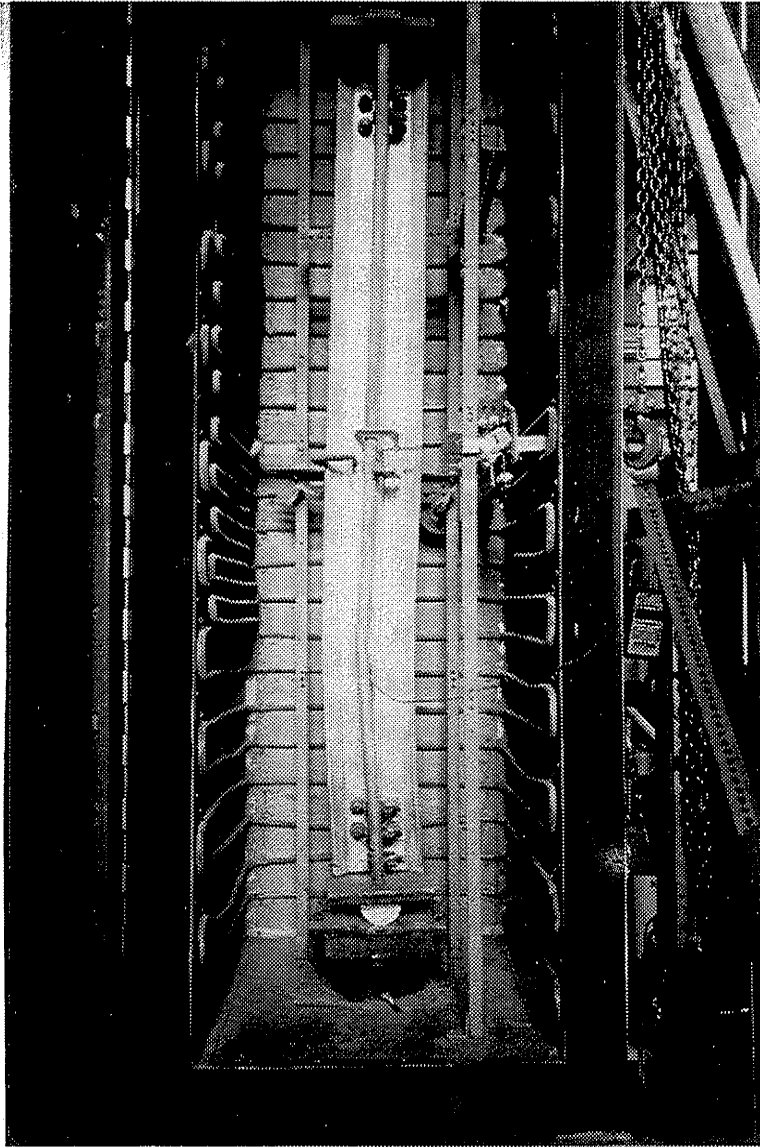


FIGURE 5.41
BG-40 Specimen at Failure

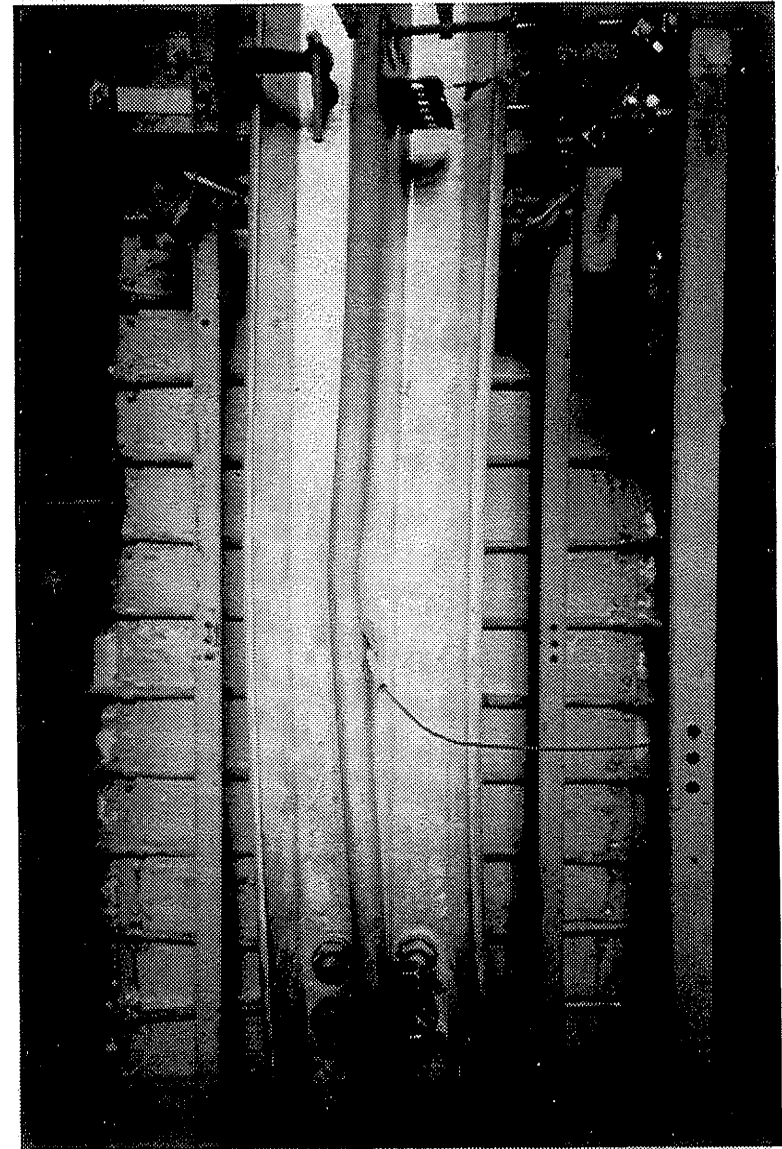


FIGURE 5.42
BG-40: Distortion of Web at Failure

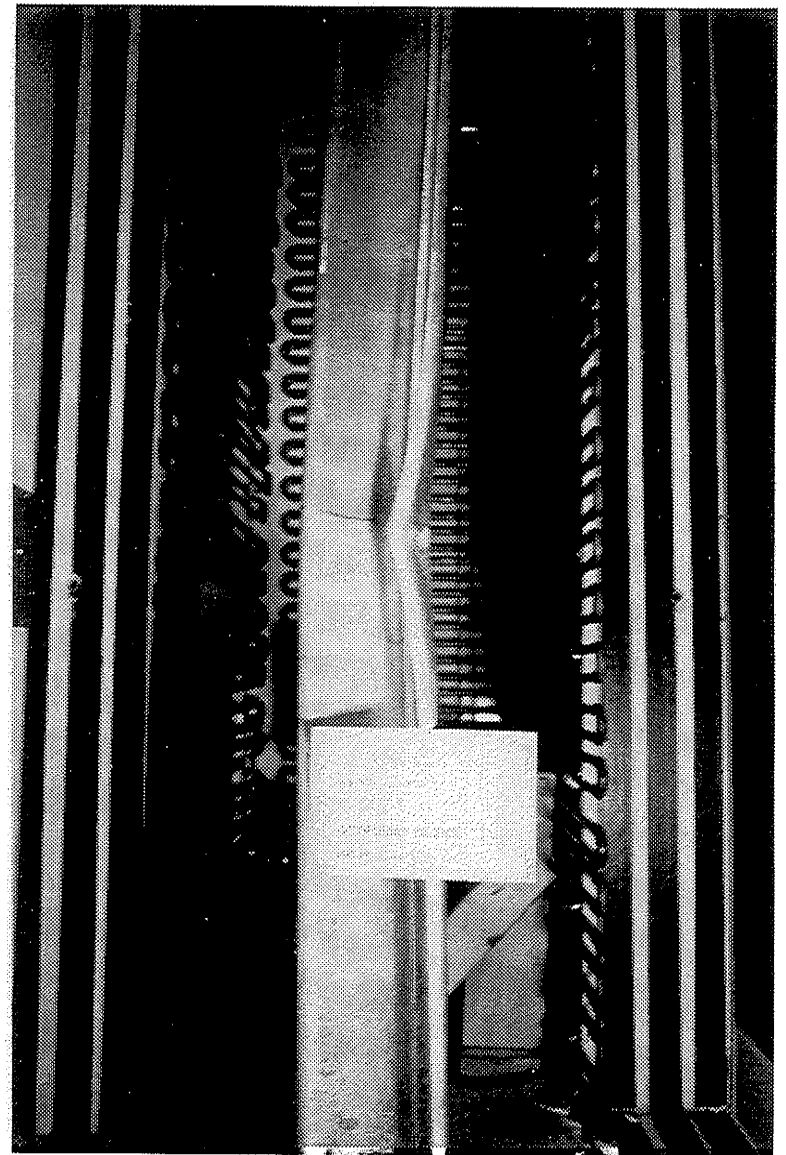
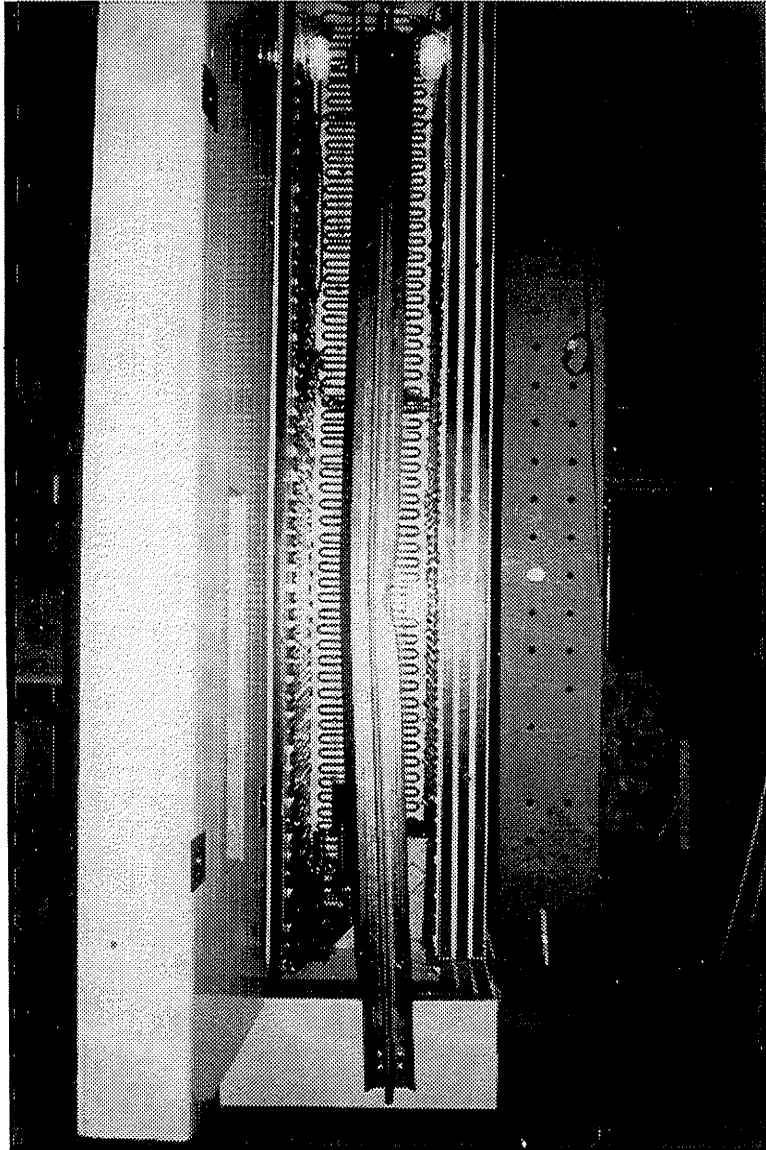


FIGURE 5.43
BG-100 Specimen after Failure

BG SPECIMEN ANALYSIS

CAN\CSA-S136-M89

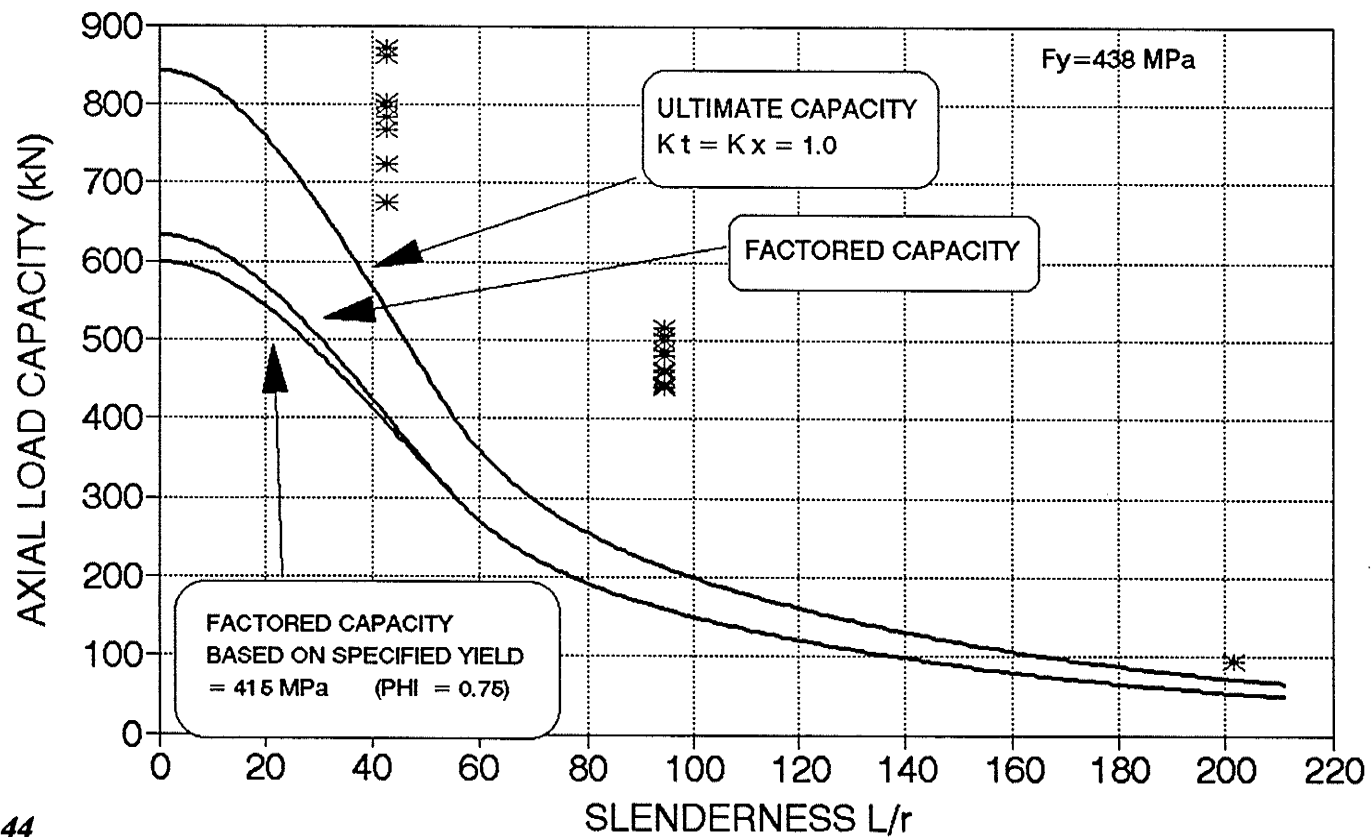


FIGURE 5.44
BG Section Analysis: CAN/CSA-S136-M89

BG SPECIMEN ANALYSIS

CAN/CSA-S136-M89

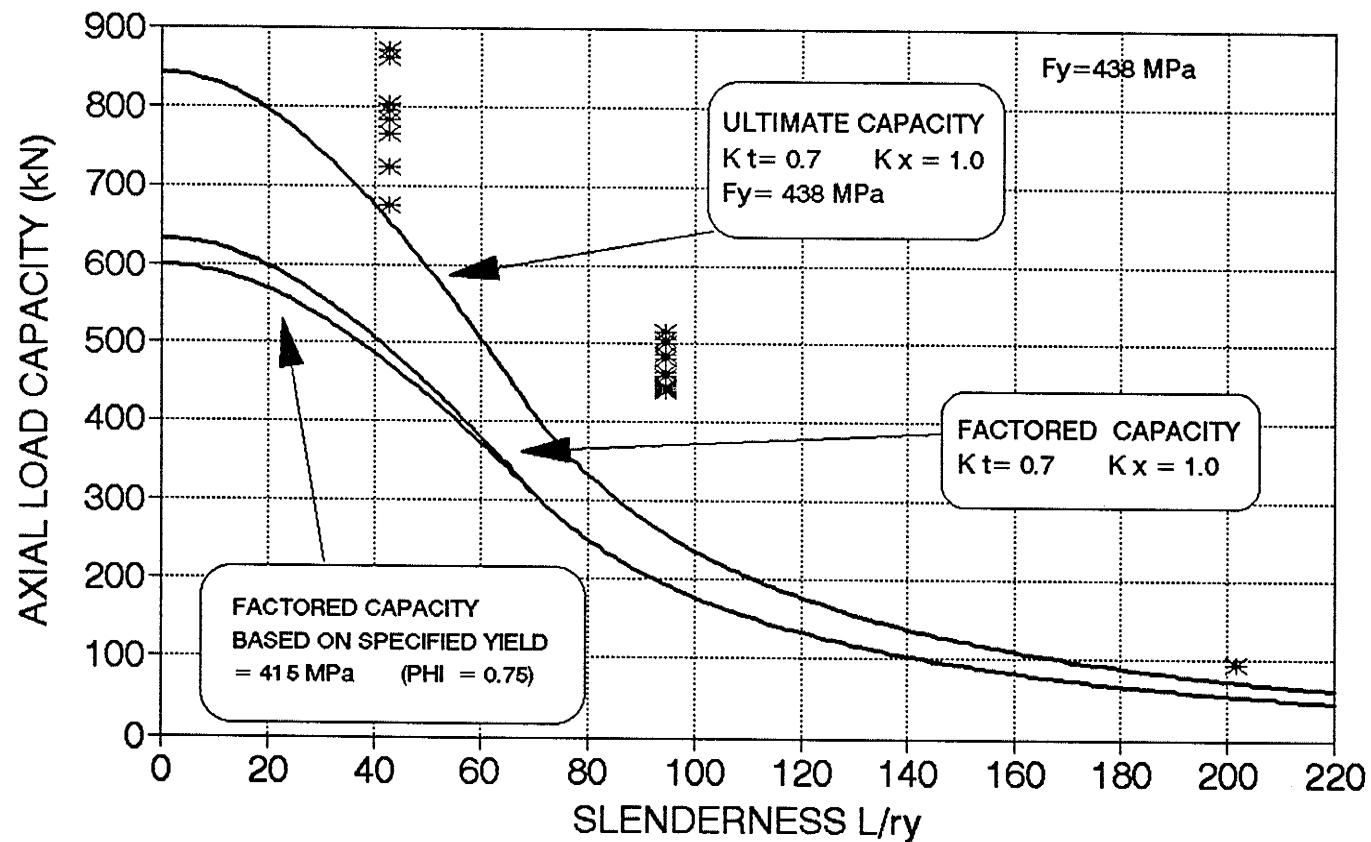


FIGURE 5.45

BG Section Analysis: CAN/CSA-S136-M89

$K_t = 0.7$

BG SPECIMEN ANALYSIS

ASCE MANUAL 52

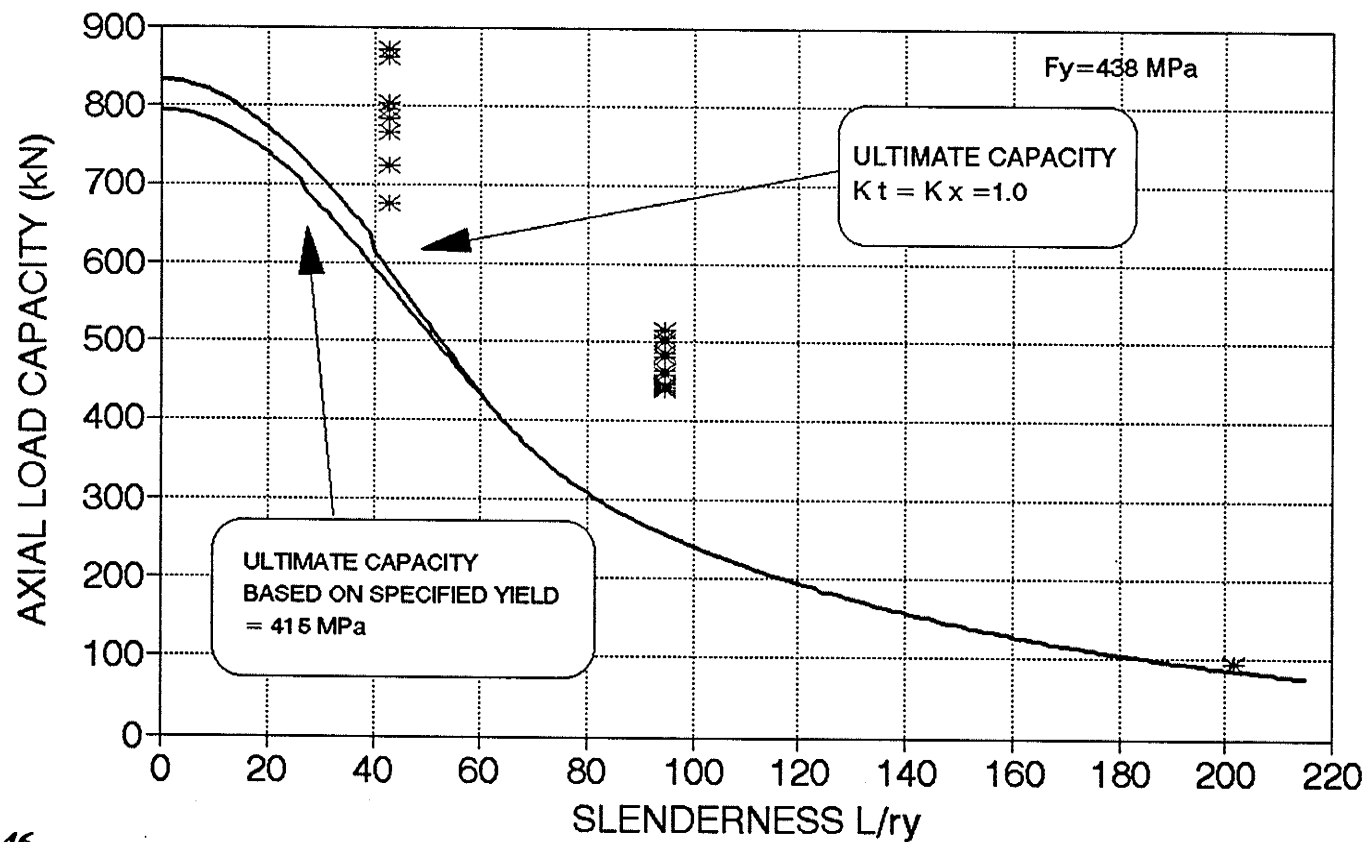


FIGURE 5.46
BG Section Analysis: ASCE Manual 52

BG SPECIMEN ANALYSIS

ASCE MANUAL 52

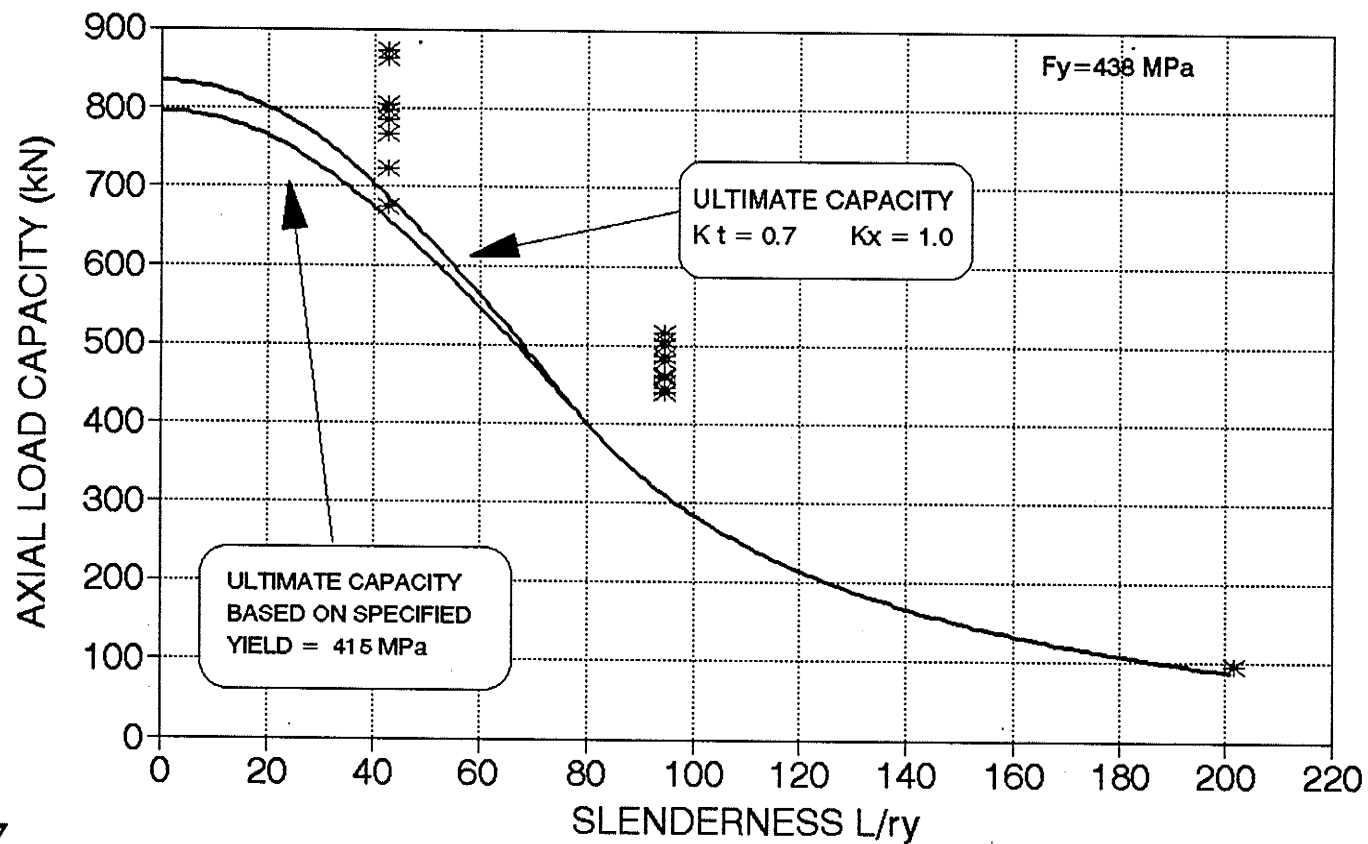


FIGURE 5.47

BG Section Analysis: ASCE Manual 52
 $K_t = 0.7$

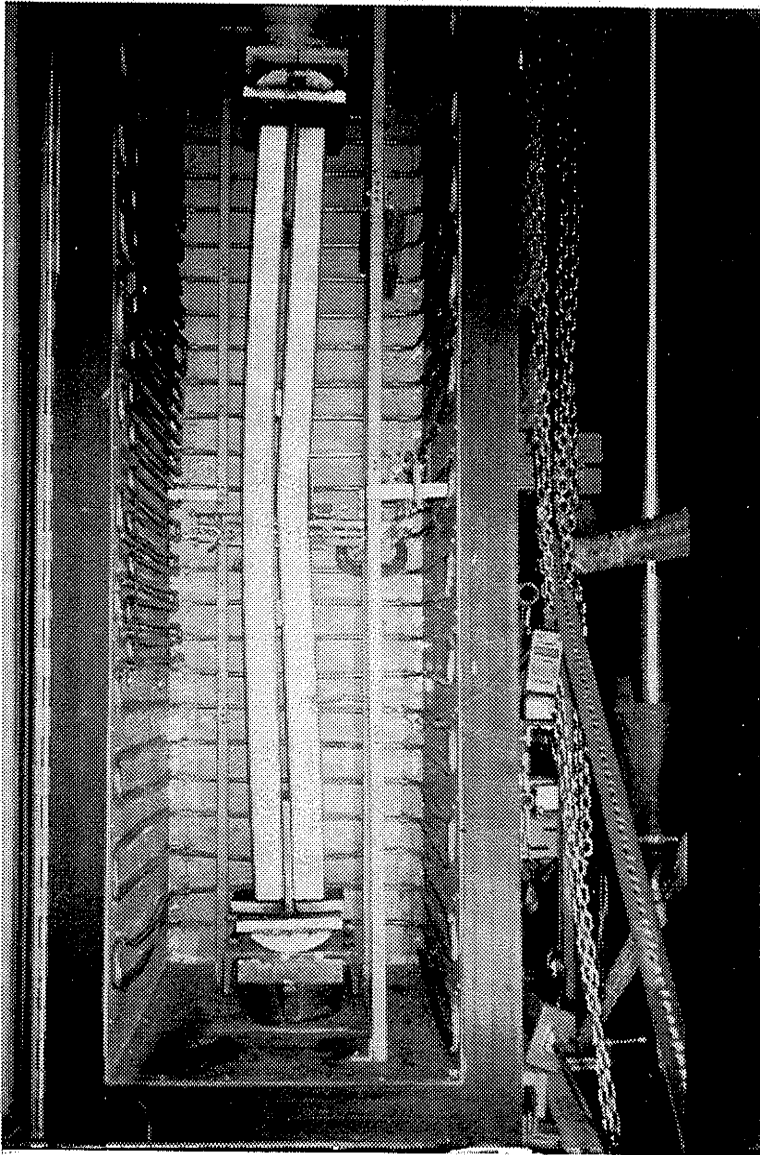


FIGURE 5.48
BN-40 Specimen at Failure

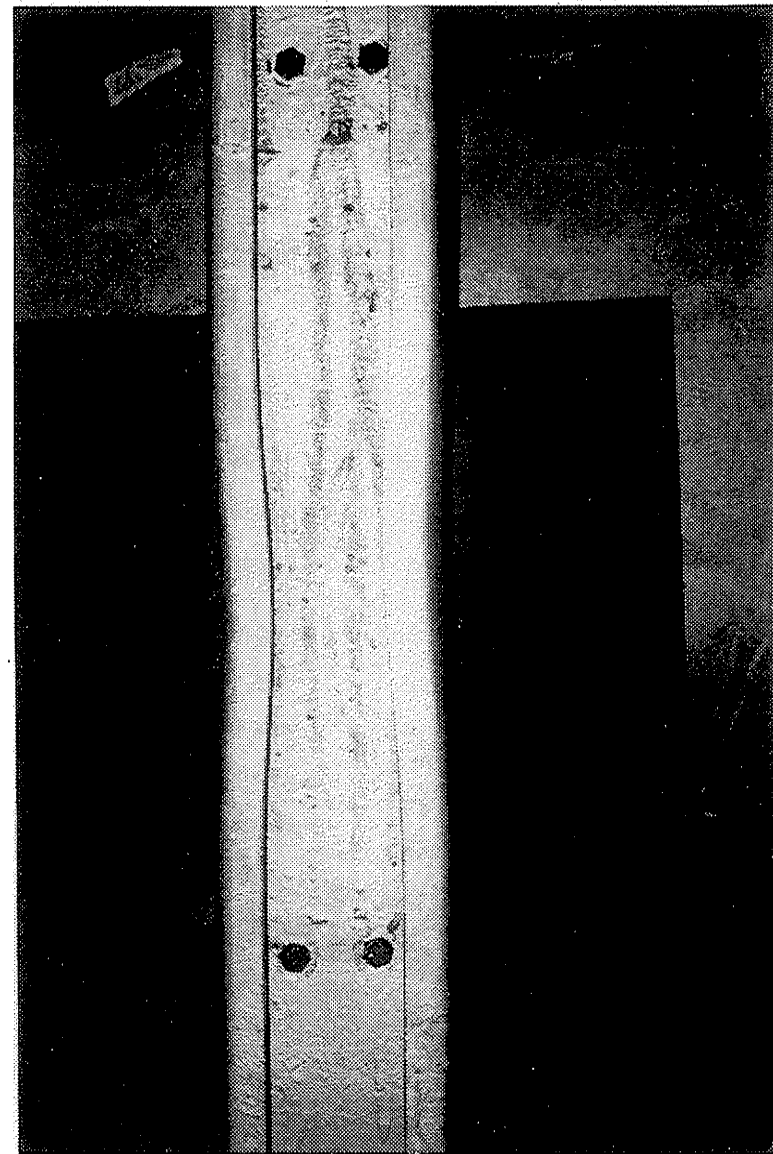


FIGURE 5.49
BN-40 Specimen Lip Distortion

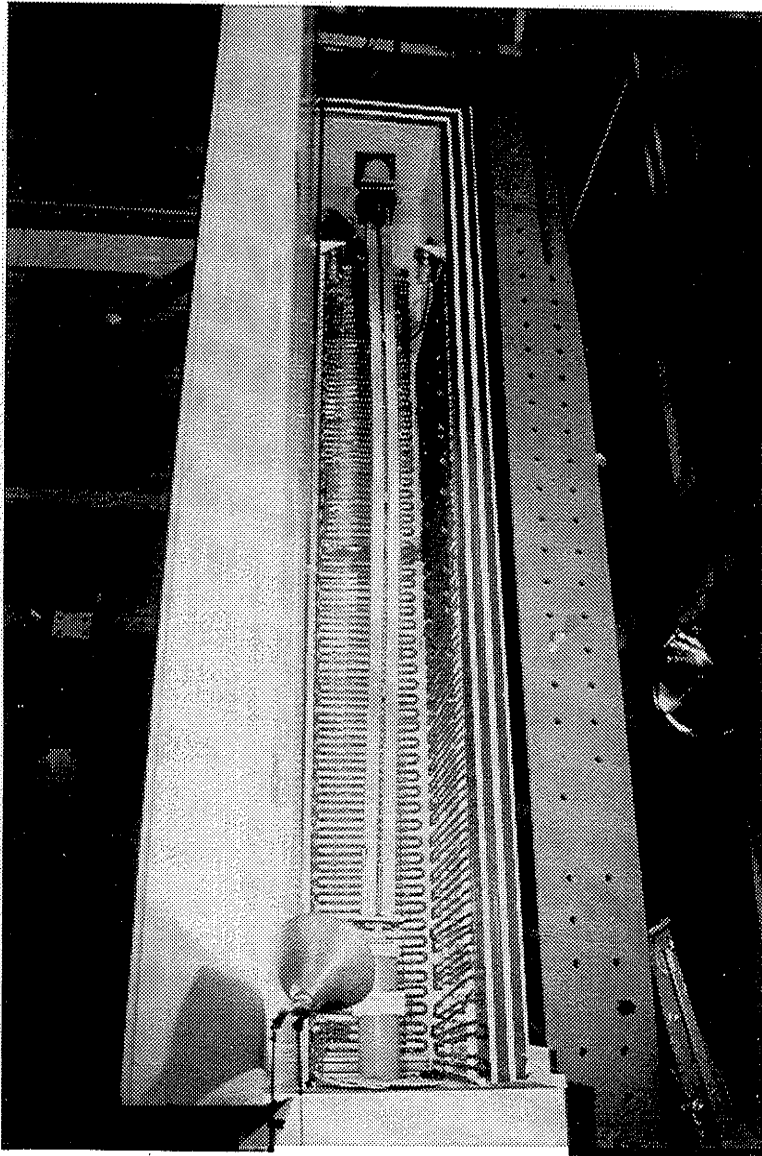


FIGURE 5.50
BN-100 Specimen at Failure

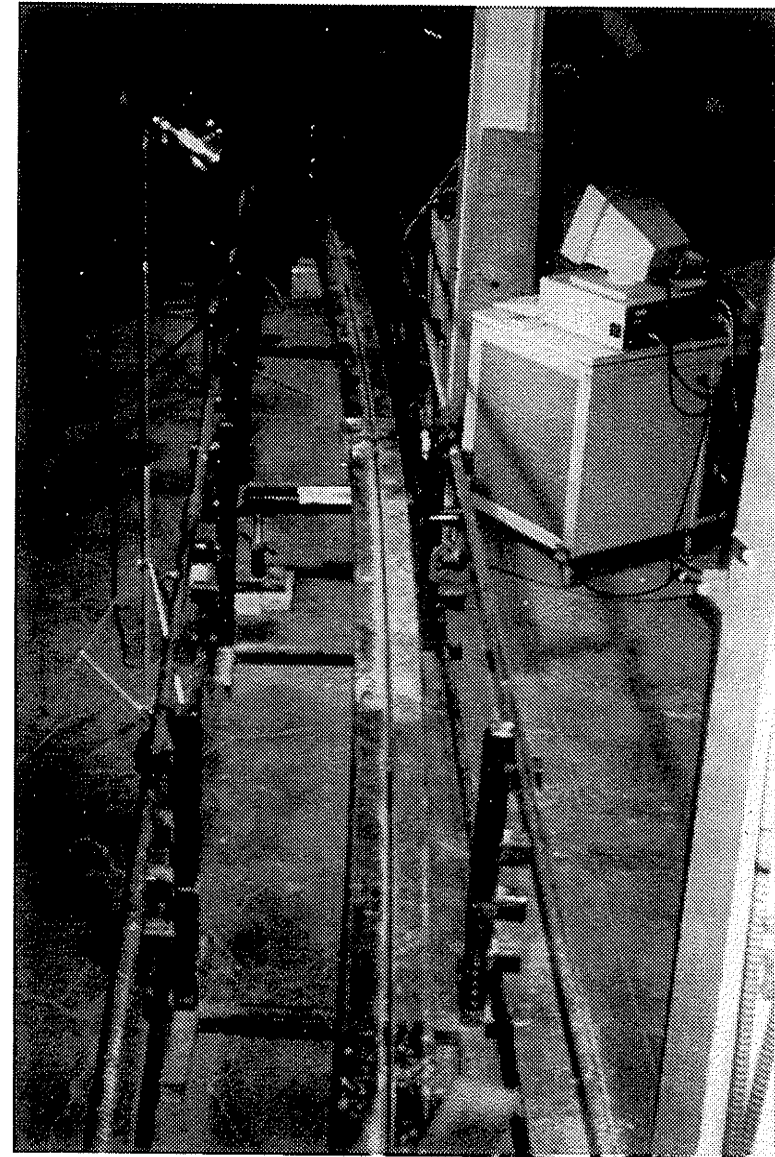


FIGURE 5.51
BN-200 Specimen at Failure

BN SECTION TESTS

CAN/CSA-S136

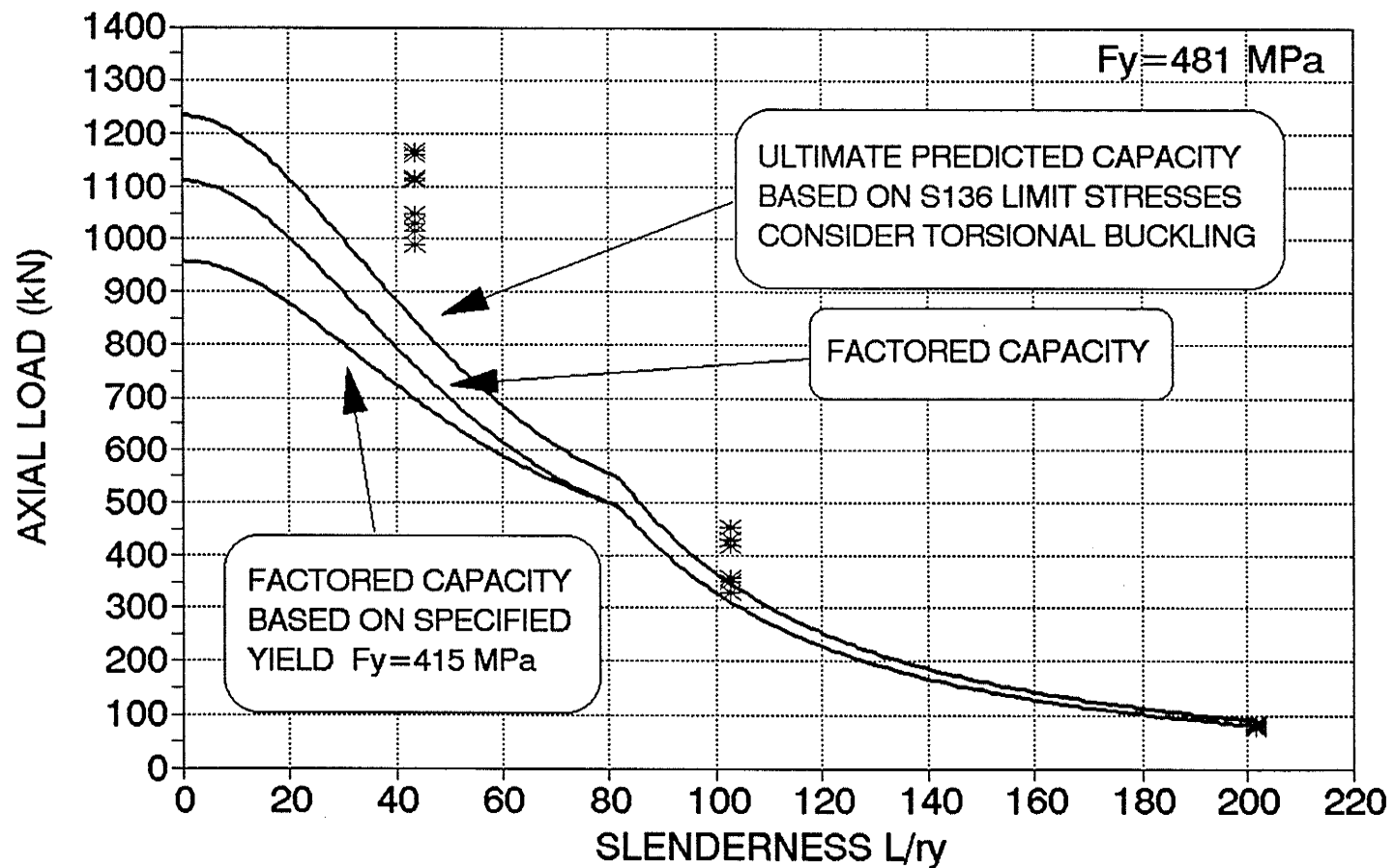


FIGURE 5.52
BN Section Analysis: CAN/CSA-S136-M89

BN SECTION TESTS

CAN/CSA-S136

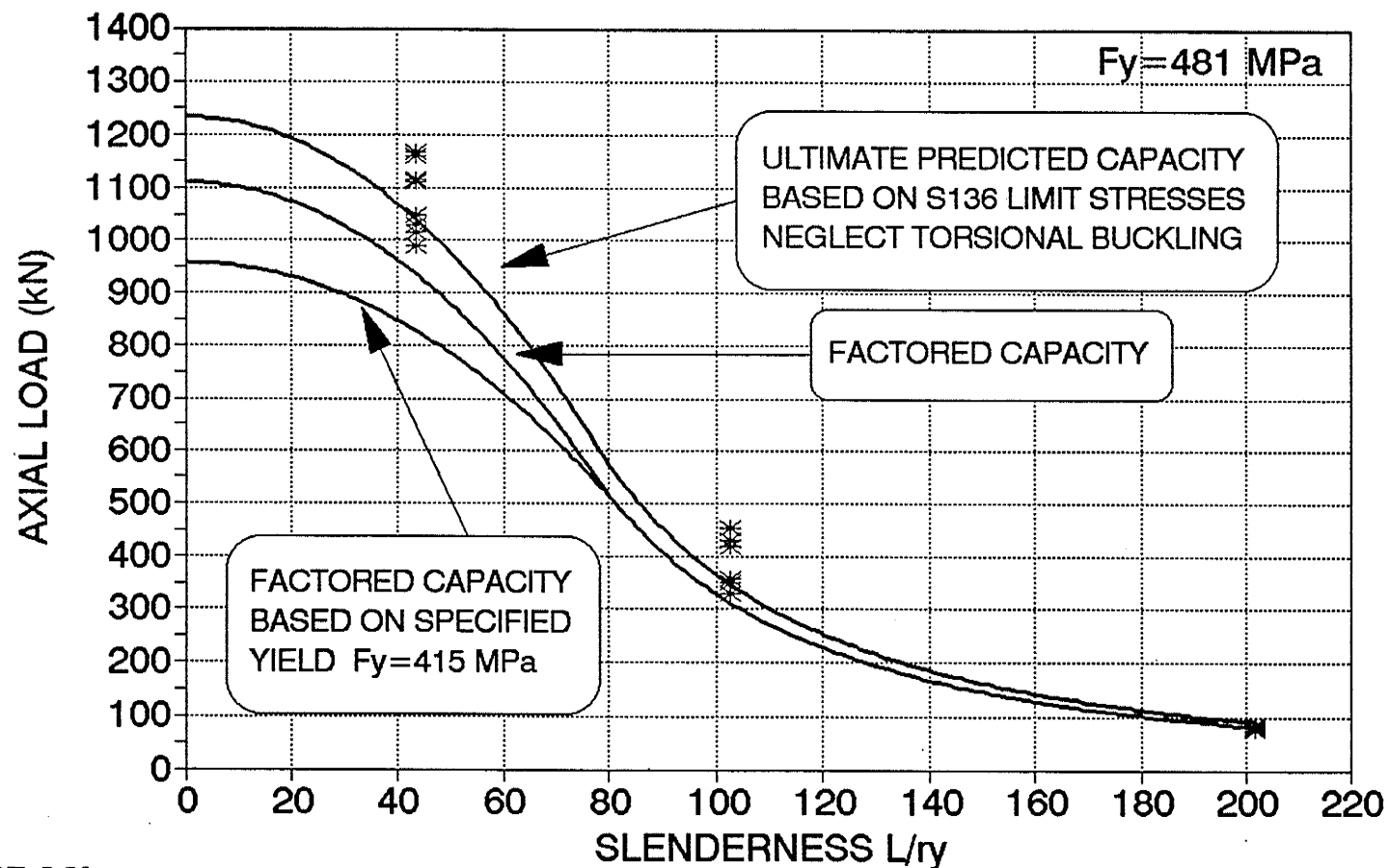


FIGURE 5.53
BN Section Analysis: CAN/CSA-S136-M89
Neglecting Torsional Buckling

HBN SECTION TESTS

CAN/CSA-S136

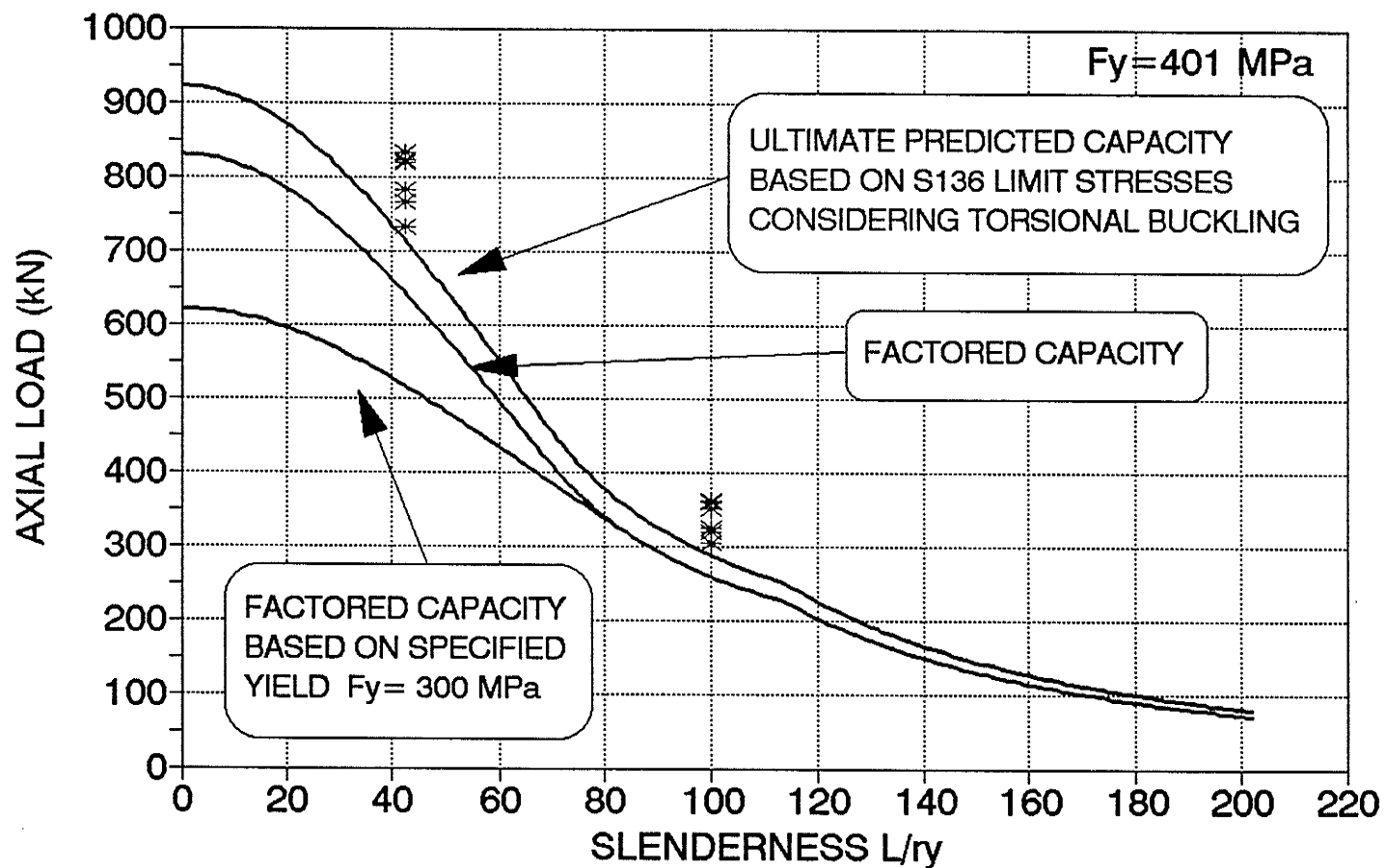


FIGURE 5.54
HBN Section Analysis: CAN/CSA-S136-M89

HBN SECTION TESTS

CAN/CSA-S136

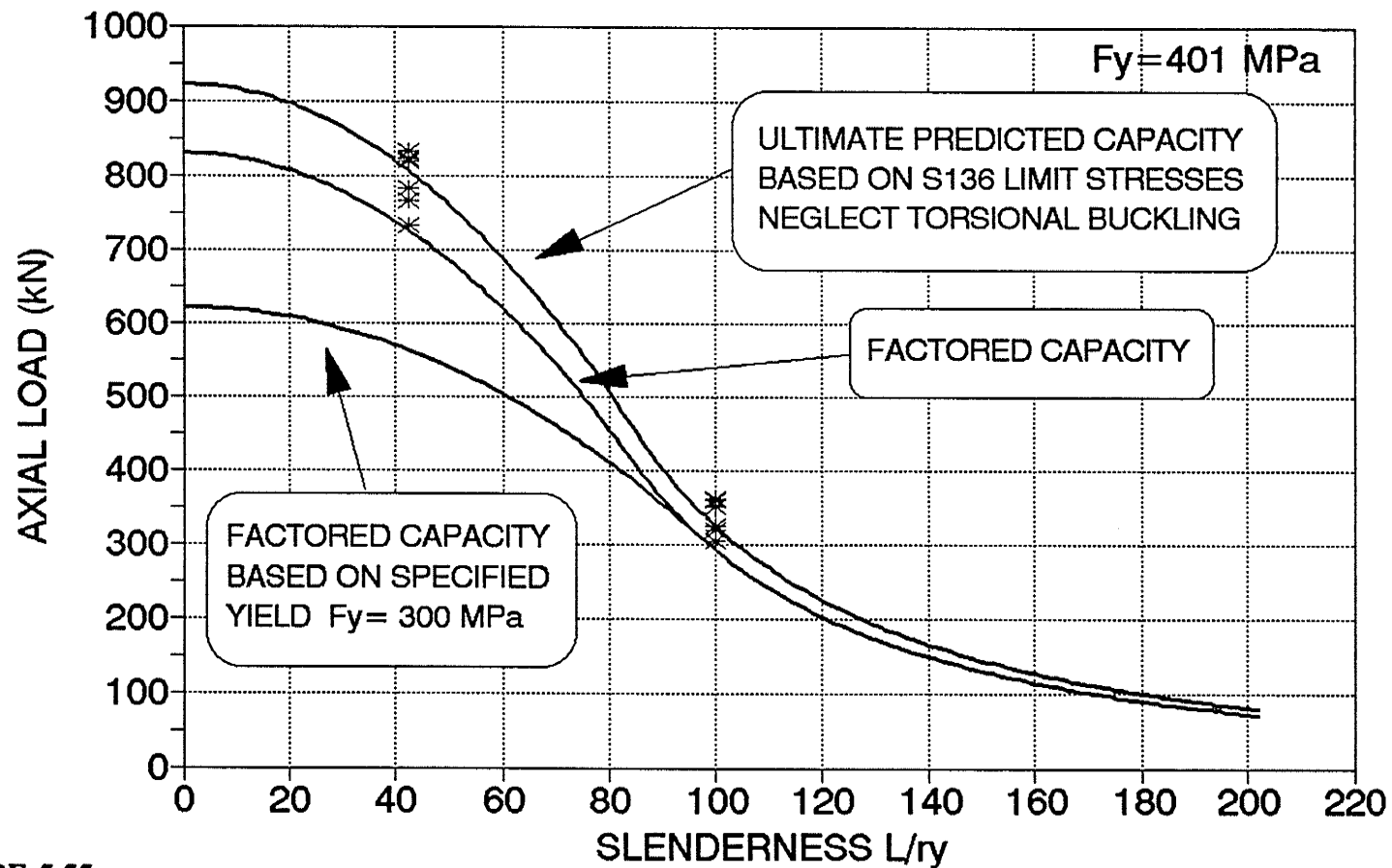


FIGURE 5.55
HBN Section Analysis: CAN/CSA-S136-M89
Neglecting Torsional Buckling

BN SECTION TESTS

CAN3-S16.1

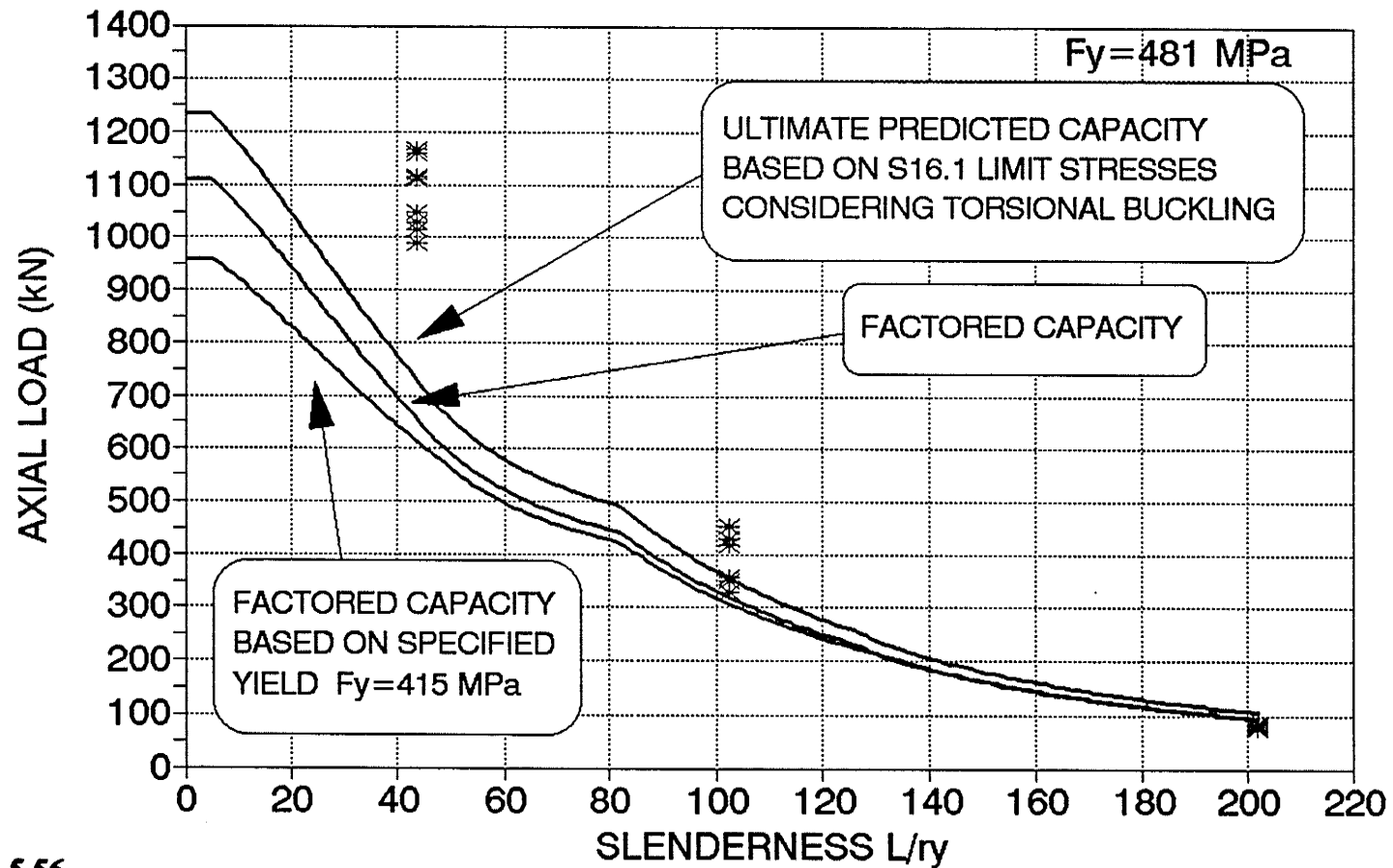


FIGURE 5.56

BN Section Analysis: CAN/CSA-S16.1-M89

BN SECTION TESTS

CAN3-S16.1

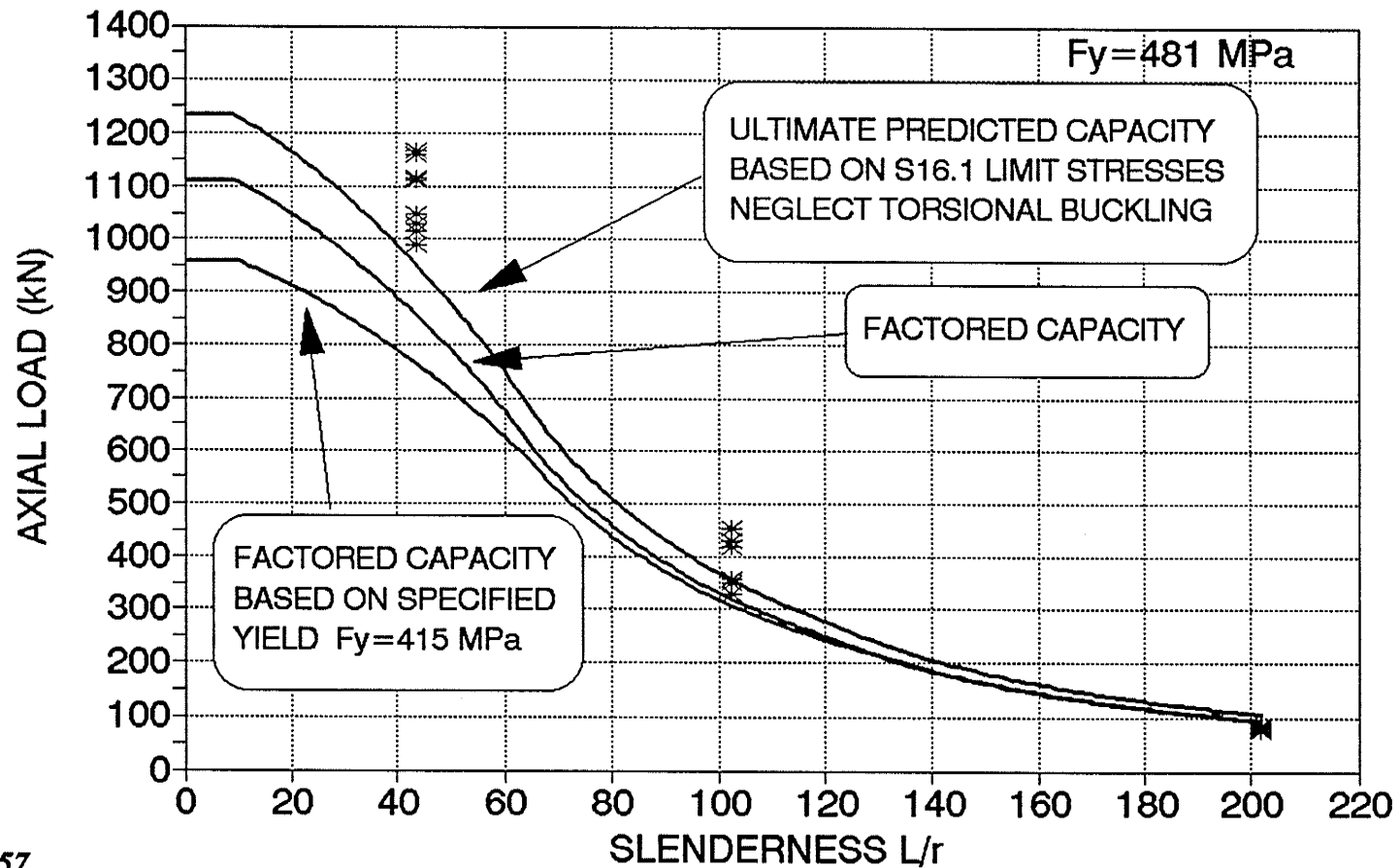


FIGURE 5.57

BN Section Analysis: CAN/CSA-S16.1-M89

Neglecting Torsional Buckling

HBN SECTION TESTS

CAN3-S16.1

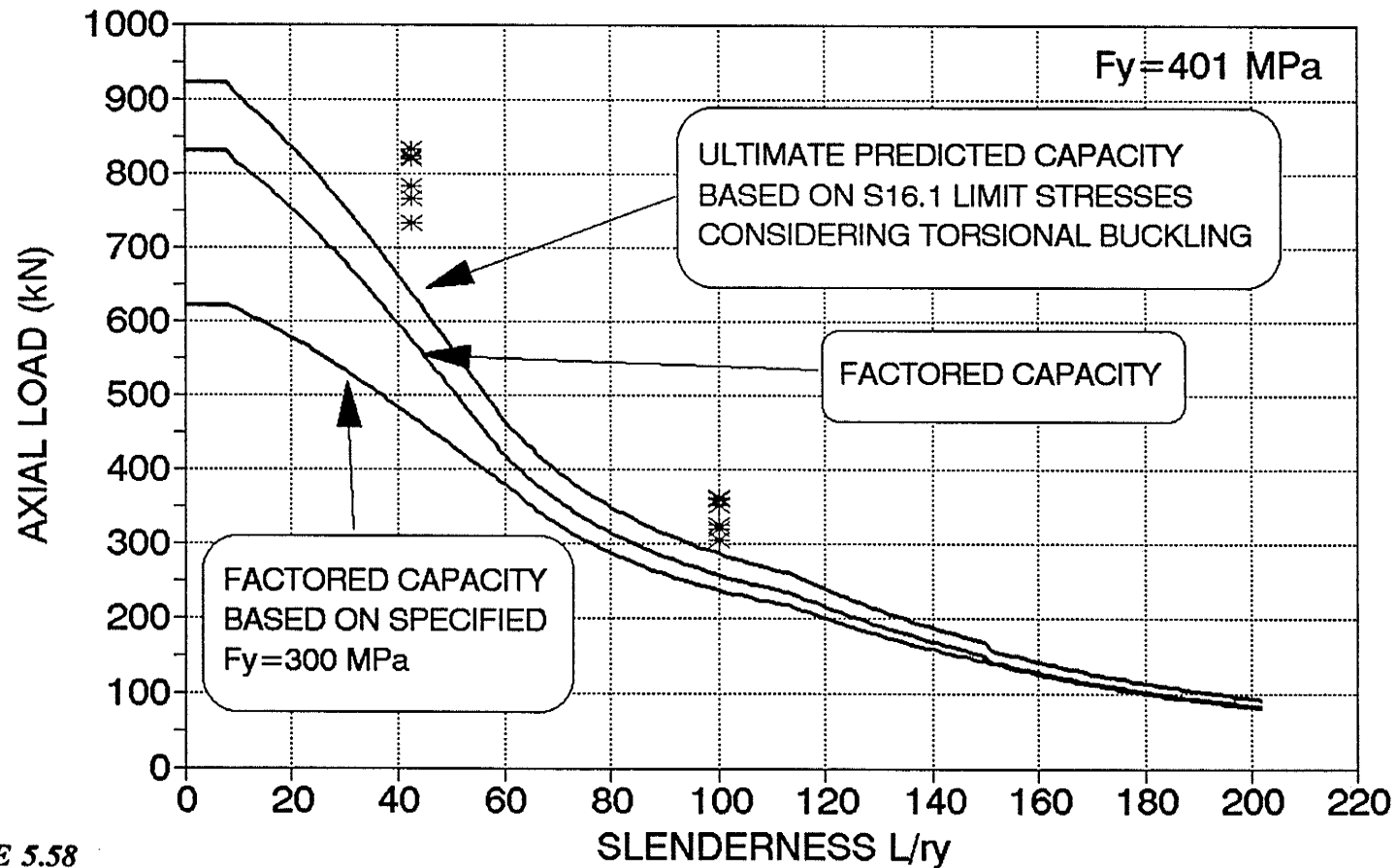


FIGURE 5.58

HBN Section Analysis: CAN/CSA-S16.1-M89

HBN SECTION TESTS

CAN3-S16.1

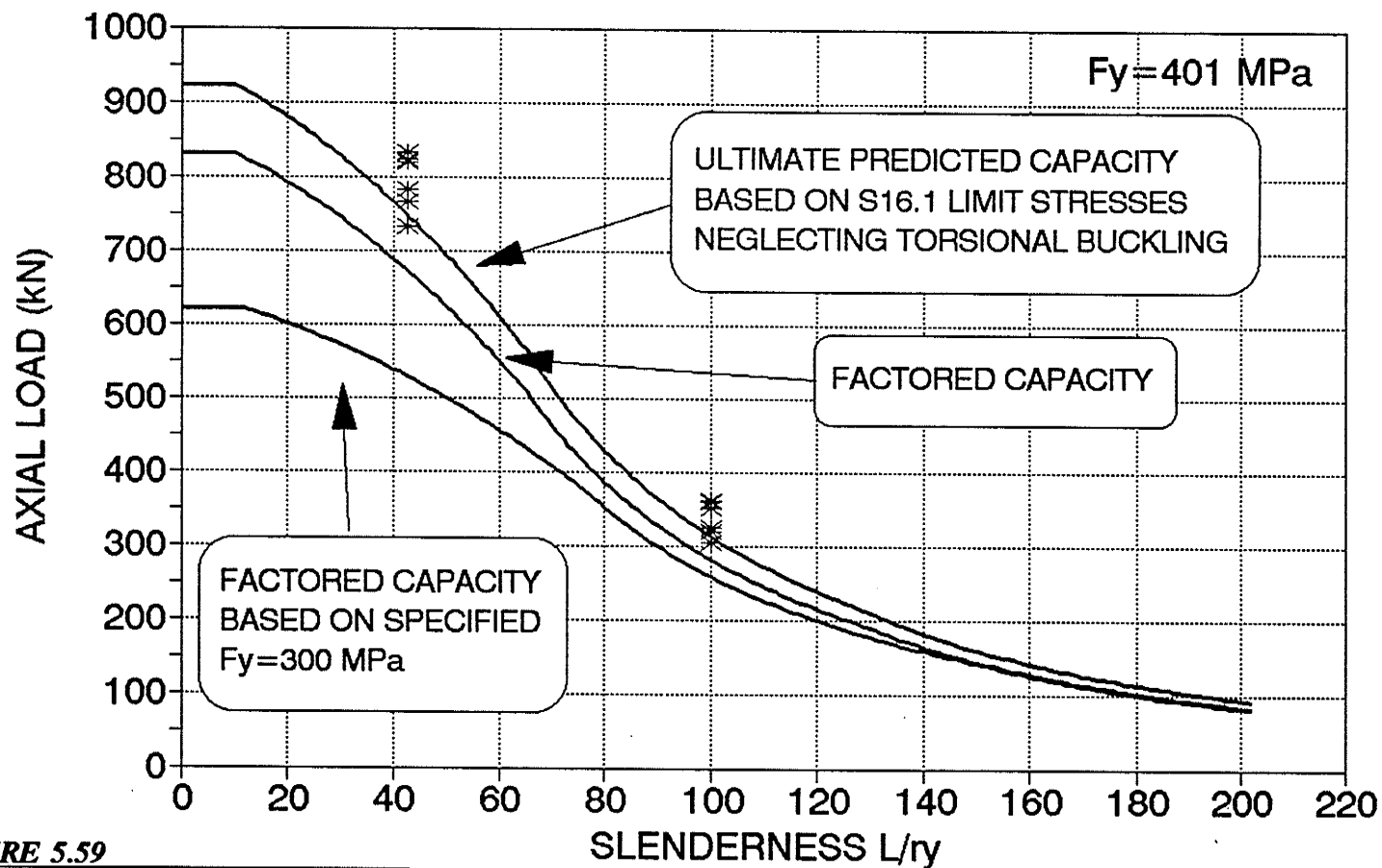


FIGURE 5.59

HBN Section Analysis: CAN/CSA-S16.1-M89

Neglecting Torsional Buckling

BN SECTION TESTS

ASCE MANUAL 52

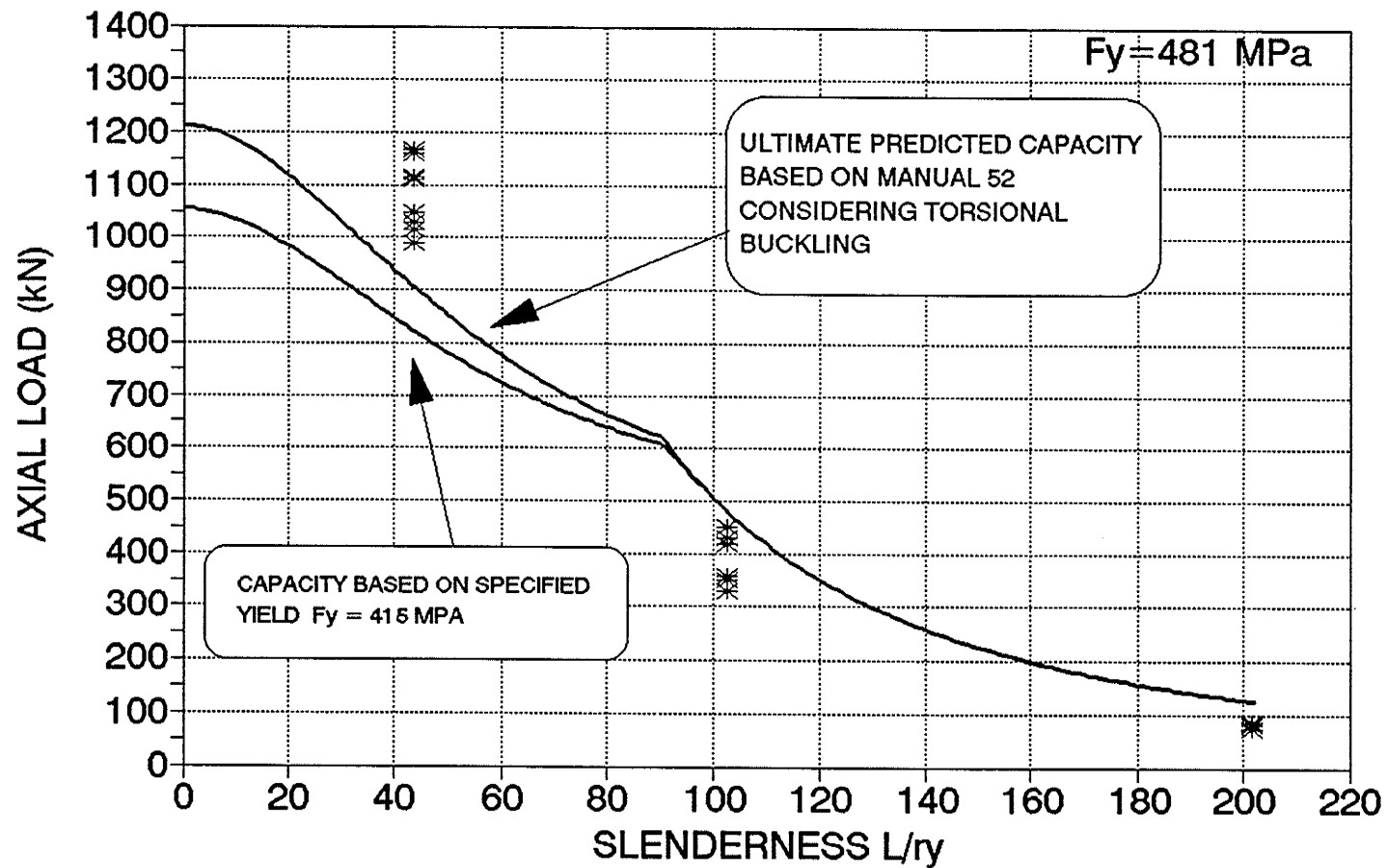


FIGURE 5.60
BN Section Analysis: ASCE Manual 52

BN SECTION TESTS

ASCE MANUAL 52

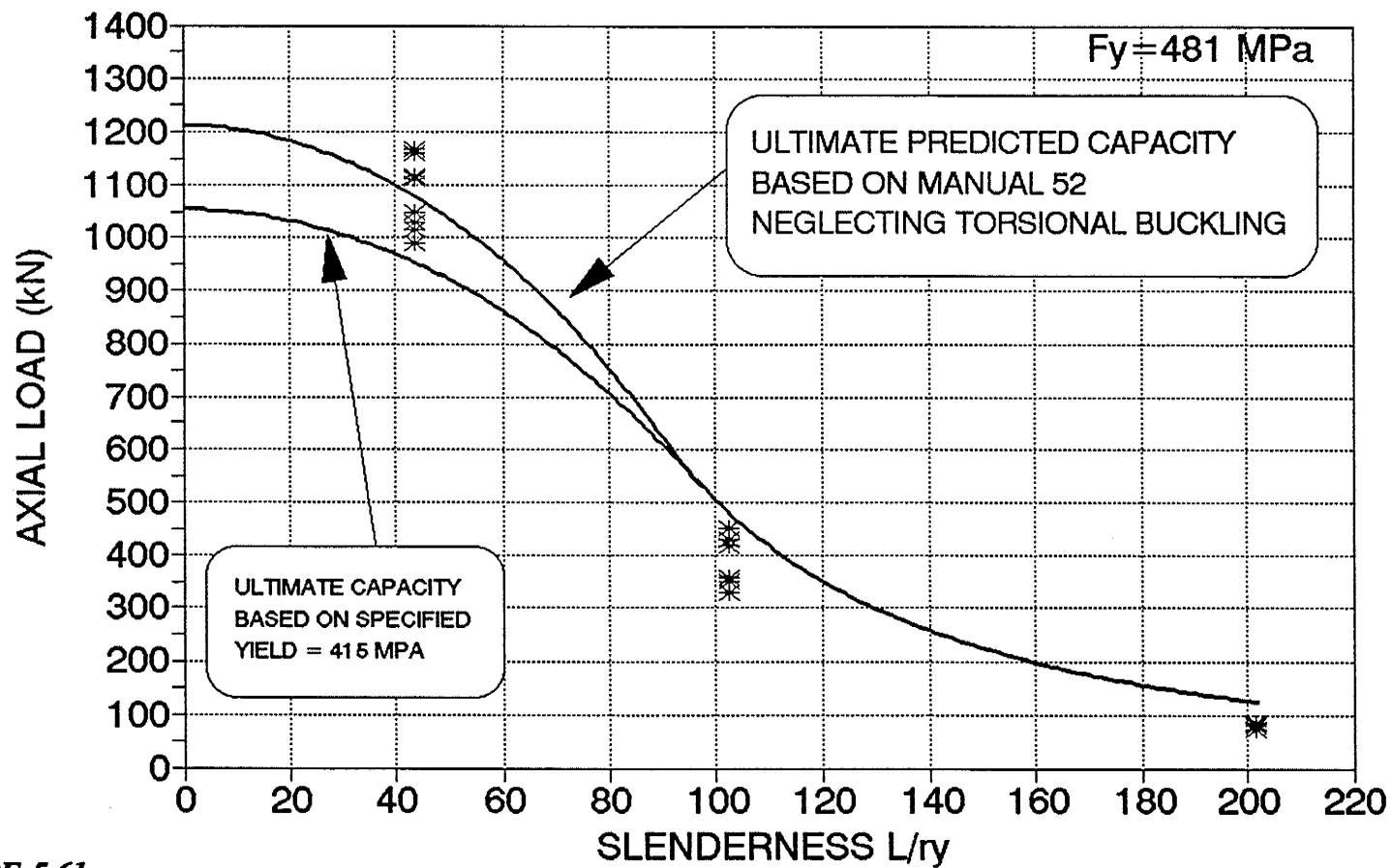


FIGURE 5.61
BN Section Analysis: ASCE Manual 52
Neglecting Torsional Buckling

HBN SECTION TESTS

ASCE MANUAL 52

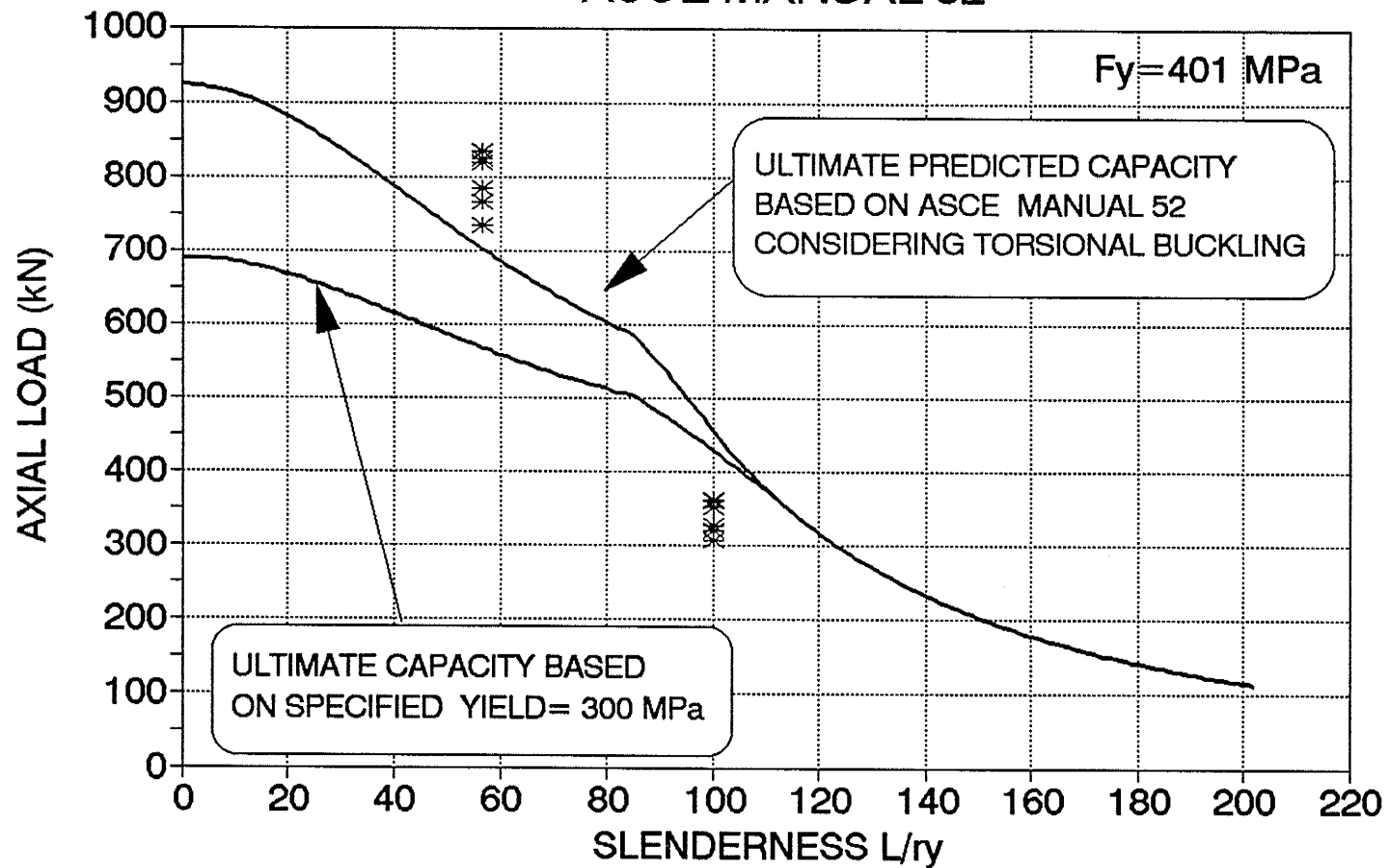


FIGURE 5.62

HBN Section Analysis: ASCE Manual 52

HBN SECTION TESTS

ASCE MANUAL 52

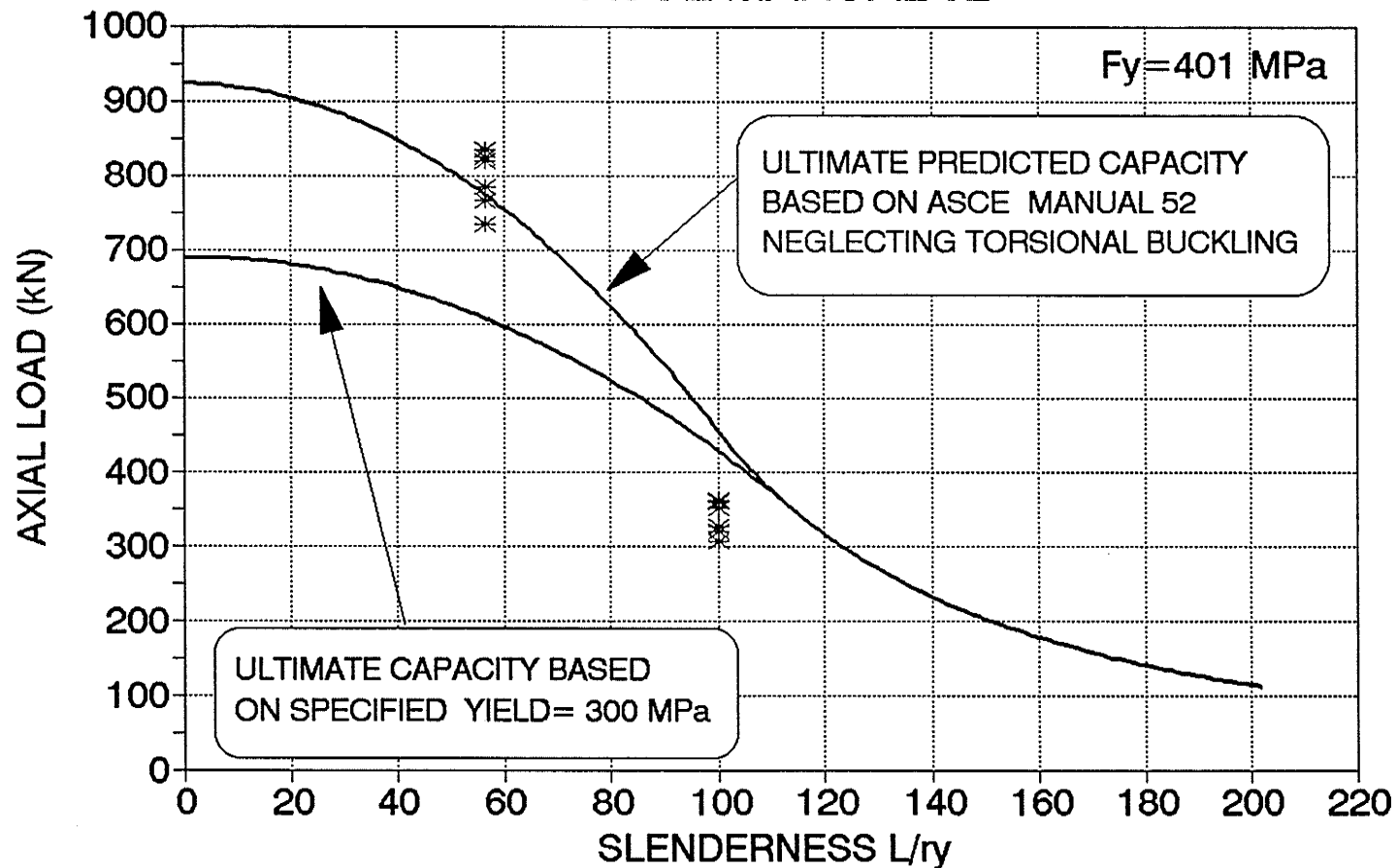


FIGURE 5.63

HBN Section Analysis: ASCE Manual 52

Neglecting Torsional Buckling

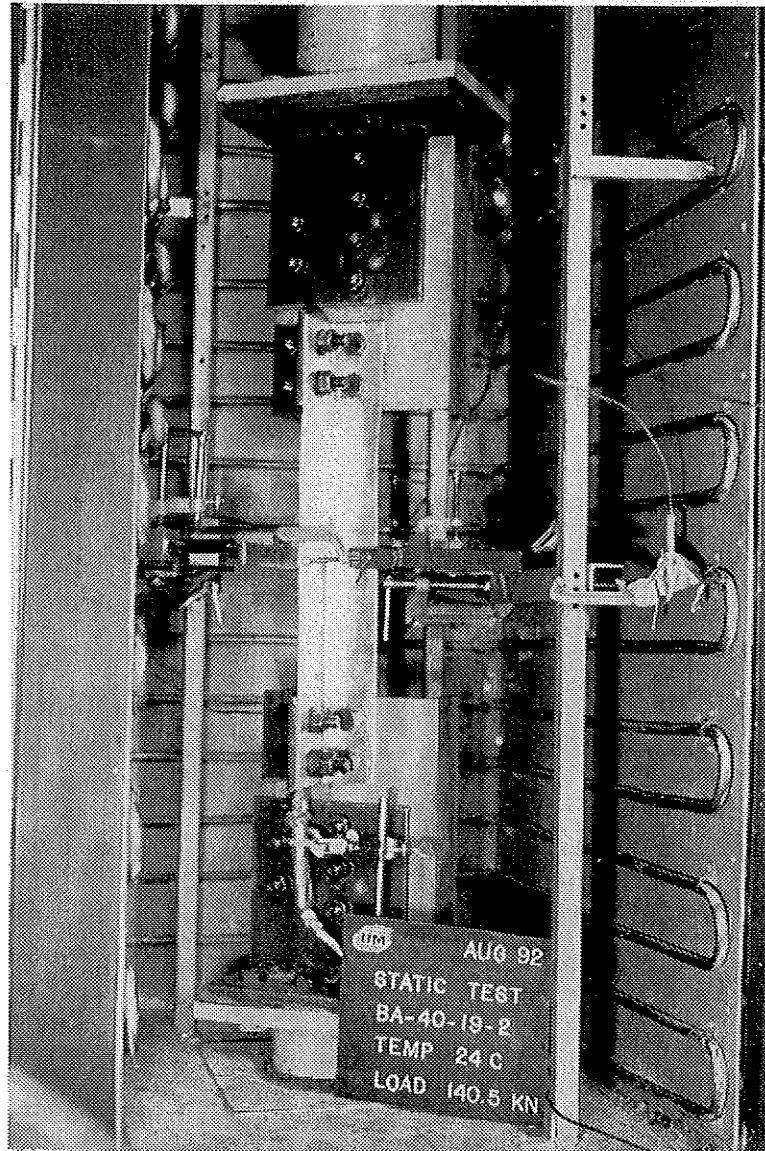
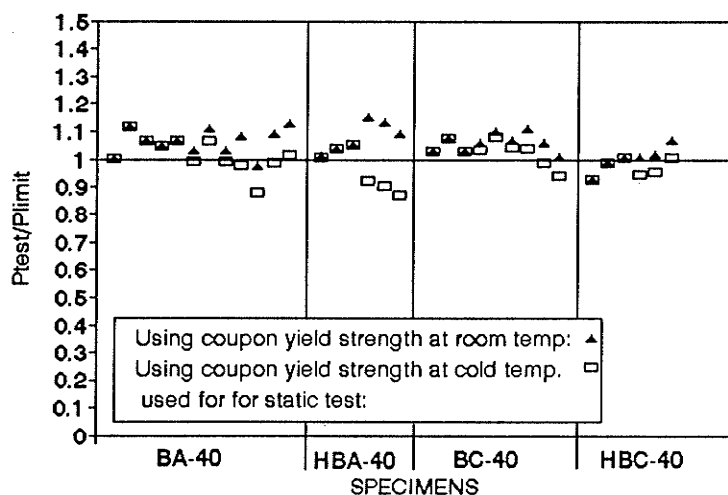


FIGURE 5.64
BA-40 Specimen with Both Legs Connected

RATIO OF EXPERIMENTAL RESULTS TO PROPOSED UPPER LOAD LIMIT FOR SHORT UNSTIFFENED ANGLES



PROPOSED COMPRESSIVE STRENGTH LIMIT FOR UNSTIFFENED ANGLES LOADED THROUGH ONE LEG

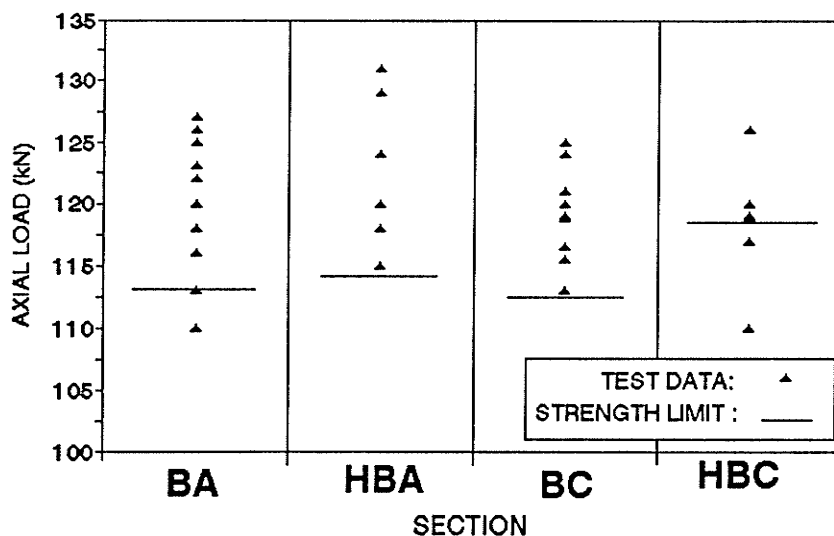


FIGURE 5.65

*Proposed Upper Limit Compressive Strength for
Unstiffened Angles Loaded Through One Leg*

Experimental .vs. Design Capacity Based On Modified ASCE Manual 52

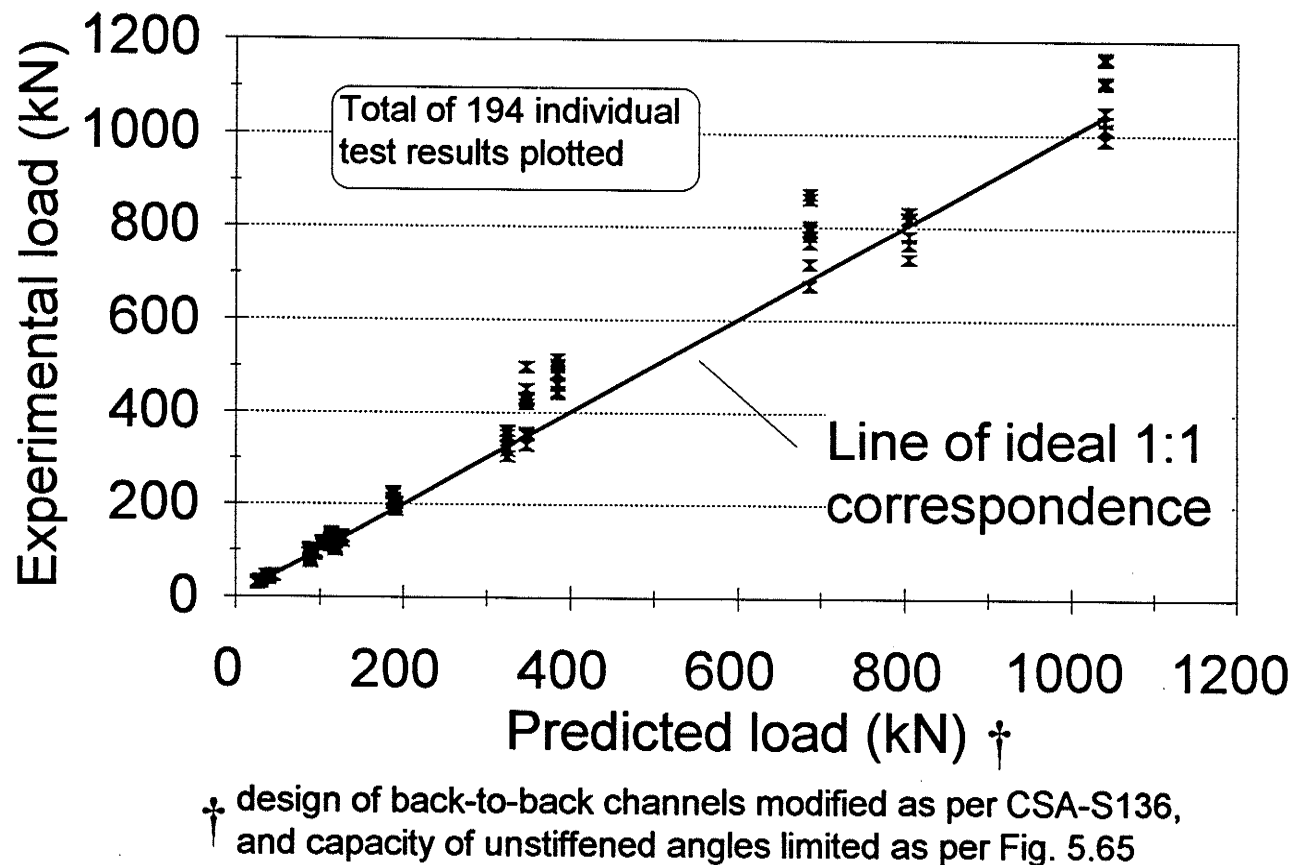
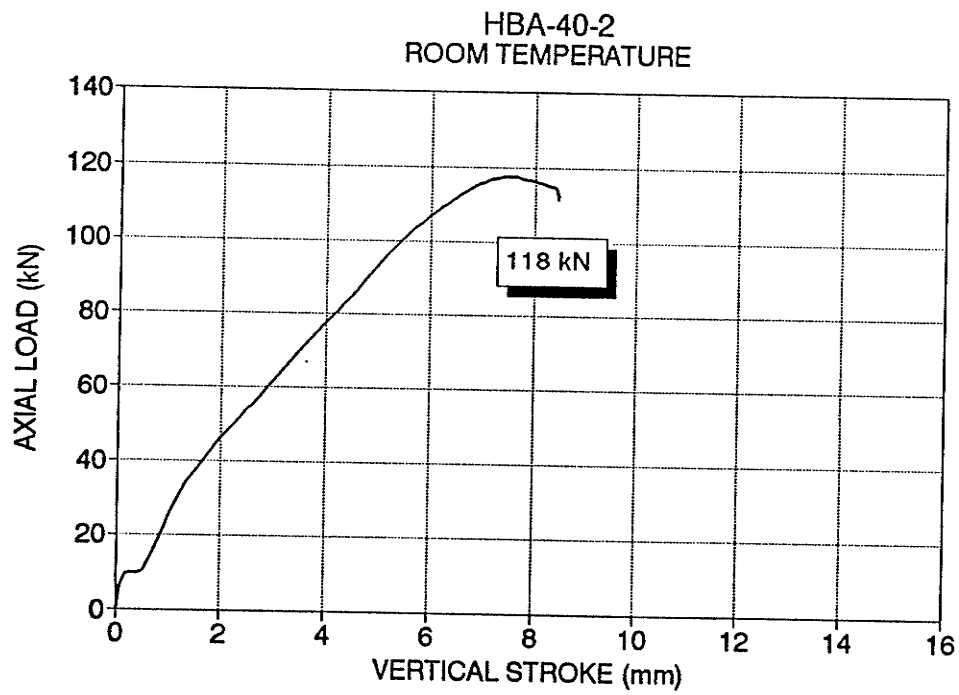
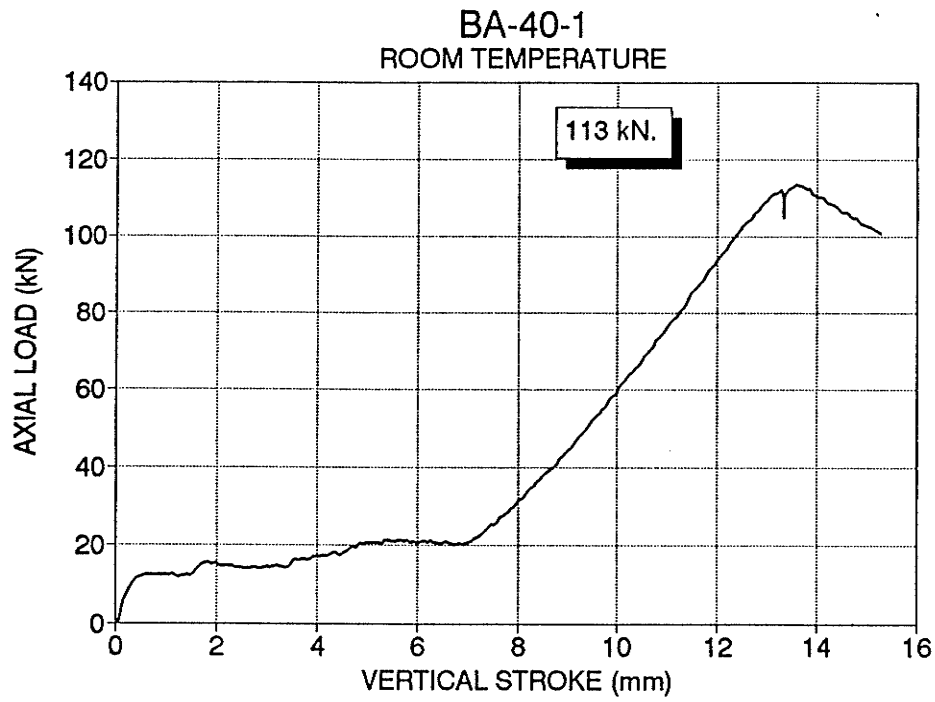


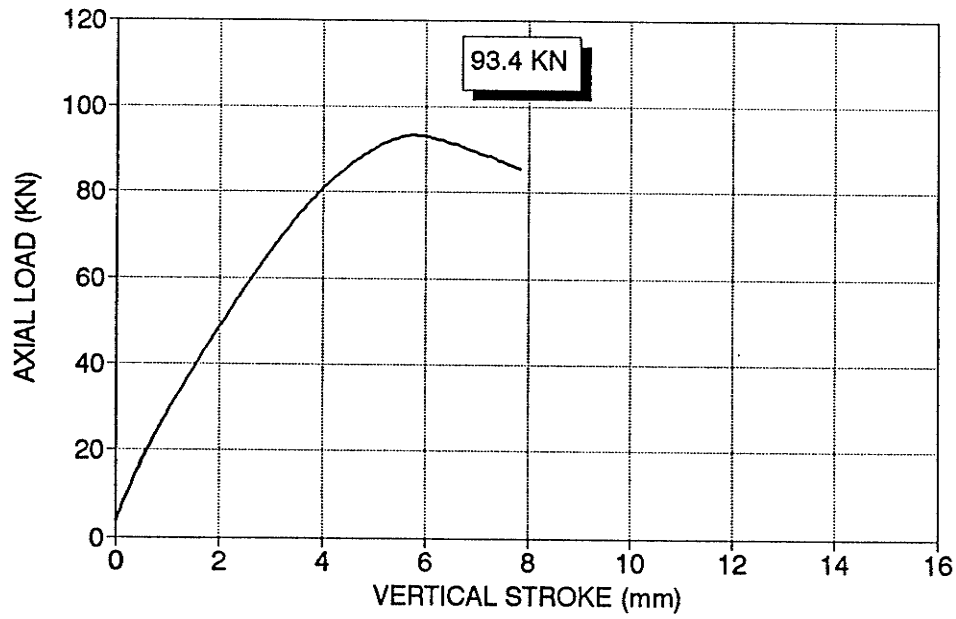
FIGURE 5.66

Comparison of test results to Modified ASCE Manual 52 Predicted loads

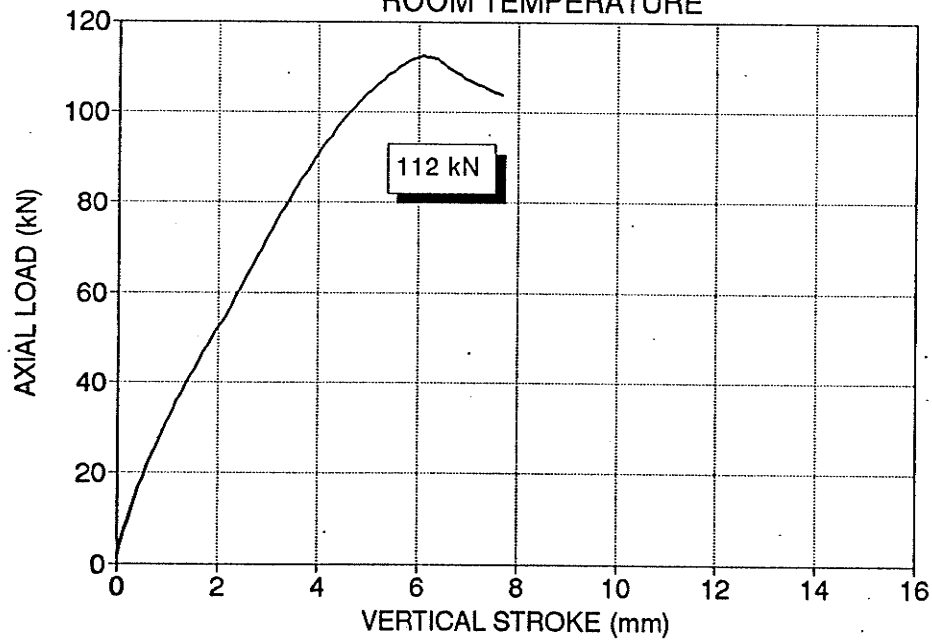
APPENDIX A



A.1 Typical Load-Displacement curves for Specimens BA-40 and HBA-40



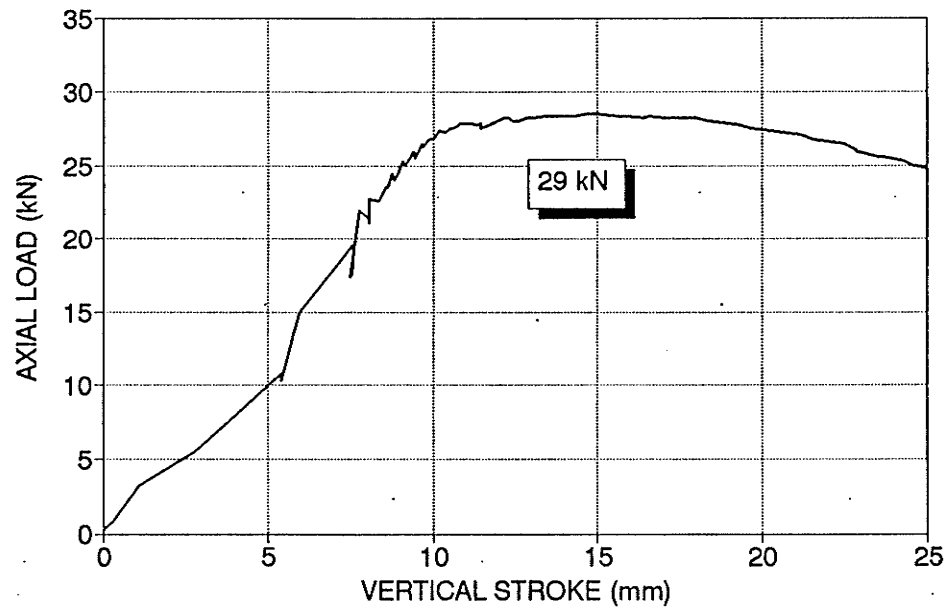
HBA-100-2
ROOM TEMPERATURE



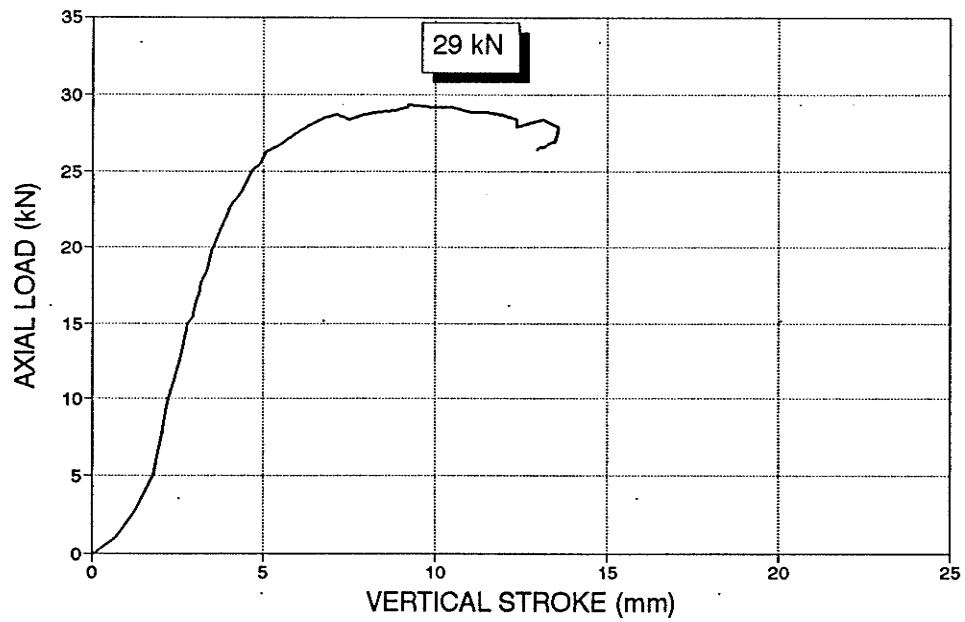
A.2 Typical Load-Displacement curves for Specimens BA-100 and HBA-100

BA-200-1
ROOM TEMPERATURE

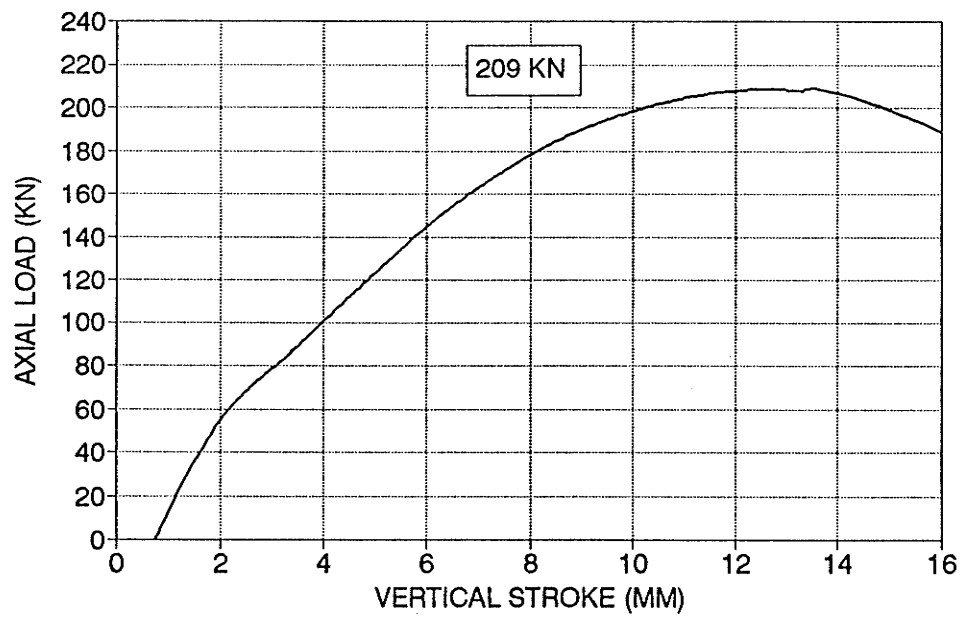
200



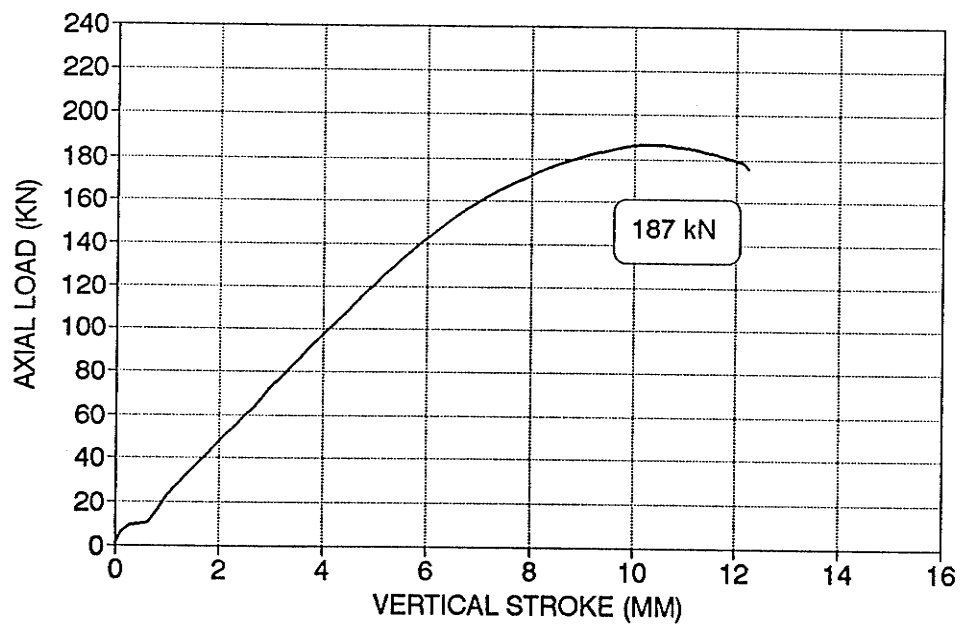
HBA-200-1
ROOM TEMPERATURE



A.3 Typical Load-Displacement curves for Specimens BA-200 and HBA-200



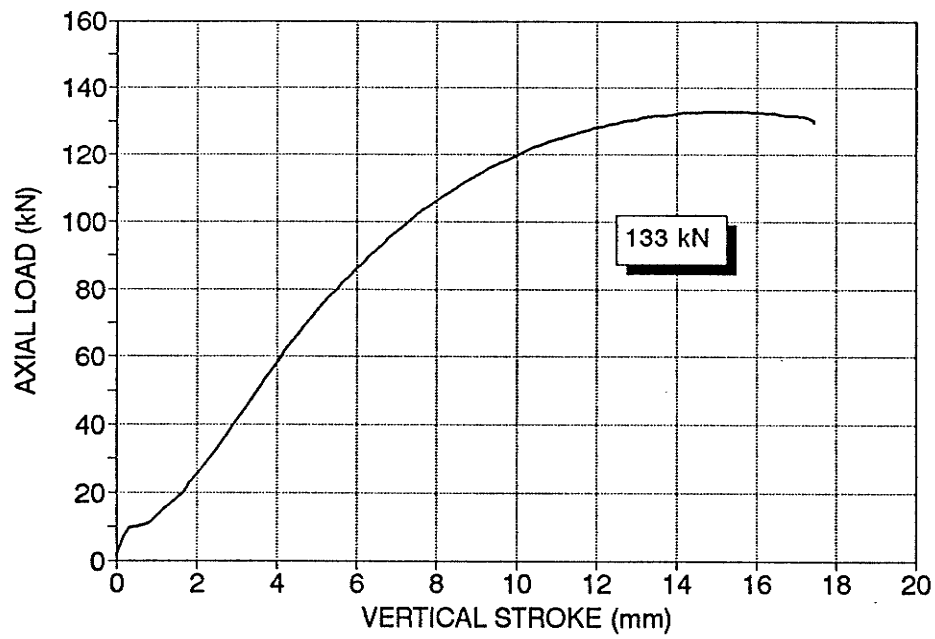
HBB-40-2
ROOM TEMPERATURE



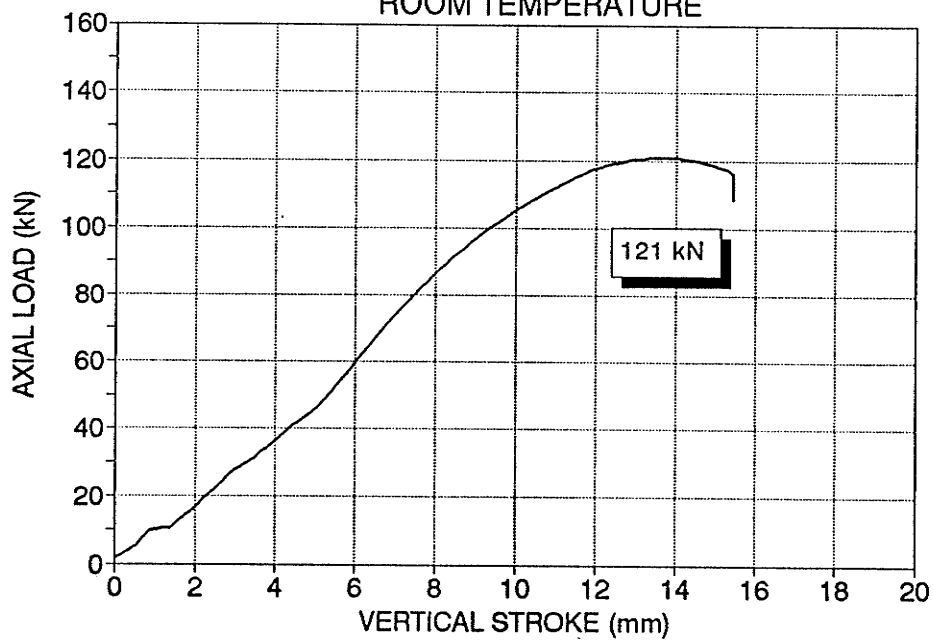
A.4 Typical Load-Displacement curves for Specimens BB-40 and HBB-40

BB-100-1
ROOM TEMPERATURE

202

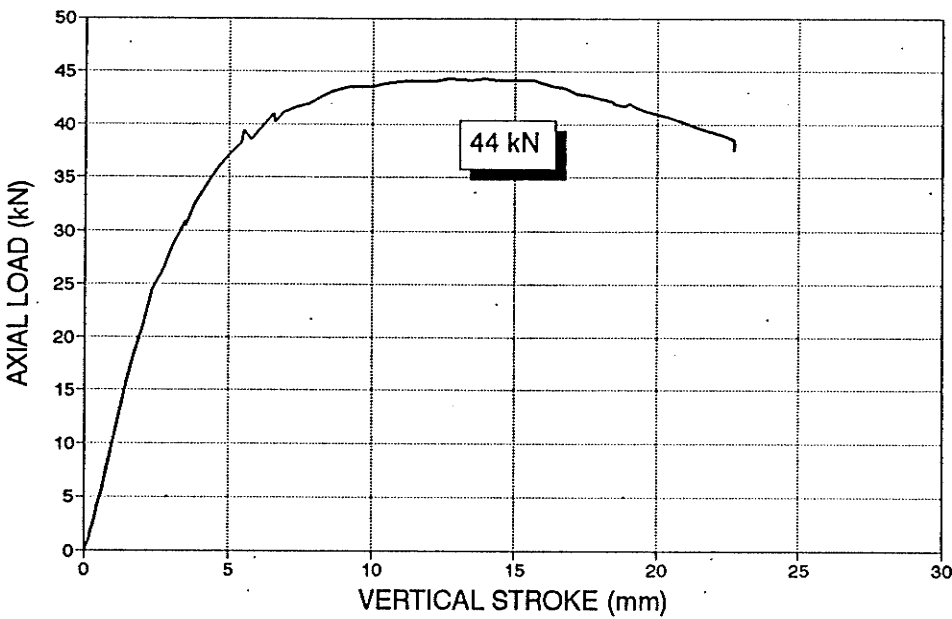


HBB-100-2
ROOM TEMPERATURE

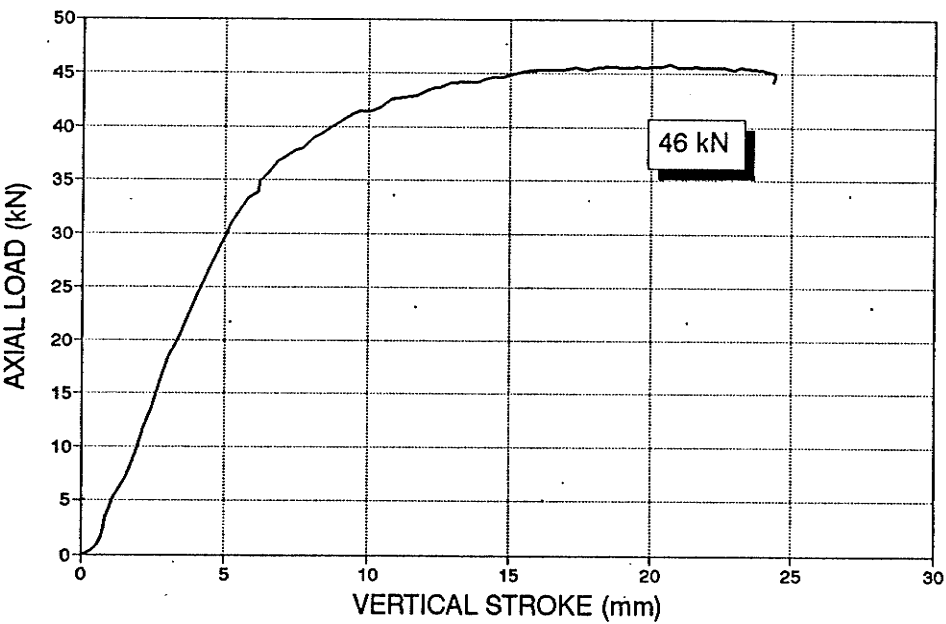


A.5 Typical Load-Displacement curves for Specimens BB-100 and HBB-100

HBB-200-1
ROOM TEMPERATURE

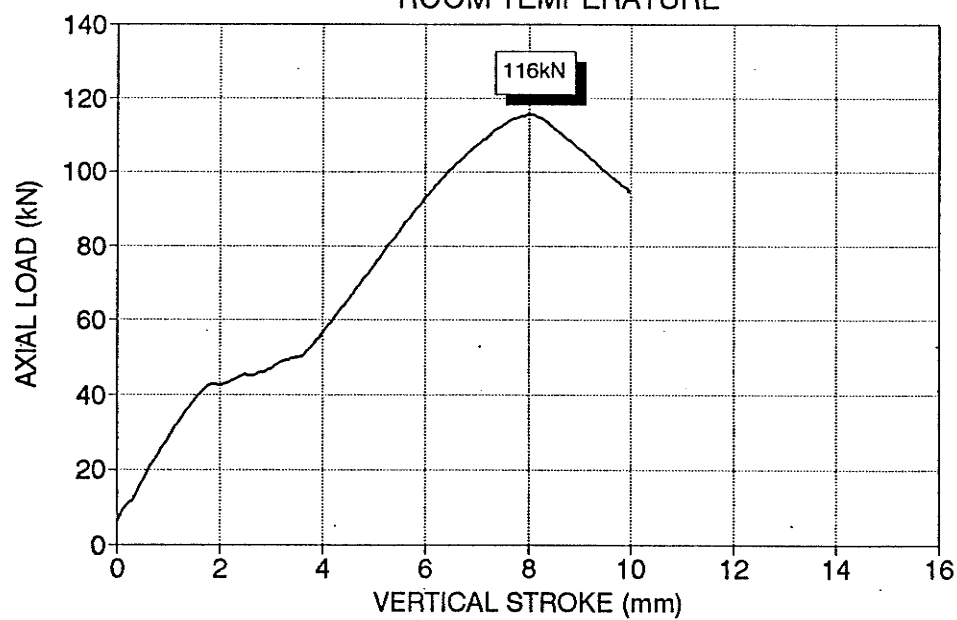


BB-200-2
ROOM TEMPERATURE

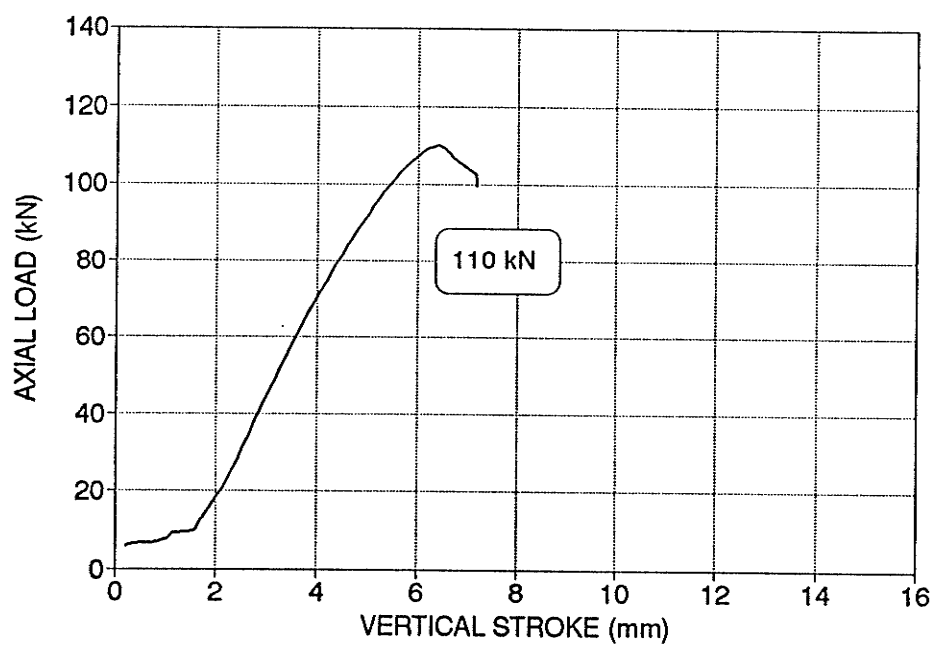


A.6 Typical Load-Displacement curves for Specimens BB-200 and HBB-200

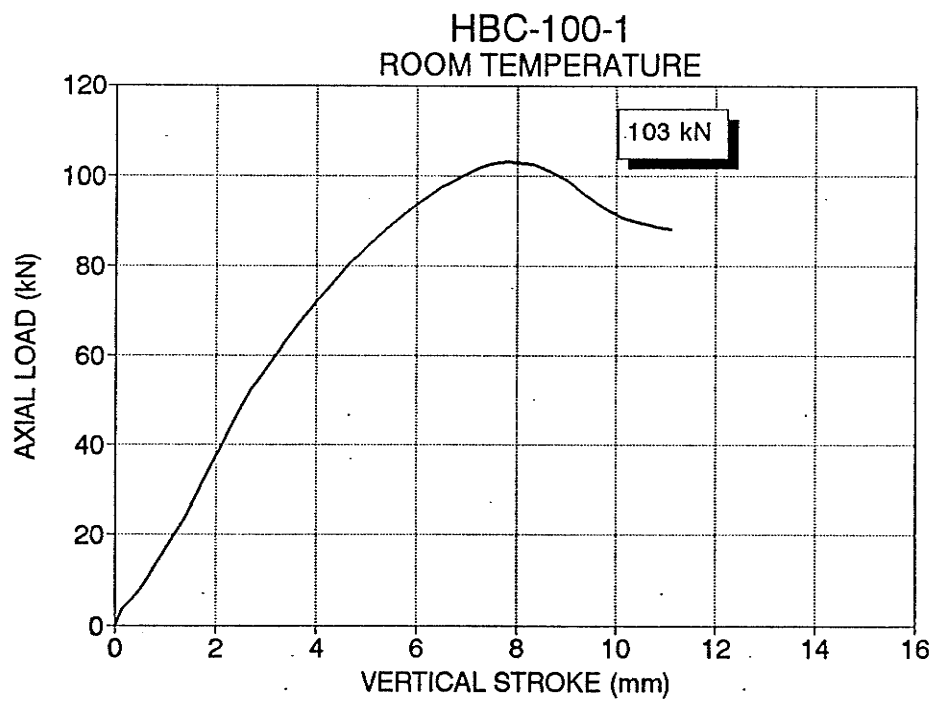
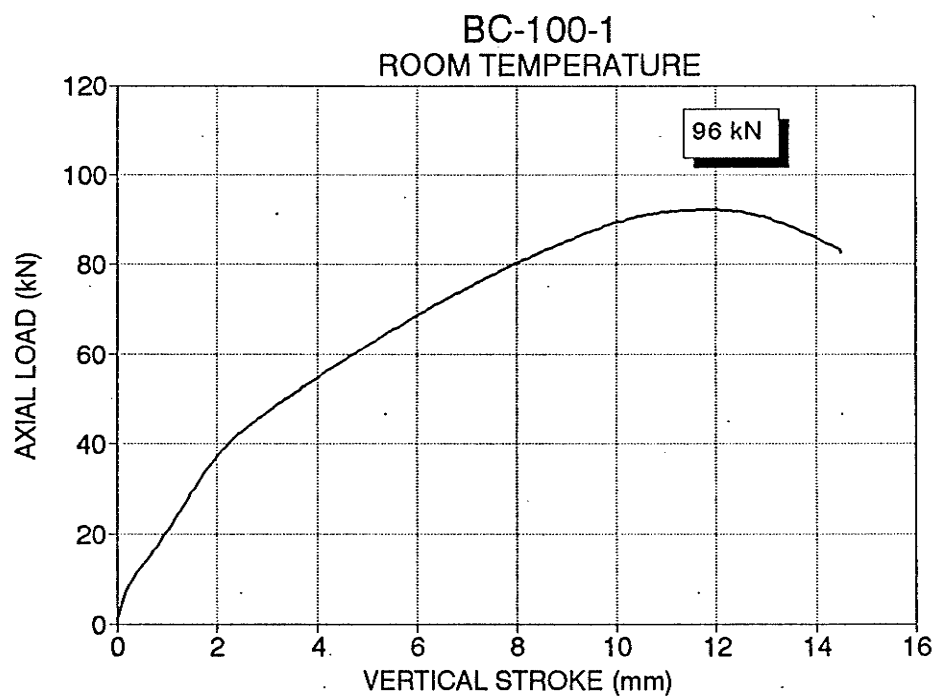
BC-40-1
ROOM TEMPERATURE



HBC-40-1
ROOM TEMPERATURE



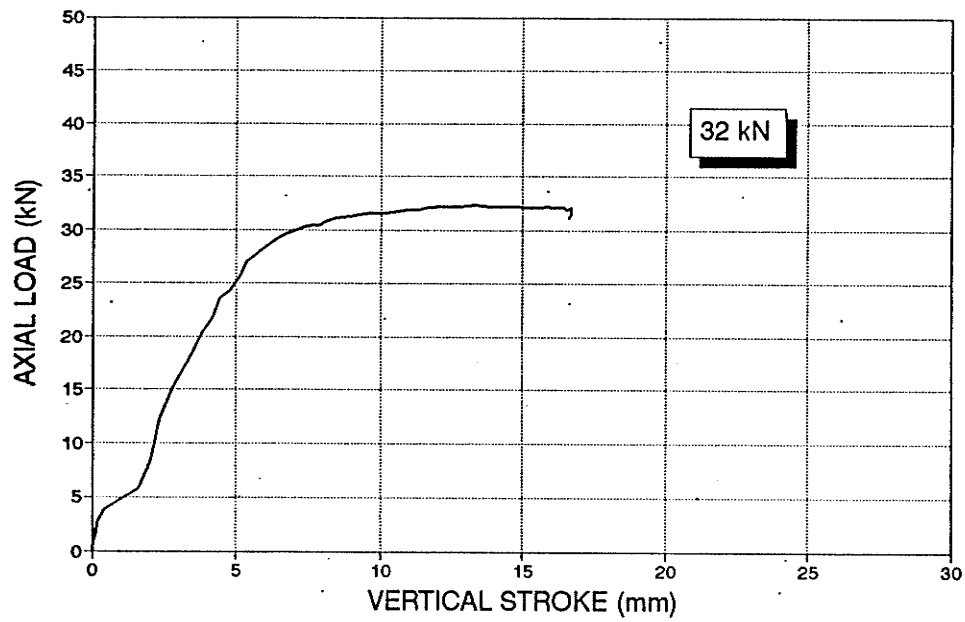
A.7 Typical Load-Displacement curves for Specimens BC-40 and HBC-40



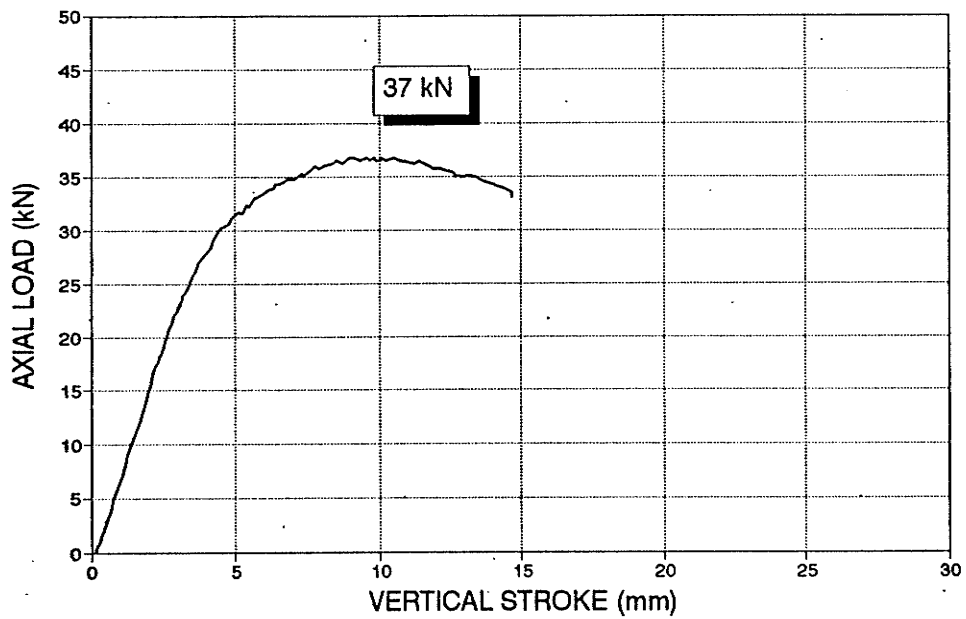
A.8 Typical Load-Displacement curves for Specimens BC-100 and HBC-100

BC-200-1
ROOM TEMPERATURE

206



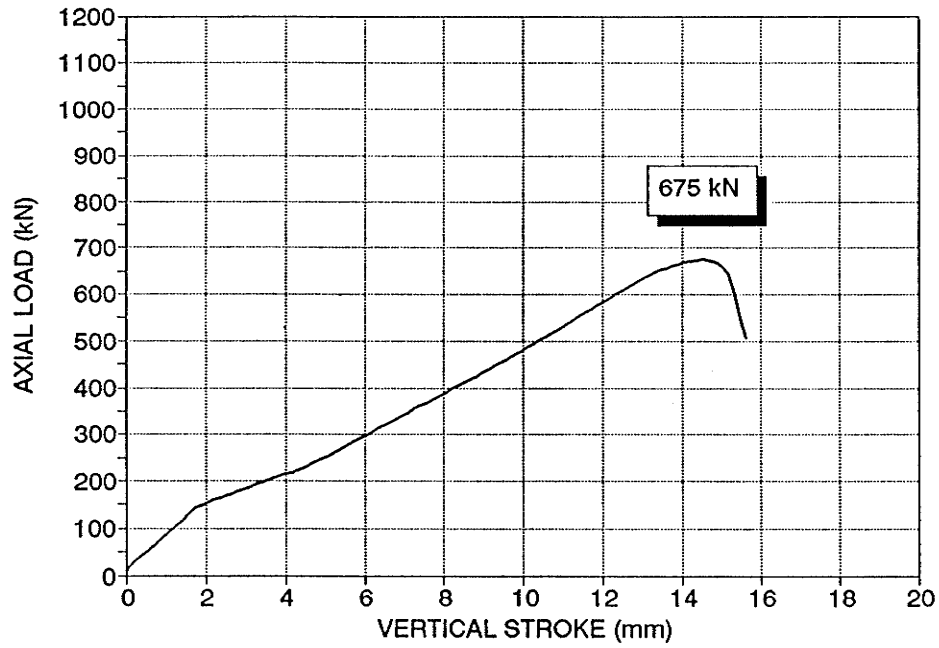
HBC-200-1
ROOM TEMPERATURE



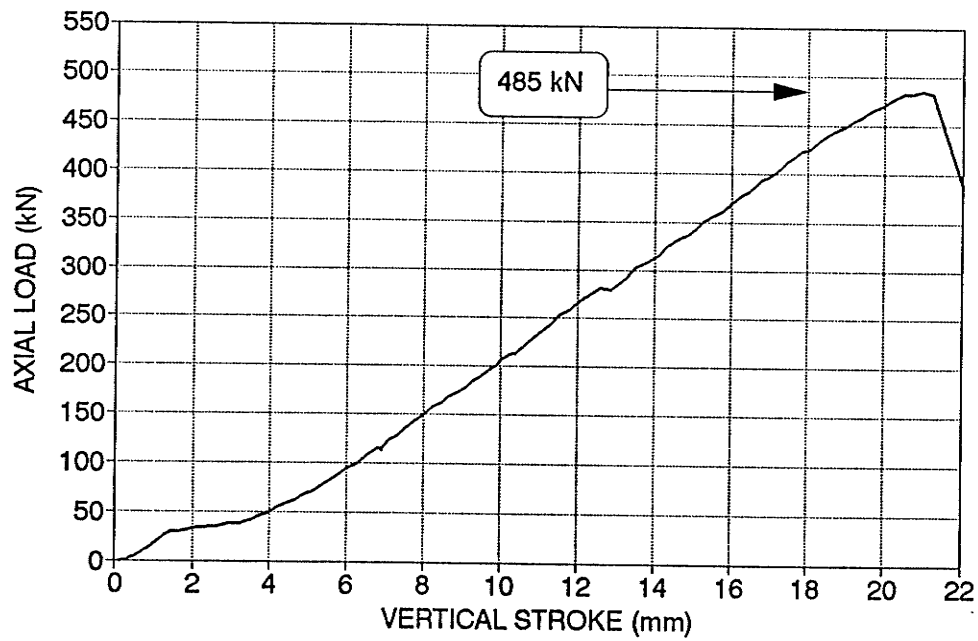
A.9 Typical Load-Displacement curves for Specimens BC-200 and HBC-200

BG-40-1
ROOM TEMPERATURE

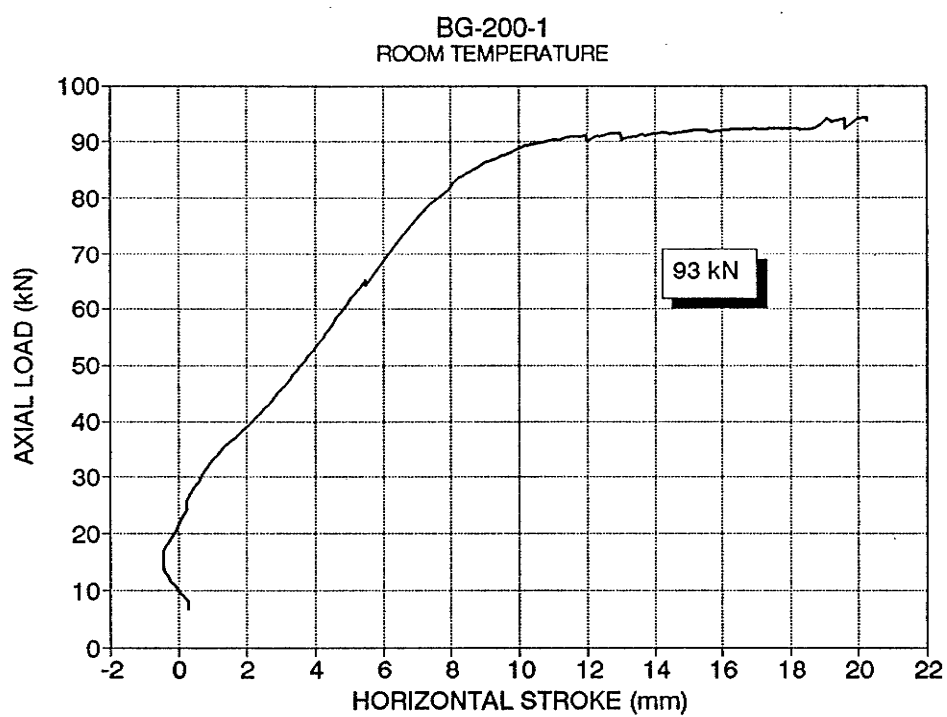
207



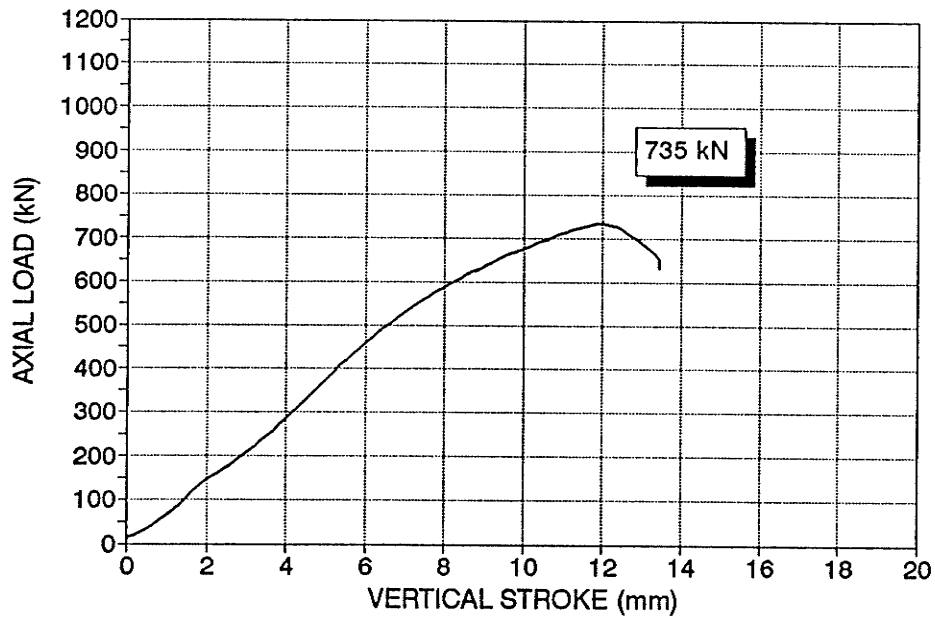
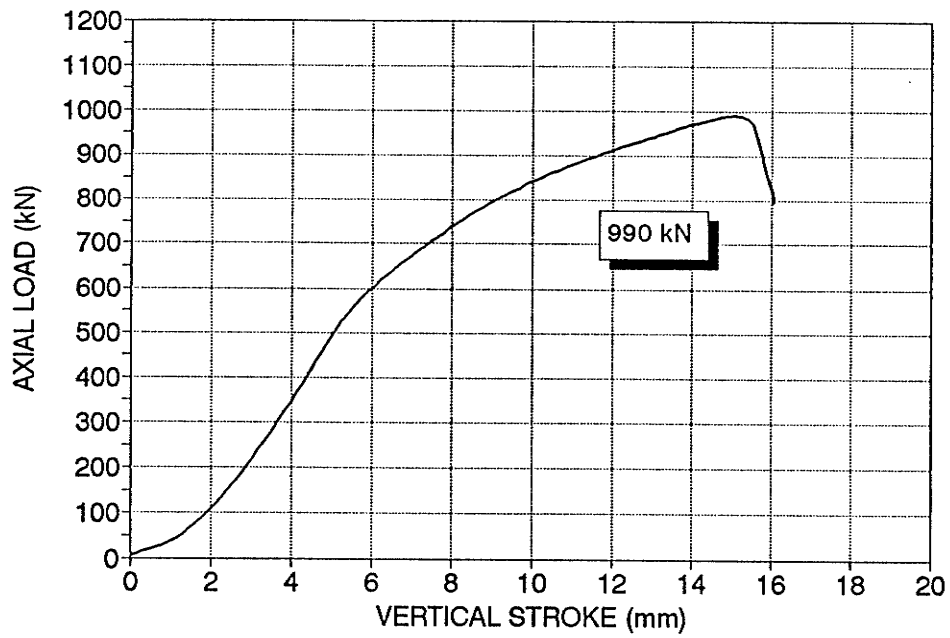
BG-100-1
ROOM TEMPERATURE



A.10 Typical Load-Displacement curves for Specimens BG-40 and BG-100



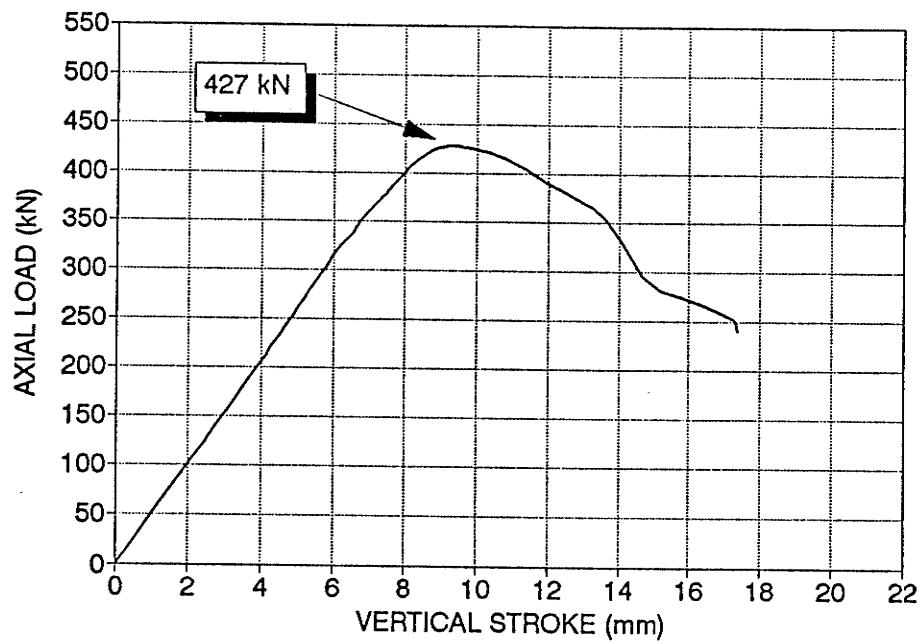
A.11 Typical Load-Displacement curves for Specimens BG-200



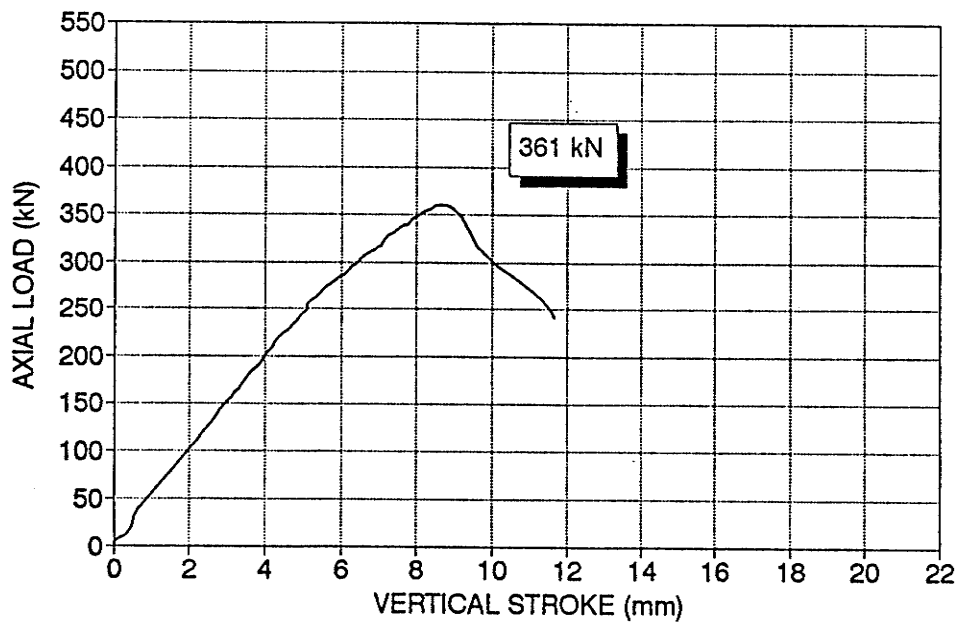
A.10 Typical Load-Displacement curves for Specimens BG-40 and BG-100

BN-100-2
ROOM TEMPERATURE

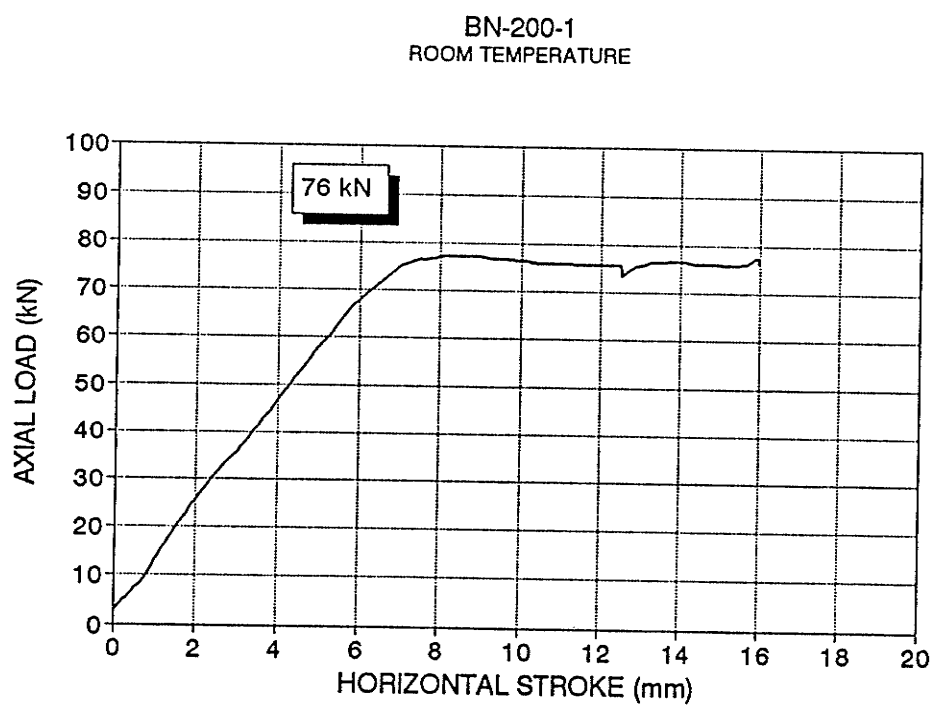
210



HBN-100-1
ROOM TEMPERATURE



A.13 Typical Load-Displacement curves for Specimens BN-100 and HBN-100



A.14 Typical Load-Displacement curves for Specimens BN-200

APPENDIX B

DESIGN EXAMPLES

Determine the capacity of section BA-40 using ASCE MANUAL 52

Section properties:

$$\text{Area} = 530 \text{ mm}^2$$

$$\text{Min radius of gyration} = 13.6 \text{ mm}$$

$$\text{Width-thickness ratio } w/t = 60.1/3.95 = 15.2$$

$$\text{Measured yield strength } F_y = 469 \text{ MPa} = 68 \text{ ksi}$$

Determine reduced effective yield stress (Section 4.7.3)

$$(w/t)_{\text{lim}} = 80/\sqrt{F_y} \text{ (ksi)} = 9.7$$

$$(w/t)_{\text{lim}} < w/t < 144/\sqrt{F_y}$$

$$\begin{aligned} \text{Therefore } F_{\text{cr}} &= (1.677 - 0.677(w/t)/(w/t)_{\text{lim}})F_y = 41.9 \text{ ksi} \\ &= 289 \text{ MPa} \end{aligned}$$

Determine effective length from Section 4.7.4.2

$$\begin{aligned} \text{Length between centroid of bolted connections} &= 552 - 50 - 50 \\ &= 452 \text{ mm} \end{aligned}$$

$$\text{Slenderness } L/r = 452/13.6 = 33.23$$

$$\text{From item 4.7-7: } KL/r = 60 + 0.5 (L/r) = 76.6$$

(for members with normal framing eccentricities at each end, and $L/r < 120$)

Allowable compression (Section 4.6)

$$\frac{KL}{r} < C_c - \pi \sqrt{\frac{2E}{F_{\text{crit}}}} - \pi \sqrt{\frac{2 \cdot 200000}{289}} - 116.9$$

$$\therefore F_a = \left[1 - \frac{1}{2} \left(\frac{KL/r}{C_c}\right)^2\right] F_{crit} = 227 \text{ MPa}$$

$$C_r = 227 \text{ MPa} \times 530 \text{ mm}^2 / 1000 = 120 \text{ kN}$$

Determine the capacity of section BA-200 using Manual 52

Reduced effective yield stress (Section 4.7.3)

$$F_{cr} = 295.5 \text{ MPa (as above)}$$

Determine effective length from Section 4.7.4.2

Length between centroid of bolted connections = 2760-50

$$= 2710 \text{ mm}$$

$$\text{Slenderness } L/r = 2710/13.6 = 199.3$$

$$\text{From item 4.7-8: } KL/r = (L/r) = 199.3$$

(for members unrestrained against rotation at both ends, and $L/r > 120$)

Allowable compression

$KL/r > C_c$ therefore in the elastic range

$$F_a = 286000 / (KL/r)^2 = 7.2 \text{ ksi} = 49.7 \text{ MPa}$$

$$C_r = 49.7(530 \text{ mm}^2) / 1000 = 26 \text{ kN}$$

Determine the capacity of HBA-40-100 section using CSA-S136-M89 Clause 6.7.4

Use section properties provided in first example

Reduced critical buckling stress

$$F_p = \frac{0.833\pi^2 E}{[(KL/r_y)^2 + (5b/t)^2]}$$

$$F_p = \frac{0.833\pi^2 E}{(0.7*452/13.6)^2 + (5*60.1/3.95)^2} = 259.8 \text{ MPa}$$

Calculate inelastic stress level

$$F_a = F_y - \frac{(F_y)^2}{4F_p} = 257.3 \text{ MPa} \quad \text{when } F_p > F_y/2$$

Check local buckling as per Clause 6.6.3.2

$$f = \frac{k\pi^2 E}{12(1-\mu^2)(w/t)^2} = \frac{0.43*\pi^2*200000}{12(1-0.3^2)(60.1/3.95)^2} = 335.8 \text{ MPa}$$

Local buckling critical stress is greater than F_p , therefore it is not critical

Calculate effective area of section (Clause 5.6.2)

$$W_{lim} = 0.644\sqrt{kE/f} = 0.644\sqrt{\frac{0.43 \times 200000}{257.3}} = 11.79$$

$W_{actual} = 15.2$ is greater than W_{lim} . Therefore area is not fully effective

Reduced flat width

$$B = 0.95\sqrt{kE/f} \left[1 - \frac{0.208}{(w/t)}\sqrt{kE/f} \right] = 13.03$$

Reduced effective area

$$A_{eff} = 530\text{mm}^2 - 3.95\text{mm} \times 2 \times (15.2 - 13.03) \times 3.95 = 462.3\text{mm}^2$$

Calculate axial resistance

$$C_r = \phi A_{eff} F_a = 0.75 \times 462.3 \times 257.3\text{MPa}/1000 = 89\text{kN}$$

Calculate axial resistance of BC-100 Specimen using CSA-S37-M86

Section properties

$$\text{Area} = 595 \text{ mm}^2$$

$$r = 18.4$$

$$w/t = 65.5/4 = 16.38$$

$$F_y = 477 \text{ MPa}$$

Determine the reduced effective yield stress (Clause 6.2.5)

$$200/\sqrt{F_y} < \frac{w}{t} < 380/\sqrt{F_y}$$

$$\therefore F_y - F_y \left[1.677 - 0.677 \left(\frac{w/t}{200/\sqrt{F_y}} \right) \right] = 222.6 \text{ MPa}$$

Dimensionless slenderness parameter λ

$$K = 0.9 \text{ for two bolt connection}$$

$$L = 1840 - 50 - 50 = 1740 \text{ mm between centres of bolt groups}$$

$$\lambda = \frac{KL}{r} \sqrt{\frac{F_y}{\pi^2 E}} = 0.9$$

From CSA-S16.1 for $0.15 < \lambda < 1.0$

$$C_r = \phi A F_y (1.035 - 0.202\lambda - 0.222\lambda^2)$$

For $KL/r < 120$, $\phi = 0.72$

$$\therefore C_r = 0.72 * 595 \text{ mm}^2 * 222.64 * (0.673) = 64 \text{ kN}$$

Note: the capacity is also checked against a lower limit provided by the value of C_r at $L/r = 120$, where ϕ is increased to $= 0.9$. This value is found to be 61 kN. Therefore the factored compressive resistance is 64 kN.

Calculate Capacity of BG-200 section according to CSA-S136-M89

Section properties

A	= 1925 mm ²	L	= 8445 mm (between hinges)
r _x	= 41.88 mm	(axis of symmetry, and rotation about hinge)	
r _y	= 41.52 mm		
x _o	= distance between centroid and shear centre =24.13 mm		
r _o	= 63.72 mm	β	= 0.857
G	= 78000 MPa	J	= 10256 mm ⁴
C _w	= 3.6*10 ⁹	I _{ps}	= 781546 mm ³
F _y	=438 MPa		

Calculate the flexural buckling critical stress (Clause 6.6.2)

Note that although the radius of gyration r_x is slightly smaller than r_y , the slenderness ratio will be based on r_y since the rotation at the hinge occurs about this axis.

$$F_e = \frac{\pi^2 E}{(KL/r)^2}$$

$$F_e = \frac{\pi^2(200000)}{(1.0(8445)/41.88)^2} = 48.6 \text{ MPa}$$

Calculate the torsional flexural buckling critical stress (Clause 6.6.3.1)

$$F_{st} = \frac{1}{2\beta} [F_s + F_t - \sqrt{(F_s + F_t)^2 - 4\beta F_s F_t}]$$

where

$$F_t = \frac{1}{A(r_o)^2} \left[GJ + \frac{\pi^2 E C_w}{(K_t L)^2} \right]$$

$$F_t = \frac{1}{1925(63.72)^2} [(78000)(10266) + \frac{\pi^2 E (3.604 \times 10^9)}{(1.0(8445))^2}] = 115.2 \text{ MPa}$$

F_s - flexural buckling strength about axis of symmetry

$$F_s = \frac{\pi^2 E}{(KL/r)^2} = 48.6 \text{ MPa}$$

Substituting these values in the expression for F_{st} provides the torsional flexural buckling stress as

$$F_{st} = 44.1 \text{ MPa} < F_e$$

Therefore torsional flexural buckling governs. The critical elastic buckling stress is given by

$$F_p = 0.833 F_{st} = 37.1 \text{ MPa}$$

Since this stress is less than $F_y/2$, the compressive stress is in the elastic region, and

$$F_a = F_p = 37.1 \text{ MPa}$$

The section should now be checked to determine if any of the flat widths exceed the limits imposed by Clause 5.6 of the Standard. However since the stress level is so low, a quick check of the most conservative limit, assuming an unstiffened element, with $k=0.43$ gives

$$W_{lim} = 0.644 \sqrt{0.43 E / 37.1} = 31.0$$

Which equates to a flat width of $31.0(4.0 \text{ mm}) = 124.0 \text{ mm}$. None of the elements have a flat unstiffened width of this limit, therefore it can be seen that the section area is fully effective.

The factored compressive resistance is then calculated as

$$C_r - \phi A_{eff} F_a = 0.75(1925)(37.1)/1000 = 54 \text{ kN}$$